

POLITECNICO DI MILANO

Scuola di Ingegneria Civile, Ambientale e Territoriale
Corso di Laurea Magistrale in

BUILDING AND ARCHITECTURAL ENGINEERING



REAL SCALE CYCLIC TESTS FOR SEISMIC ASSESS OF CONCENTRICALLY BRACED FRAMES

Supervisor:

Chiar.mo Prof. Carlo Andrea CASTIGLIONI

Correlator:

Dott. Ing. Alper KANYILMAZ

Master thesis of:

Rico Umberto
Matricola 852308

Academic Year 2014/2015

Index

1. Introduction	4
1.1. EN 1993-1-1 design approach for concentrically braced frames	5
1.2. MEAKADO PROJECT	6
1.3. Thesis objectives.....	6
2. State of the Art	8
2.1. Experimental researches about hysteretic behaviour of concentrically bracings	9
3. Design of test specimens	18
3.1. Introduction	18
3.2. Experimental tests definition.....	19
3.2.1. Steel characterization.....	21
3.3. Design Procedure	22
3.3.1. Model of Pendulum Frame	23
3.3.2. Bolts.....	24
3.3.3. Main elements of the frame	24
3.3.3.1. Beam-to-column joints.....	26
3.3.3.2. Pinned base connection of the column.....	28
3.4. Bracing system.....	30
3.4.1.1. Buckling check of the compressed element following the l'EC3	31
3.4.1.2. Tightening torque	33
3.4.1.3. Connection joint to the main members	35
3.4.1.4. Mid-plate connection	38
3.4.2. Evaluation of the bearing capacity of the tension and compression diagonal	39
4. Experimental setup	40
4.1. Test bench	40
4.1.1. Load application device.....	44
4.1.2. Out-of-plane restraints	45
4.2. Instrumentation.....	46
4.2.1. Linear displacement potentiometers	46
4.2.1.1. Operational principle.....	46
4.2.1.2. Calibration.....	47
4.2.1.3. Pots layout	48
4.2.2. Uni-axial strain gauges	54
4.2.2.1. Operational principle.....	54
4.2.2.2. Technical characteristics of the strain gauges	54
4.2.2.3. Layout e strain gauges description.....	55
4.3. Data acquisition system and load application	59

5. Experimental results.....	60
5.1. Loading protocol.....	60
5.2. Sign convention	63
5.3. Performance states	64
5.4. Test 1: X-shaped frame 2L60x8	65
5.4.1. Loading history	65
5.4.2. Global overview	66
5.4.3. Columns	67
5.4.4. Bracings behaviour	68
5.5. Test 2: X-shaped frame No mid connection 2L60x8.....	70
5.5.1. Loading history	70
5.5.2. Global overview	71
5.5.3. Columns	71
5.5.4. Bracings behaviour	72
5.6. Test 3: Single diagonal moment resisting frame 2L60x8	74
5.6.1. Loading history	74
5.6.2. Global overview	75
5.6.3. Column and beams.....	76
5.6.4. Bracings behaviour	76
5.7. Test 5: X-shaped frame 2L70x7	78
5.7.1. Loading history	78
5.7.2. Global overview	79
5.7.3. Bracings behaviour	80
5.8. Test 7: Single diagonal frame 2L70x7.....	81
5.8.1. Loading history	81
5.8.2. Global behaviour	82
5.8.3. Bracings behaviour	84
5.9. Test 15: No-bracings and no-gussets frame	85
5.9.1. Loading history	85
5.9.2. Global overview	86
5.10. Test 16: No bracings frame.....	88
5.10.1. Loading history	88
5.10.2. Global behaviour	89
5.11. Test 13: X-braced frame 2L60x8.....	92
5.11.1. Loading history	92
5.11.2. Global behaviour	93
5.11.3. Column and beams.....	104
5.11.4. Bracings behaviour	104

5.11.5. Energy dissipation	105
5.12. Test 17: Pinned X-braced frame 2L60x8	112
5.12.1. Loading history	112
5.12.2. Global overview	113
5.12.3. Column and beams.....	114
5.12.4. Bracings behaviour	115
5.13. Test 18: Pinned X-braced frame 2L70x7	116
5.13.1. Loading history	116
5.13.2. Global overview	117
5.13.3. Columns	118
5.13.4. Bracings behaviour	119
5.14. Test 19: Pinned single diagonal frame 2L70x7	120
5.14.1. Loading history	120
5.14.2. Global overview	121
5.14.3. Column and beams.....	122
5.14.4. Bracings behaviour	122
5.15. Test 23: Single diagonal pinned frame 2L60x8	124
5.15.1. Loading history	124
5.15.2. Global overview	125
5.15.3. Columns and beams	126
5.15.4. Bracings behaviour	126
6. Analysis of test results.....	128
6.1. Energy dissipation	128
6.1.1. Bolts slip and ovalization	128
6.1.2. Bracings buckling	132
6.1.3. Idealization of the brace	135
6.1.4. Strength and stiffness comparison	136
6.1.5. Overstrength from compression diagonal	138
6.1.6. Pinned vs moment resisting frame	141
6.1.7. Gusset plate	142
6.1.8. Reserve ductility of the frame	144
7. Initial connection stiffness	147
8. Conclusions. Future research.	155
APPENDIX A – Lab report about specimens monoaxial tensile tests.....	157
APPENDIX B – Complete bill of materials and design papers	159
Bill of materials	159
Bill of fasteners	160
Graphic charts.....	161

APPENDIX C – BRACINGS BEARING CAPACITY	223
Bearing capacity brace-gusset plate connection	223
Compression and tension brace resistance	227
Compression profile classification	227
Tension diagonal strength	227
Buckling and strength of compression diagonal	228
Block tearing	229
APPENDIX D – DESIGN OF PINNED FRAME ELEMENTS	230
Hollow beam resistance and stability to compression according to EC3	230
Hollow beam resistance and stability to compression according to EC3	232
Weldings design and check.....	235
APPENDIX E – instrumentation layout	237
Potentiometers layouts	237
APPENDIX F – bolt slip.....	243
References	246
Acknowledgements	248

INDEX OF FIGURES

Figure 1. Calculation framework for bracings configurations: a) Tension only b) Tension / Compression	5
Figure 2. Design values scheme	6
Figure 3. Force-displacement cycles of a rod axially loaded to symmetrical loading history	8
Figure 4. Force-displacement cycles of a braced frame	8
Figure 5. Tests specimens	10
Figure 6. Maximum bearing capacity for each loading cycle. Single diagonal frame configuration	11
Figure 7. Maximum bearing capacity for each loading cycle. Cross-diagonal configuration frame	11
Figure 8. Cycle force-displacement for single diagonal specimens	12
Figure 9. Force-displacement cycle of cross configuration braced specimens	12
Figure 10. Asymmetrical deformed configuration	13
Figure 11. Adimensional energy absorbed for each loading cycle	13
Figure 12. Comparison between numerical and real behaviour	14
Figure 13. Hysteretic response of a brace undergoing inelastic cycles	15
Figure 14. Construction detail of the tested specimen	16
Figure 15. Generic scheme of the frame	18
Figure 16. Frame configuration during the tests	19
Figure 17. Samples extracted from angular profiles of the braces for tensile tests	21
Figure 18. Conceptual scheme of a) MRF and b) PF (measures in meters)	23
Figure 19. Braced pendulum frame	23
Figure 20. Front view of MRF (measures in meters)	25
Figure 21. Front view of PF (measures in meters)	25
Figure 22. Beam-column joint in MRF	26
Figure 23. Construction details of beam-column connection (measures in mm)	26
Figure 24. Beam-column joint in PF	27
Figure 25. Construction details of beam-column connection (measures in mm)	27
Figure 26. Pinned base plate in MRF	28
Figure 27. Detail of pinned base plate in MRF	28
Figure 28. Construction details of pinned base plate in PF	29
Figure 29. Detail of pinned base plate in MRF	29
Figure 30. Front view of the PF configurations (measures in meters)	34
Figure 31. Front view of the MRF configurations (measures in meters)	34
Figure 32. Angular gusset plate welded to the main members	35
Figure 33. Modular connection system in MRF	35
Figure 34. Modular connection system in PF	36
Figure 35. Construction details of corner connection modular systems in MRF (measures in mm)	37
Figure 36. Construction details of corner connection modular systems in PF (measures in mm)	37
Figure 37. Steel mid-plate of the bracing system	38
Figure 38. Construction detail of the mid-connection (measures in mm)	38
Figure 39. MRF Test setup (measures in meters)	41
Figure 40. PF Test setup (measures in meters)	42
Figure 41. View of the test bench	43
Figure 42. Load transmission device of frames (measures in mm)	44
Figure 43. Fixing phase of the load cell to the MRF	44
Figure 44. Sphere joint welded to the specimen	45
Figure 45. Sphere joint welded to the specimen	45
Figure 46. Electric scheme of a stick linear potentiometer	46
Figure 47. Calibration of a potentiometer through digital micrometer	47
Figure 48. Linear regression line of a pot	47

Figure 49. Pots for horizontal displacement of the frame	48
Figure 50. Pots for horizontal displacements (real test bench)	49
Figure 51. Potentiometers for measuring braces buckling in X configuration frame	50
Figure 52. Pots for buckling measurement of the brace in one diagonal configuration	50
Figure 53. Pots for relative slide evaluation of the braces	51
Figure 54. Scheme for rotation calculation of the beam-column joint	52
Figure 55. Potentiometers for rotation of beam-column joints	52
Figure 56. Pots for base plate slip	53
Figure 57. Potentiometers for the measurement of base plates sliding	54
Figure 58. Structure of an electrical sheet strain gauge	55
Figure 59. Installed strain gauges: a) on continuous brace b) on right column c) on the bottom beam ..	55
Figure 60. Strain gauges layout	56
Figure 61. Detail of the bracings strain gauge installation	57
Figure 62. Installation details of the strain gauges on the main members a) column of MRF b) beam of MRF c) column of PF	58
Figure 63. Data acquisition systems	59
Figure 64. Storey drift definition	60
Figure 65. Loading protocol definition on control unit of actuator	62
Figure 66. Adopted sign convention: a) positive frame displacement b) negative frame displacement	63
Figure 67. 2L60x8 X-braced frame specimen on test bench	65
Figure 68. Loading history	65
Figure 69. Initial step hysteresis loops- Coordinates for initial stiffness	66
Figure 70. a) Frame hysteresis loop . b) Initial steps-global	67
Figure 71. Load trend on columns	67
Figure 72. Load on bracings over times. Data derived by strain gauges records.	68
Figure 73. Axial forces over drift applied during test.	69
Figure 74. Loading history	70
Figure 75. Global test hysteresis loops	71
Figure 76. Load trend on columns	72
Figure 77. Load on bracings over times. Data derived by strain gauges records.	72
Figure 78. Axial forces over drift applied during test.	73
Figure 79. Specimen on test bench	74
Figure 80. Loading history	74
Figure 81. Global test hysteresis loops	75
Figure 82. Load trend on columns	76
Figure 83. Load on bracings over time and displacement applied.	77
Figure 84. Trend of load on brace and columns. Comparison. Force distribution scheme	77
Figure 85. Specimen on test bench	78
Figure 86. Test 5: loading history	78
Figure 87. Test 5: global test hysteresis loops.	79
Figure 88. Test 5: axial load over time and displacement imposed (experimental results)	80
Figure 89. Test 7: Specimen on test bench before test initiation	81
Figure 90 Test 7: loading history	81
Figure 91. Test 7: Global test hysteresis loops	82
Figure 92. Test 7: plastic hinge during post-buckling phase (0.62% of drift)	83
Figure 93. Test 7: plasticization of diagonal edge (0.62% of drift)	83
Figure 94. Test 7: collapse mechanism of brace (0.69% of drift)	84
Figure 95. Test 7: diagonal axial load – displacement applied (experimental results)	84
Figure 96. Specimen on test bench	85
Figura 97. Test 16: loading history	85

Figure 98. Global test hysteresis loops.....	86
Figure 99. Web angles yielding.....	87
Figure 100. Test 16: specimen on test bench.....	88
Figure 101. Test 16: loading history.....	88
Figure 102. Initial stiffness.....	89
Figure 103. Global test hysteresis loops.....	90
Figure 104. Test 16: gusset plates yielding. T-stub section.....	90
Figure 105. Beam-column node rotation.....	91
Figure 106. Yielding mechanism of the gusset plates.....	91
Figure 107. Test 13: loading history.....	92
Figure 108. Initial stiffness (plot at first ± 6 mm cycle).....	93
Figure 109. First slip occurred when frame under compression, force peak value 665 kN, drift -0,23% (plot at first compression peak of ± 8 mm cycle) (2800 s time step).....	94
Figure 110. Bearing capacity reduction (plot at first compression peak of ± 8 mm cycle) (5550).....	94
Figure 111. Second slip (plot at first compression peak of ± 12 mm cycle, drift -0,46 %, force peak value 675 kN) (6550 s time step).....	95
Figure 112. First slip occurred when structure under tension (plot at first tension peak of ± 13 mm cycle, drift +0.51%, force peak value 703 kN) (6950 s time step).....	95
Figure 113. Continuous brace buckling, +0.59 % (+15 mm) drift cycle, force peak value 750 kN (9850 s time step).....	96
Figure 114. 4. plastic hinge is formed at mid-span of the north-west continuous diagonal.....	96
Figure 115. 5. Plastic hinge formed after first in-plane buckling on mid-span of NE diagonal.....	96
Figure 116. Global behaviour. Stiffness deterioration. (13080 s time step).....	97
Figure 117. Plasticization of frame nodes.....	97
Figure 118. Plasticization, cracks opening and propagation at NW discontinuous diagonal.....	98
Figure 119. Global behaviour. Brace axial load-drift ratio. (15150 s time step).....	98
Figure 120. Crack opening at plastic hinges yet presented at frame nodes.....	99
Figure 121. Global behaviour (17150 s time step).....	100
Figure 122. Failure along the stitch plate bolts in mid-span of the north-east discontinuous diagonal. (second frame tension peak of ± 30 mm). Gross-section separation at mid-span of NE discontinuous brace. Cracks, initiated after plastic hinge formation, propagate.....	100
Figure 123. Global behaviour (18150 s time step).....	101
Figure 124. Failure at mid-span of the north-west continuous diagonal (first frame compression peak of ± 38 mm cycle).....	101
Figure 125. Global behaviour (20200 s time step).....	102
Figure 126. Frame at test end; yielding at gusset.....	102
Figure 127. Main phases on a drawing.....	102
Figure 128. Load trend on beams.....	104
Figure 129. Axial load of bracings over time and displacement applied.....	105
Figure 130. Calculation scheme hysteresis loop area.....	105
Figure 131. Energy dissipation for each cycle.....	106
Figure 132. Scheme of global (a) and local (b) buckling mechanism.....	107
Figure 133. Curve of cumulative energy dissipated during test 13.....	107
Figure 134. Compare cumulate the energy dissipation comparison. Test 13 vs Test 16.....	108
Figure 135. Cumulative energy dissipation of positive displacement loops.....	109
Figure 136. Calculation scheme.....	109
Figure 137. Cumulative energy of negative drift cycle loops.....	110
Figure 138. Cumulate energy dissipation during positive drift cycle vs negative drift cycle loops.....	111
Figure 139. Energy dissipation for each cycle (Test13 vs Test3).....	111
Figure 140. Specimen on test bench.....	112

Figure 141. Loading history.....	112
Figure 142. Initial stiffness	113
Figure 143. Global test hysteresis loops	114
Figure 144. Buckling mechanism of the system. Brace touched the beam.	114
Figure 145. Load trend on columns.....	115
Figure 146. Pre-buckling phase axial loops in bracings	115
Figure 147. Specimen on test bench.....	116
Figure 148. Loading history.....	116
Figure 149. Initial step and global test hysteresis loops.....	118
Figure 150. Load trend on columns.....	118
Figure 151. Bracing axial load over time and displacement applied	119
Figure 152. Detail of plastic hinge on continuous brace.	119
Figure 153. Specimen on test bench.....	120
Figure 154. Loading history.....	120
Figure 155. Hysteresis loops after buckling and at test end.	121
Figure 156. Trend of load on brace and columns. Comparison. Force distribution scheme.	122
Figure 157. Bracings axial load over time and displacement applied.....	123
Figure 158. Buckling of diagonal (+0.19% drift applied).....	123
Figure 159. Specimen on test bench.....	124
Figure 160. Loading history.....	124
Figure 161. Global hysteresis loops pre-yielding and after yielding of the brace.....	125
Figure 162. Trend of load on brace and columns. Comparison. Force distribution scheme.	126
Figure 163. Bracings axial load over time and displacement applied.....	127
Figure 164. Buckling of diagonal. (+0.19% drift applied)	127
Figure 165. Test 5: base shear – drift.....	128
Figure 166. Scheme of involved force at bolt connection	129
Figure 167. Slip and its effects on internal surface of brace at connection to gusset.....	129
Figure 169. Bolt holes ovalization at brace joints ends.....	131
Figure 169. Test 3-7-18-23. Evaluation of axial buckling load of brace through base shear (values about test 5)	132
Figure 170. Diagonal inflexion over axial load in bracings	133
Figure 171. Test 3-7-19-23: bracing behaviour idealization	135
Figure 172. Test 7: calculation scheme of frame global stiffness.....	137
Figure 173. Hysteresis loops comparison	138
Figure 174. X-braced vs Single diagonal frame - initial stiffness.....	139
Figure 175. X-braced vs Single diagonal frame - global behaviour	140
Figure 176. Global behaviour semi-rigid vs pinned frame	141
Figure 177. Global base shear-drift behaviour of the frame with and without gusset plate connections	142
Figure 178. Geometry of beam-to-column connection	143
Figure 179. Initial stiffness comparisons of X-braced semi-rigid and pinned frames.....	143
Figure 180. Initial stiffness comparisons of semi-rigid and pinned frames.....	143
Figure 181. Peak base shear reached in the tests	144
Figure 182. Ductility resources of the 2L60x8 braced frame	145
Figure 183. Ductility resources of the 2L70x7 braced frame	145
Figure 184. Base shear and Drift values at various instances (A, B, C, D, E)	146
Figure 185. Specimen X60 during post buckling and after bracings' complete failure	146
Figure 186. Semi-rigid beam-to-column connection.....	147
Figure 187. Geometrical scheme for deriving parameters	148
Figure 188. Angle and gusset cross-section for stiffness estimation.....	149

Figure 189. Connection geometry for estimation of connection stiffness: (a) positive bending; (b) negative bending.....	150
Figure 190. Web angles and gusset cross-section for moment strength estimation	152
Figure 191. Connection geometry for estimation of connection strength: (a) positive bending; (b) negative bending.....	153
Figure 192. Configurations of braced frame tested	156
Figure 193. Values of lab tensile test of specimens	157
Figure 194. Values of lab tensile test of specimens	158
Figure 195. Values of lab tensile test of specimens	158
Figure 196. Test 1. Slip at bracings node.	243
Figure 197. Test 2. Slip at bracings node.	243
Figure 198. Test 3. Slip at bracings node.	244
Figure 199. Slip at bracings node.....	244
Figure 200. Slip at bracings node.....	244
Figure 201. Slip at bracings node.....	245
Figure 202. Slip at bracings node.....	245

INDEX OF TABLES

Table 1. Cyclic tests list. **test 2,6,10 not shown in table: they refer to X configuration with continuous diagonal not bolted to mid-plate.....	20
Table 2. Mechanical characteristics of the used steel.....	21
Table 3. Profiles geometrical properties of the MRF and PF main members	24
Table 4. Bracings geometrical properties	30
Table 5. Design data for interconnectors spacings.....	31
Table 6. Geometric characteristics of the diagonal in the section of anchorage	31
Table 7. Specimens geometrical properties.....	33
Table 8. Tightening combined method: initial applied torque	33
Table 9. Tightening combined method: nut additional rotation	33
Tabella 10. Loading protocol definition according to ECCS (1986).....	61
Table 11. Loading protocol of tests	62
Table 12. Sign convention of test parameters	63
Tabella 13. Test 1: displacement cycles	66
Table 14. Test 2: displacement cycles	70
Table 15. Test 3: displacement cycles	75
Table 16. Test 7: displacement cycles	79
Table 17. Test 7: displacement cycles	82
Table 18. Test 16: displacement cycles	86
Table 19. Test 16: displacement cycles	89
Table 20. Test 13: displacement cycles	93
Table 21. Percentage of contribution in energy dissipation	108
Table 22. Ratio about energy dissipation	109
Table 23. Energy dissipation comparison.....	109
Table 24. Cumulate energy dissipated	110
Table 25. Comparison of energy dissipation between tests (13vs3vs16)	111
Table 26. Displacement cycles	113
Table 27 Test 18: displacement cycles	117
Table 28. Test 19: displacement applied.....	121
Table 29. Test 23: displacement cycles	125
Table 30. Numerical values obtained for various inelastic mechanisms.....	130
Table 31. Comparison between design and experimental values about buckling axial load in compression diagonal	134
Table 32. Stiffness and strength tests comparison.....	136
Table 33. Rotational stiffness of web angles connection.....	149
Table 34. Segment stiffness derivation	151
Table 35. Global rotational stiffness derived by gusset plates	151
Table 36. Summary of rotational stiffness	152
Table 37. Evaluation of P_{ui} , load generating plastic hinges	154
Table 38. Ultimate moment strength for rotational directions	154
Table 39. List of steel elements for moment resisting frame assembly.....	159
Table 40. List of steel elements for pinned frame assembly	160

ABSTRACT

This thesis investigates the cyclic performance of concentrically braced frame, designed according to EN 1993-1-1 prescriptions. Two basic structures, a semi-rigid and a pinned one were studied using full-scale experiments to determine their flexural strength, stiffness, and ductility. Different bracings configurations and profiles sections have been tested. The experimental study foresees quasi-static cyclic tests conducted by imposing increasing amplitude cycles displacement to the frame. The analysed configurations encompass both active diagonal frame case, only one tension active diagonal, and a frame with no diagonals (only gusset plates).

From full-scale brace experiments, cross-section width-thickness and slenderness ratios are shown to influence the brace axial deformation ductility, such that a larger width-thickness ratio and a smaller slenderness tend to reduce ductility.

The analysis of the obtained results allowed to evaluate the contribution provided by main frame elements to the global behaviour of the frame and the influence of the compression diagonal through the bracings systems. The experimental results also highlighted an underestimation of standards about the bearing capacity of the compression bracing due to an overestimation of the free-buckling length. The experimental tests analysed in this thesis are part of the research project funded by “*European Research Fund for Coal and Steel*”, named “MEAKADO Project RFSR-CT-2013-00022”.

1. Introduction

Steel Concentrically Braced Frames (CBFs) have been used for years in steel construction sector. Their seismic performance has been extensively studied. These studies have produced guidelines for brace and connection design to give the desired capacity under seismic events. These guidelines, however are generally too conservative and actually could produce CBFs that are ineffective in seismic events. This project aims to better define the performance of these CBFs, thereby allowing more specified guidelines for design. Design approach of current standards, such as EN 1993-1-1, supposes structure as resistant to seismic event with a return period equal either to the service life of the structure without developing any significant damages to structural elements (SLS – service limit state), or higher than service life limit avoiding collapse (ULS – ultimate limit state). In order to reach the goal, standards indicate design procedure to provide the required stiffness, strength and enough degree of ductility. Ductility results effective since represents the skill of the structure to generate plastic deformations before structural collapse occurs, constituting a fundamental resource in case of seismic design. Adopting the so called “capacity design”, it is possible to control the collapse mechanism of the structure, the areas in which energy will be dissipated. Some elements are designed to plasticize during a seismic event while others to remained within the elastic range.

Enough overstrength and stiffness must be provided to non-dissipative elements in order to concentrate plasticizations. Thus, design procedure recommends to develop a collapse mechanism occurring after local plasticization areas. It also suggests to guarantee a global response able to provide sufficient stability also in case of local buckling or plasticization deriving from hysteretic behaviour of the structure. [1] [2] The degree of design ductility depends on many parameters, among which the structural elements configuration.

In case of simple CBFs, it is standard practice to ignore any lateral resistance provided by the nodal connection devices of between frame elements, such as gusset plates. In other words, the beam-column connections are assumed to be pinned, when in fact the presence of the gusset plate can add significant lateral stiffness to the joint. The actual stiffness of the frame is complex in nature due to the behaviour of the gusset-brace system. When the brace member is subject to tension demands, the gusset plate will experience an added compressive stress in conjunction with the tensile stresses induced by the brace. This compressive stress is associated with the rotation of the beam-column joint as the CBF drifts laterally. The extent of this rotation is dependent on the amount of lateral drift and also the dimensions of the frame. The overall stiffness of the CBF is thus a combination of that provided by the brace member and gusset plate connection to both brace and beam-column. This total stiffness will vary significantly depending on the relevant level of frame drift. At low cyclic demands the stiffness of the CBF will have similar contributions from both the tension and compressive gusset-brace system. As these cyclic demands increase and the brace and/or gusset plate experience buckling from compression loading, the lateral stiffness of the frame will become predominantly dependent on the tension resistance of the gusset-brace system only. These observations were also made by Goggins *et al.* (2005) for cyclic tests on brace members only. Currently, standard practice in Europe (CEN 2004) is that CBFs are designed so that yielding of the diagonals in tension will take place before failure of the connections and before yielding or buckling of the beams or columns. In the analysis of the structure, in frames with diagonal bracings only the tension diagonals are taken into account, while in frames with V bracings, both the tension and compression diagonals are taken into account for the seismic action. If a non-linear static (pushover) global analysis or non-linear time history analysis is used and certain criteria are met, both tension and compression diagonals can be taken into account in the analysis of any type of concentric bracing system.

1.1. EN 1993-1-1 design approach for concentrically braced frames

In the case of concentrically-braced frames, capacity design normally implies the use of diagonal bracing members as the main dissipative elements, while providing adequate overstrength factors for other frame members and components to ensure compliance with the selected failure mode. EN 1998-1-1 rely on the capability of parts of the structure (dissipative zones) to resist earthquake actions beyond their elastic range. In the case of concentrically-braced frames, Eurocode 8 assumes that only tension diagonals participate in the lateral resistance of earthquake-induced loading, and hence, in these structures dissipative zones are mainly located in the tension diagonals. This approach is different from that followed in other seismic codes. Furthermore, buckling as well as yielding of structural elements (beams and columns) must be avoided. Structure has to resist seismic loads without losing vertical stability.

Diagonal elements could be arranged to X or V configurations. At any configuration corresponds a different seismic behaviour. Braced frame current design guarantees that seismic energy dissipation is performed locating plasticization areas on tension diagonals, neglecting compression diagonal contribution. Ultimate dissipative behaviour on diagonals is achieved by adopting following prescriptions:

- evaluation of design loads on bracing has to be derived from schemes in which only tension diagonal is considered as active, as shown in *Figure 1a*;
- non-dimensional slenderness $\bar{\lambda}$ must be higher than 1.3, in order to avoid columns overloading after buckling on compression diagonal (reference scheme of *Figure 1b*). Furthermore, non-dimensional slenderness has to be equal or less than 2 so to provide a good dissipative level to bracings undergone cyclic loads;
- definition of the global overstrength coefficient Ω , equal to the minimum between values of overstrength coefficients Ω_i of the single diagonals. Generic diagonal overstrength coefficient is equal to the ratio design plastic resistance of tension diagonal over the corresponding stress induced by the seismic action.

$$\Omega = \Omega_{min} = \min \Omega_i$$

$$\Omega_i = (N_{pl,Rd,i}^d / N_{Ed,i}^d) = \min \Omega_{min}$$

- to achieve a global dissipative behaviour of the structure, ensuring uniform distribution of ductility along diagonal, Eurocode 8 (EC8) [22] stipulates that the maximum value of the overstrength should not exceed the minimum value by more than 25% (*homogeneity strength condition of dissipative members*).

$$\Omega_{max} / \Omega_{min} \leq 1.25$$

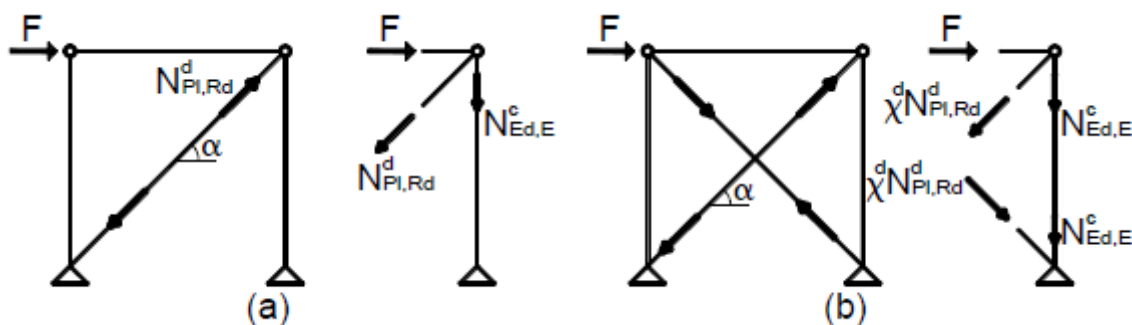


Figure 1. Calculation framework for bracings configurations: a) Tension only b) Tension / Compression

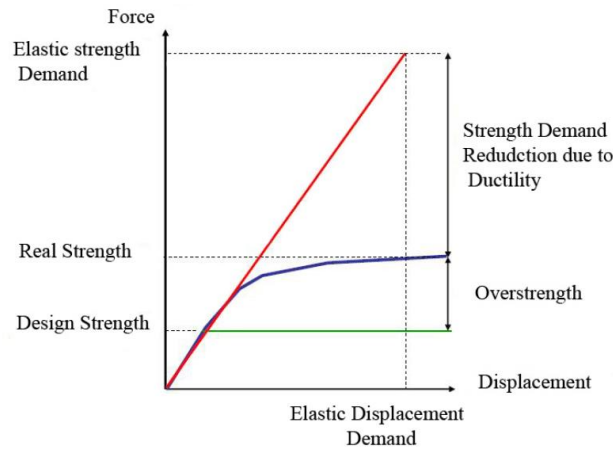


Figure 2. Design values scheme

During plastic behavior is reasonable to assume that compression diagonals have all reached the condition of instability and therefore, according to standards prescriptions, is correct to disregard their resistance. On the contrary, in the phase of elastic behavior, compression diagonals influence the global behavior of the structure in terms of frequency and vibration modes, hence the definition of seismic design actions (Figure 2).

1.2. MEAKADO PROJECT

Cost of a detailed structural design required to ensure high levels of ductility in seismic-resistant steel buildings is difficult to justify economically in low and moderate seismic risk geographical areas. EC8 provides seismic design rules based on strength, without any requirements for ductility, in case of braced frames designed in low ductility class and low dissipative structural behavior; it assigns a behavior factor between 1.5 and 2. The resistance estimation of the structural elements must be done following EC3 requirements. Despite the popularity of these low dissipative systems, their global behavior and their inelastic performance is not completely investigated. Indeed, experimental research projects of recent years have all been performed in order to analyze the behavior of structures designed for high seismicity areas. The research project promoted by "EU - European Research Fund for Coal and Steel referred to as" "MEAKADO", whose objective is to thoroughly investigate the behavior of structures designed for low areas and/or moderate seismicity. The results obtained will help to improve the current guidelines provided by EC8 thus developing specific design methodologies for these kinds of structures, ensuring an adequate level of reliability and cost effectiveness of the project.

1.3. Thesis objectives

The present thesis analyzes the experimental study of a real-scale concentrically steel braced frame arranged to X with low dissipative behavior, designed according to current dell'EC3 provisions. The experimental study deals with quasi-static cyclic tests conducted by imposing increasing amplitude drift cycles to a real scale braced frame. L-profiles are coupled together by means of bolted steel stitches for constituting bracings.

Main aim of the test is to investigate, limited to the profiles used, the hysteretic behavior of the diagonal elements, by placing greater focus on:

- evaluation and analysis of buckling axial load in compression diagonal;
- contribution provided by compression diagonal to lateral stiffness of the frame;

- provision given by elements of base structure (beams, columns and beam-to-column connection components) to global behaviour of the frame.

CBFs are strong, stiff and ductile, making them ideal for seismic framing systems. The inelastic behaviour of the brace provides most of the ductility, but in order to fully utilize the frame, the connections and framing members must also be taken into account. Therefore, it was important to consider not only the performance of the brace when designing, but also the ability for the connections and the framing members to withstand the strength and deformation demands transferred from the brace during cyclic loading. Through these considerations, a maximum amount of energy can be dispersed before the system fails.

A number of ductile detailing requirements are applicable to CBF design. The current procedure is generally rational, but recent research demonstrates increased inelastic deformation capacity may be developed with some modifications to the connection design; these potential modifications are discussed later in this document.

As summarized by Hines et al. (2009), collapse performance of CBF systems that possess limited ductility appears to be impacted less by a system's strength than by its reserve capacity. It is therefore proposed to reconsider the design of braced frames in low and moderate seismic regions as moderate-ductility dual systems.

2. State of the Art

Inelastic response of a concentrically X-braced frame under seismic loads, is mainly connected to hysteretic behaviour of diagonal bracings. A perfect knowledge about bracings behaviour under cyclic axial loads, is fundament to improve design and modelling of a braced frame. Graph of *Figure 3* is representative of the cyclic behaviour of axially loaded rod, in which P_y is the plastic strength of the rod under tension, while δ_y is the correspondent plastic deformation. Otherwise behaviour under compression results strongly non-linear, due to buckling phenomena.

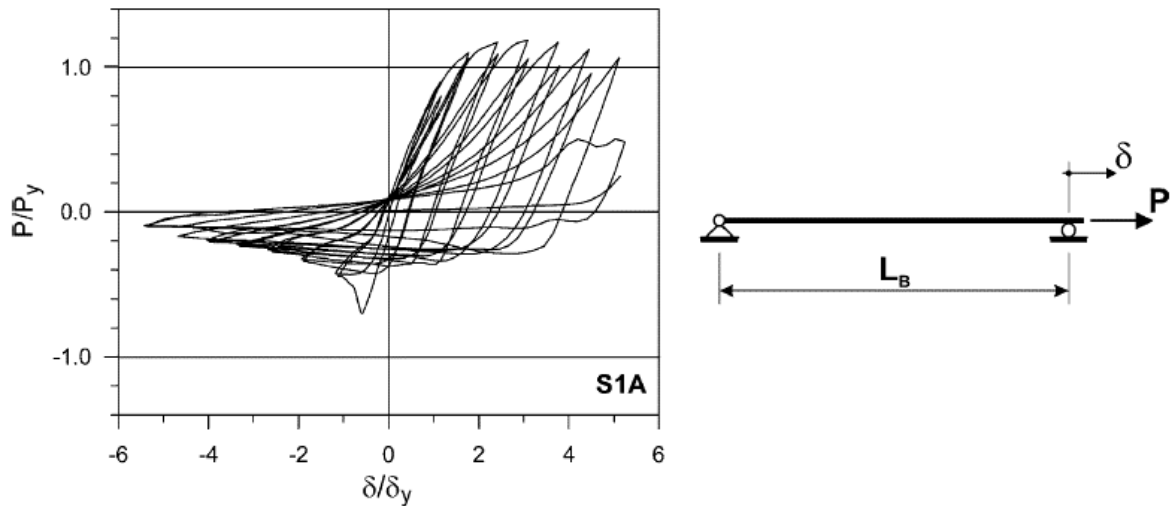


Figure 3. Force-displacement cycles of a rod axially loaded to symmetrical loading history

Graph of *Figure 4* represents the typical cyclic behaviour of a concentrically braced frame undergone incremental horizontal displacement.

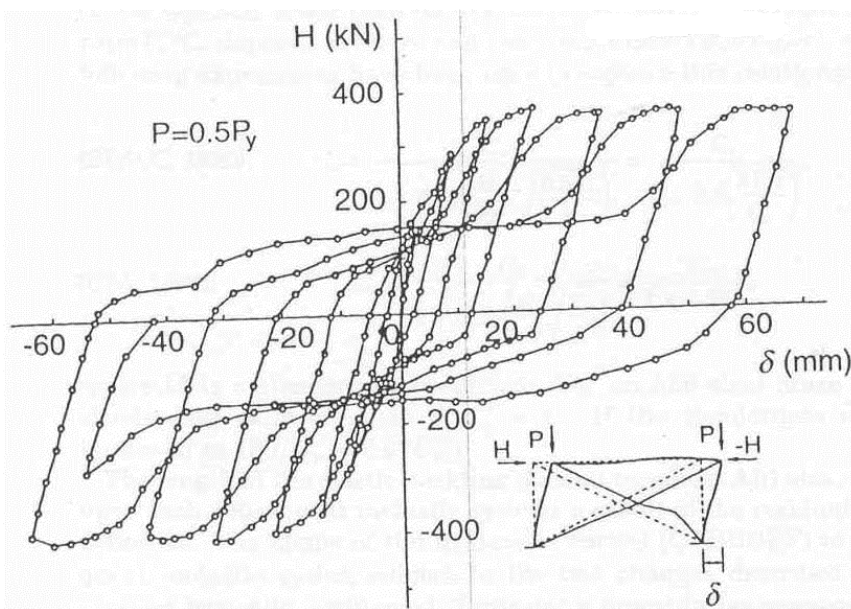


Figure 4. Force-displacement cycles of a braced frame

Assuming that main structural members remain in the elastic field, the behaviour of the braced frame could be summarized in three main phases:

1. phase 1 in which no buckling phenomena of compression diagonal occurred: braced frame behaviour is elastic and load reversal bring the entire structure to recover its initial undeformed situation;
2. phase 2 in which instability occurred in compression diagonal while the one under tension behaves again elastically: in this range a global strength and lateral stiffness reduction appear;
3. phase 3 in which yielding of tension diagonal occurred: additional lateral stiffness reduction could be observed. Strength of diagonal is also reduced for both stresses phases of compression and tension.

2.1. Experimental researches about hysteretic behaviour of concentrically bracings

Steel Concentrically Braced Frames (CBFs) have been used for years in steel construction and therefore have been studied for seismic performance (Inoue *et al*, 1978, Wakabayashi *et al*, 1980, Lee *et al*. 2005). These studies have produced guidelines for brace element and connection design to give a desired capacity under seismic events. Results of these studies implemented in codes in form of defining overstrength and response modification factors.

Because of conceptual framework used in the current guidelines, the structure is designed using results from elastic analysis; so a great number of these experimental studies were performed within the elastic range. Cyclic testing of conventional braced frames shows that these braces buckle in compression and yield in tension. Plastic hinges occur after the brace has buckled and the stiffness and resistance of the frame decreases.

Shaishmelashvili and Edisherashvili (1973) have conducted an experimental study on dynamic characteristics of large-scale models of multi-story steel frame building with different vertical bracings. They have tested some large-scale models of a 9-story building with 12 different bracing schemes in free and forced (resonance) vibration states. In the performed tests only linear behaviour of the structure has been considered.

Suzuki *et al*. (Feb.1975) performed an experimental study on the elasto-plastic behaviour of tensile braced frames to obtain the restoring force characteristics of low-rise steel structures. Alternating horizontal force was applied at the second floor under a constant vertical load, paying attention to the behaviour of two columns subjected to varying axial forces. Test specimens consisted of one-story, one-bay frames with wide flange sections and braces of round steel bars. The relation between shear force and displacement in each column was investigated by numerical analysis. According to the results, the elasto-plastic behaviour of the two columns is obviously different; one is subjected to additional tensile force and the other to additional compressive force. From these results, it was found that the restoring force characteristics of braced frames are stable but that the hysteresis loops in each column become unstable because of the additional compressive force.

Main experimental and analytical studies performed last 30 years about cyclic loads, have highlighted the relation between the dissipative capacity of diagonals and three major parameters:

- slenderness ratio;
- constraints conditions at diagonals edges;
- transversal section of the element.

One of the first experimental studies on the inelastic cyclic behaviour of concentrically steel braced frames was performed in 1977 by *Wakabayashi, Nakamura and Yoshida* [5]. Samples were tested both in single diagonal configuration and cross-configuration. The test devices are designed so that external forces were absorbed only by braces. As illustrated in Figure 5, analysed diagonal elements was 50x50x6 mm H-cross section and steel plates were welded at their edges in order to compose the connection to test actuator by means of high strength bolts. In the cross-configuration, steel reinforcing plates are welded at intersection of diagonals. The tests have analysed braced meshes of increasing slenderness, respectively of 40, 80, and 120 with different weaker axis orientation of the cross section with respect to the plane of the frame. Tests with both monotonous and cyclic load with increasing amplitude of displacement, have been done. Up to a maximum amplitude equal to 4% of the height of the frame.

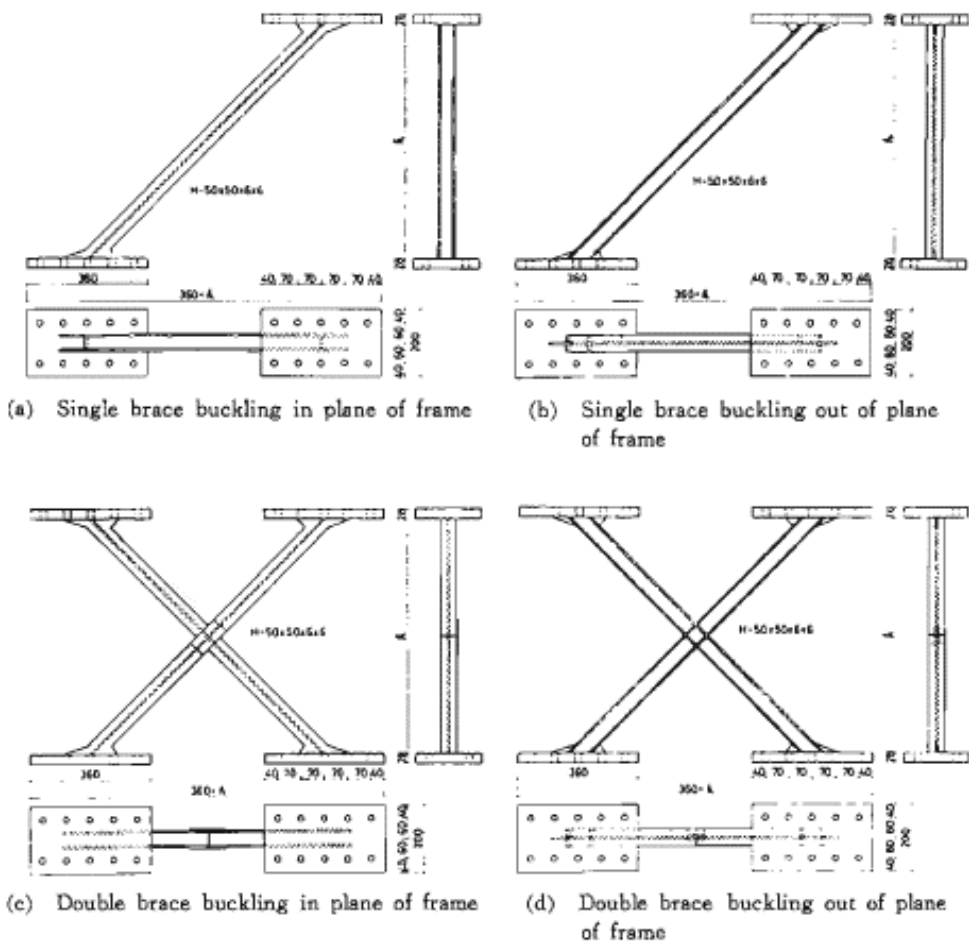


Figure 5. Tests specimens

Graphs of *Figure 6* and *Figure 7* report maximum values about bearing capacity q for any loading cycle applied, respectively for single and X-braced configuration. Maximum resistance undergoes a drastic reduction as loading cycles increase.

Besides, specimens with slender diagonals, (named SIC3, SOC3, DIC3 e DOC3) show a maximum resistance comparable to the value of yielding of tension diagonal during first loading cycle; specimens with squat diagonals (named SIC1, SOC1, DIC1, DOC1) have shown similar during initial loading cycle, a maximum resistance lower than the yielding stress of tension diagonal. Indeed, compression diagonal, tends to be arranged in straight rectilinear configuration to act as tense element as load is reversed: slender diagonal recover more quickly un-deformed shape than squat diagonal, since these latter oppose a greater resistance.

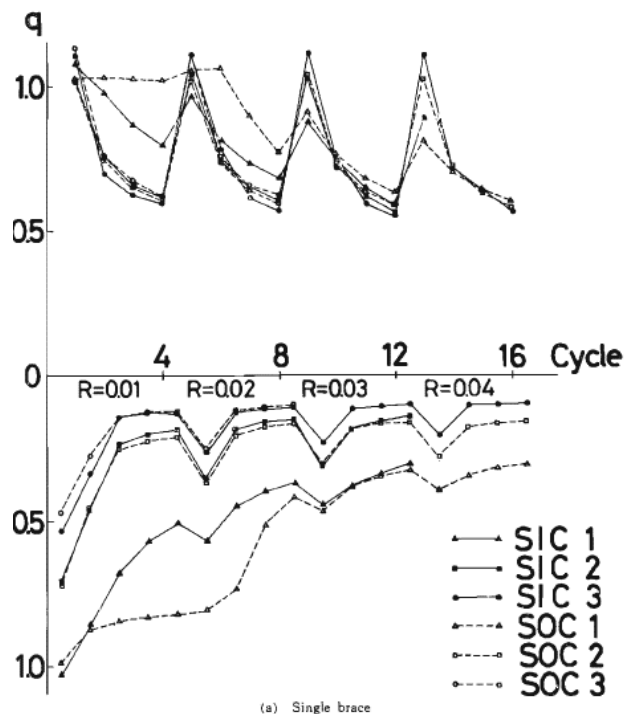


Figure 6. Maximum bearing capacity for each loading cycle. Single diagonal frame configuration.

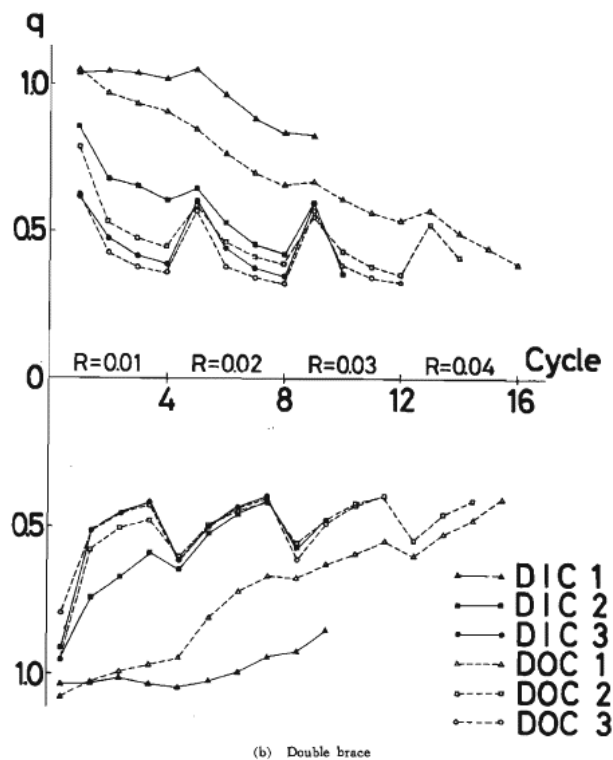


Figure 7. Maximum bearing capacity for each loading cycle. Cross-diagonal configuration frame.

Working out the experimental results obtained on a total of 24 samples it was possible to characterize the behavior of the two configurations analyzed.

The graph of *Figure 8* is representative of the force displacement cycle that characterizes the configurations with single diagonal from which it is possible to note a progressive reduction of the strength and stiffness in subsequent stages of loading and unloading to the first cycle; the overall shape of the cycle, however, remains unchanged. Analyzing the deformed configurations of these samples it was observed that the condition of buckling is manifested by the formation of plastic hinges at mid-span and at diagonal extreme edges.

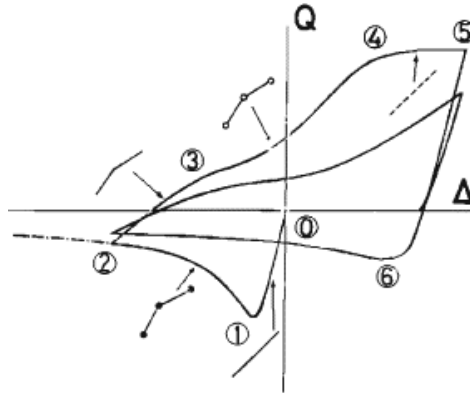


Figure 8. Cycle force-displacement for single diagonal specimens

Graph of *Figure 9* is instead representative of force displacement cycle that characterizes the diagonal meshes arranged to cross configuration in which it is possible to notice a sudden reduction of the stiffness in correspondence of point 3 caused by buckling of compression diagonal. Accumulation of plastic deformations in the diagonals causes a net loss of resistance in the cycles subsequent to the first. Unlike what was seen for specimens with single diagonal, it is possible to observe a change of the shape of the force-shift cycle loop to the vary of number and amplitude of loading cycles. The samples deformed configuration is symmetrical for first load cycles while becomes asymmetrical for the subsequent cycles due to the plastic deformations which occur in the diagonal segment between the joints ends and the mid-span: this experimental conclusion is shown pictured in *Figure 10*.

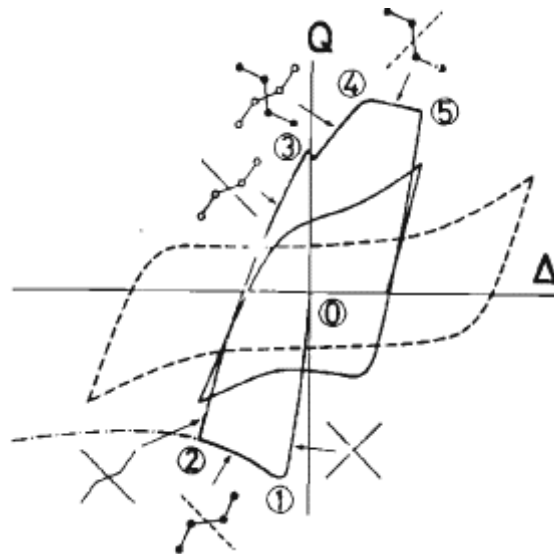


Figure 9. Force-displacement cycle of cross configuration braced specimens

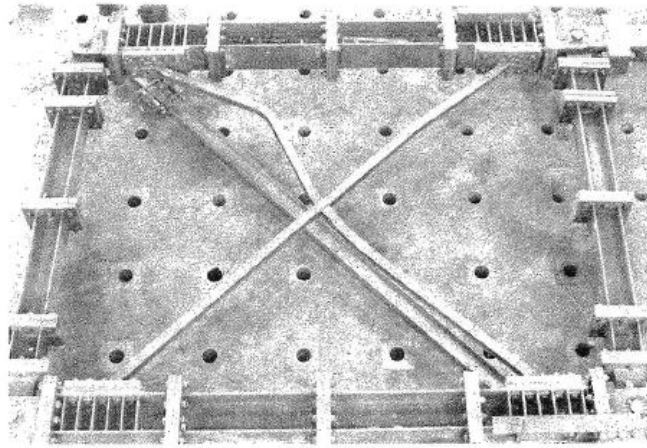


Figure 10. Asymmetrical deformed configuration

Additional situation highlighted by this experimental research is connected to energy adsorbed by specimens tested. Figure 11 shows trend of adimensional energy ζ absorbed by diagonals for each loading cycle. Conclusions follow by curves analysis:

- energy absorption decreases while loading cycles increase, starting from second cycle;
- stronger diagonals absorbed more energy than leaner (slender);
- elements with same slenderness show comparable levels of energy absorbed between them, regardless of the fact that the instability has occurred in or out of plane.

Also energy absorbed by considering as active only tension diagonal (slip model) has been plotted. Energy dissipated according to this model results lower than all other cases: this means energy absorbed by compression diagonals is anything but negligible.

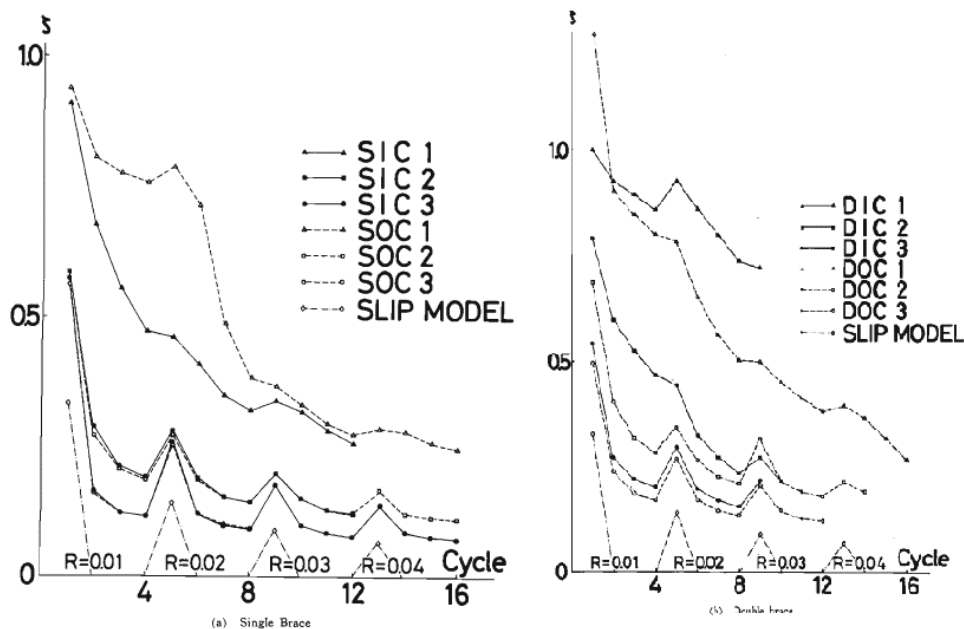


Figure 11. Adimensional energy absorbed for each loading cycle

During 1981 Popov e Black [6] have performed a study about the cyclic response of 24 elements composed by 6 different sections and variable slenderness values (40, 80, 120): experimental results

highlighted that buckling load resistance is strictly and directly connected to the slenderness of elements. Less slender components showed a lower resistance degradation comparing to those leaner.

Starting from 80s first research projects about numerical model calibration initiated. Procedure was performed according to results carried out by real scale experimental tests.

Ballio, Castiglioni e Perotti [7] [8] have studied the cyclic behaviour of axially loaded elements in order to evaluate performances of elements subjected seismic loads. Quasi-static cyclic tests have been performed on single storey frame with several bracings configurations: profiles coupled to L and C sections. The aim was to achieved enough data in order to calibrate the numerical model. *Figure 12* shows how the final model reproduced with good approximation the real behaviour of the frame.

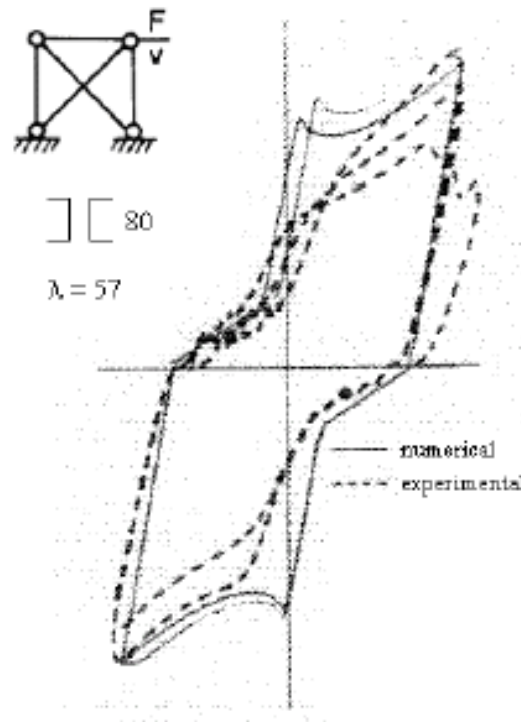


Figure 12. Comparison between numerical and real behaviour

Some of the performance issues that inhibit the use of CBFs are pinching of the hysteretic curve, “soft-storey” response, premature fracture of brace members at their central hinge location and beam or column fracture due to highly stiff gusset plate connection regions. The hysteretic response of a brace undergoing inelastic cycles of tension and compression is illustrated in *Figure 13a*. The unsymmetrical nature of the response curve of a single brace requires that braces must be used in pairs that are oriented in opposite directions. The resulting hysteretic curve for a symmetrical, two brace system is illustrated in *Figure 13b*.

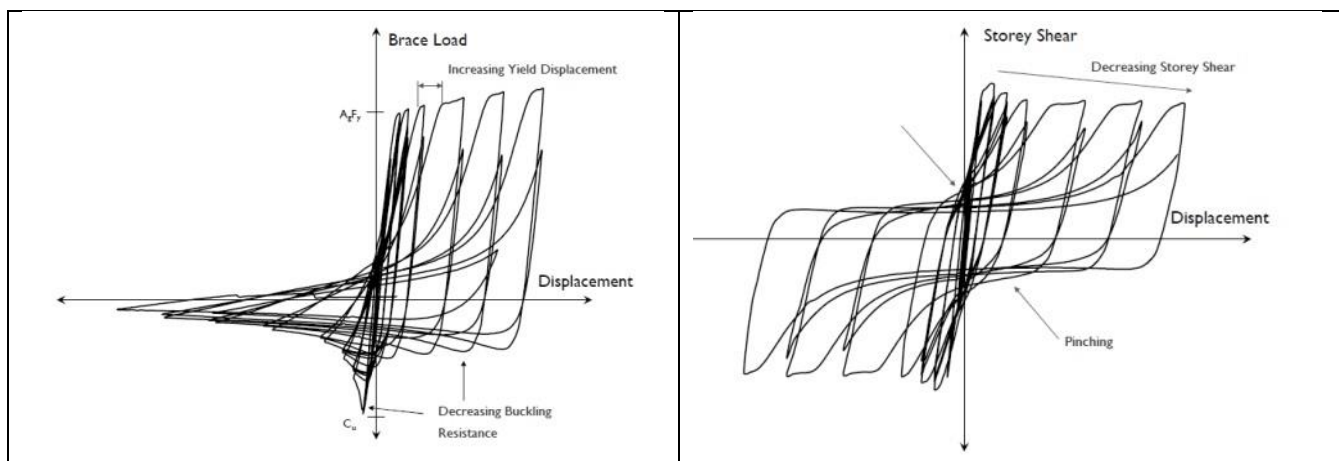


Figure 13. Hysteretic response of a brace undergoing inelastic cycles

After several cycles the plastic hinge region at the centre of the brace accumulates damage which results in a decreased buckling load. This leads to further pinching of the hysteresis and a reduction in the peak storey shear in each cycle. This phenomenon becomes more pronounced as brace slenderness is increased (Tremblay, 2001). Seismic performance of a lateral force resisting system is often measured by the energy dissipated (the area under the hysteretic curve). Concentrically braced frames have limited ability to dissipate energy due to their pinched hysteretic response. A lack of energy dissipation means that CBFs can exhibit relatively large lateral displacements and risk collapse during long duration, strong motion shaking (Whittaker et al., 1991). Designers can enhance the energy dissipation of a CBF by selecting members that have high compressive resistances relative to their cross-sectional area.

Shademan (2005) analytically studied the effects of different X-braced steel frames and their effects on the structural performance using pushover analysis. It was concluded that different bracing scheme configuration can have significant effect on overall structural performance.

In 2013 *Metelli, Bregogli e Marchina* [9] have presented a report at “XV Convegno ANIDIS” about an experimental study about the hysteretic behaviour of concentrically bracings composed by flat plates. Welded diagonal as well bolted joints solutions have been investigated. *Figure 14* shows the construction detail of the tested configurations.

Sample was subjected to 50 increasing amplitude displacement cycles until a maximum drift equal to 4.6% of its height; the experimental study has shown the correctness of the theoretical predictions on buckling lengths, whose values are lower than those normally used in the calculations of professional practice, which considers an overestimate of the slenderness due to safety issues. Results also allowed to validate a numerical model for the analysis of plastic buckling and the hysteretic behavior of the braces, which could be a simple tool for the evaluation of the dynamic behavior of nonlinear multi-storey buildings made with Concentrically braced frames.

Experimental studies showed the design features that affect the cyclic behavior of the braces. Attention has been focused towards diagonal elements which have the task of dissipating the seismic energy input by deforming plastically. The factor that most affects the cyclic response is the slenderness of the diagonals: it was observed that the slender elements have a lower dissipation capacity and a greater chance of suffering of local rupture phenomena at the points in which are formed the plastic hinges. Also the shape of the section resulted as one of the parameters that influences diagonal element performances in terms of energy dissipation and resistance. Anyway, the presented research has been conducted on frames designed for high seismic risk areas with the aim of maximizing the energy dissipation capacity of the diagonal elements and to avoid brittle collapse of the structure.

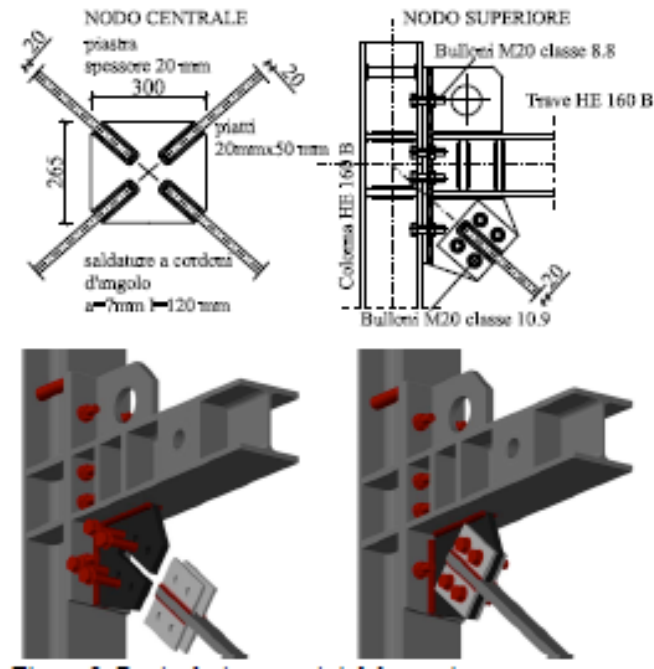


Figure 14. Construction detail of the tested specimen

Furthermore, other recent researches and analysis of steel frames in structures that experienced seismic damage is at the forefront of quantifying reserve strength in low-ductility steel frames (Tremblay et al., 1995; Davaran et al., 2014; Stoakes and Fahnestock, 2014). This evidence is the basis for the development of more cost-effective, low-ductility steel frames.

In 1995, analysis of numerous structures after the 1994 Northridge earthquake by Tremblay et al. highlighted specific failures in the steel frames. Among the types of failures observed were: weld fractures in the beam-to-column and flange connections, buckling of brace members, shearing of web bolts, and fracture joints in both welded and bolted flanges. Despite these failures, none of the structures had collapsed. The study recommended further research investigating collapse performance be performed to study how failure of certain members would affect failure of other non-structural members that may cause danger to people inside of the buildings (e.g. broken glass).

In a study performed at University of Illinois at Urbana-Champaign by Stoakes and Fahnestock in 2011, eight different beam-column connections were tested via a hydraulic actuator. The study was performed to better understand behavior of these connections under loads as it relates to the reserve capacity of a steel frame. In general, such connections are considered pin connections for simplicity of design and analysis, but this study proved that such connections have significant moment resistance and ductile properties.

In a study performed at École Polytechnique by Davaran et al. in 2014, six different steel brace connections were tested to examine their brace re-engagement behavior upon failure of the connection. The brace connections were loaded axially along the brace until brace reengagement was observed; the ultimate loading value was compared to the expected loading value based on brace configuration and steel thicknesses. The study showed that in all 6 tests, brace re-engagement resulted in re-development of compressive strength of the brace connection. The study also showed that re-engagement compressive strength is dependent upon the gusset plate buckling resistance. In cases where the connection failure was symmetrical, compression strength was increased by more than twice the

expected compressive strength in bearing; asymmetrical connection failures resulted in a slightly lower compressive strength upon reengagement. The study also concluded that controlled weld failure prior to gusset buckling can lead to a re-engagement compressive strength nearly 2.5 times that of the strength assumed from the brace re-engaging the gusset plate in bearing.

The previous studies performed by Tremblay et al., 1995, Davaran et al., 2014, and Stoakes and Fahnestock, 2011 all acknowledge that low-ductility steel braced frames have some inherent reserve capacity. The studies also recognize sources of such reserve capacity. Even though most of the studies have quantified the various sources of reserve capacity under certain controlled situations, none of them have applied the findings to an entire structural system in terms of feasibility in actual applications.

3. Design of test specimens

Design procedure of the experimental tests has been described in this chapter. In particular, detailed description of the structural elements of test frames have been provided, and list of test program have been presented. All the test specimens have been designed according to EC3 recommendations.

3.1. Introduction

Figure 15 shows the generic test sample which represents one floor of a concentrically X-braced multi-storey building, with dimensions corresponding to realistic sizes of a building frame, yet limited by testing facilities.

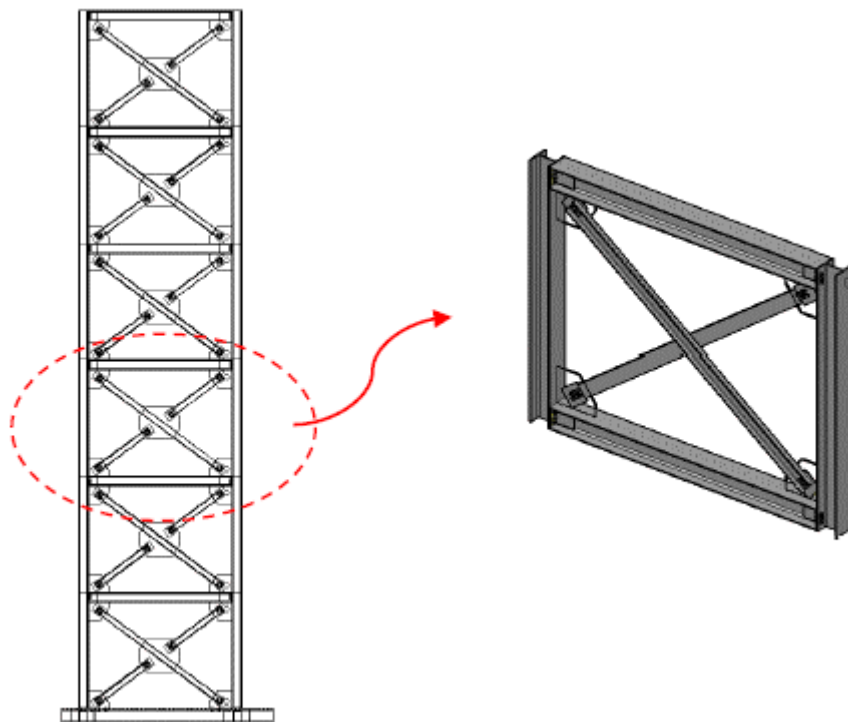


Figure 15. Generic scheme of the frame

Test program consists of 24 quasi-static cyclic tests of a frame of 1 level and 1 bay (2.60 m height and 4.30 length). This program permits investigating in detail the contribution of frame effect on global behaviour, and the contribution of compression diagonal, with several bracings profiles. 3 different double angle profiles have been used. The angles have been arranged back-to-back, essentially forming a tee section, by means of steel interconnectors.

The generic test sample consists of two distinct structural systems:

1. structure formed by the main members: beams, columns, and connecting elements between them;
2. bracing system composed of tension and compression diagonals, connected together in the middle by means of a steel plate.

Two beam-column joint solutions have been designed to connect the main members to the bracing system: bolted angular gusset plates in moment resisting frame (MRF) and hinged gusset plates in pinned frame (PF).

3.2. Experimental tests definition

The frame has been tested vertically connected to a counter frame. Hydraulic jack actuator applies the load to the upper beam through a bolted connected transfer beam. A displacement controlled loading protocol was used based on ECCS 45 recommendations. Tests have been performed in a quasi-static regime with application of a displacement amount at 0.4 mm/s.

Figure 16 shows the general configurations of tests that have been performed. Table 1 lists instead all tests performed in chronological sequence.

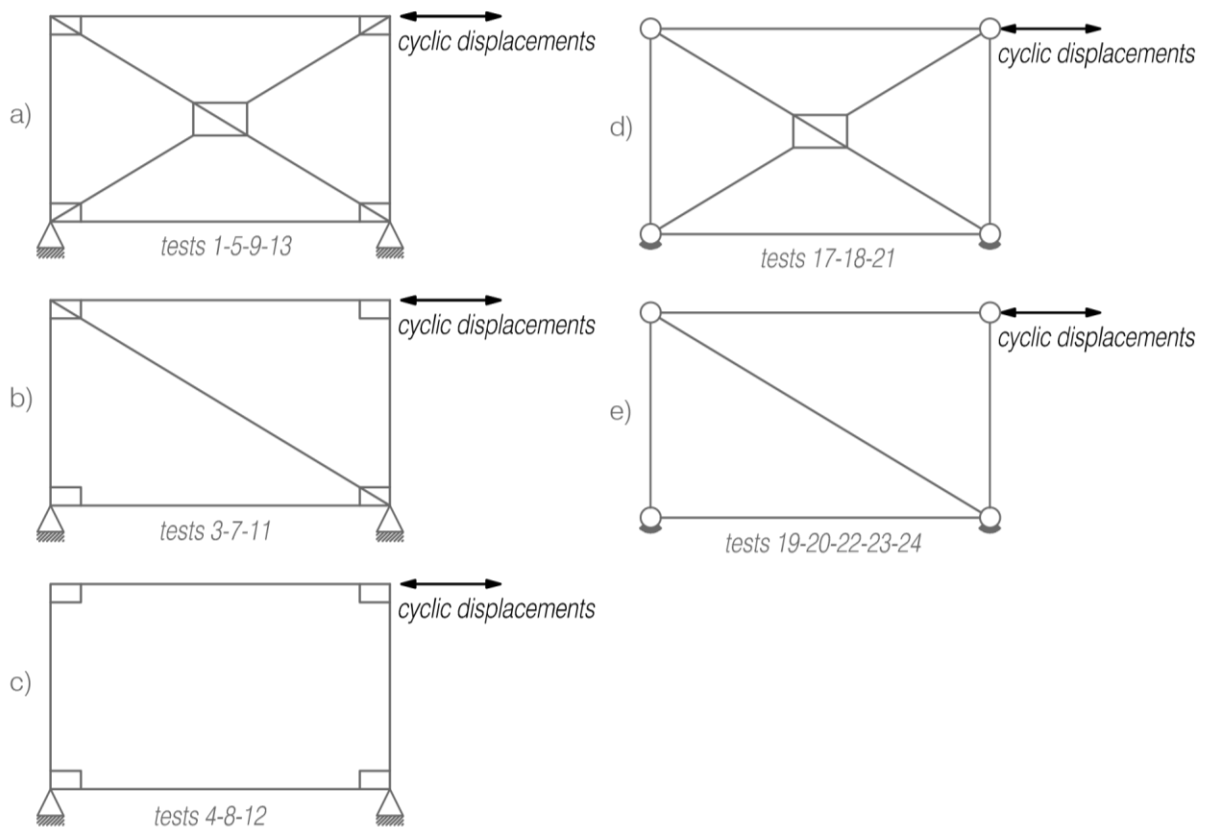


Figure 16. Frame configuration during the tests: a) Both active diagonals in MRF b) Only one active diagonal in MRF c) Only frame effect in MRF d) Both active diagonals in PF e) Only one active diagonal in PF

# Test	Profile	Conn.	Structure type	Notes
1	2L60x60x8	4M16	FRAME	X bracing no prestressed bolts
3	2L60x60x8	4M16	FRAME	Only tension diagonal
4			ONLY ANGULAR GUSSETS	
5	2L70x70x7	4M20	FRAME	X bracing
7	2L70x70x7	4M20	FRAME	Only tension diagonal
8			ONLY ANGULAR GUSSETS	
9	2L80x80x8	4M20	FRAME	X bracing
11	2L80x80x8	4M20	FRAME	Only tension diagonal
12			ONLY ANGULAR GUSSETS	
13	2L60x60x8	4M16	FRAME	X bracing with prestressed bolts
14			EMPTY	
15			NO GUSSET	
16			EMPTY NEW	
17	2L60x60x8	4M16	PINNED	X bracing
18	2L70x70x7	4M20	PINNED	X bracing
19	2L70x70x7	4M20	PINNED	Only tension diagonal
20	2L80x80x8	4M20	PINNED	Only tension diagonal
21	2L80x80x8	4M20	PINNED	X bracing
22	2L80x80x8	4M20	PINNED	Only tension diagonal
23	2L60x60x8	4M16	PINNED	Only tension diagonal
24	2L70x70x7	4M20	PINNED 50% PRESTRESSED BOLTS	Only tension diagonal

Table 1. Cyclic tests list.

**test 2,6,10 not shown in table: they refer to X configuration with continuous diagonal not bolted to mid-plate

3.2.1. Steel characterization

In order to evaluate mechanical properties of the steel used for main members, diagonals and connection elements, uni-axial tensile tests are carried out from rectangular specimens following the standards UNI EN 6892-1 and UNI EN 10002-1; tests are performed at “Laboratorio Prove e Materiali” of “Politecnico di Milano”. Table 2 reports the tests results. Figure 17 shows the rectangular specimens extracted from the bracings profiles. Complete account of tensile tests provided by the laboratory is reported on Appendix A.

Description	Steel used	Sample code	Sample dimension				f_y [MPa]	$f_{y,media}$ [MPa]	f_u [MPa]	$f_{u,media}$ [MPa]
			Initial length [mm]	Thickness [mm]	Width [mm]	Cross section [mm ²]				
Beam	S355JR	1B-1	90	13.38	19.97	267.2	374	374.67	549	547.00
		1B-2	90	13.55	19.92	269.9	375		544	
		1B-3	90	13.42	20.19	270.9	375		548	
Column ⁽¹⁾	S355JR	2C-1	50	$\phi = 10$ mm		78.5	357	362.00	561	559.33
		2C-2	50	$\phi = 10$ mm		78.5	344		535	
		2C-3	50	$\phi = 10$ mm		78.5	385		582	
Connection element of beam-column joint	S275JR	3L-1	80	10.3	19.86	204.6	363	364.67	491	489.67
		3L-2	80	10.32	20.57	212.3	368		492	
		3L-3	80	10.25	21.03	215.6	363		486	
Steel gusset plate	S275JR	8AB-1	100	16.16	21.33	344.7	385	387.33	513	517.00
		8AB-2	100	15.98	20.5	327.6	384		515	
		8AB-3	100	15.87	20.2	320.6	393		523	
Diagonal	S275JR	11A-1	70	7.92	20.16	159.7	339	349.00	462	462.33
		11A-2	70	7.94	20.01	158.9	366		457	
		11A-3	70	7.94	18.65	148.1	342		468	
		11B-1	70	6.98	19.83	138.4	341	336.33	482	478.67
		11B-2	70	7.03	20.65	145.2	328		475	
		11B-3	70	6.99	19.57	136.8	340		479	
		11C-1	70	7.9	20.23	159.8	337	346.67	464	465.00
		11C-2	70	7.96	20.27	161.3	343		471	
		11C-3	70	8.06	19.63	158.2	340		460	

(1) Tensile tests on cylindric sample

Table 2. Mechanical characteristics of the used steel



Figure 17. Samples extracted from angular profiles of the braces for tensile tests

3.3. Design Procedure

Two specimens were designed using concentric braces. This chapter reports and describes their configurations. Boundary frames dimensions have been selected to be representative of bay dimensions for frames located into a test-bed structure. The boundary frame with an aspect ratio (L/h) of 1.65 is taken from multi-storey building system where L and h are the bay width and the height of the specimen respectively. The actual scale of the boundary frame is 1:1 of the prototype adapting it to limitations of the testing apparatus.

Figure 18 shows conceptual scheme of both frames. MRF has an height of 2.60 m and a length of 4.30 m, dimensions evaluated in correspondence of the beams and columns centroid axes. The inter-storey is different from values of constructive practical: the choice has been constrained by dimensions of the contrast bench frame used for experimental tests. Components such as beams and columns have been designed conservatively with the intention of reusing the frame.

PF structure was developed from previous research performed by prof. Perotti, and reviewed by an advisory panel. Columns and column base plates were present, while bracings connection joints and upper beam have been designed. The dimensions of the frame, referred to the beams-columns centroid axes are equal to moment resisting frame: 4.30 m per 2.60m.

Diagonal elements are inclined by an angle $\vartheta=30^\circ$ with respect of the horizontal axis and they have a length of 5.00 m. Because of operational issues, the diagonal elements idealization is done tracing the axes passing through the centroid of the diagonal boltings. If the gravity axes are not concentric, the resulting couples must be considered in design of the members.

All beams and columns dimensions as well as connection angles were same for all specimens to specimen to allow a more uniform comparison of the strength, stiffness and seismic energy dissipation capacity of several proposed retrofit designs.

This simplified scheme has been the starting point for real frame design, through the following steps:

1. main frame members definition through the choice of beams and columns profiles and connecting elements in correspondence of beam-column joint;
2. specific design of columns base joints that is able to allow rotation;
3. choice of the profiles to adopt as bracing system, in relation to the guidelines defined by the research project MEAKADO;
4. bracing connecting elements definition, especially:
 - a. design of a specific modular system for the connection of the diagonal elements to the main members;
 - b. design of steel mid-plate for the mutual connection of the two diagonals in correspondence of the centre of the frame;

The entire structure has been sized according to EC3 actual version prescriptions; in the context of this report are reported only the main design actions about the diagonal elements in relation to:

- bearing capacity of tension diagonal element;
- compressed diagonal resistance and stability;
- shear bearing capacity of the bolting consisting of diagonal and connecting tissue to main members;
- *block tearing* resistance.

The constructive elements adopted are described in the following paragraphs. At the end of the design phase, construction drawings and definition of the constructive details have been produced. the documentation has been reported in the APPENDIX B.

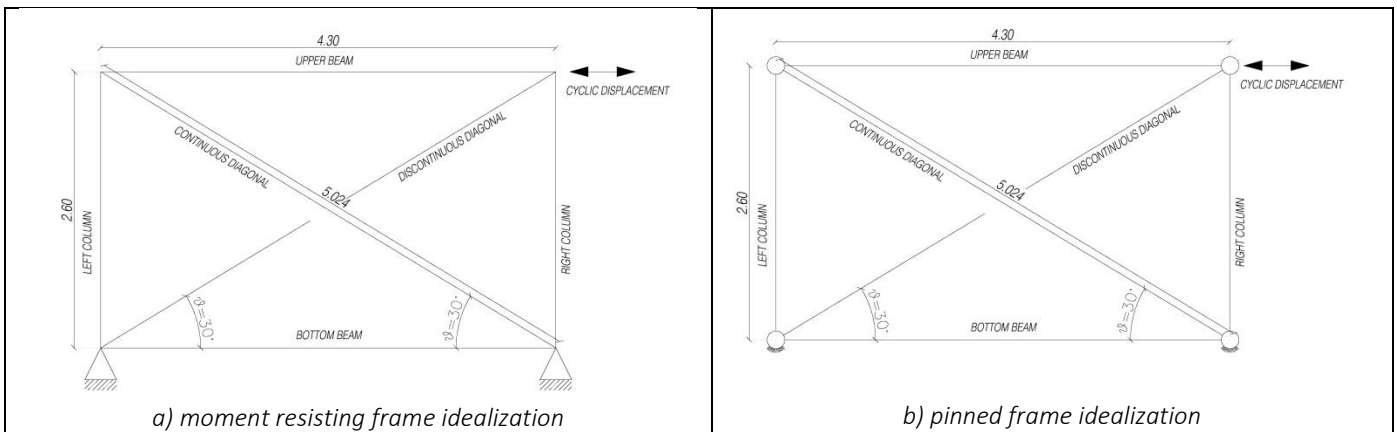


Figure 18. Conceptual scheme of a) MRF and b) PF (measures in meters)

3.3.1. Model of Pendulum Frame

The generic structure needs a first modelling phase in which it has been done a geometric-mechanical idealization of the connections between different structural parts that aren't exactly coincident with real parts. The structural scheme of the *pendulum frame* has been used. Beam-column joints have been outlined as hinges so that to provide relative rotation between the elements without transmitting bending moment [10]. *Figure 19* shows the assumed conceptual scheme of a pinned structure. It is able to bear vertical loads, but it results unstable in respect to horizontal actions, such as seismic load, wind load, or actions related to geometrical imperfection (2^{nd} order effect). A bracing system has been added in order to transfer horizontal loads to foundation, eliminating the lability of standing elements of the structure.

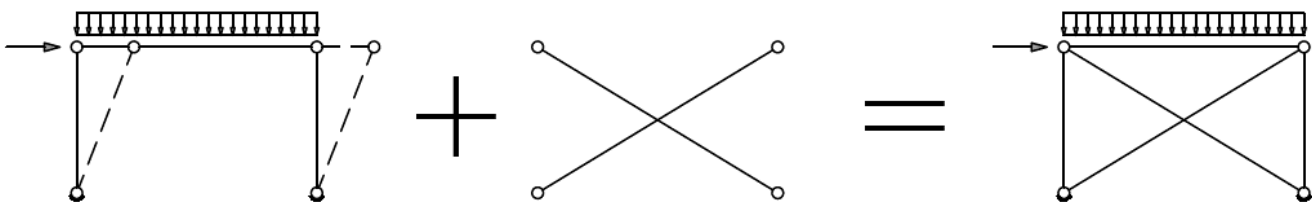


Figure 19. Braced pendulum frame

No-correspondence between axes of the numerical model and centroid axes in the real structure requires a careful regard in modelling the hinged diagonals elements. I.e., in the numerical model hinges are placed at the intersection of geometric axes, while in the real case, they have a different position, due to the presence of angular connection profiles. [11]. EC3 allows to size steel bracings through two different methodologies:

- both tension and compression diagonal have to be considered as resistant: in this case it has to be verified mainly the compressed element due to the buckling risk;
- only the tense bracing has to be considered as resistant, leaving out the static contribution of the compression diagonal.

X-shaped connecting rods work as truss in both the approaches, carrying only axial loads.

3.3.2. Bolts

The connection system screw-nut-washer is high resisting steel with controlled tightening as indicated by norm EN 14399 – 4 (HV system). In particular, an hexagonal partial threaded bolt class of resistance 10.9 with ultimate breaking strength of 1000 MPa; an hexagonal nut class of resistance 10.9 and a double washer: one under the bolt head and the other next to the nut. The typology of bolts used are reported:

- M20 and M22 prestressed bolts for diagonal-gusset plate connection;
- M20 non-prestressed bolts for interconnections between the bracings angle profiles;
- M24 non-prestressed bolts for beam-column connection joint and for corner gusset plates;
- M27 non-prestressed bolts for the connection of base plate to the fixed beam of test bench.

3.3.3. Main elements of the frame

Figure 20 shows in detail the MRF, designed in order to remain in the elastic field up to the maximum push load driven by the load cell. Main members are constituted by an upper and a bottom beams sections HE 300 A with a span of 4.00 m. The two columns are HE 300 B with an height of 3.00 m. Steel used for these profiles is S355JR. The total frame dimensions are 4.60 m per 3.10 m. Main members are assembled so that beams and columns geometric axes overlap with the pendulum frame simplified scheme. Angular gusset plates have been designed in correspondence of beam-column joints,. They are bolted both to the beam that to the column flange, so to form a semi-rigid connection.

Figure 21 represents the PF scheme. The upper beam is RHS 250x150x10 cross-section with a span of 3.98 m. The two columns are HE 200 A profile with an height of 3.00 m: the steel used is S355JR. The system has been then settled directly to the fixed beam of the test bench. The overall frame dimensions are the same of the moment resisting frame if we refer at centroid axes. The beams and columns geometric axes overlap with the frame simplified scheme. Bolted steel plates are designed for node connections of the pinned frame. Table 3 reports the geometrical properties of the profiles.

Structural Element	Cross section profile	MAIN MEMBERS: geometrical properties of the section												
		h	b	a	e	r	Area	Linear Mass	Axis x-x			Axis y-y		
		[m]	[mm]	[mm]	[mm]	[mm]	[cm ²]	[kg/m]	J _x	W _x	i _x	J _y	W _y	i _y
								[cm ⁴]	[cm ³]	[cm]	[cm ⁴]	[cm ³]	[cm]	
beam	HE 300 A	290	300	8.5	14	27	112.5	88.3	18263	1260	12.7	6310	421	7.49
column	HE 300 B	300	300	11	19	27	149.1	117	25166	1680	13	8563	571	7.58
beam	RHS 250x150x10	250	150	10	10	15	74.5	58.5	6092	487	9.04	2723	363	6.0
column	HE 200 A	190	200	6,5	10	18	58.83	42.3	3692	388.6	8.28	1326	133.6	4.98

Table 3. Profiles geometrical properties of the MRF and PF main members

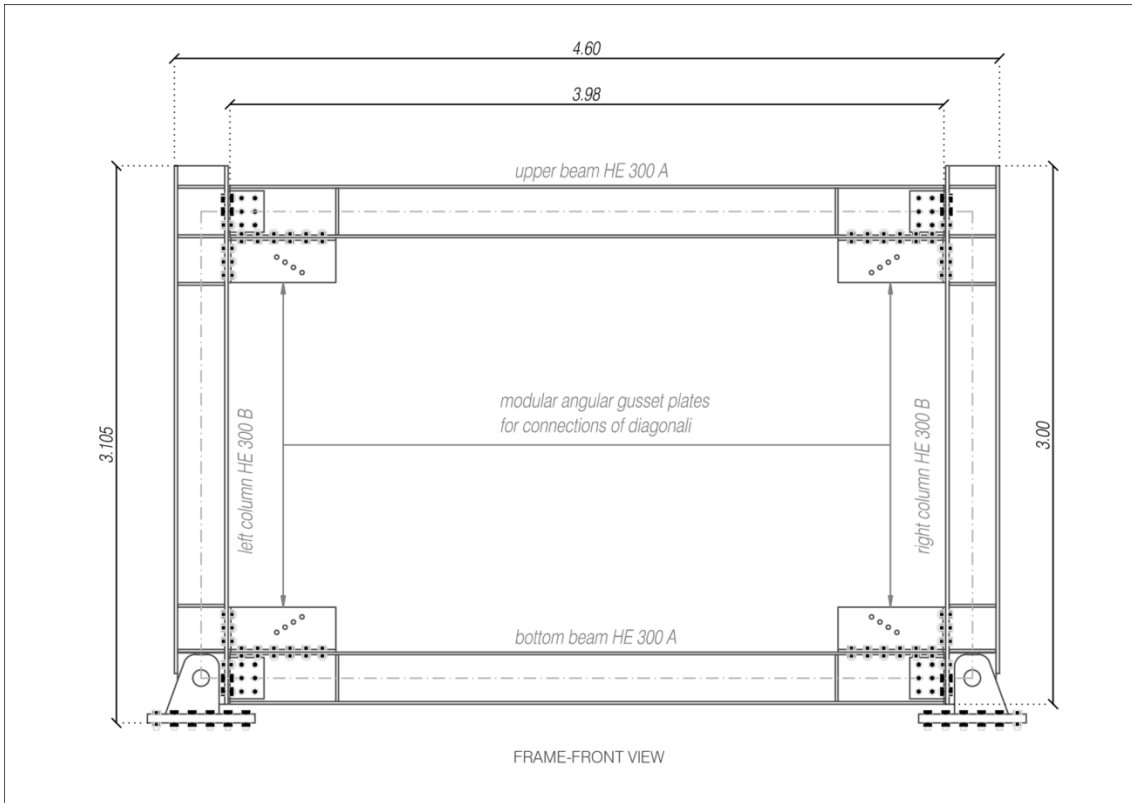


Figure 20. Front view of MRF (measures in meters)

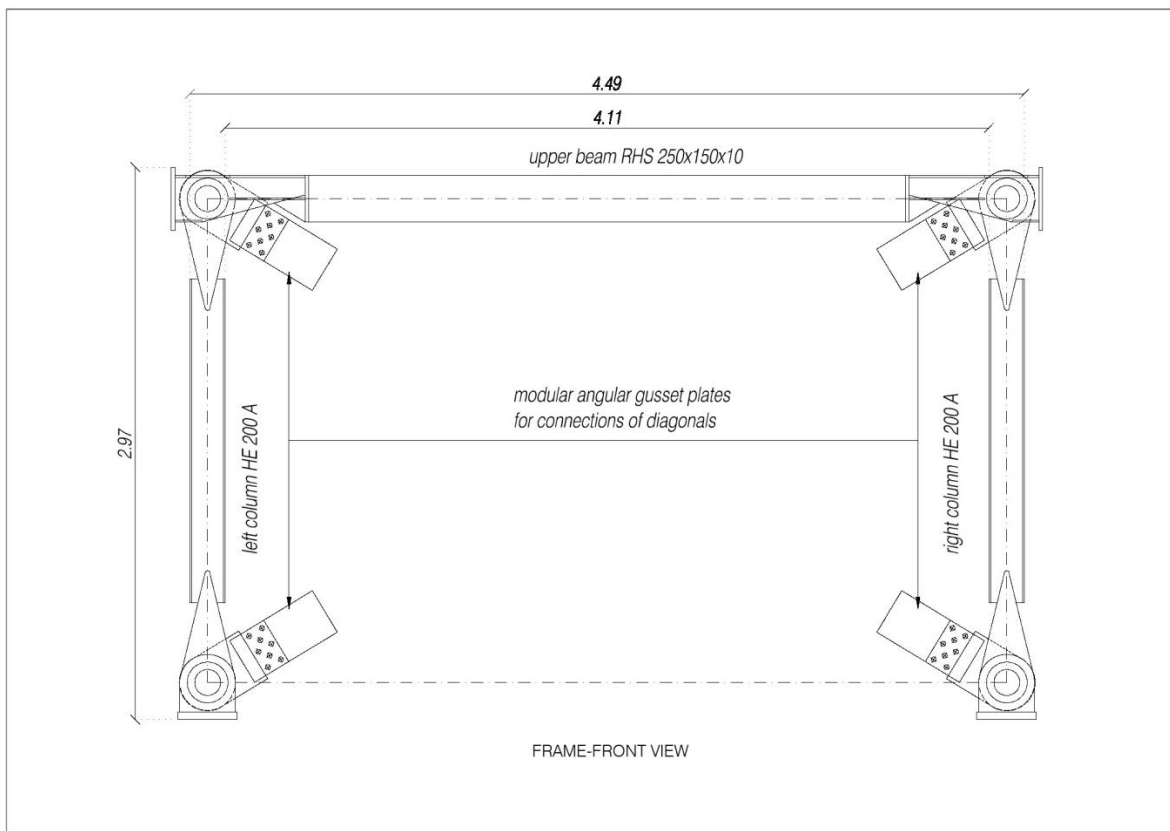


Figure 21. Front view of PF (measures in meters)

3.3.3.1. Beam-to-column joints

Beam-column connection has been designed using steel double web angle bolted both to the column flange that to the beam web. The girder is connected to the column through a shear plate connection. Bolts are $\Phi 24$ mm non pre-stressed class of resistance 10.9. The plate has been designed and checked for the limit states of shear rupture, shear yielding, block shear and bearing strength at the bolt holes. This connection is characterized by a suitable rotational capacity and a low flexural bearing capacity, so that to reproduce the ideal behaviour of the hinge constraint, yet supposed in the pendulum frame scheme [10]. Additional large gusset plates reduce the effective brace length and make the brace buckling profile more severe.

Stiffening plates have been placed in the column web ends aligned to the beam flanges, in order to avoid preferential areas of possible weakness in the connection. The plates are welded to columns through double angular weldings of 4 mm. Additional steel plates with a section of 10 mm are welded on the beam web edges, under the beam-column shear connection so that to increase the resisting section of the beam web. *Figure 22* shows the realized joint meanwhile the *Figure 23* shows the constructive details of the connection.

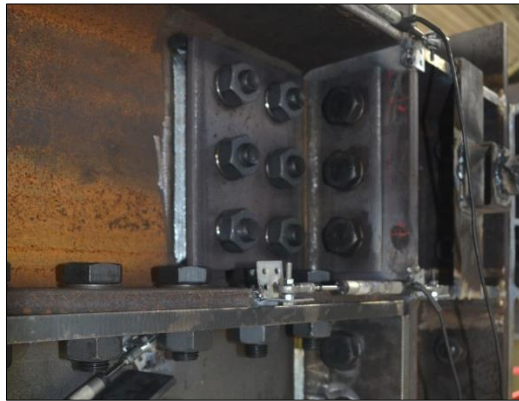


Figure 22. Beam-column joint in MRF

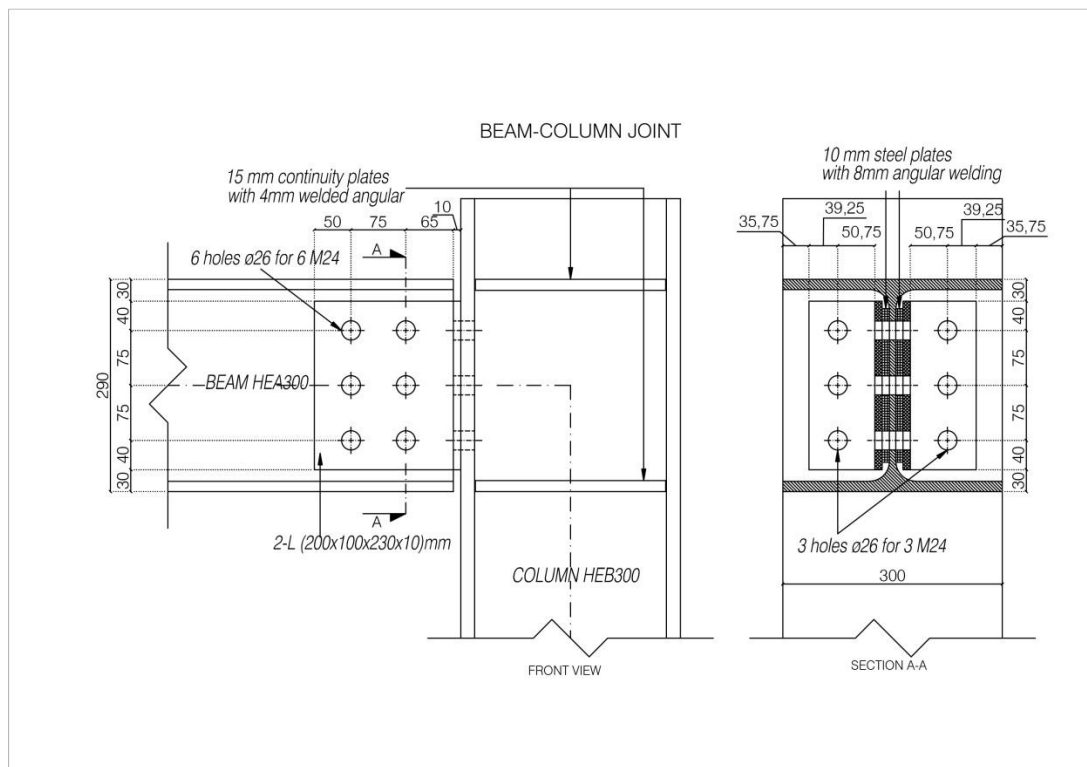


Figure 23. Construction details of beam-column connection (measures in mm)

Pinned frame has been designed providing simple beam-column connection in order to realize a joint which is assumed no moment transmitting. The purpose is to realize the ideal constraint behaviour of the hinge. Although some friction still remain at surfaces interface.

Beam, columns, and the steel plates for the diagonal connection, are designed in such a way to fit one each other in correspondence of the nodes. The elements are then kept together by a pin, a steel cylinder with diameter $\Phi 140$ mm that passes through each member and allow the node to rotate. *Figure 24* shows in detail the hinged joint.

Additional steel plates with a section of 10 mm are welded on the beam ends, for increasing the rigidity in its connection at node. Section of the beam decreases coming near the node in order to allocate the gusset plate on which is fixed the bracing and let it rotate. *Figure 25* represents the constructive details of the connection.



Figure 24. Beam-column joint in PF

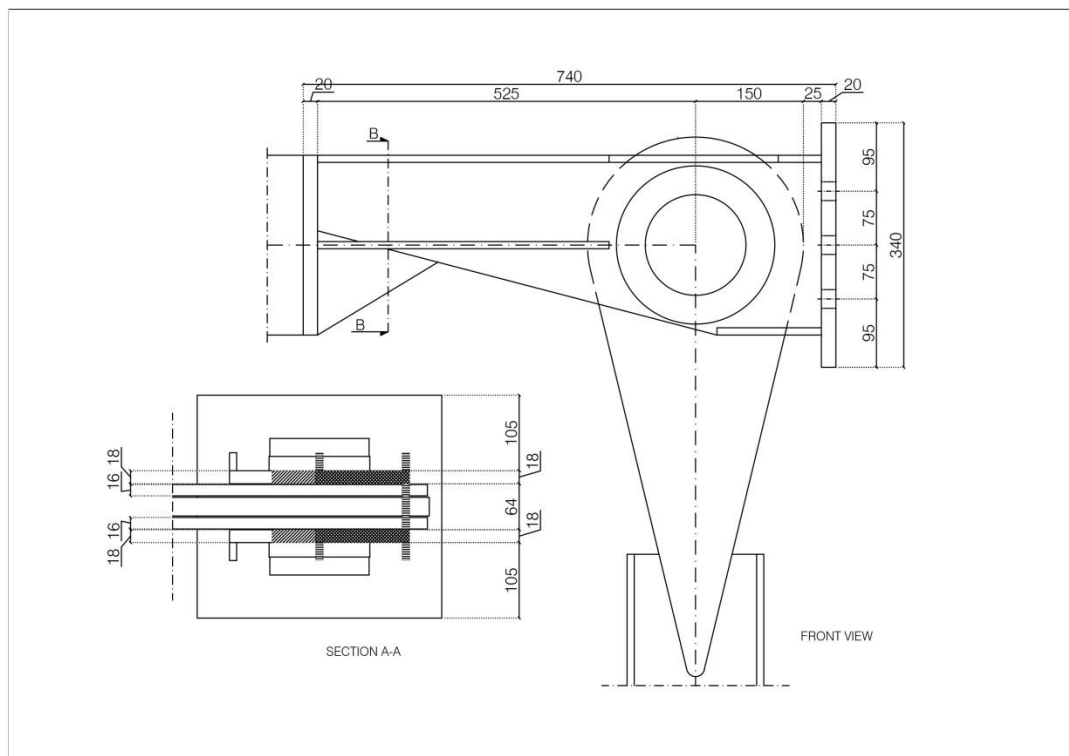


Figure 25. Construction details of beam-column connection (measures in mm)

3.3.3.2. Pinned base connection of the column

A pinned base has been designed at column end in order to create the hinge constraint. *Figure 26* shows its real configuration and the construction details. This type of connection is formed by two mounting plates continuous penetration welded to a flat base and drilled to accommodate the pin; an equal drilled hole is also present at the end of the column web to allow insertion of the pin and realize the kinematic expected. The pivot pin is connected to the fixed test beam by means of a set of 12 bolts, 30mm diameter and class of resistance 10.9. The pin is 90 mm diameter realized with S355JR steel, and it is sized so as to withstand the maximum shear force generated by the traction of the diagonal elements and support the self-weight of the frame. Pin has been treated with special substances in order to decrease the friction effect at the interface between surfaces; an appropriate safety device has been designed to prevent any sliding of the pin in z-axis.



Figure 26. Pinned base plate in MRF

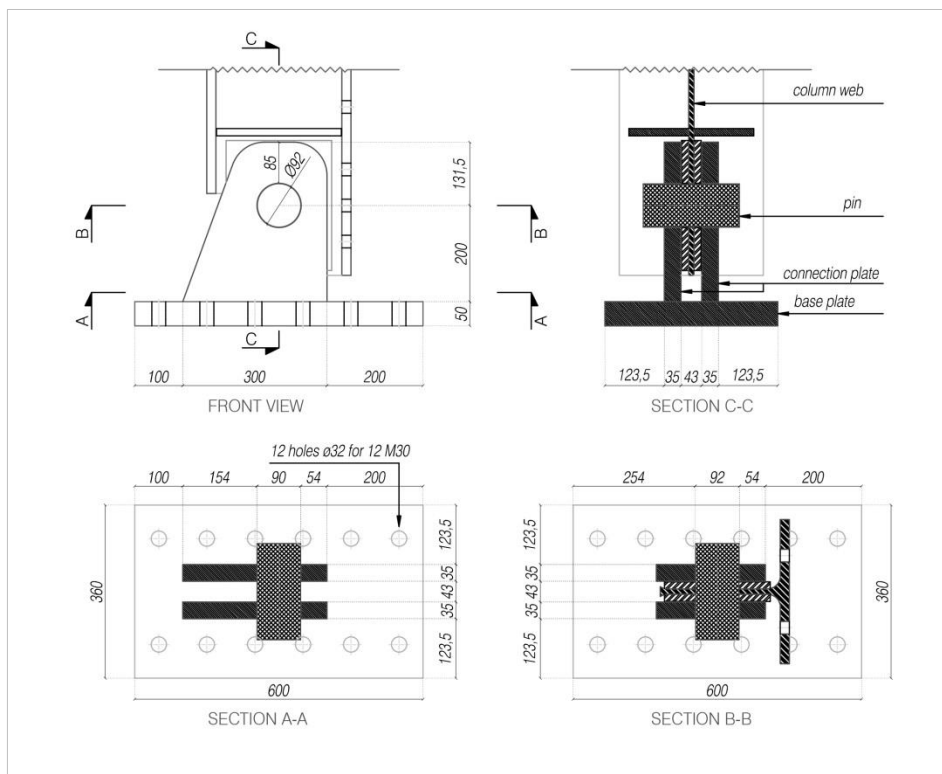


Figure 27. Detail of pinned base plate in MRF

The base plate connection of the PF has not been designed. It has been taken from an existing frame, previously designed and tested for a project of prof. Perotti. Base plate is similar to the one used in MRF. The detailing is the only think that changes. Wence the frame has been adapted to the existing base plate. The element is composed by a 40 mm thickness horizontal steel plate in which two steel vertical plates are fully penetration welded. These latters have a $\Phi 140$ cm hole for accommodating the cylindrical pin. Base plates have been fixed to the bench beam by a set of 6 threaded rods closed by means of pre-stressed nuts, in order to avoid as much as possible the base sliding. A steel plate 50 mm thickness has been added to raise the frame for reaching same height of jack attack of the MRF. It is placed in between the base plate and the bench anchor beam.

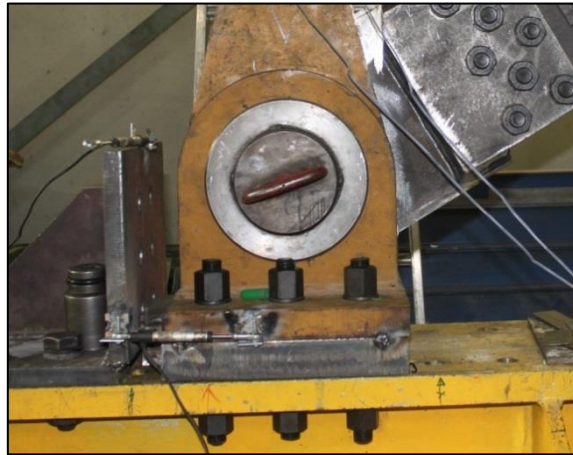


Figure 28. Construction details of pinned base plate in PF

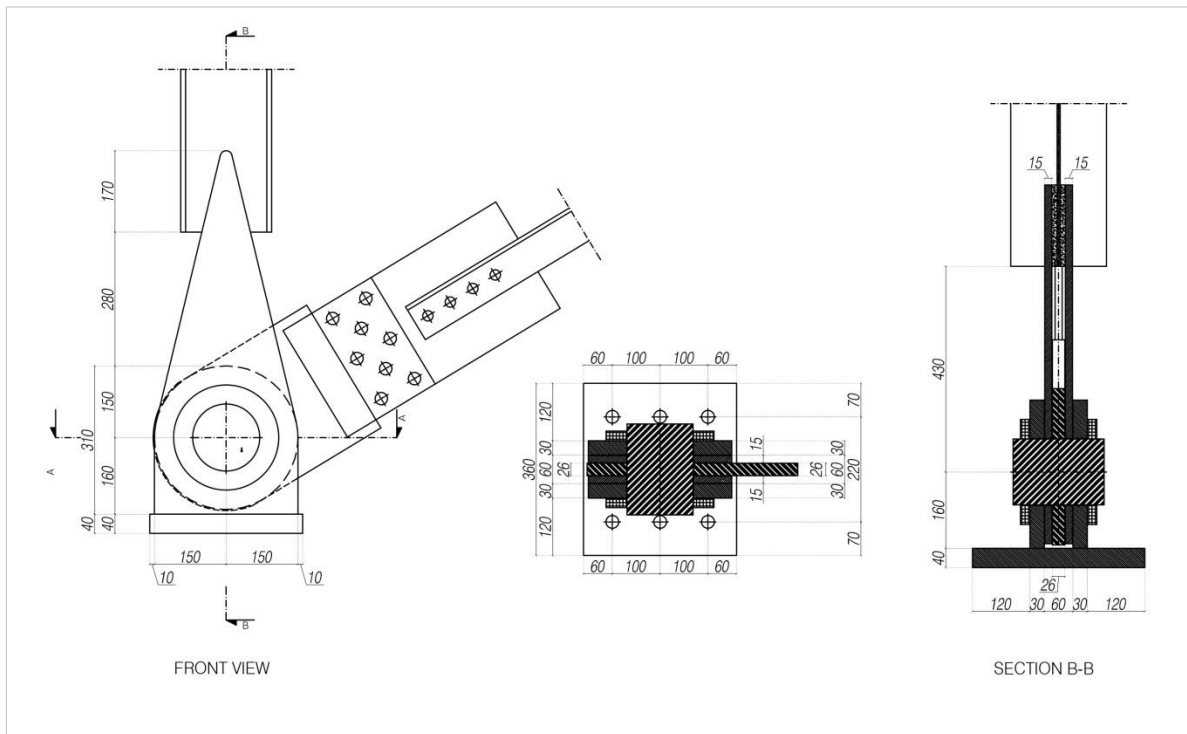


Figure 29. Detail of pinned base plate in MRF

3.4. Bracing system

Relative bracing system has been adopted. *Figure 30* and *Figure 31* show configurations of the frames. The cross bracing system is composed by a discontinuous diagonal split in two semi-diagonals of 1.95 m (DIS 1 e DIS 2 in red colour) and a continuous diagonal of 4.10 m (CON in green colour) connected together through a steel mid-plate. Both the diagonals are composed by angular profiles coupled together to form tee section. They are composed of steel S275JR hot-rolled formed, inclined of an angle $\vartheta = 30^\circ$ with respect to the horizontal. Profiles have been stiffened by means of bolted interconnectors appropriate spaced. Centroid axes of the bracing system overlap with the ideal lines shown in conceptual scheme of the pendulum frame. Angular gusset plates have been designed to connect bracings to main members of the frame. Double L-profiles arranged to tee section have been used. Steel interconnectors join the profiles by means of $2\Phi 20$ non pre-stressed bolts in constant spacing sequence. The details are shown in *Figure 30* and *Figure 31*. The following profiles have been tested:

- L-profile 60x60x8 mm
- L-profile 70x70x7 mm
- L-profile 80x80x8 mm

Table 4 summarizes the geometrical properties of the steel bracing profiles.

EC3 requires buckling check for composite rods either in contact or at a reduced distance to main members, joined with steel interconnectors. Neglecting the effect of shear stiffness, the same approach as for simple rod can be used if the following requirements are respected:

- stitch plates must be linked to the profiles by means of bolts or weldings at intervals not greater than $15 \cdot i_{min}$, where i_{min} is the minimum radius of gyration of main component. Therefore it corresponds to the inertia radius of single L-profile.

The interconnectors were detailed such as to reduce the length of the brace in order to prevent displacements both in the in-plane and out-of-plane directions. The intended result was a more stable, less pinched hysteretic loops with less stiffness and strength degradation under reversed cyclic loading. *Table 5* reports geometrical indications for stitch plates design. *Table 6* summarizes bracings geometrical characteristics of section at corner gusset plate and mid-plate connection.

Structural element	Profile	BRACINGS: sections geometrical properties													
		a	e	r	r_1	t	d	Area	Linear Mass	Axis x-x			Axis y-y		
		[mm]	[mm]	[mm]	[mm]	[mm]	[mm]	[cm ²]	[kg/m]	J_x	W_x	i_x	J_y	W_y	i_y
diagonal	2L 60x8	60	8	8	4	15	17.9	18.05	14.18	58.4	13.21	1.8	172.86	26.03	3.08
diagonal	2L 70x7	70	7	9	4.5	15	19.7	18.8	14.76	84.6	15.96	2.12	223.77	28.87	3.45
diagonal	2L 80x8	80	8	10	5	15	22.5	24.5	19.32	144.4	23.86	2.42	366.05	39.59	3.86

Table 4. Bracings geometrical properties

INTERCONNECTORS SPACINGS CHECK			
i_{\min}	1.8	cm	<i>Inertia radius L-profile 60x8 mm</i>
	2.12	cm	<i>Inertia radius L-profile 70x7 mm</i>
	2.42	cm	<i>Inertia radius L-profile 80x8 mm</i>
$p_{2,\max}$	31.80	cm	<i>Maximum padding spacing</i>
$p_{2,\max,CON}$	27.65	cm	<i>Maximum spacing between interconnectors in continuous brace CON</i>
$p_{2,\max,DIS1/2}$	25.00	cm	<i>Maximum spacing between interconnectors in discontinuous braces DIS 1 e DIS 2</i>

Table 5. Design data for interconnectors spacings

Element	Profile	Steel type	L	e_1	e_2	p_1	d_0	$T_{int.}$
			[m]	[mm]	[mm]	[mm]	[mm]	[mm]
CON diagonal	2L 60x60x8	S275JR	4.10	30	25	55	18	15
DIS1-DIS2 diagonal			1.95					
CON diagonal	2L 70x70x7		4.10		30			
DIS1-DIS2 diagonal			1.95					
CON diagonal	2L 80x80x8		4.10		40		22	
DIS1-DIS2 diagonal			1.95					

Table 6. Geometric characteristics of the diagonal in the section of anchorage

3.4.1.1. Buckling check of the compressed element following the l'EC3

The bearing capacity of the compressed element is evaluated using this following formula:

$$N_{b,Rd} = \chi \cdot \beta_A \cdot A \cdot \frac{f_y}{\gamma_{M1}}$$

in which:

- A is the nominal area of the cross section;
- f_y is the yielding stress of the material;
- β_A is a reduction coefficient for the nominal area that takes into account local buckling phenomena: it is equal to 1 for class 1,2 and 3 sections, while it is equal to the ratio A/A_{eff} for class 4 section.

$N_{b,Rd}$ values have been defined for each bracing section. They are reported in APPENDIX C. χ is the reduction coefficient for the correspondent buckling mode and it is evaluated as following:

$$\chi = \frac{1}{\phi + \sqrt{\phi^2 - \bar{\lambda}^2}} \quad \text{with } \chi \leq 1$$

The coefficient ϕ is defined as:

$$\phi = 0.5 \cdot [1 + \alpha \cdot (\bar{\lambda} - 0.2) + \bar{\lambda}^2]$$

where α is the imperfection coefficient that depends on buckling curve of the compression diagonal.

The relative slenderness $\bar{\lambda}$, depending on the section class, is given by:

$$\bar{\lambda} = \sqrt{\frac{A \cdot f_y}{N_{cr}}} \quad \text{for class 1,2 and 3 section}$$

$$\bar{\lambda} = \sqrt{\frac{A_{eff} \cdot f_y}{N_{cr}}} \quad \text{for class 4 section}$$

N_{cr} represents the elastic critical load that activates the phenomenon of instability; if the flexural buckling phenomenon manifests itself before other forms of instability it is equal to:

$$N_{cr} = \min \left\{ \frac{\pi^2 \cdot E \cdot J_x}{L_{0,x}^2}, \frac{\pi^2 \cdot E \cdot J_y}{L_{0,y}^2} \right\}$$

In which:

- E is the Young elastic modulus of the cross section;
- J is the momentum of inertia;
- L_0 is the buckling length of the element;
- – the subscript x y identify the principal axes of the cross section.

If the compressed element has the edges constrained effectively in position with respect to the lateral displacements the buckling length L_0 can be assumed, in favor of security, equal to the geometric length L of the element.

In conclusion buckling resistance of the compressed element depends on three factors:

1. slenderness of the element, in turn depending on the constraint of the elements;
2. geometrical properties of the cross section;
3. type of steel used.

A correct definition of buckling length is a key step in verification of a compressed element. For the X-shaped frames the buckling length of the diagonals is assumed equal to half of continuous diagonal length. Whereas a 4.10 m length with constant section the effective buckling length is therefore equal to $L_0=0.5 \cdot L=2.05$ m. In case of only one brace the buckling length coincides exactly with the entire constant section part of the diagonal continues and is therefore equal to $L_0=L=4.10$ m.

Table 7 summarizes the geometrical properties of the specimens.

Bracing configuration		L [m]	L _{0,x} [m]	L _{0,y} [m]	λ _i	λ _x	λ _y	λ _{rel,x}	λ _{rel,y}
2L60x8	X bracings configuration	2.05	2.05	2.05	86.81	113.89	66.56	1.31	0.76
	One continuous diagonal bracing configuration	4.10	4.10	4.10		227.78	133.12	2.62	1.53
2L70x7	X bracings configuration	2.05	2.05	2.05		96.70	59.42	1.11	0.68
	One continuous diagonal bracing configuration	4.10	4.10	4.10		193.40	118.84	2.23	1.37
2L80x8	X bracings configuration	2.05	2.05	2.05		84.70	53.11	0.97	0.61
	One continuous diagonal bracing configuration	4.10	4.10	4.10		169.42	106.22	1.94	1.22

Table 7. Specimens geometrical properties

3.4.1.2. Tightening torque

A set of 4 prestressed bolts have been used for braces connection to corner gusset plate and mid-plate. The size depends on the cross-section profile used in the bracing system:

- 16 mm in class 10.9 HV for the 2L 60x8 mm profile
- 20 mm in class 10.9 HV for 2L 70x7 mm and 2L 80x8 mm profiles.

A torque wrench has been used for tightening bolts. All bolts were tightened to be snug-tight. As provided by means of the combined method in accordance with EN 1090-2, coefficient of torque performance k, reported by the manufacturer, must be in the range of values between 0.10 and 0.16. This method consists in a first tightening phase of the bolts by imposing a torque moment equal to 75% of pre-load and a second phase in which will be turned the nut of an additional angle function of the total thickness that has to be tightened (including the thickness of the washers). Table 8 and Table 9 summarize values calculated for the two types of bolts to be pre-stressed.

BOLT	d [mm]	RESISTANCE CLASS	f _{ub} [N/mm ²]	A _{res} [mm ²]	F _{p,c} (EN1090-2) [kN]	k	M _r (EN1090-2) [N*m]	Initial torque
								75% M _r [N*m]
M16	16	10.90	1000.00	157.00	109.90	0.13	228.60	171.44
M20	20	10.90	1000.00	245.00	171.50	0.13	445.90	334.43

Table 8. Tightening combined method: initial applied torque

Additional rotation			
BOLT	d [mm]	Condition on t [mm]	Angle of rotation [°]
M16	20	t < 32	60
		32 ≤ t < 96	90
		96 ≤ t ≤ 160	120
M20	20	t < 40	60
		40 ≤ t < 120	90
		120 ≤ t ≤ 200	120

Table 9. Tightening combined method: nut additional rotation

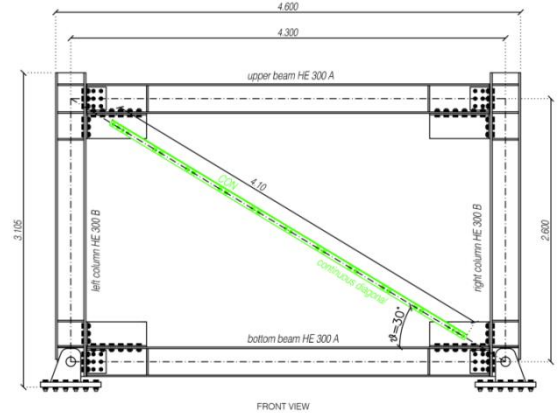
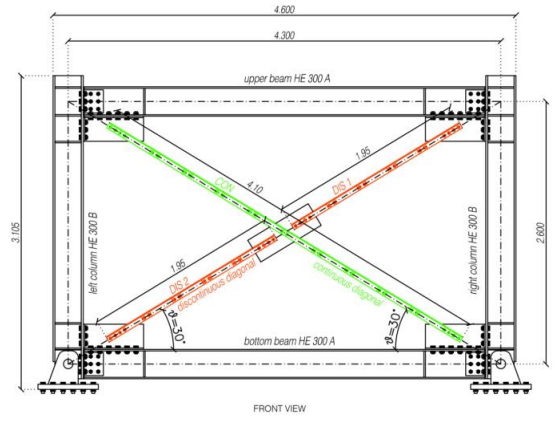
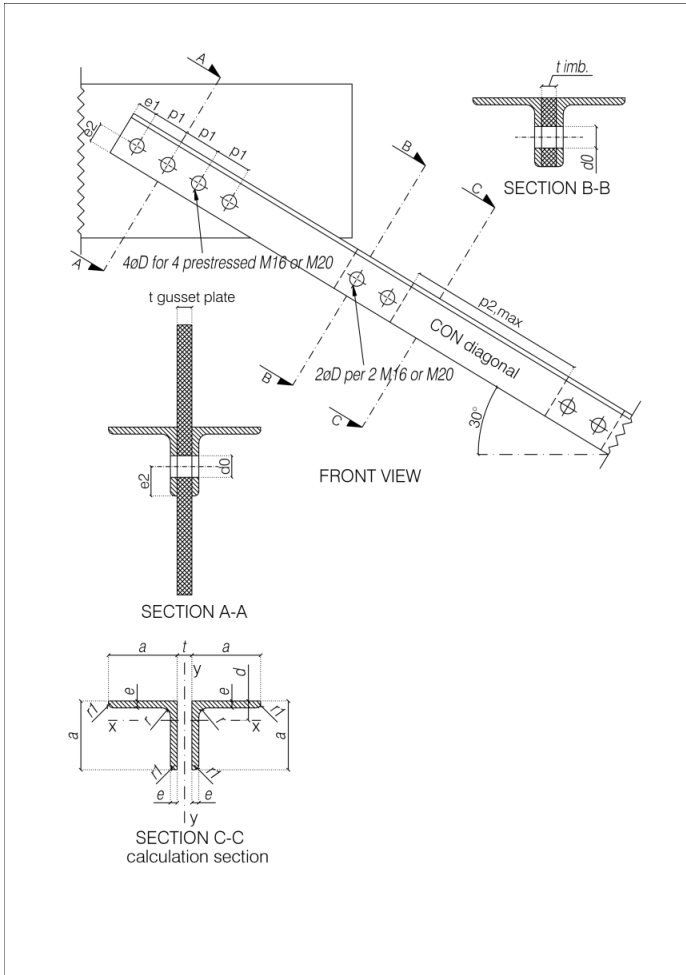


Figure 31. Front view of the MRF configurations (measures in meters)

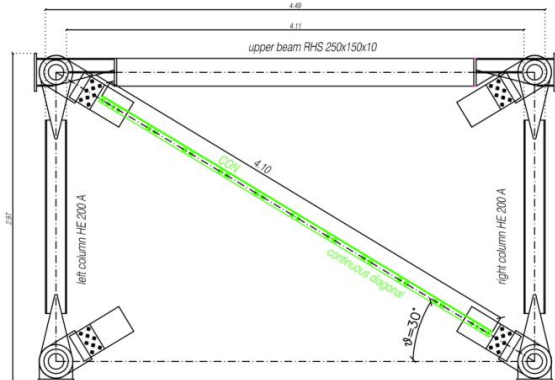
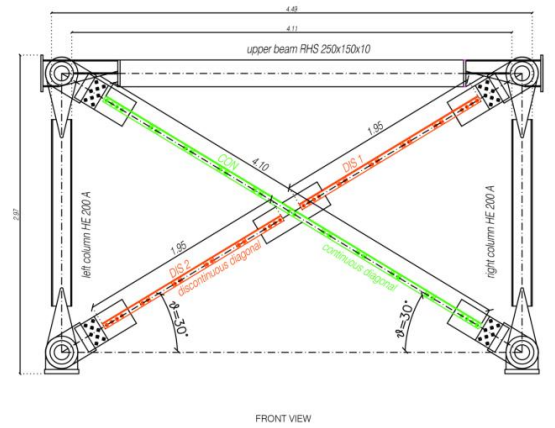
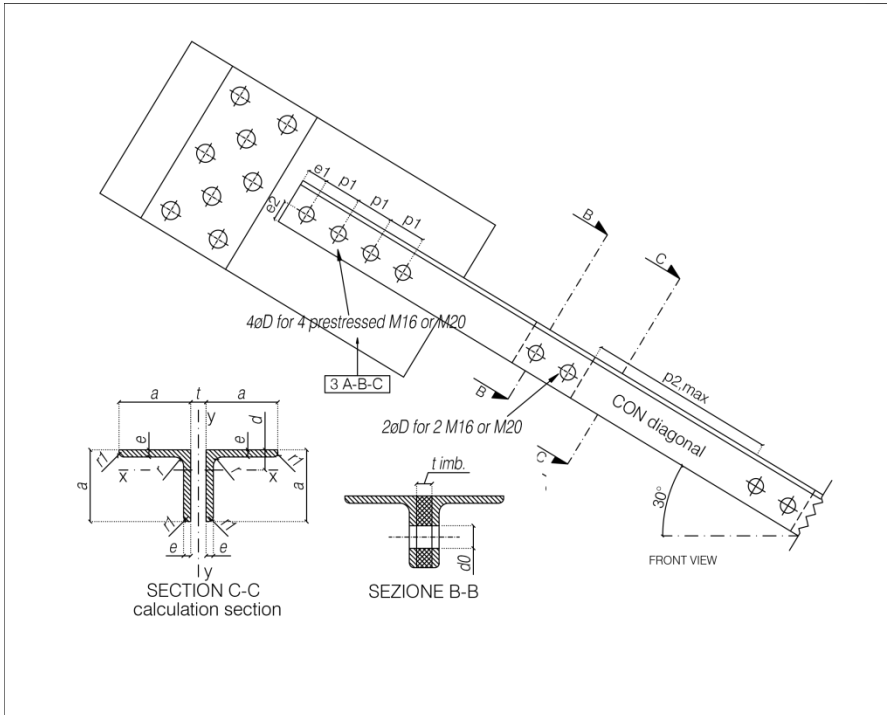


Figure 30. Front view of the PF configurations (measures in meters)

3.4.1.3. Connection joint to the main members

Joints connecting beams-columns-diagonals perform the function to transfer loads between different oriented elements; bracings are dimensioned just assuming axial loads and ideal presence of hinges at their ends.

Figure 32 shows the angular steel gusset plate of a moment resisting frame. The connection has been directly welded to the web of the beam and column.



Figure 32. Angular gusset plate welded to the main members

The need to perform tests with different types of diagonals using the same base frame has suggested the design of a modular connection system no longer welded but bolted to the main members; the welded gusset plate solution is in fact more costly in terms of time as operationally, more complex to perform and moreover leads to a lower precision in positioning of the connecting element. Figure 33 reports the corner connection system of MRF. It is composed by three steel plates welded together in order to mould a single element. This has been bolted to the column web using 12 M24 bolts and to the beam web with 6 M24 bolts; bolts are class of resistance 10.9 non pre-stressed. Diagonals of the bracing system are bolted to the central vertical plate by means of a modular connection consisting in the use of 4 pre-stressed bolts class of resistance 10.9. The diameter is variable depending on the profiles cross-section: 16 mm for 2L profiles 60x60x8 mm, 20 mm for 2L-profiles 70x70x7 mm and 80x80x8 mm.



Figure 33. Modular connection system in MRF

The same approach has been adopted for the design of pinned frame angles joints. Modular steel gusset plates have been realized in order to facilitate the replacement of different diagonals during test. The element has been placed in between column edge and beam end, locked in the inner part of the hinge. The cylindrical pin holds the element in place, and leaves it free to rotate in order to not provide bending moment resistance. Some friction persists in between the elements. The modular corner plates are composed by two steel elements:

- A steel element designed to remain mounted on the frame during all the tests. It is formed by two rectangular steel plate 20 mm thickness fully-penetrated welded to a 26 mm thickness bent part. This latter has a $\Phi 14$ mm hole to accommodate the pin. The element has been designed in order to be a clamp in which an additional rectangular steel plate will be bolted by a set of $\Phi 26$ mm high strength bolts.
- A rectangular steel plate thought to be dismissed and replaced after each test. It is 15 mm thickness and it has got two sets of holes for boltings. First set of $\Phi 26$ mm holes for its connection to the steel element that is fixed and rotates in the beam-column joint. A string of 4 $\Phi 18$ mm or $\Phi 20$ mm (dependent on the cross-section bracing profiles used on a specific test) for the bracings bolting.



Figure 34. Modular connection system in PF

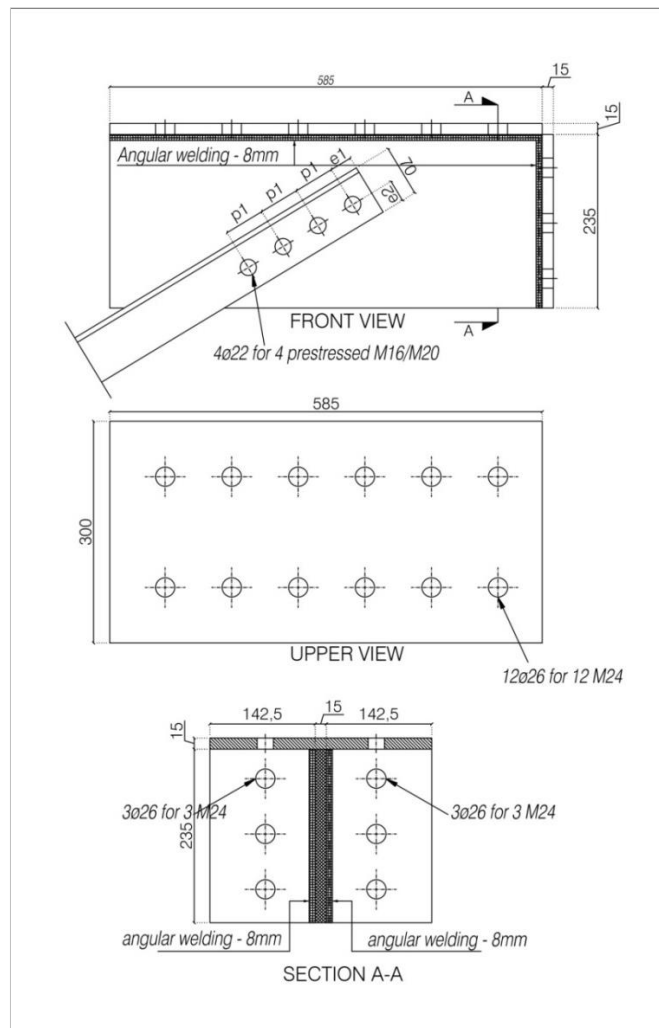


Figure 35. Construction details of corner connection modular systems in MRF (measures in mm)

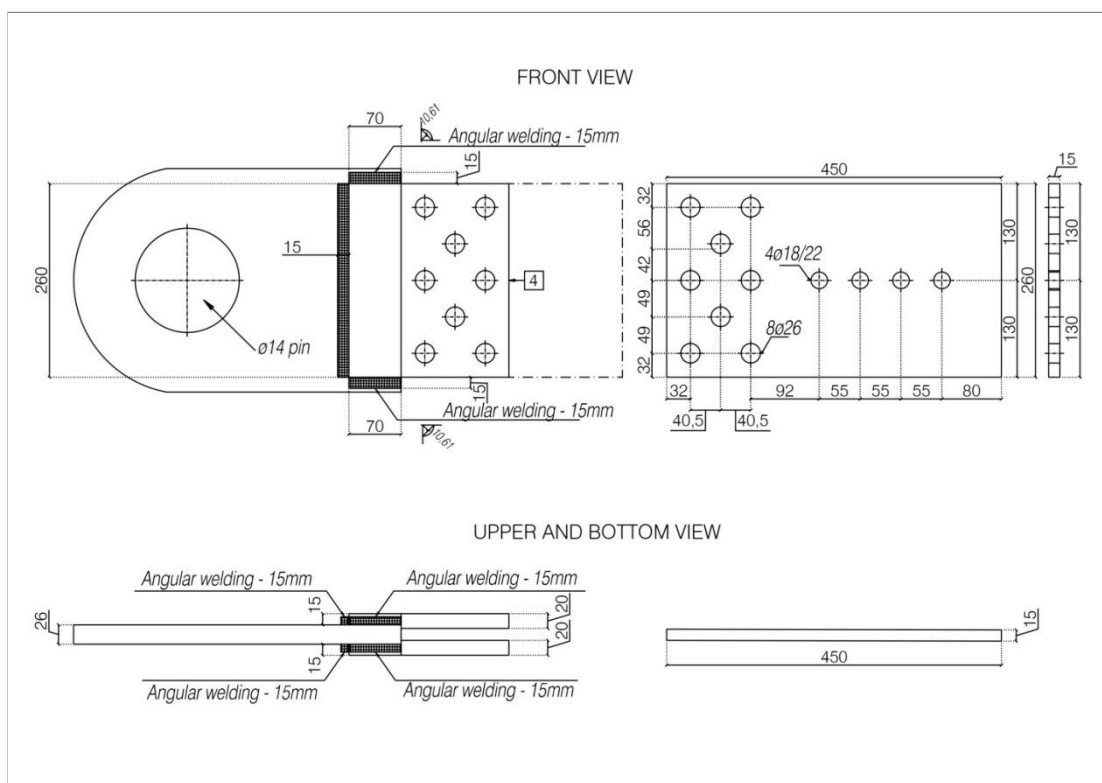


Figure 36. Construction details of corner connection modular systems in PF (measures in mm)

3.4.1.4. Mid-plate connection

Diagonals in X-configuration frame have been bolted to a steel mid-plate. It consists in a 15 mm thickness rectangular steel S275JR plate. In particular, discontinuous diagonals are bolted through a set of 4 pre-stressed bolts class of resistance 10.9 HV, while the continuous diagonal is connected using 2 bolts having with same mechanical characteristics. They have variable diameter depending on cross section of the element:

- 16 mm in class 10.9 HV for the 2L 60x8 mm profile
- 20 mm in class 10.9 HV for 2L 70x7 mm and 2L 80x8 mm profiles.

Figure 37 shows the mid-plate connection assembled and Figure 38 the construction details.

The mid-plane node is representative of a constraint to instability of the compressed element. It has been designed to limit the slenderness of the diagonals. Therefore dimensioning of diagonal in-plane effect has been done considering as effective length half of the continuous diagonal.



Figure 37. Steel mid-plate of the bracing system

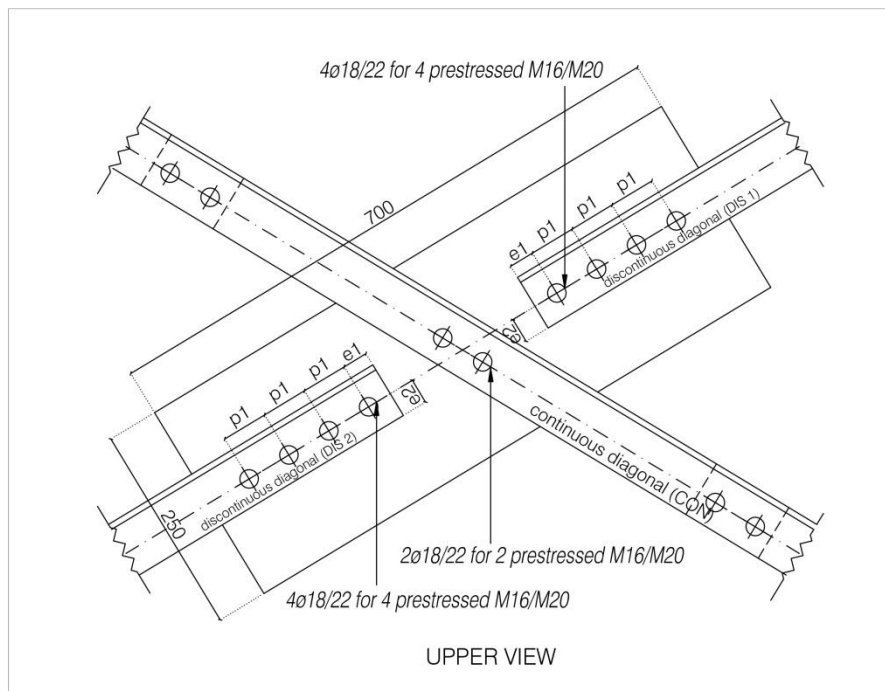


Figure 38. Construction detail of the mid-connection (measures in mm)

3.4.2. Evaluation of the bearing capacity of the tension and compression diagonal

Computation of the resistances following the standard l'EC3, has been reported in APPENDIX C, in particular regarding at:

- ultimate plastic strength of the diagonal in tension;
- strength and buckling of the compression diagonal;
- shear bearing capacity of the bolted connection composed by the gusset plate at beam-column connection and the diagonal element and realized using pre-stressed bolts so to avoid sliding;
- block tearing resistance.

Tables reported in appendix show values about strength of the section. Safety coefficients have been assumed equal to the unit. Subscripts, equations and references have been reported below.

$N_{pl,Rd} = \frac{A \cdot f_y}{\gamma_{M0}}$	plastic resistance of gross section	EC3 1-1 par. 6.2.3
$N_{u,Rd} = \frac{\beta_3 \cdot A_{net} \cdot f_u}{\gamma_{M2}}$	design ultimate resistance of net-section	EC3 1-1 par. 6.2.3
$N_{c,Rd} = \frac{A \cdot f_y}{\gamma_{M2}}$	design compression resistance	EC3 1-1 par. 6.2.4
$N_{b,Rd} = \chi \cdot \frac{A \cdot f_y}{\gamma_{M1}}$	compression buckling resistance	EC3 1-1 par. 6.3.1
$F_{s,Rd} = F_{p,c} \cdot \frac{k_s \cdot n \cdot \mu}{\gamma_{M3}}$	slip resistance of bolted union	EC3 1-8 par. 3.9.1
$F_{b,Rd} = \frac{k_1 \cdot a_b \cdot f_u \cdot d \cdot t}{\gamma_{M2}}$	bearing resistance of bolted union	EC3 1-8 par. 3.6.1
$F_{d,u,Rd} = 0.9 \cdot \frac{A_{net} \cdot f_u}{\gamma_{M2}}$	connection resistance in hollow-section	EC3 1-8 par. 3.10.3
$V_{eff,1,Rd} = \frac{f_u \cdot A_{nt}}{\gamma_{M2}} + \frac{(1+\sqrt{3}) \cdot A_{nv} \cdot f_u}{\gamma_{M0}}$	block tearing resistance for centroid load	EC3 1-8 par. 3.10.2
$V_{eff,2,Rd} = \frac{0.5 \cdot f_u \cdot A_{nt}}{\gamma_{M2}} + \frac{(1+\sqrt{3}) \cdot A_{nv} \cdot f_u}{\gamma_{M0}}$	block tearing resistance for non-centroid load	EC3 1-8 par. 3.10.2

Detailed calculation diagram has been reported in APPENDIX C.

4. Experimental setup

The following chapter explains all the equipment adopted to perform tests. This section provides specific details on experimental setup, design considerations for the specimens, instrumentation and method of data acquisition. Two boundary frames previously designed and constructed were used, but modified to accommodate different beam-to-column connections as well as gusset connections. Additional design checks were carried out to make sure the boundary frame and its connections were safe for the contemplated applications.

4.1. Test bench

Tests have been performed in “Laboratorio Prove Materiali” of Politecnico di Milano, from 11th February to 29th April of the year 2016.

Figure 39 and *Figure 40* outline vertical positioned specimens. Load is applied at the top of the right column through a transfer beam, connected to the load cell. The transfer truss is coupled to an electromechanical actuator with maximum load capacity, both in traction and in compression, amount at 750 kN; the actuator is connected to a counter fixed frame, consisting of a column and two truss systems inclined at 60° toward each other. A double row of 29 mm diameter holes equally spaced at 75 mm intervals is provided on its inward flange to allow the jack to be positioned at the required height. Anchorage of counter-frame to the strong laboratory slab is realized by means of 100 mm diameter anchors. Truss systems are jointed to the columns via end plate connections and the foundation slab using 60 mm anchor bolts.

The frame was tested under its own dead load. No additional dead load was applied to the frame or its columns. To prevent global buckling of the members, specimens have been restrained out-of-plane.

The specimens are attached using a bolted connection to the foundation beam of the test bench, acting as a mounting, in correspondence of the two frame base plate column base. This supporting girder is fastened to the laboratory slab by means of appropriate high strength threaded rods. The anchor beam was established laboratory component prior to this research and the specimen geometry and base plates were adapted to it. Its top flange is provided with a double row of 29 mm diameter holed to fit in bolts 27 mm in diameter, equally spaced at 100 mm intervals, so as to realize a wide range of different mounting positions.

Figure 41 represents the real scale test bench. Main elements of the experimental setup have been highlighted, particularly:

1. Foundation beam of the test bench in which the frame is bolted;
2. Lateral reaction frame to avoid the out-of-plane buckling of the specimens;
3. Electro-mechanical actuator with its steel reaction wall;
4. An actuator control unit data acquisition of potentiometers;
5. A load acquisition unit applied and the strain gauge measurements;
6. Stationary instrumentation column for the measurement of the horizontal frame displacement.

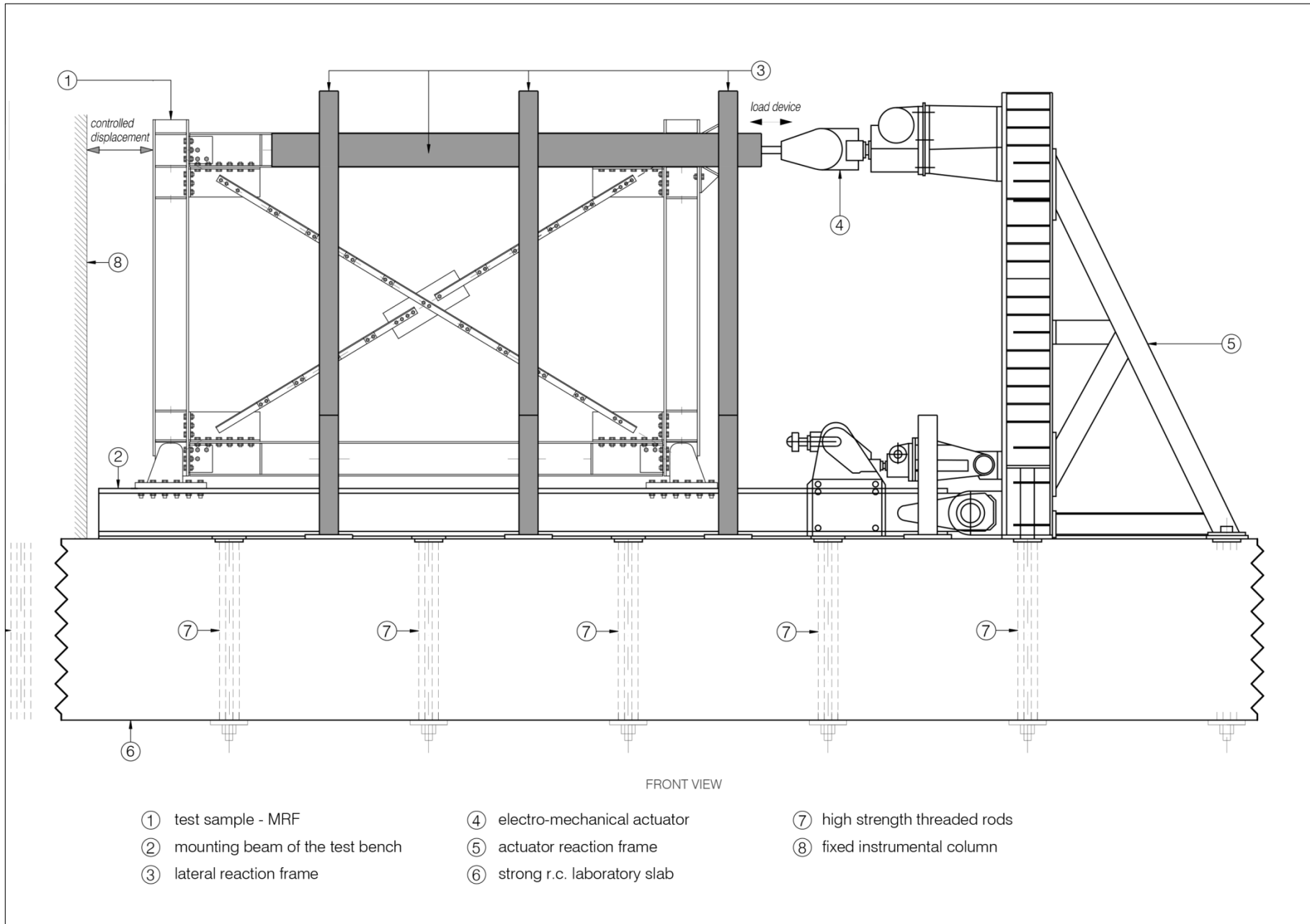


Figure 39. MRF Test setup (measures in meters)

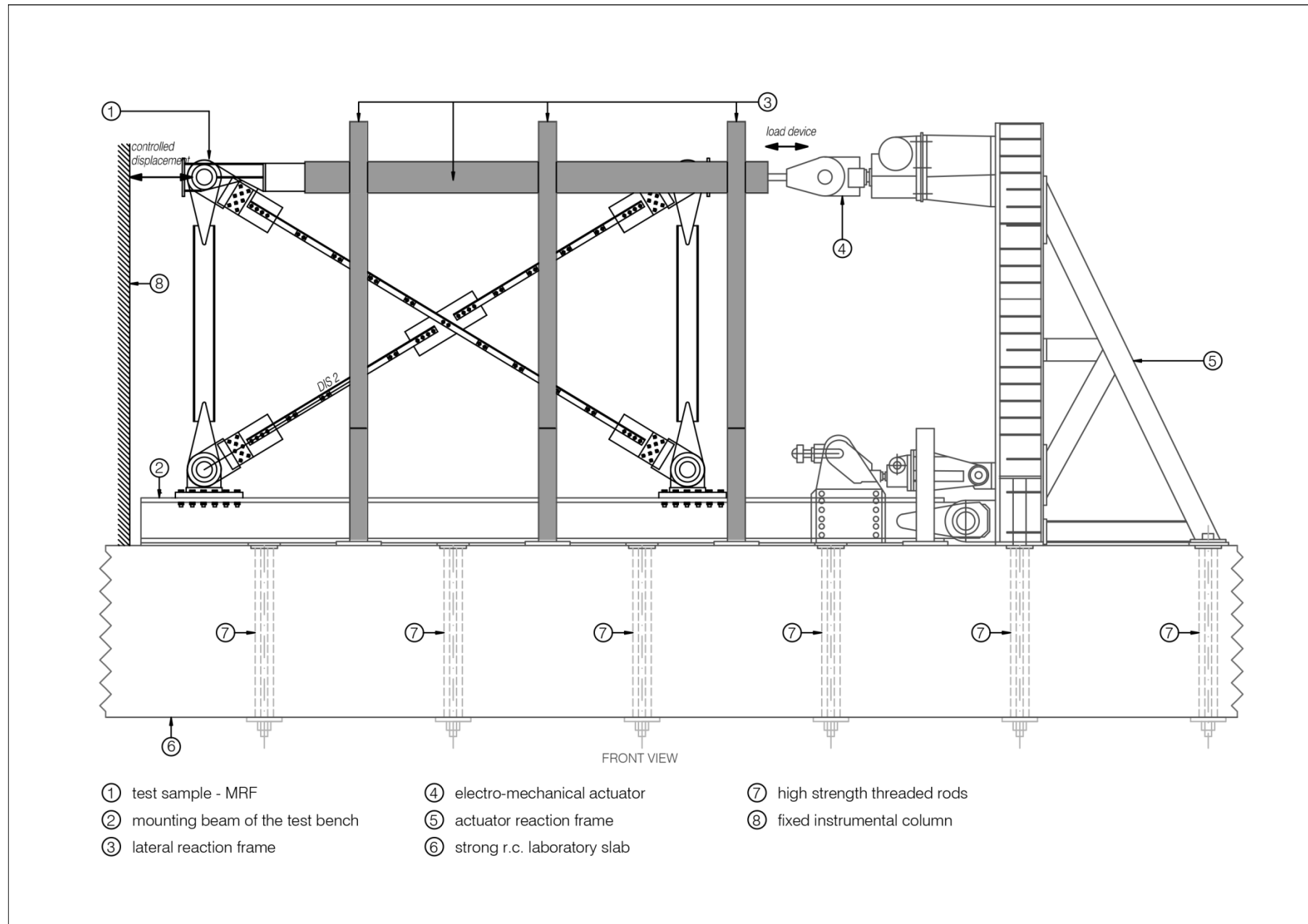


Figure 40. PF Test setup (measures in meters)

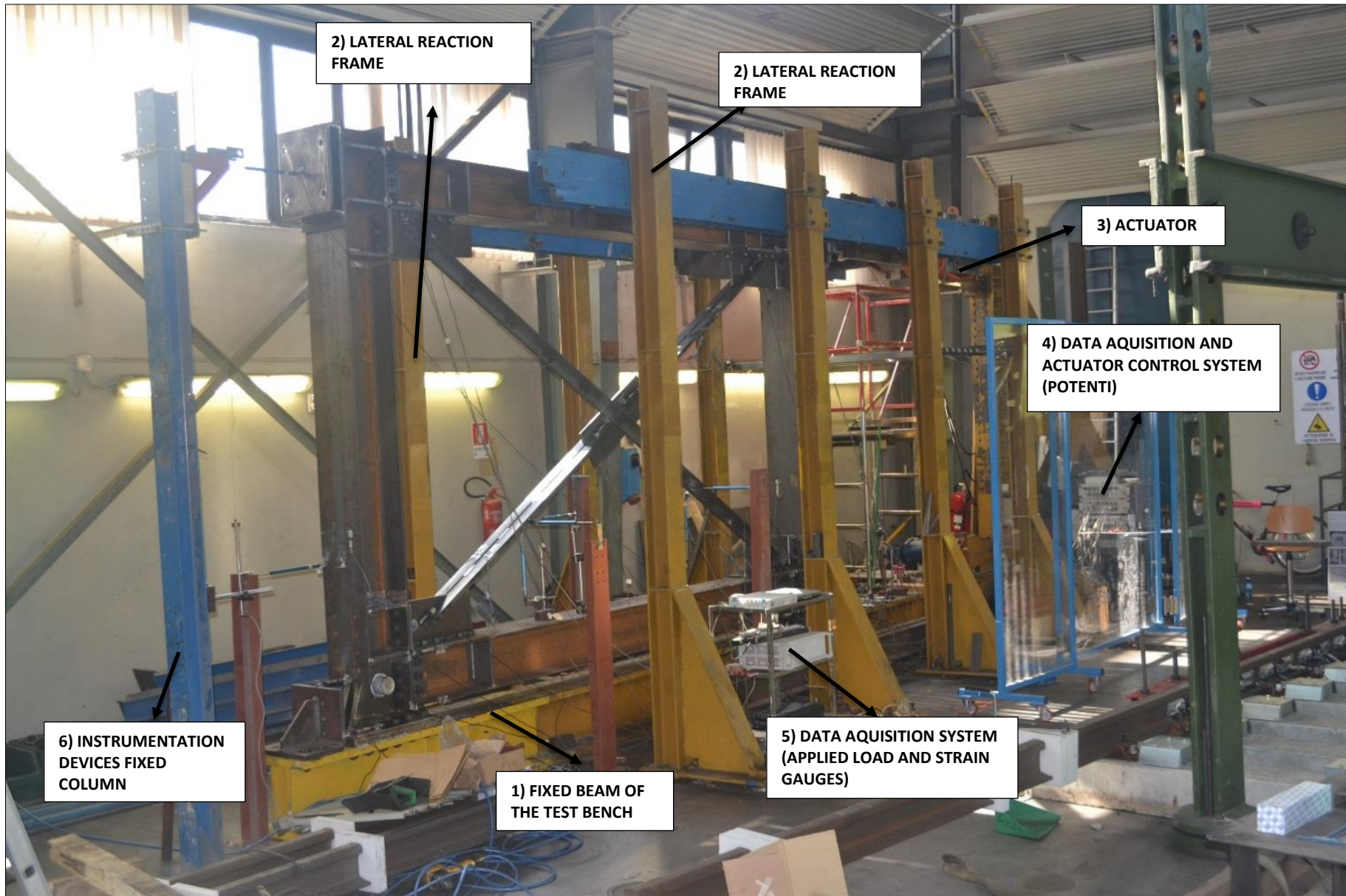


Figure 41. View of the test bench

4.1.1. Load application device

Scheme in *Figure 42* demonstrates the electro-mechanical actuator that transfer load to the frame through a system of plates realized in steel S355JR, welded together, and bolted at the top of the right column by means of 8 high strength bolts 30 mm 10.9 HV.

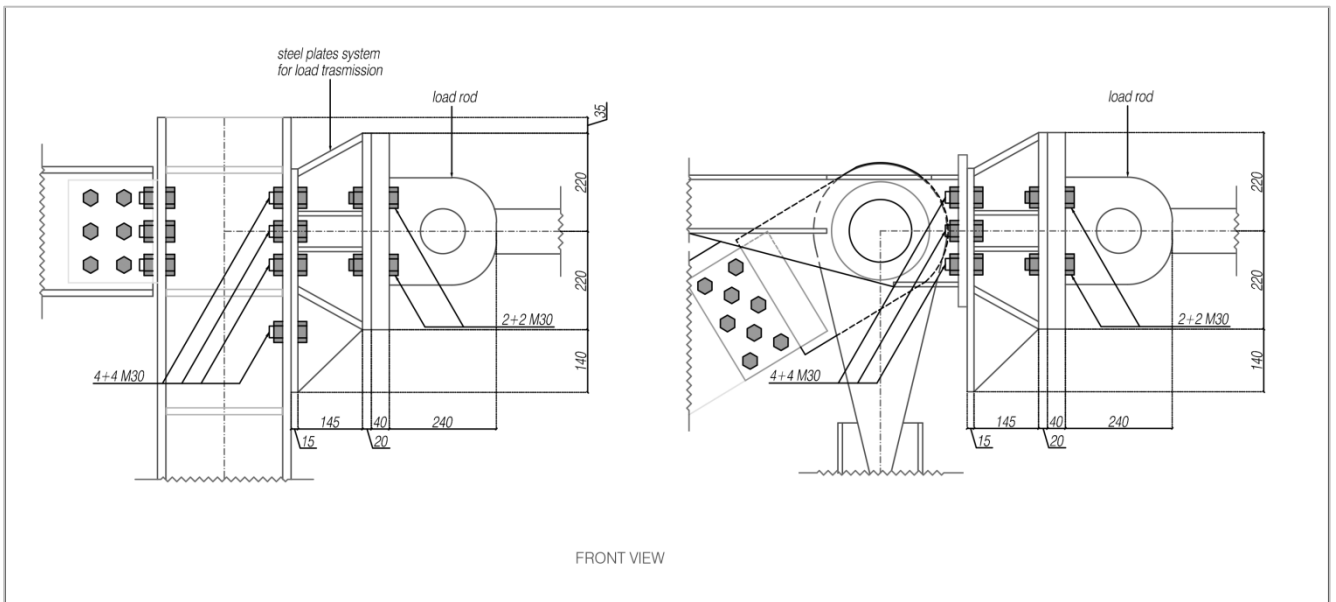


Figure 42. Load transmission device of frames (measures in mm)

The girder beam is joined to the frame through an intermediate steel plates transmission system using 4 M30 high strength bolts; *Figure 43* shows the fixing phase of the truss to the MRF upright corner.



Figure 43. Fixing phase of the load cell to the MRF

A problem with the methodology used to control the actuator was identified during first test. Irregularities were noted in the actuator performance, due to a clearance in the sphere of the device inside it. The actuator control script resulted having error that had been overlooked. It has been created a Matlab script that has helped to clear the results and adjust the curves in force-displacements graphs.

4.1.2. Out-of-plane restraints

Out-of-plane displacement of the specimens is prevented by four roller supports cantilevering from two counter-frames present on the east and west side of the specimen. The rollers were aligned to act (if necessary) at the mid-level of the upper beam level. A gap of approximately 3mm was left between the beam web and each roller so that the roller would only be engaged if out-of-plane deflections closed that gap. Contrast frames are rigidly coupled to the slab by means of high strength threaded rods. *Figure 44* and *Figure 45* show the out plan contrast system described above. The out-of-plane restraints did not inhibit vertical movement.

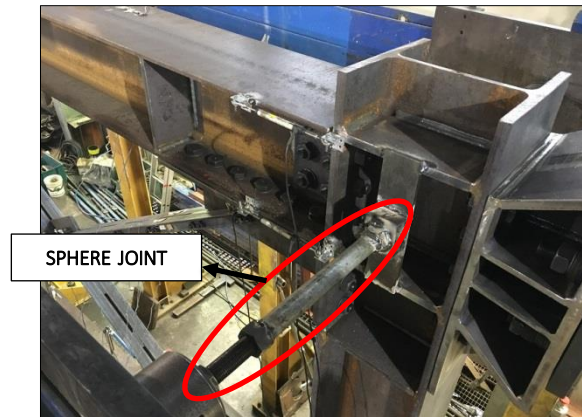


Figure 44. Sphere joint welded to the specimen

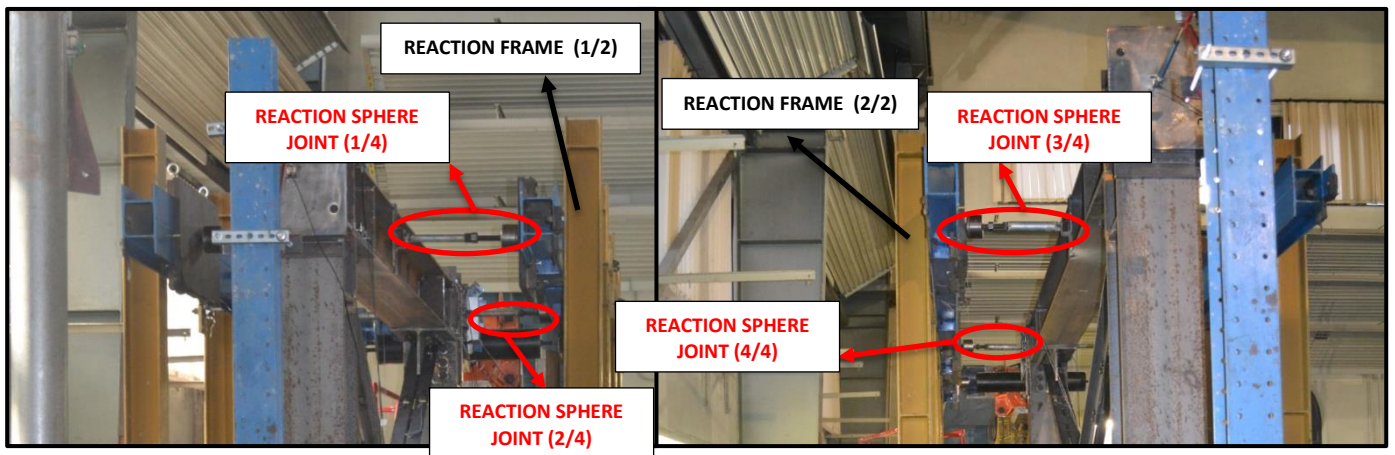


Figure 45. Sphere joint welded to the specimen

4.2. Instrumentation

The specimens were instrumented with stick linear potentiometers composed by sphere joints for measuring absolute or relative displacement of specific points of the specimen. Stick pots and string pots were used to measure out-of-plane displacement, rotation, elongation, slip and uplift.

The measurement of strain in members and diagonals is provided by mono-axial strain gauges installed in crucial points of the frames.

4.2.1. Linear displacement potentiometers

4.2.1.1. Operational principle

A linear potentiometer is a transducer able to convert a physical quantity input, precisely the displacement, into an electrical signal. *Figure 46* shows the electrical device details. Essentially it is constituted by a conductive track with an high resistance R (order of $k\Omega$), fed with a DC voltage of 5-10 V, and a movable contact able to displace along the conductor. Each variation in the moving contact, which is integral with the frame element surface, causes a change in the resistance and consequently a variation of the output voltage V_u , the latter measured by a voltmeter.

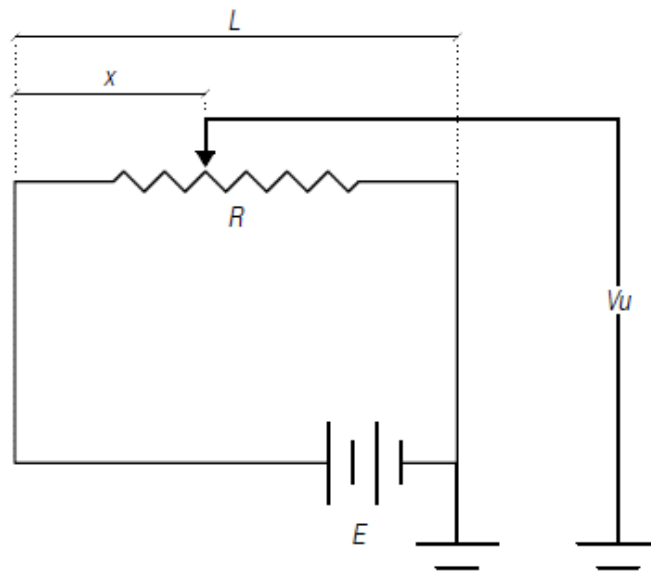


Figure 46. Electric scheme of a stick linear potentiometer

Defined E the supply voltage, and L the length of the conductor, the displacement x is therefore calculated thanks to the following formula:

$$V_u = E \cdot \frac{x}{L}$$

4.2.1.2. Calibration

Calibration is the experimental procedure that defines the relationship between the output and the input of an instrument starting from a measure known.

Calibration of potentiometer is obtained by forming a calibration cycle in which known values of displacement are supplied to the input by means of a digital micrometer Mitutoyo, fixed to the same potentiometer. Starting from the zero wiring of the potentiometer, 10 increasing values have been chosen and assigned moving the pot at regular intervals until the end of the race; at each shift imposed has been related a different voltage value at the output. The detected data are then processed using a linear regression in order to obtain the calibration curve in analytical form. In *Figure 47* is shown the pot calibration phase while in *Figure 48* the obtained calibration generic line.

They have been used potentiometers Penny & Giles model SLS190 with useful electrical stroke of 205 mm and 255 mm and potentiometers Gefran Sensors PZ12 model A 25 and PZ 12 model A 50 having a useful electrical stroke respectively of 25 mm and 50 mm.



Figure 47. Calibration of a potentiometer through digital micrometer

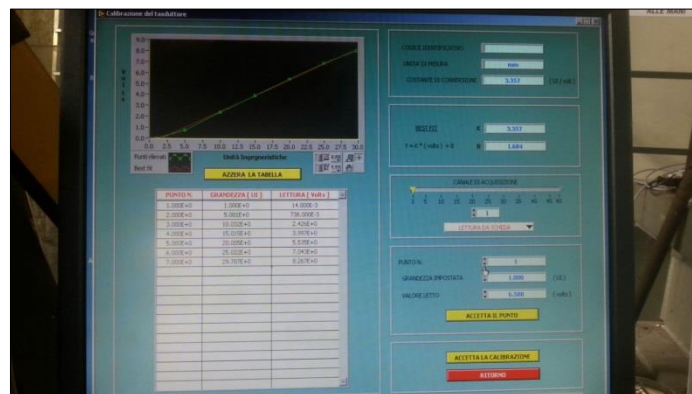


Figure 48. Linear regression line of a pot

4.2.1.3. Pots layout

APPENDIX D bares the layout of potentiometers installed on both the frames. While, a detailed description is reported in the following paragraphs, related to the specific displacement to measure.

Potentiometers for horizontal displacement of the frame

Horizontal floor displacement is recorded and assessed at the intersection between axis of left pillar and axis of the upper beam. *Figure 49* shows how one end of the instrument is directly fixed to the frame while the other is made integral to a fixed instrumentation column. Potentiometer 26 provides, for all the tests, the quantification of frame displacement in the horizontal direction. Lateral displacement of frame is also recorded by a string pot positioned in parallel to the previous one. This solution allows to synchronize the recorded measurements with the two acquisition control units dedicated respectively to the potentiometers and strain gauges.

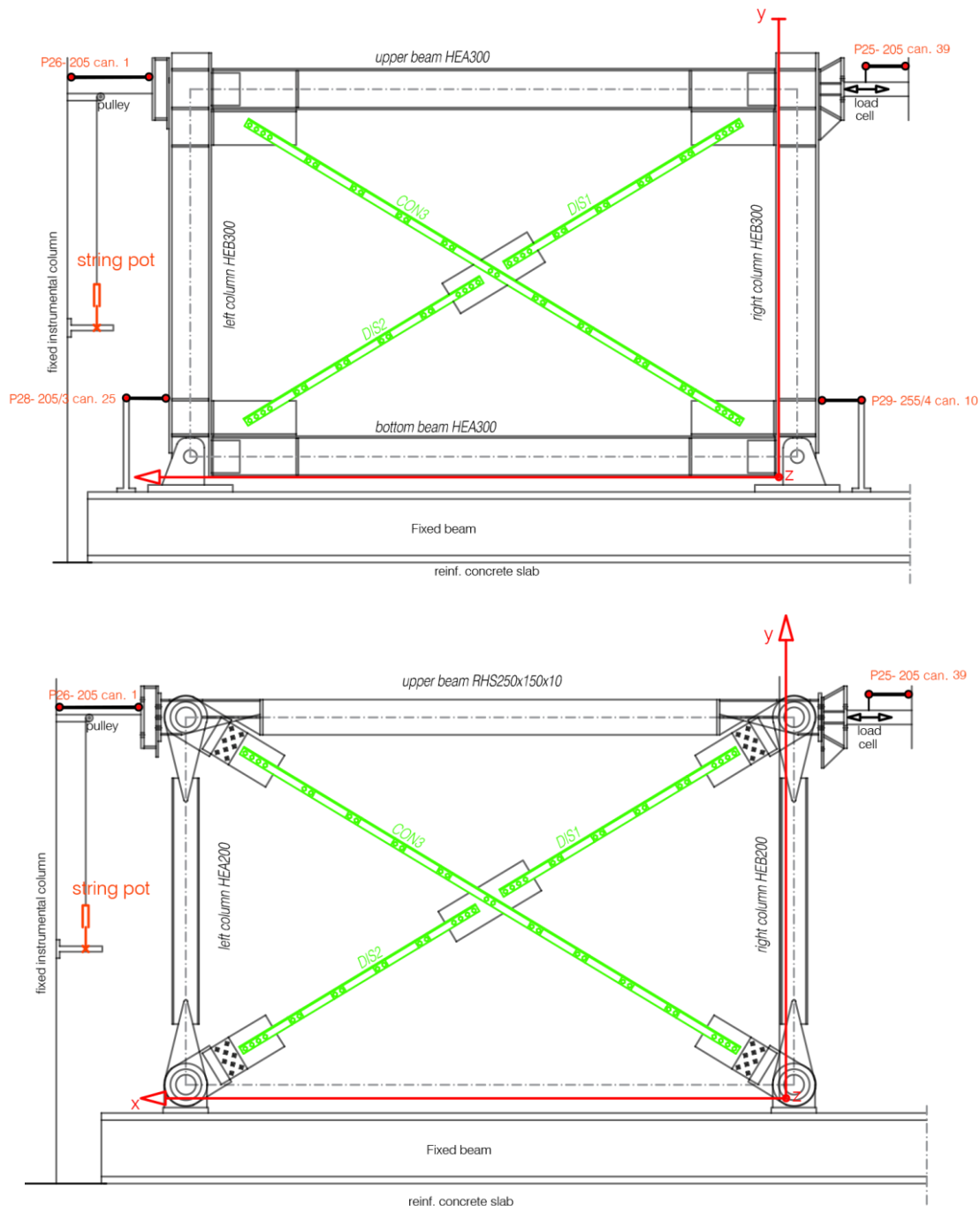


Figure 49. Pots for horizontal displacement of the frame

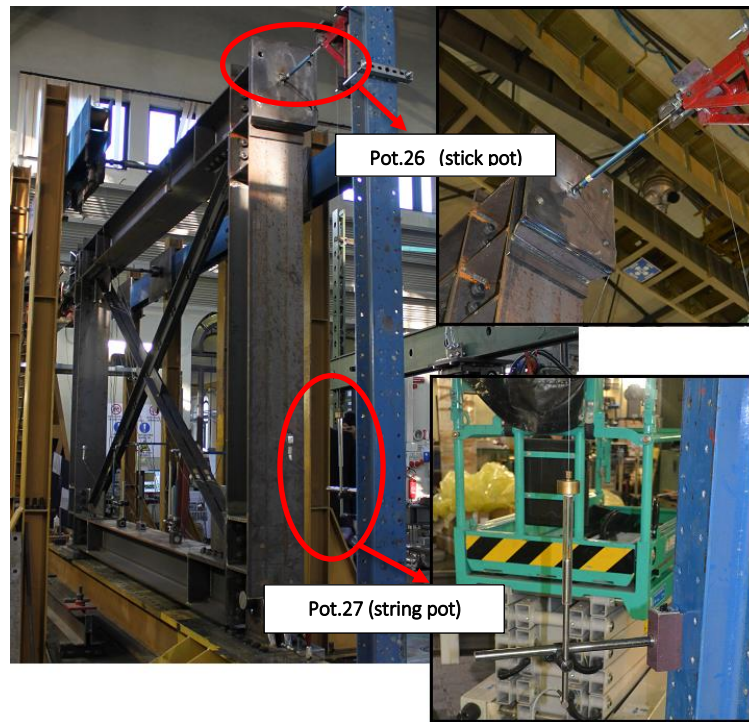
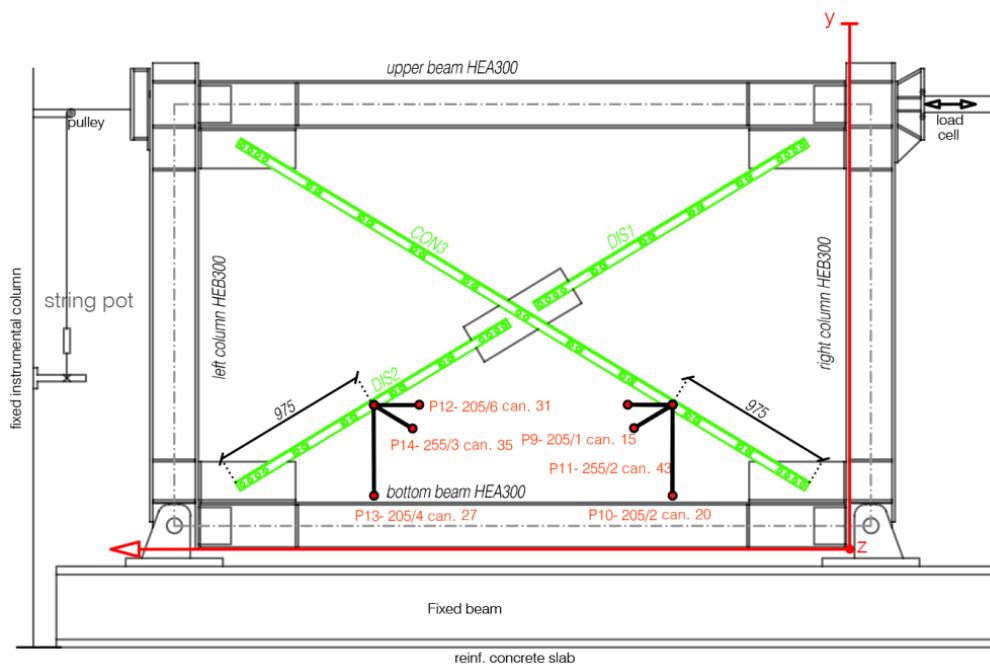


Figure 50. Pots for horizontal displacements (real test bench)

Brace Potentiometers

Braces have been instrumented with a set of three potentiometers: two 205 mm stroke pots for measuring the in-plane buckling (x and y directions) and one 255 mm stroke pot for the out-of-plane (z direction). They have been placed in correspondence of the point of maximum free buckling length.

Figure 51 shows the potentiometers mounted on the X-bracings configuration samples. Magnetic bases have been used for having a suitable installation. Bases are integral with the lower beam and the two side instrumentation columns welded to the strong laboratory slab. Due the ease of installation, measures have been recorded only in the midpoints of the lower half continuous brace (Pot. 9,10,11) and the midpoint of the discontinuous DIS 2 (Pot. 12,13,14).



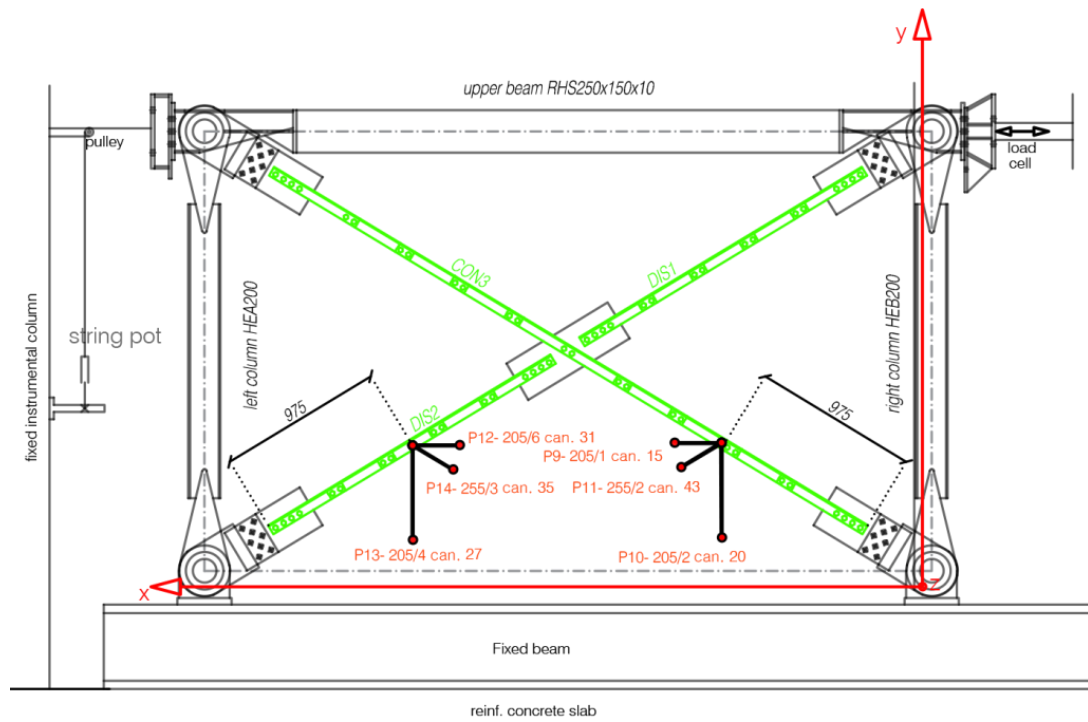


Figure 51. Potentiometers for measuring braces buckling in X configuration frame

In tension diagonal configuration, the free buckling length is increased. Therefore, the point to be monitored has been adjusted and shifted as indicated in the respective layout. Figure 52 shows the pots installed on the specimen. In order to reach an handy installation, pots are fixed next to the midpoint of the brace at a distance of 18 cm from the same.

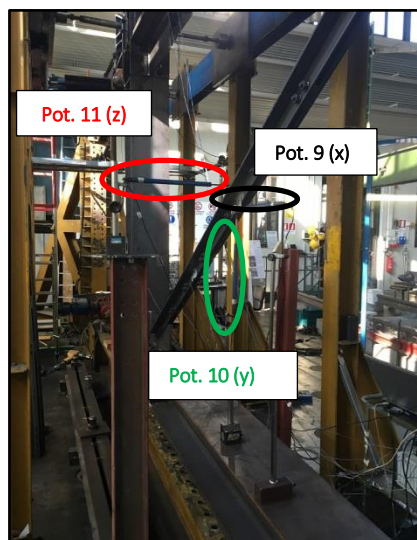


Figure 52. Pots for buckling measurement of the brace in one diagonal configuration

Potentiometers for measuring the sliding at the braces ends

Pots 19, 20, 21, 22, 23 e 24 are placed in specific points in order to pick up the relative displacement between brace and the relative angular steel gusset plate in which it is fixed. 25 mm stroke pots have been installed, lined up to the direction of the stretching/shortening deformations of the brace. Importance in slippage calculation regards its contribution in energy dissipation. Pots are shown in detail in Figure 53.

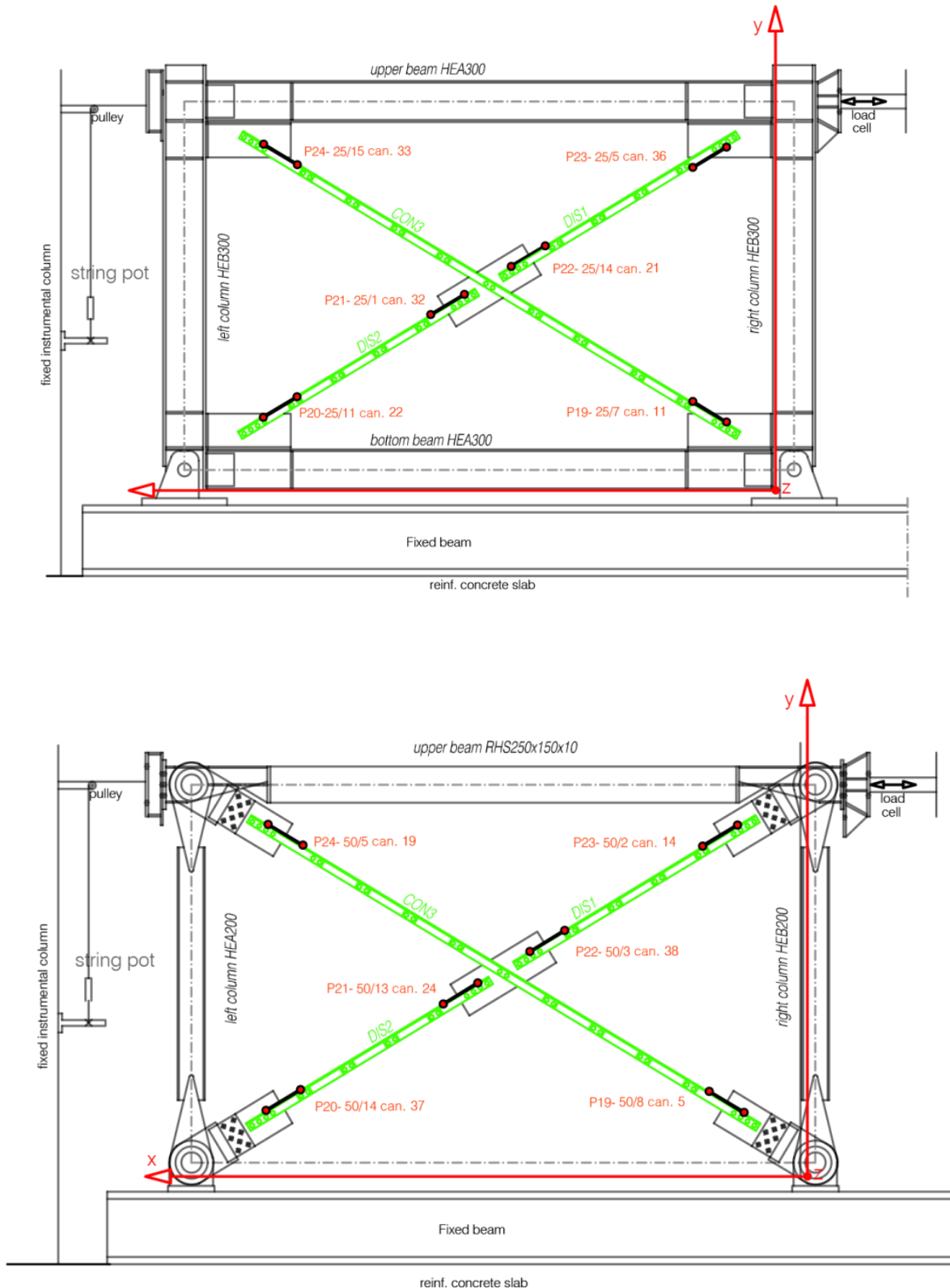


Figure 53. Pots for relative slide evaluation of the braces

Potentiometers for beam-column rotation

Beam-column joints have been instrumented in order to record rotation between members. Relative rotation of members has been recorded only in the MRF, where coupled pots have been used: 1-2, 3-4, 5-6, 7-8. The following expression explains rotation shown in the scheme of Figure 54:

$$\alpha = \frac{(d_1 - d_2)}{b}$$

In which:

- d_1 and d_2 are respectively the records of pots 1 e 2
- b is the distance along y direction, between two pots

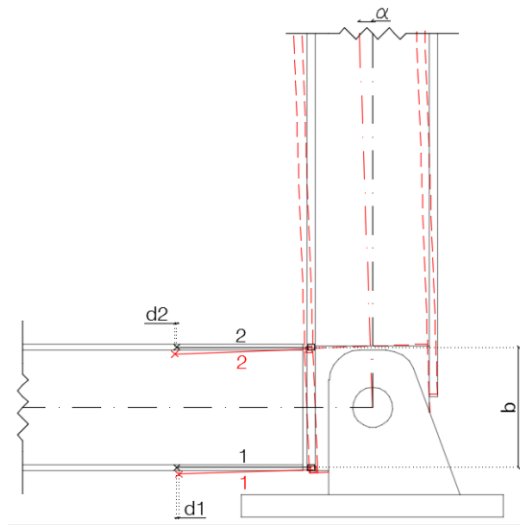


Figure 54. Scheme for rotation calculation of the beam-column joint

50mm stroke pots have been attached, as shown in Figure 55, so to record local rotation across each node between the two structural elements, beam and column. They are fixed from column points aligned to the flanges of the beam.

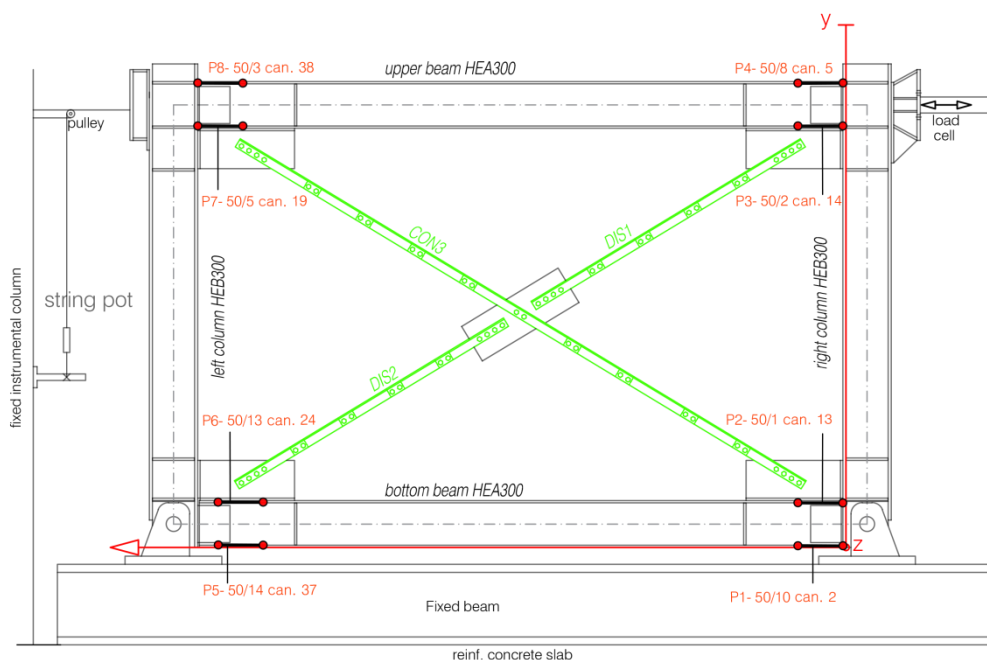


Figure 55. Potentiometers for rotation of beam-column joints

Potentiometers for picking up the base steel plate sliding

Base plate slippage is recorded by means of two potentiometers. An additional angle gusset plate has been bolted next to the bases. Here, pots 15 and 17 with 25 mm stroke have been installed in order to record any relative displacement between instrumental beam and, respectively, the left and right base plates. As much potentiometers 16 and 18 have been placed in order to evaluate the displacement of the bottom part of the left and right column. They have been positioned in correspondence of the centre of axis rotation. *Figure 57* shows the lateral angular steel brackets bolted to the fixed bench by means of 4 high strength bolts 24 mm diameter.

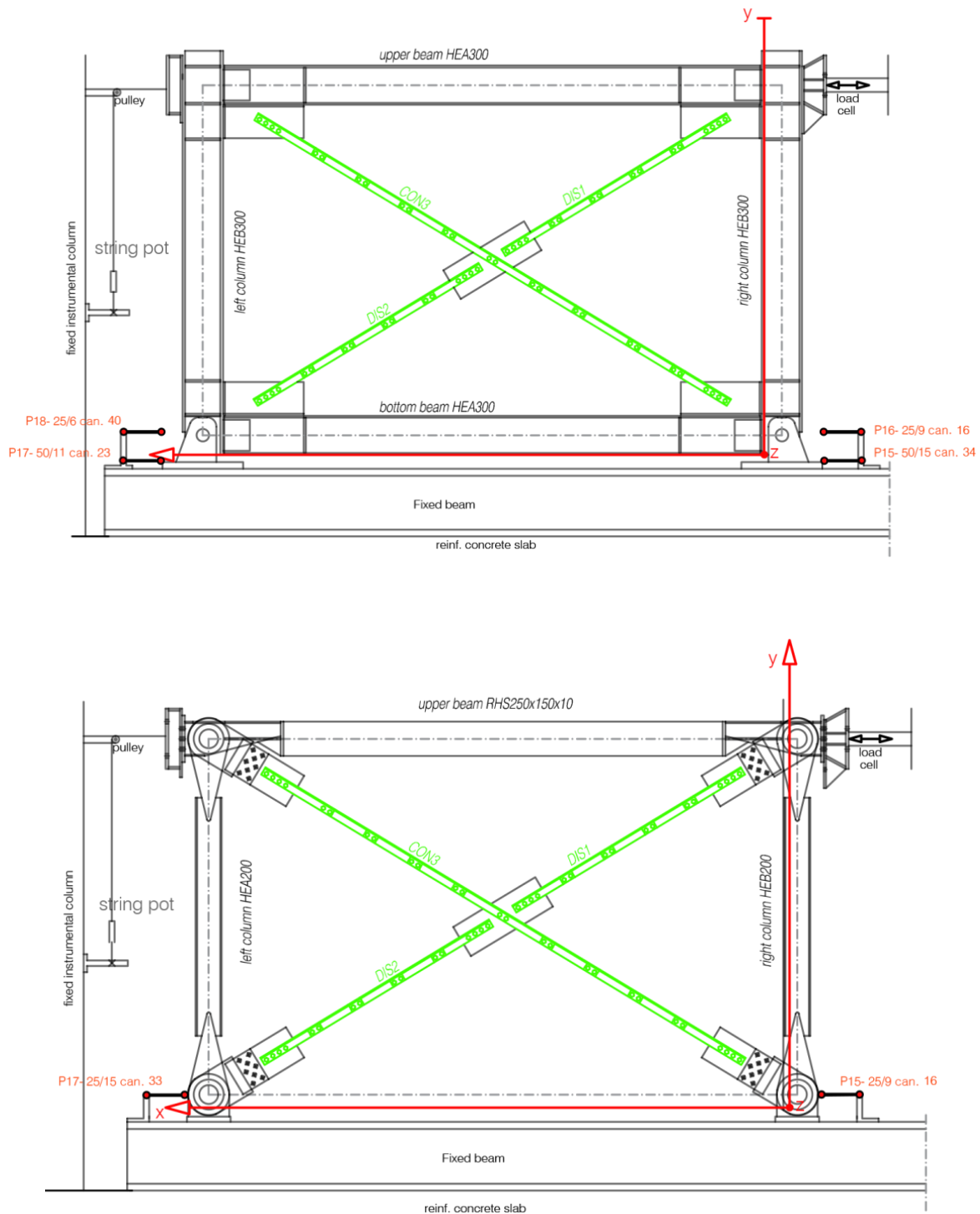


Figure 56. Pots for base plate slip

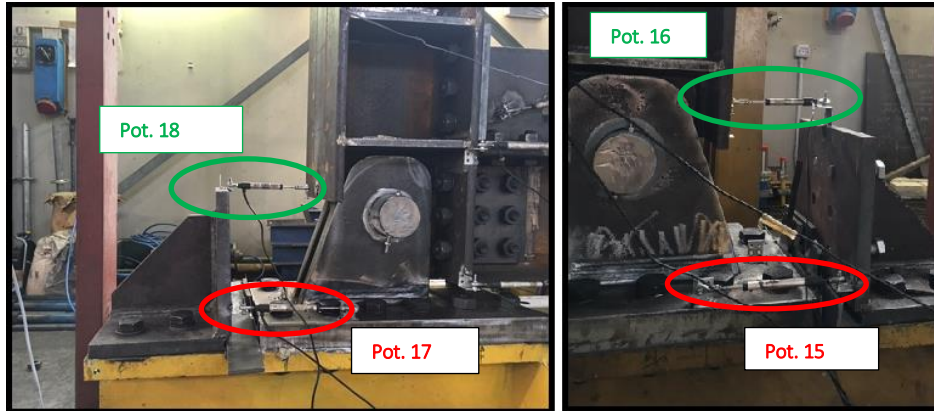


Figure 57. Potentiometers for the measurement of base plates sliding

4.2.2. Uni-axial strain gauges

In order to evaluate internal forces in bracings, columns and beams, uni-axial strain gauges have been installed. These instruments detect small dimensional strains of a body subjected to mechanical stress. Knowing physical and mechanical characteristics of the material, internal actions are derived from deformations values.

4.2.2.1. Operational principle

Uni-axial strain gauges are based on the principle of a variation in the conductor wire resistance with which they are made in relation to the deformation which the thread itself is subjected. Assuming that the original electric resistance of the wire gauge is R , the induced deformation produces a resistance change ΔR described by the following equation:

$$\frac{\Delta R}{R} = G_f \cdot \frac{\Delta L}{L} = G_f \cdot \varepsilon$$

In which:

- G_f is defined as Gauge Factor that express the strain gauges sensitiveness
- L is the initial length of the device
- ΔL is the length variation subjected by the element

4.2.2.2. Technical characteristics of the strain gauges

3 wires electrical sheet strain gauges are applied to specific points of the frame structure elements. They are strain gauges model Ltd FLA-6-350-11-3LT, manufactured by Tokyo Sokki Kenkyujo Co., composed by a resistance of 350Ω , 6 mm grid length and a Gauge Factor equal to 2.12. All the strain gauge devices are connected to the control logic unit by a 3 wires quarter bridge connection.

Figure 58 shows in detail the internal structure of a strain gauge: a thin metal sheet grid-shaped is photoetched on a gossamer support composed of insulated resin; copper terminals are connected to the grid for the electrical connection.

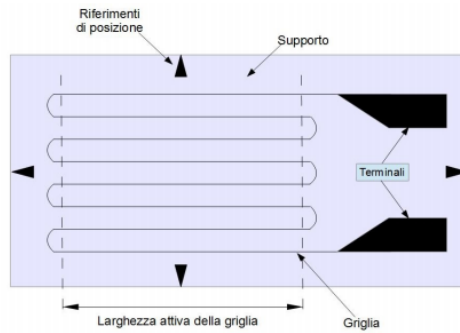


Figure 58. Structure of an electrical sheet strain gauge

Application of strain gauges on frame elements is realized according to the following steps:

1. removal, with the aid of a grinder, of any type of finishing present on the metal surface;
2. cleaning, in the bonded area performing a one-way movement, using an absorbent gauze soaked in acetone. After cleaning tracking the bonding location;
3. strain gauge bonding;
4. strain gauge coverage with a polyethylene sheet applying pressure for about one minute;
5. removal of the polyethylene sheet and positioning of a protective block below the connection cable and over the strain gauge.

Figure 59 shows the strain gauges placed on the main areas of the specimen.

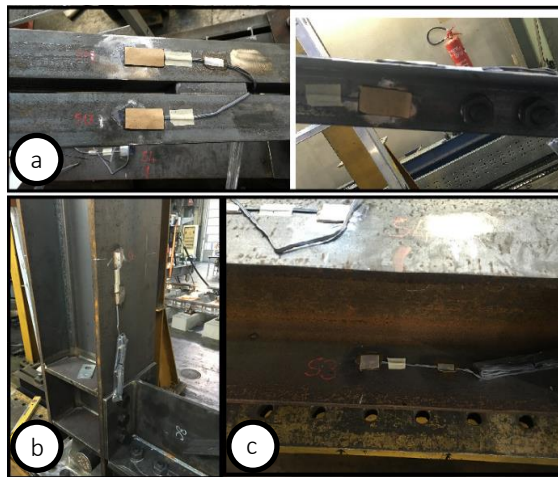


Figure 59. Installed strain gauges: a) on continuous brace b) on right column c) on the bottom beam

4.2.2.3. Layout e strain gauges description

Considerations about axial force calculation are reported in the following paragraph. Starting from the strain gauge measurements. The gauges have been placed in pairs to permit determination both the axial strain and curvature in each position. Figure 60 represents the complete layout of both the specimens: the MRF and the PF.

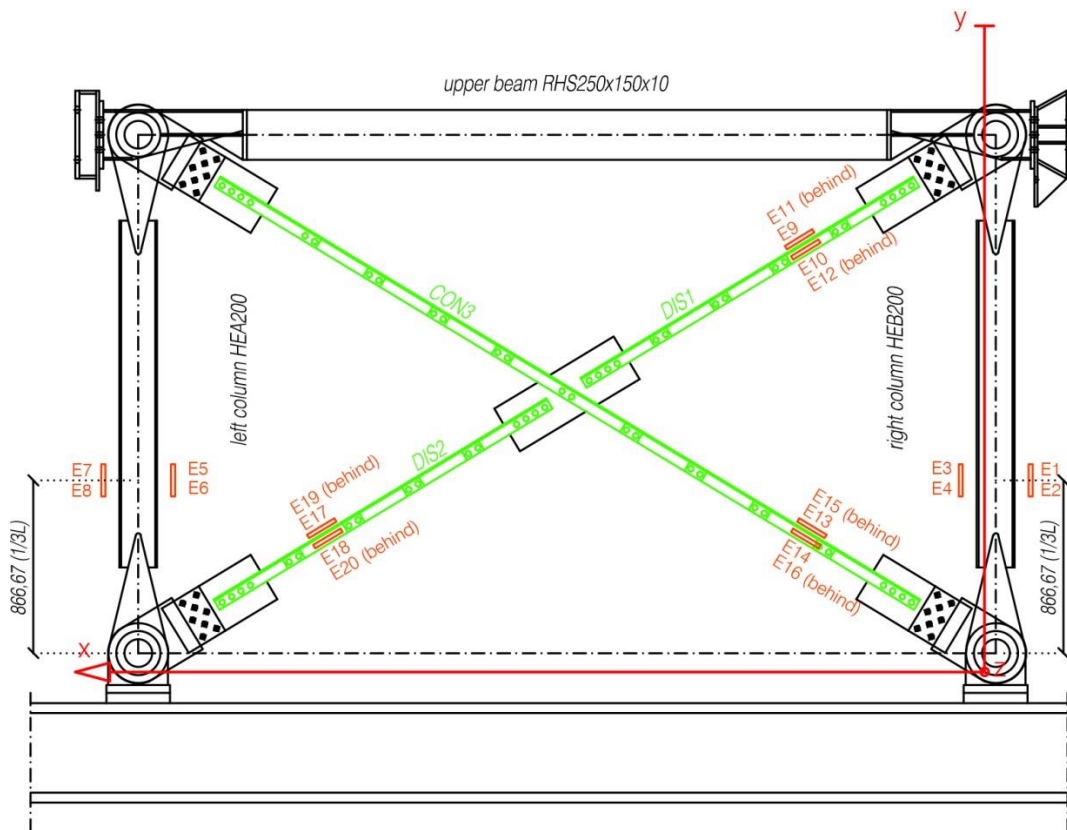
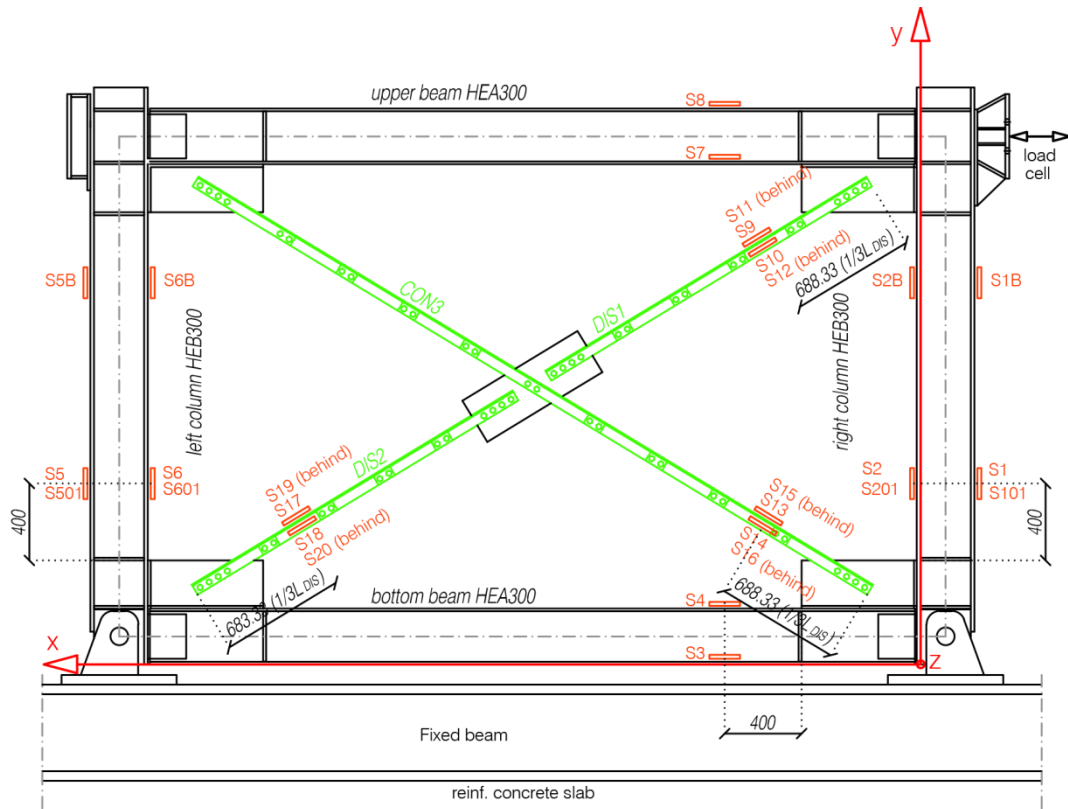


Figure 60. Strain gauges layout

Strain gauges on braces

Axial actions in bracings have been calculated starting from strains measured the 4 uni-axial strain gauges installed according to the diagram of *Figure 61*. Strain gauges along brace have been placed sufficiently distant from the plastic hinge generation point: high profile deformations can in fact lead strain gauge to the break, invalidating the data recorded.

Internal axial force acting on the generic diagonal is obtained with the following relation:

$$N_{CON} = A_{CON} \cdot \bar{\epsilon}_{CON} \cdot E$$

In which:

- A_{CON} is the cross-section area of each brace:
 18.05 cm² for the 2L 60x8 mm profile
 18.80 cm² for the 2L 70x7 mm profile
 24.50 cm² for the 2L 80x8 mm profile
- $\bar{\epsilon}_{CON}$ is the average strain measured by the set of 4 gauges;
- E is the Young elastic modulus of the steel assumed equal to 210 000 MPa.

In the compression phase of the diagonal, the average strain allows to delete the strain aid given by the flexion [13].

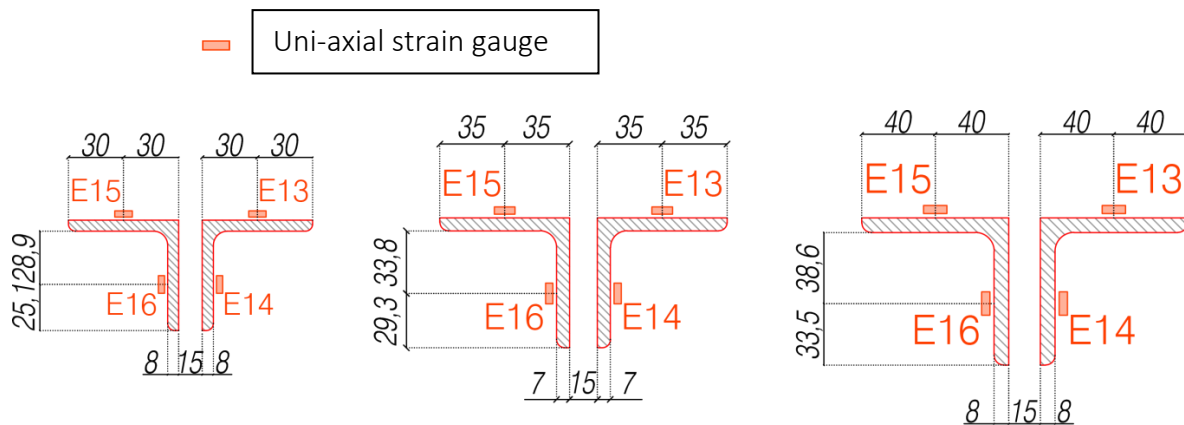


Figure 61. Detail of the bracings strain gauge installation

Beam and column strain gauges

Strain gauges placed on beams and columns were positioned at centre of the outside flanges, on the most extreme fibre, as exhibited on diagram of *Figure 62*. In the columns they were located 400 mm from the corner gusset plates, where the steel would remain elastic. The beam locations were similar. Strain gauges in pinned frame have been put at 1/3 of the column height. The axial force acting on each element is obtained by using the deformation data detected by the strain gauges according to the formula:

$$N = A \cdot \bar{\epsilon} \cdot E$$

In which:

- A is the cross section area of beam or column, respectively:
88.3 cm² e 117 cm² for beam and column of the MRF
74.5 cm² and 58.83 cm² for beam and column of the PF;
- $\bar{\epsilon}_{CON}$ is the average deformation measured by each pair of strain gauges;
- E is the steel Young elastic modulus assumed equal to 210 000 MPa.

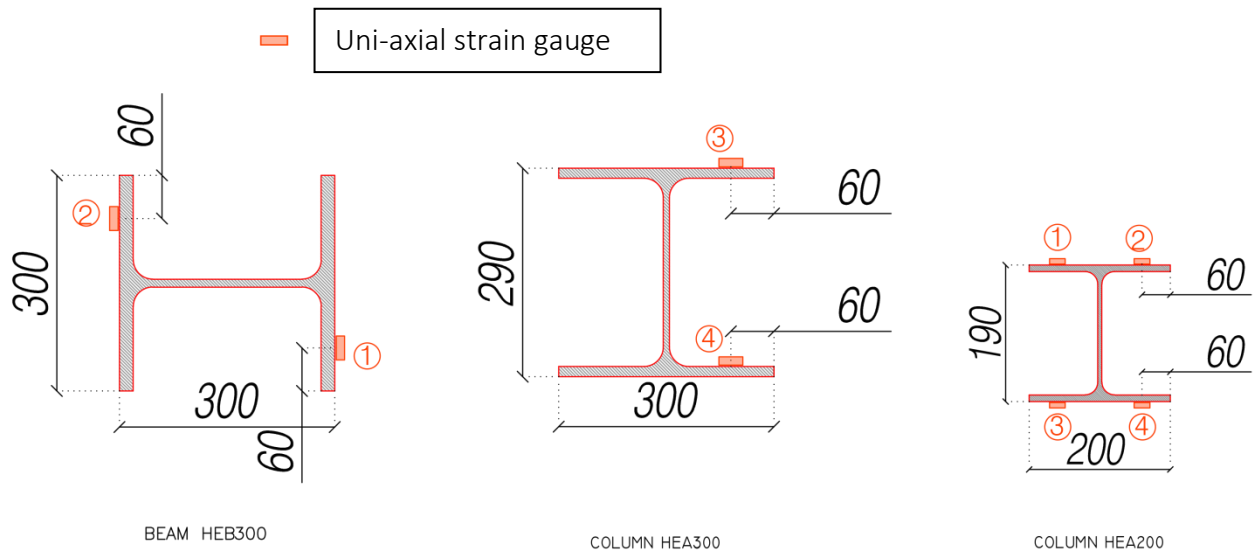


Figure 62. Installation details of the strain gauges on the main members a) column of MRF b) beam of MRF c) column of PF

4.3. Data acquisition system and load application

Two distinct data acquisition units working in parallel have been used, both with an acquisition frequency of 1 Hz. The first unit, is composed by:

- a SPIDER 8 data acquisition unit that records the displacements of the string potentiometer and the load applied;
- a MGC data acquisition system that amplifies and records the strain gauges deformation.

Second unit, in addition to acquiring the measurements taken by stick potentiometers through three analog amplifiers, deals with application of loading protocol. In particular, the load reversal occurs automatically thanks to the actuator control software that follows the values of the horizontal displacement recorded by the potentiometer 26.

Synchronization of data is given by same acquisition frequency and comparison of the frame horizontal displacement extent, recorded with both different units. *Figure 63* shows the two control unit systems.

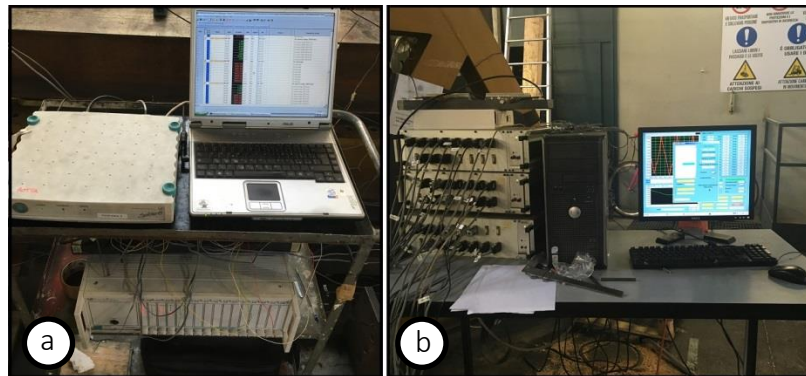


Figure 63. Data acquisition systems: a) loading cell and strain gauges b) actuator control and stick pots

5. Experimental results

Chapter 5 describes each of the experiments in a separate section. This summary includes the force-drift response for each specimen and describes the progression of yielding and damage through the tests. Photographs, thermography files and plots supplement the descriptions. Each test presented divided into subchapter representing main topics investigated for each specimen, particularly:

- Loading history in terms of drift;
- Base shear-displacement;
- Columns force trend;
- Bracings behaviour;

The same subsections follow for each test developed during program. Furthermore, loading protocol and sign convention adopted, equal for all tests are presented in this section.

Storey drift is defined as the percentage ratio between lateral displacement δ pushed to the frame by the loading jack, and the interstorey height h , equal to 2600 mm. *Figure 64* shows the concept.

$$drift [\%] = \frac{\delta}{h} \cdot 100$$

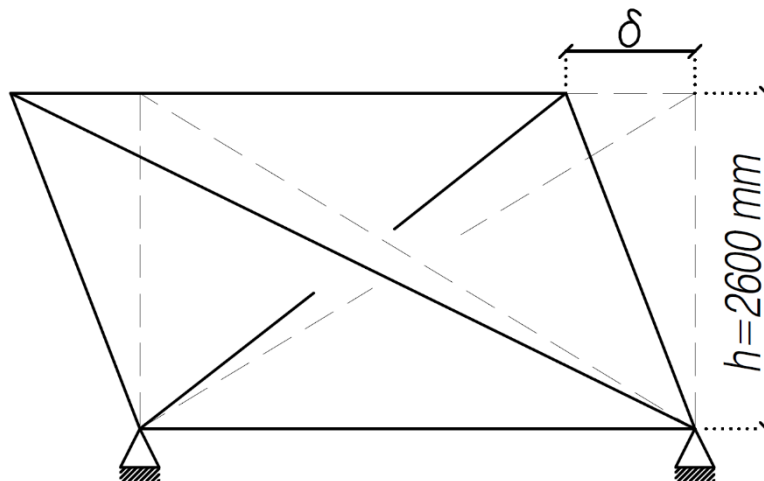


Figure 64. Storey drift definition

5.1. Loading protocol

Drift control tests have been chosen. Load control tests could be tricky since bearing capacity could lower after first few cycles due to instability, bringing the test to the end. Therefore, continuing the test, a loss of resistance in a single element has been observed not necessarily implying a lowering in bearing capacity of the structure.

Complete reversal cyclic loads deteriorates the structure resistance faster than partial reversal loads. The amount of cycles to undergo to the structure for each maximum imposed drift, has been estimated in order not to be too high so to avoid low-cycle fatigue, and simulate as much as possible a real earthquake. Specimen has been stressed using a drift control procedure, following a loading protocol defined according to l'ECCS Recommendations (1986) [14]. *Table 10* shows cyclic displacement definition scheme, as specified by ECCS (1986). δ_y , representing the limit displacement in elastic field, is the parameter that control the cyclic loads. Vertex + o – specify if displacement bring to compression or tension.

N° of cycles	Interval	
1	$\delta_y^+/4$	$\delta_y^-/4$
1	$2\delta_y^+/4$	$2\delta_y^-/4$
1	$3\delta_y^+/4$	$3\delta_y^-/4$
1	δ_y^+	δ_y^-
3	$(2+2n)\delta_y^+$	$(2+2n)\delta_y^-$
n=0,1,2,3,...		

Tabella 10. Loading protocol definition according to ECCS (1986)

δ_y definition has been modified from ECCS (1986) specifications. It recommends the execution of a tension and compression monotonic test for each specimen in order to obtain values of elastic limit displacements. Tests analysed in this document, adopt as elastic limit the displacement that bring the brace element in tension to yielding. Monotonic tests have not been performed, so δ_y have been defined using the following procedure.

Tension tests on specimens of diagonal braces gave average values of the yielding stress as follow:

$$f_{y,60x8} = 349.00 \text{ MPa}, f_{y,70x7} = 336.33 \text{ MPa}, f_{y,80x8} = 346.67 \text{ MPa},$$

which is connected to the yielding axial load:

$$N_{y,CON} = A_{2xL60x8} \cdot f_y = 1805 \text{ mm}^2 \cdot 349.00 \text{ MPa} = 629.94 \text{ kN}$$

$$N_{y,CON} = A_{2xL70x7} \cdot f_y = 1880 \text{ mm}^2 \cdot 336.33 \text{ MPa} = 632.31 \text{ kN}$$

$$N_{y,CON} = A_{2xL80x8} \cdot f_y = 2450 \text{ mm}^2 \cdot 346.67 \text{ MPa} = 893.44 \text{ kN}$$

consequently, the strain of diagonal elements under respective yielding axial loads:

$$\Delta_l = \frac{N_{y,CON}}{A_{2xL60x8}} \cdot \frac{L_d}{E} = \frac{629.94 \text{ kN}}{1805 \text{ mm}^2} \cdot \frac{2.05 \text{ m}}{210\,000 \text{ MPa}} = 3.41 \text{ mm}$$

$$\Delta_l = \frac{N_{y,CON}}{A_{2xL70x7}} \cdot \frac{L_d}{E} = \frac{632.31 \text{ kN}}{1880 \text{ mm}^2} \cdot \frac{2.05 \text{ m}}{210\,000 \text{ MPa}} = 3.28 \text{ mm}$$

$$\Delta_l = \frac{N_{y,CON}}{A_{2xL80x8}} \cdot \frac{L_d}{E} = \frac{893.44 \text{ kN}}{2450 \text{ mm}^2} \cdot \frac{2.05 \text{ m}}{210\,000 \text{ MPa}} = 3.56 \text{ mm}$$

Half of the continuous brace length has been considered as effective length of the diagonal L_d . Therefore, referring to pendulum frame, the interstorey drift that bring continuous diagonals to yielding:

$$\delta_{y,2xL60x8} = \frac{\Delta_l}{\cos \theta} = \frac{3.41 \text{ mm}}{\cos 30^\circ} = 3.94 \text{ mm}$$

$$\delta_{y,2xL70x7} = \frac{\Delta_l}{\cos \theta} = \frac{3.28 \text{ mm}}{\cos 30^\circ} = 3.78 \text{ mm}$$

$$\delta_{y,2xL80x8} = \frac{\Delta_l}{\cos \theta} = \frac{3.56 \text{ mm}}{\cos 30^\circ} = 4.11 \text{ mm}$$

Therefore a value of about $\delta_y = 4.00 \text{ mm}$ has been chosen, equivalent to a drift of 0.15 %.

Also load cycles definition for plastic field differs from ECCS (1986) standards. Intermediary cycles have been imposed in order to better investigate the frame response in plastic field. *Table 11* summarizes loading protocol adopted for tests.

N° of cycles	Interval	
	1	$\delta_y^+/4$
1	$2\delta_y^+/4$	$2\delta_y^-/4$
1	$3\delta_y^+/4$	$3\delta_y^-/4$
1	δ_y^+	δ_y^-
3	$n+\delta_y^+$	$n+\delta_y^-$
3	$2k+\delta_y^+$	$k \delta_y^-$
$\delta_y^+ = \delta_y^- = 4 \text{ mm}$		
$n=1,2,3,4,5,6$		
$k=4,5,6,7,\dots$		

Table 11. Loading protocol of tests

Loading protocol and the actuator jack have been controlled automatically by a software. The load reversal follow outputs of the potentiometer n.26. The control unit of the jack is shown in *Figure 65*.

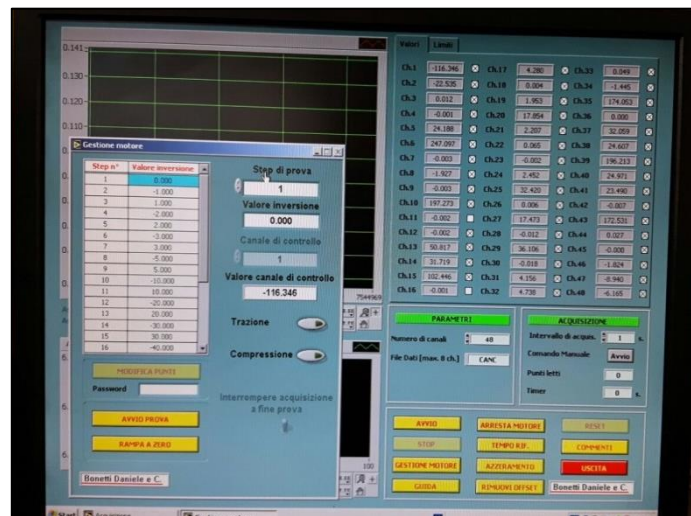


Figure 65. Loading protocol definition on control unit of actuator

5.2. Sign convention

Figure 66 reports the detail about convention adopted, in which:

- δ is the lateral displacement applied to the frame;
- V is the load applied by the jack, defined as base shear.

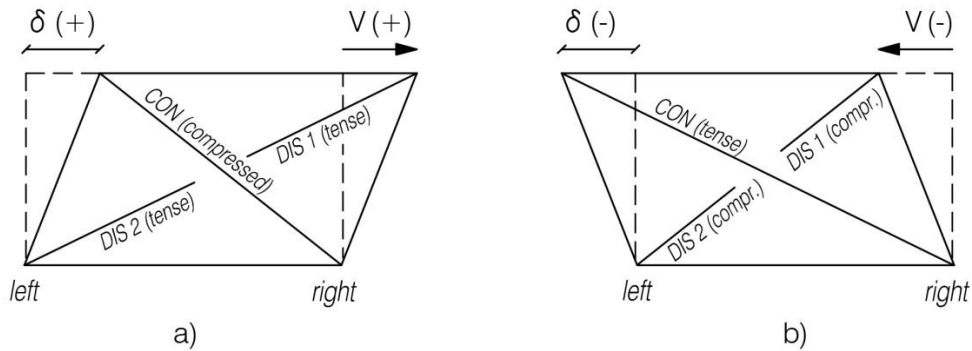


Figure 66. Adopted sign convention: a) positive frame displacement b) negative frame displacement

A positive displacement implies continuous diagonal in compression and discontinuous diagonals in tension. Table 12 summarizes conventions adopted for quantities measured during tests.

Element	Symbol	Sign	Meaning
Horizontal displacement of the frame	δ	+	Frame displacement on the right
			Compressed continuous diagonal
			Tension discontinuous diagonal
			Beams strain gauges in compression
		-	Frame displacement on the left
			Tension continuous diagonal
			Compressed discontinuous diagonal
			Beams strain gauges in tension
Applied load	V	+	Horizontal displacement of the frame on the right
		-	Horizontal displacement of the frame on the left
Compression on continuous diagonal	N_{CON}	+	Horizontal displacement of the frame on the right
Tension on continuous diagonal		-	Horizontal displacement of the frame on the left
Compression on discontinuous diagonal	$N_{DIS1}; N_{DIS2}$	+	Horizontal displacement of the frame on the right
Tension on discontinuous diagonal		-	Horizontal displacement of the frame on the left
Diagonal inflection in-plane	γ	+	Displacement of the measurement point to the lower beam

Table 12. Sign convention of test parameters

5.3. Performance states

Here they are presented a general and theoretical description of performance states that were identified based on the expected yield and failure mechanisms of the system. There are two tiers of yield mechanisms: primary and secondary. The primary yield mechanisms are brace buckling and yielding. Secondary yield mechanisms are those which occur in the rest of the system components and connections after primary yielding initiates. Yielding in the gusset plates, yielding in the framing members, interface weld cracking and separation, and bolt-hole elongation are secondary yield mechanisms. Failure modes occur when significant system strength is lost. Brace fracture occurs when there is complete fracture of the brace through the cross section. This usually occurs after there is excessive local buckling at the plastic hinge location and a crack initiates, a tear forms and fracture occurs. Failure modes may also be gusset plate weld fracture and shear tab bolt fracture. Other failure modes including brace fracture at the net section, fracture of beams or columns and tearing of gusset plates, however these modes of failure were not observed during these tests. Performance states are used to describe the state of damage. Yielding (i), buckling (ii) and fracture (iii) are the mechanism performance states. Brace fracture, shear tab bolt fracture and weld crack initiation and separation are failure mode performance states. The performance states are separated into an initial (1), moderate (2) and severe (3) level to quantify degree of damage.

i. *Yielding*

Yielding occurs in the braces, gusset plates, framing elements and connections. Yielding in the brace is estimated by strain gauge measurements. The gusset plates yield significantly, as resulted by test 14, and with clear progression through the performance state levels. Yielding also is found in the framing members and connection elements. Yielding also occurred around the bolt holes connection. Typically the yielding occurred in the column web in the area between the gusset plate connection and the work point of the brace. Yielding also occurred in the column flanges when bending of the column occurred.

ii. *Buckling*

Buckling performance states are defined by the degree of deformation and are in the initial, moderate and severe range. The compressive resistance of the brace is slightly reduced after in-plane buckling deformation level. The severe buckling state occurs when the buckled shape of the member takes on a new form. The normal buckled shape has a smooth curve profile but a plastic hinge begins to form when the $P-\delta$ moments increase and exceed the plastic capacity of the brace. When the buckled member hinges the shape takes on a more triangular form and loses its smooth curve. This “triangular” form concentrates inelastic strains into the plastic hinge of the brace.

iii. *Fracture*

Brace fracture occurs when a tear propagates through the entire cross section of a member. Brace fracture often occurs at a plastic hinge where the cross section of the brace is subject to extremely high local stresses and deformation. Fracture can occur in any structural member or system component however only brace, weld and bolt fractures were noted in this research.

iv. *Bolt Hole Yielding, Elongation and Fracture*

Shear plate connections were used for beam-column connections. These connections are known to be relatively flexible but to have significant moment resistance at large connection rotations. With these connections at high drift levels, yielding is concentrated around the bolt holes. This yielding is observed in the whitewash around the bolts and in line with the bolts. Bolt hole elongation occurs which lessens the stress on the bolt but eventually shear fracture, SF.

5.4. Test 1: X-shaped frame 2L60x8



Figure 67. 2L60x8 X-braced frame specimen on test bench

5.4.1. Loading history

Test 1 was performed after bench assessment. Control system and recording devices have been checked as well as precautions adopted. Once the loading protocol have been activated, stresses developed into sections. From third loading cycle, some imperfections results in loading mechanism. The actuator was applying displacement to the structure without loading it. Test protocol was revised slightly for subsequent testing because of irregularities noted in the actuator performance. Checking the connection node, the transfer beam was not complete adherent to the frame. The floating clearance in the load transfer node was avoided using thin steel sheets. Furthermore, bolts has not been pre-stressed as well as indicated by standards prescriptions. Precautions was adopted starting from the second test. *Figure 68* show loading history while *Table 13* lists displacements applied.

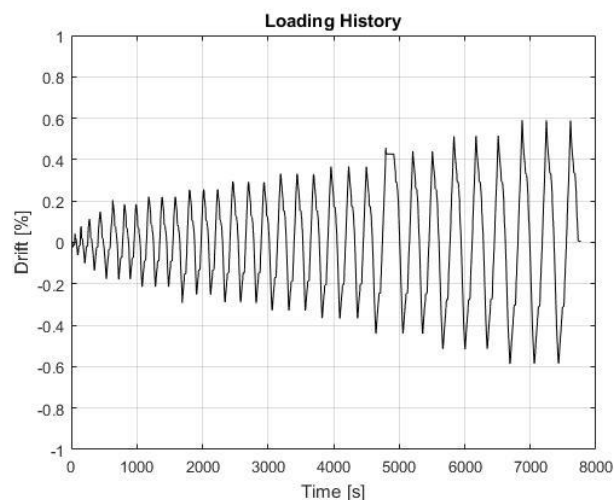


Figure 68. Loading history

Displacement step	Cycles	Cumulative n. of cycles	Displacement [mm]	Drift [%]
1	1	1	± 1	± 0.04
2	1	2	± 2	± 0.08
3	1	3	± 3	± 0.12
4	1	4	± 4	± 0.15
5	3	7	± 5	± 0.19
6	3	10	± 6	± 0.23
7	3	13	± 7	± 0.27
8	3	16	± 8	± 0.31
9	3	19	± 9	± 0.35
10	3	22	± 10	± 0.38
11	3	25	± 12	± 0.46
12	3	28	± 14	± 0.54
13	3	31	± 16	± 0.62

Tabella 13. Test 1: displacement cycles

5.4.2. Global overview

The X-braced 2L60x8 frame was the first specimen to be tested. Initial stiffness has been derived from force-drift ratio graph related to initial steps. Slope of the curve, due to the presence of the pinching zone in the plot (the flatter zone at zero force highlighted in *Figure 69*), has been calculated following the scheme reported in the graph, through the equation:

$$SLOPE_{tens} = \frac{y_1 - y_2}{x_1 - x_2}; SLOPE_{compr} = \frac{y_4 - y_3}{x_4 - x_3};$$

It reached 78.5 kN/mm for frame in tension and 72 kN/mm in compression. The slightly asymmetrical trend could be related to imperfection in adherence at interface transfer beam-frame and sliding effects. The stiffness degradation was influenced by severe drift inducing yielding processes and plastic deformation in the specimen.

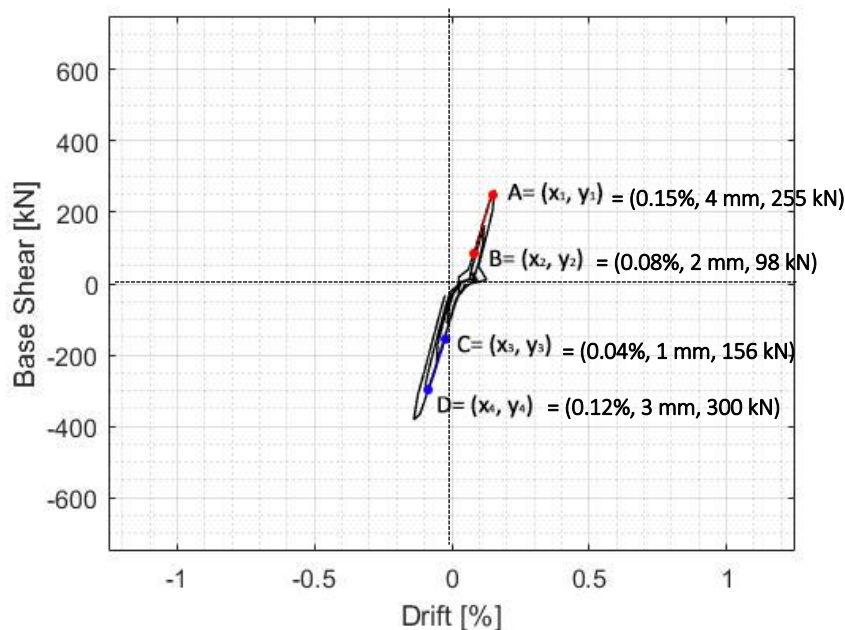


Figure 69. Initial step hysteresis loops- Coordinates for initial stiffness

Total frame hysteresis loops are reported in *Figure 70*, representing the force-drift ratio graph. Force-drift relationship indicates the inelastic deformation behaviour of the specimen. Total resistance of the frame was +485 kN and -690 kN.

Plot of force-drift ratio highlights evident dissipative phenomena (*Figure 70a*) connected to bolts slip, mainly due to a insufficient pre-tension procedure of bolts. Furthermore, local-buckling occurred along continuous diagonal during first tension peak of ± 5 mm cycle ($\pm 0.19\%$ drift) and ± 10 mm cycle (drift $\pm 0.38\%$), decreasing the bearing capacity of the whole frame, from 300 kN to 210 kN (-30%) and from 430 kN to 375 kN (-13%), respectively. After that, structure was yet able to regain its resistance thanks to hardening processes. Moreover, during last cycles, frame resulted loaded also if displacement was zero.

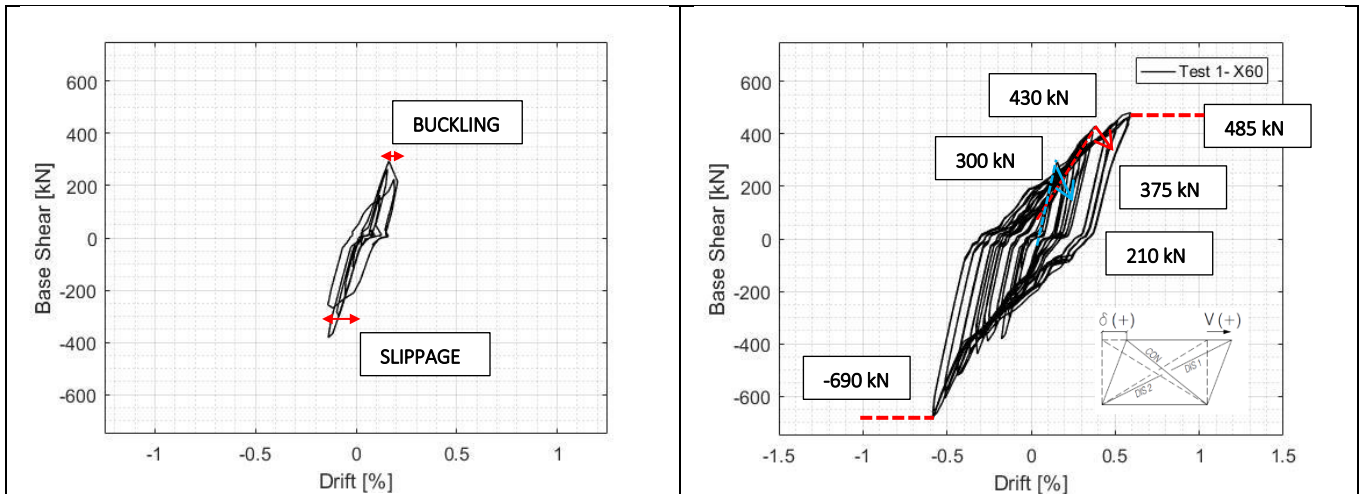


Figure 70. a) Frame hysteresis loop . b) Initial steps-global.

5.4.3. Columns

Trend of forces distribution in columns during tests followed what happened in bracings. Peak values followed by a reduction in bearing capacity, occurred simultaneously to brace buckling. Thus, stiffness lost after bracing instability made structure more narrow and free to rotate without inducing severe loads in columns.

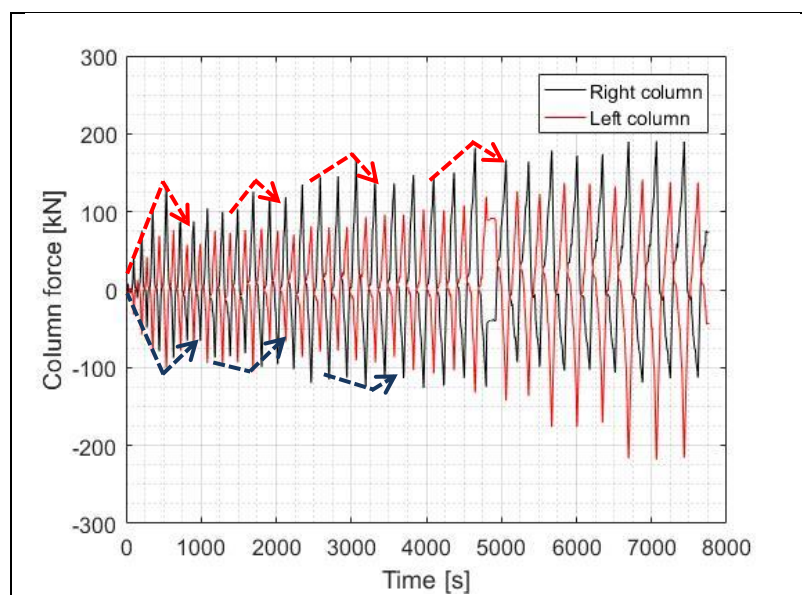


Figure 71. Load trend on columns.

5.4.4. Bracings behaviour

The balanced approach establishes a hierarchy of yielding to maximize the total ductility and inelastic capacity of the system. A sequence of desirable yield mechanisms can then be achieved prior to system failure. The desired controlling failure mode of the system is brace fracture after significant inelastic deformation has occurred. Specimen of test 1 was not loaded up to failure, but consistent plastic deformations have been appreciated among bracings.

Plot of bracing forces-time shown in *Figure 72*, describes the trend of axial forces into diagonal elements during tests. Instability effects are represented by significant drops in force values, highlighted by the arrows. First buckling occurred in discontinuous diagonal loaded in compression at +200 kN (while frame was under tension). Next cycle the bearing capacity of brace was reduced of about 46%. Trend of both diagonals remained symmetrical till buckling occurred. Yielding by tension have not been observed. During last cycles severe drift range, continuous brace could yet bear in tension 378 kN.

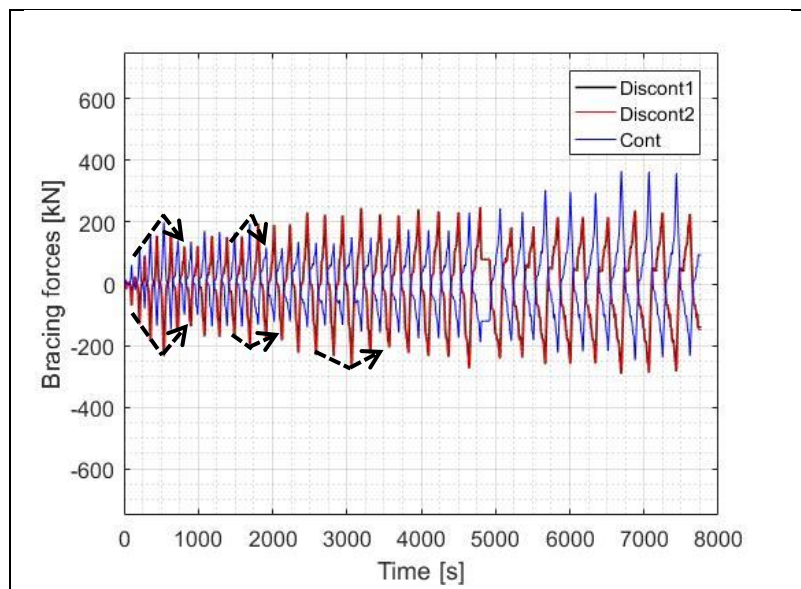


Figure 72. Load on bracings over times. Data derived by strain gauges records.

Asymmetrical trend of the axial forces in CON and DIS bracings has been reported in plots of *Figure 73*. Asymmetrical behaviour is yet particularly clear by base shear-displacement graph, where during last loading cycles specimen has revealed resistances amounting at 485 kN and 690 kN, respectively for tension and compression. The difference reached 205 kN. Higher resistance values have been reached when the continuous diagonal was under tension. The inter-storey drift has then developed buckling on bracings when undergone compression. The asymmetrical trend could be recognised as effect of the asymmetrical geometry of the frame, due to presence of two different diagonals, continuous and discontinuous. Furthermore, intrinsic geometrical imperfections of the frame as well especially the non-complete adhesion at interface between the jack and the frame when load is applied.

Figure 73 shows the axial force trend in each one of the bracings as function of lateral drift. Axial force has been derived from deformations data recorded by strain gauges on diagonals. Axial load graph represents an asymmetrical progress characterized by hysteresis loops, meaning energy dissipation due to combination of several effects such as plasticization, bolts slip or ovalization. Indeed, non-linearity could be connected to slip occurred between bracings and gusset plates. Coupling and frictional forces were overtaken, resulting in slippage and consequent energy dissipation. Thermography photos done during test confirmed the fact showing the heat production at nodes.

Higher values have been noticed comparing tension resistances between continuous and discontinuous diagonals. As results from graphs of axial load-drift ratio of bracings, discontinuous diagonal shows curves characterized by higher amplitude than the continuous one. Final cycle 0.62 % drift presents following characteristic values:

- Axial load amounting at 378 kN in tension, and 250 kN in compression in CON diagonal;
- Axial load amounting at 247 kN in tension, and 295 kN in compression in DIS1 diagonal;
- Axial load amounting at 250 kN in tension, and 300 kN in compression in DIS2 diagonal.

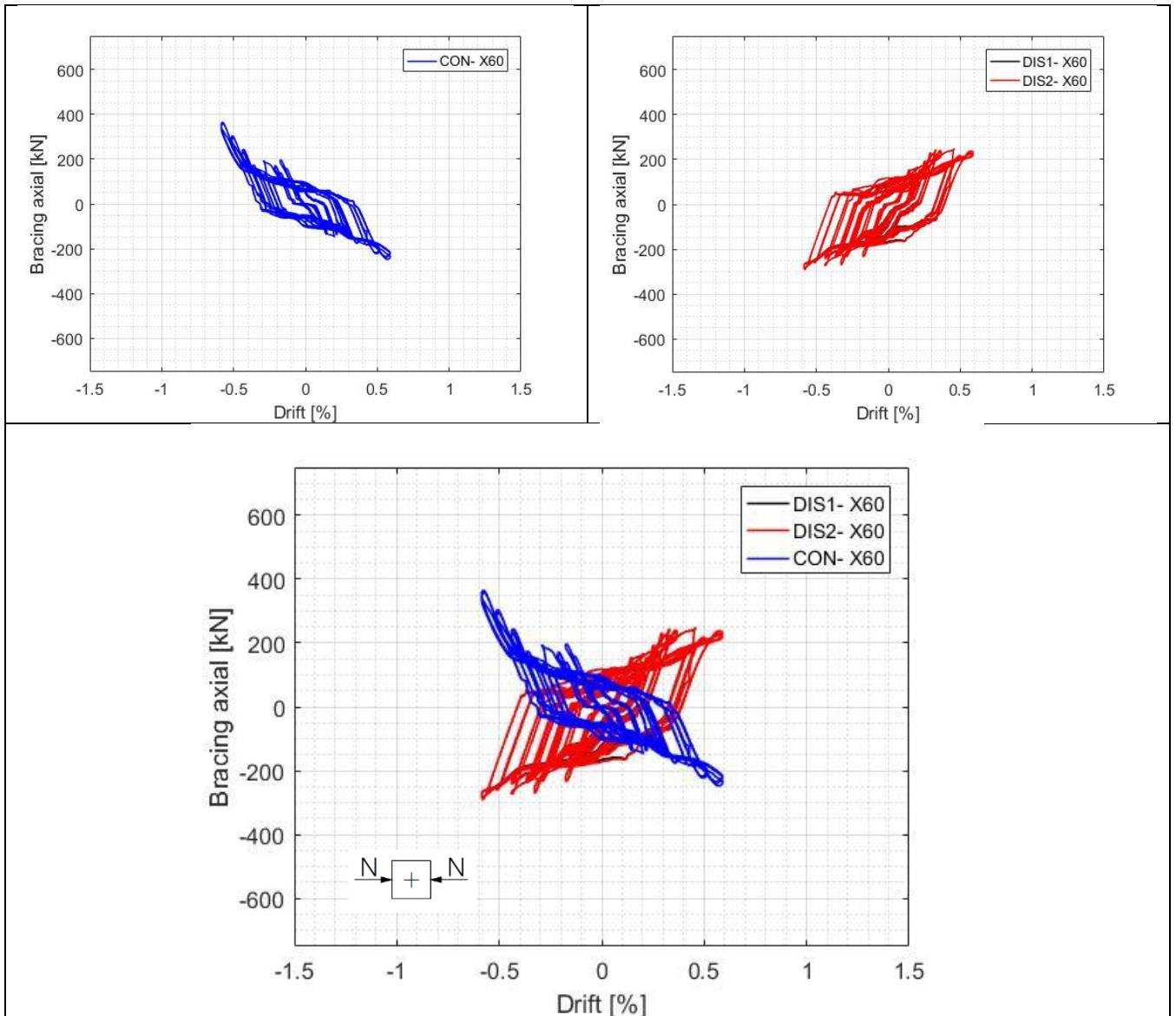


Figure 73. Axial forces over drift applied during test.

5.5. Test 2: X-shaped frame No mid connection 2L60x8

5.5.1. Loading history

After test 1 experience, assessment of the bench, control system and recording devices have been checked as well as standards prescribes. Once the loading protocol have been activated, first negative displacement has been applied to the structure. The floating clearance in the load transfer node was avoided using thin steel sheets. Frame has been undergone to 17 cycles, as reported in *Figure 74* and *Table 14*.

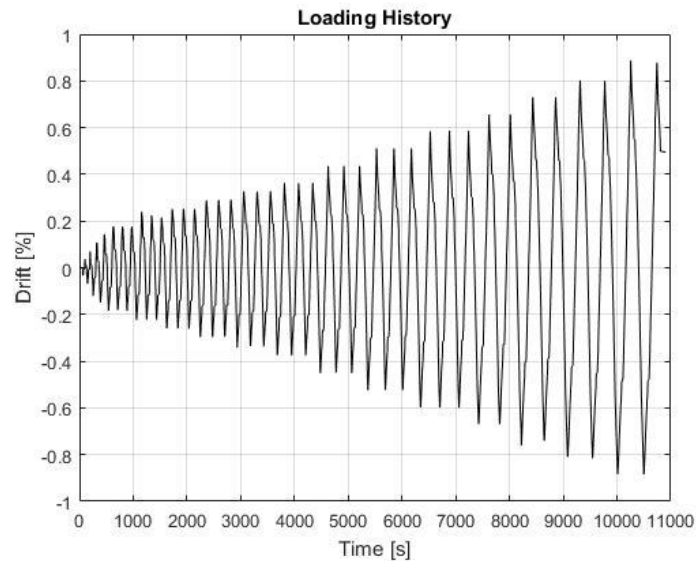


Figure 74. Loading history

Displacement step	Cycles	Cumulative n. of cycles	Displacement [mm]	Drift [%]
1	1	1	± 1	± 0.04
2	1	2	± 2	± 0.08
3	1	3	± 3	± 0.12
4	1	4	± 4	± 0.15
5	3	7	± 5	± 0.19
6	3	10	± 6	± 0.23
7	3	13	± 7	± 0.27
8	3	16	± 8	± 0.31
9	3	19	± 9	± 0.35
10	3	22	± 10	± 0.38
11	3	25	± 12	± 0.46
12	3	28	± 14	± 0.54
13	3	31	± 16	± 0.62
14	3	34	± 18	± 0.69
15	3	37	± 20	± 0.77
16	3	40	± 22	± 0.85
17	3	43	± 24	± 0.92

Table 14. Test 2: displacement cycles

5.5.2. Global overview

Test 2 was done in order to investigate the contribution of the mid-connection to global performances of the frame. Bolts of the continuous brace-mid-plate connection have been removed. Initial stiffness has been derived from initial steps curves of force-drift ratio graph, using same scheme reported in 5.4.2. It amounts at 77 kN/mm for frame in tension and 64 kN/mm in compression. The asymmetrical trend is connected to frame assessment such as residual imperfection in adherence at interface transfer beam-frame and asymmetrical configuration of the bracings geometry (continuous and discontinuous diagonal). No pre-yielding of the frame was observed.

Global behaviour of the frame has been printed and reported in *Figure 75* as force-drift ratio. Force-drift relationship provides an overview about the inelastic deformation behaviour. Total resistance of the frame was +632 kN and -773 kN. Evident slip phenomena carried out from the plot. This claim could be simply verified in bracing forces plot reported in section 5.5.4.

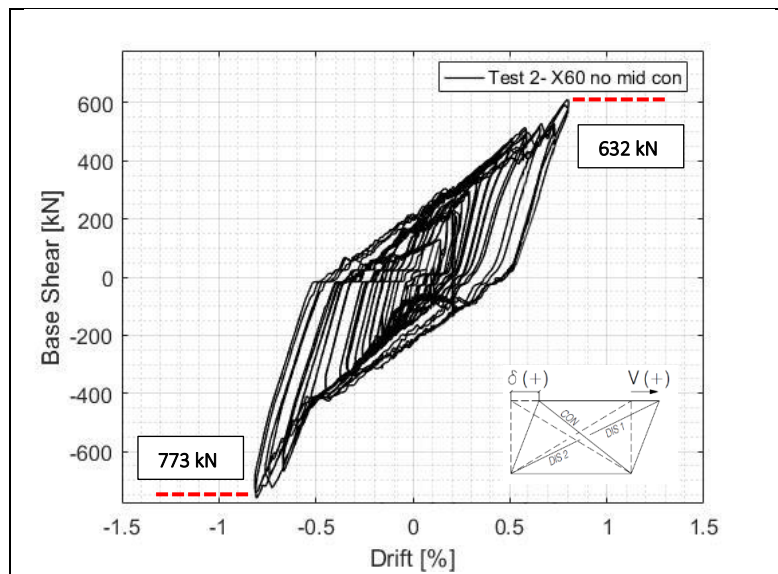


Figure 75. Global test hysteresis loops.

5.5.3. Columns

Trend of axial forces in column, shown in *Figure 76*, remained symmetrical till bracings system behaved as elastic. As soon as buckling occurred, forces in column declined. Last cycles peaks result significant, since left column showcased overloaded compared to the one on the right in which forces decreased. This means that one of the two displacement directions became weaker, due to buckling.

Throughout, forces maximum values oscillated between +156 kN and -144 kN in right column and between +225 kN and -300 kN in left column.

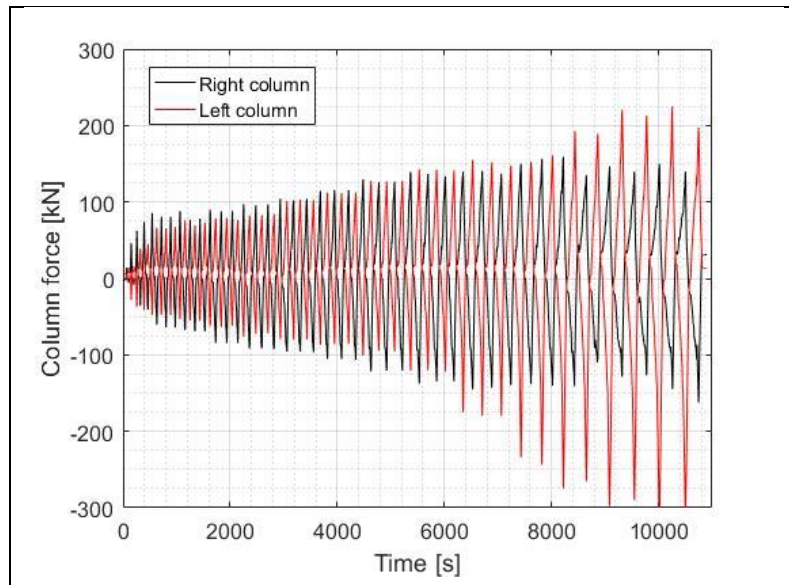


Figure 76. Load trend on columns

5.5.4. Bracings behaviour

Figure 77 shows axial forces on bracing. Continuous diagonal not retrieved instability before last displacement cycle. Conversely, discontinuous diagonal DIS2 started to buckle losing bearing capacity once it has been loaded in compression up to -194 kN, during ± 14 mm cycle (± 0.54 drift). Even if a plastic hinge was formed, DIS2 could yet bear load during post-buckling phase.

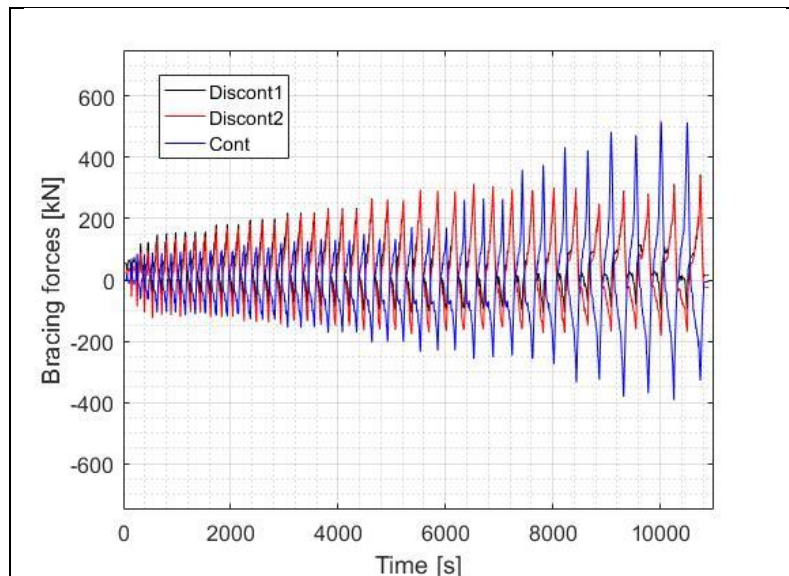


Figure 77. Load on bracings over times. Data derived by strain gauges records.

Deeper check has been done through graphs of Figure 78, where axial action-drift ratio is reported. Differences in resistance between two diagonals could be observed. Continuous diagonal reached +523 kN and -394 kN. While, shorter bracings behaved weaker. Maximum capacity reached under tension was quite similar between DIS1 and DIS2, amounting at about +350 kN. Although, during compression a gap in resistance is noticed. The difference in between was of 50% during last, as represented by flatter curves of DIS1. After plasticization, curves are characterized by a central flatter segment, increasing in slope towards reaching loading peaks. The phenomenon results more evident regarding to continuous brace, than stiffened as soon as tensile stresses increased.

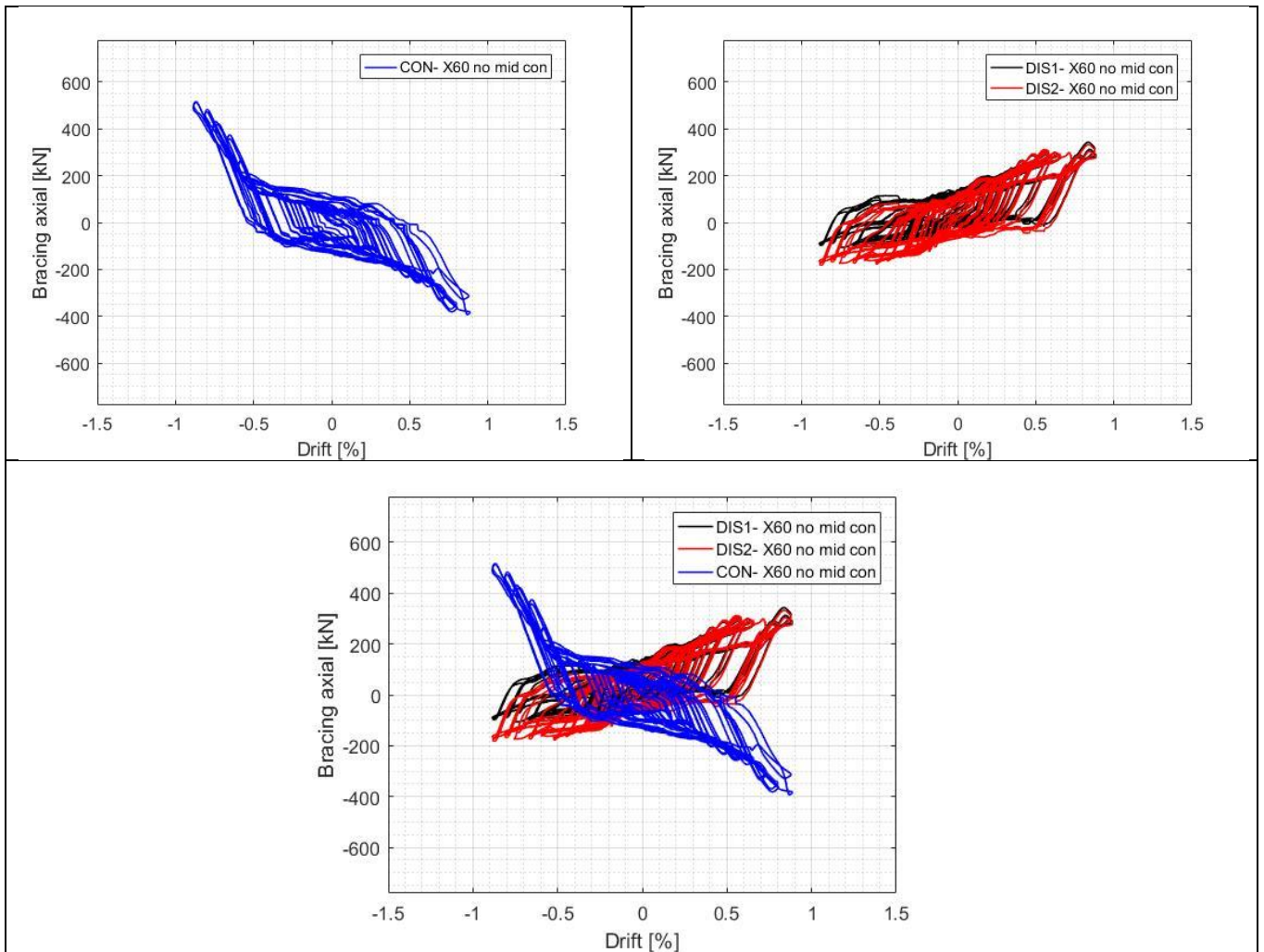


Figure 78. Axial forces over drift applied during test.

5.6. Test 3: Single diagonal moment resisting frame 2L60x8



Figure 79. Specimen on test bench

5.6.1. Loading history

Single diagonal 2L60x8 MRF was tested following displacement control loading protocol of previous tests until 12th cycle. From 13th to 15th cycle only negative displacement has been increased, till reaching -0.77% drift. First in-plane buckling of the bracing occurred during first tension peak of 0.23% drift loading cycle. After that, post-buckling behaviour of the diagonal has been better investigated through four additional cycles. Figure 80 shows loading history while Table 15 provides the schedule of displacement cycles applied.

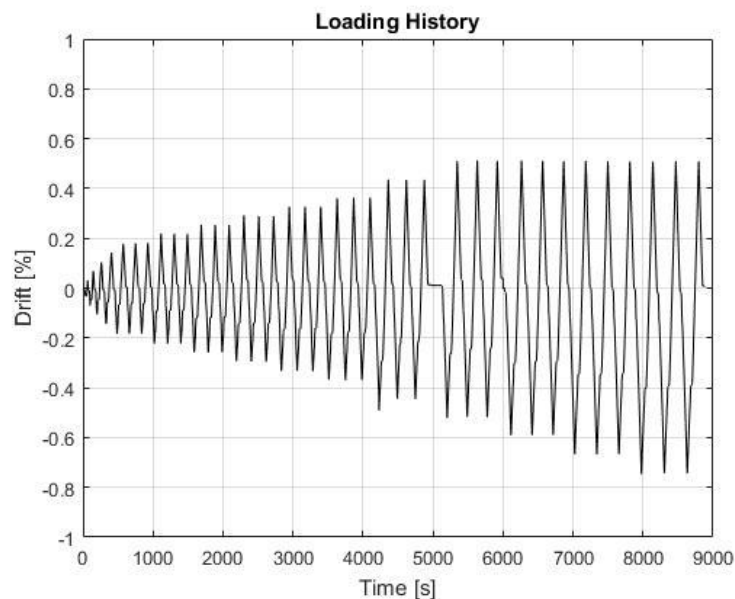


Figure 80. Loading history

Displacement step	Cycles	Cumulative n. of cycles	Displacement [mm]	Drift [%]
1	1	1	± 1	± 0.04
2	1	2	± 2	± 0.08
3	1	3	± 3	± 0.12
4	1	4	± 4	± 0.15
5	3	7	± 5	± 0.19
6	3	10	± 6	± 0.23
7	3	13	± 7	± 0.27
8	3	16	± 8	± 0.31
9	3	19	± 9	± 0.35
10	3	22	± 10	± 0.38
11	3	25	± 12	± 0.46
12	3	28	± 14	± 0.54
13	3	31	-16 +14	- 0.62 +0.54
14	3	34	-18 +14	- 0.69 +0.54
15	3	37	-20 +14	- 0.77 +0.54

Table 15. Test 3: displacement cycles

5.6.2. Global overview

Values derived from slope of curves of initial steps force-drift ratio graph amount at 51 kN/mm for frame in tension and 63 kN/mm in compression. The asymmetrical trend is linked to the configuration of the frame. Single diagonal configuration performs better when continuous brace is stressed by tension, while resulted weaker when the diagonal is under compression since it could easily buckle.

Global force-drift ratio graph has been plotted and reported in *Figure 81*. Frame hysteresis graph explains the inelastic deformation behaviour. Total resistance of the frame was +290 kN and -348 kN. The gap in-between is correct due to the asymmetry of the single diagonal frame, that results weaker in tension loading direction (diagonal under compression). Anyway bearing capacity as well as initial stiffness have been gradually deteriorated during cyclic test, after that buckling of diagonal occurred at the beginning of ±5 mm cycle (0.19% drift). Furthermore, sliding phenomena are highlighted by the plot, especially when frame was being undergone compression (continuous diagonal in tension).

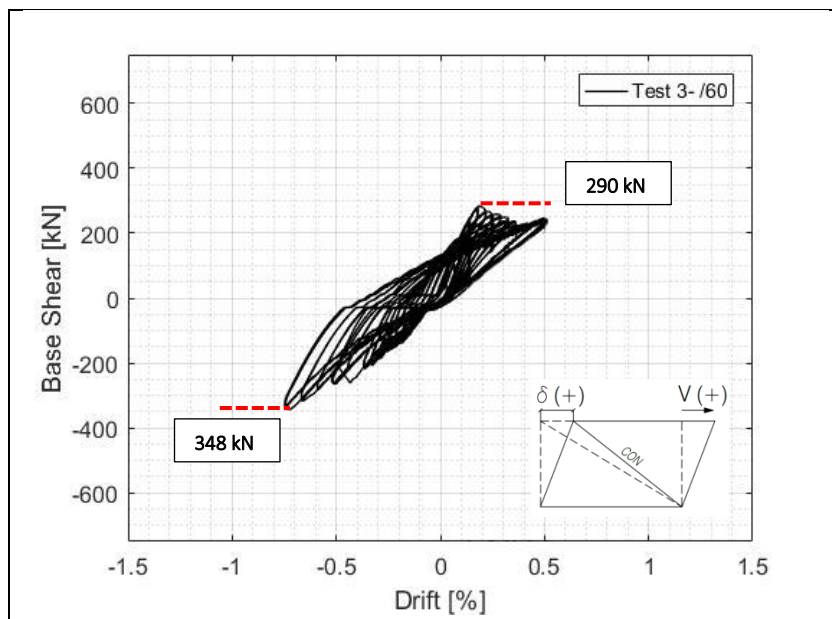


Figure 81. Global test hysteresis loops.

5.6.3. Column and beams

Forces trend in columns results unbalanced between left and right column sides. *Figure 82* shows loads, peaks and valleys. Values was 6 times more higher in left column during initial steps of test. Due to the fact that right column was more free to displace and rotate in single diagonal configuration. Continuous diagonal was connecting the south-east corner (base of right column) with edge of the left column. Thus, no hard actions developed into right column gross-section. On the other side, left column resulted stressed more to tension than compression. This is due to the fact that when the frame was being pushed under compression, continuous bracing carried up a larger portion of forces, unloading the column. While in the reverse direction, brace out came weaker so that loads weighted more on column. Furthermore, after buckling occurred in continuous brace, the abrupt released of loads on frame, caused permanent deformation to right column, that remained loaded under tension up to the end of test. Therefore, while maximum values reached in right column oscillated between +50 kN and -25 kN, on the left loads grew up +150 kN and -75 kN.

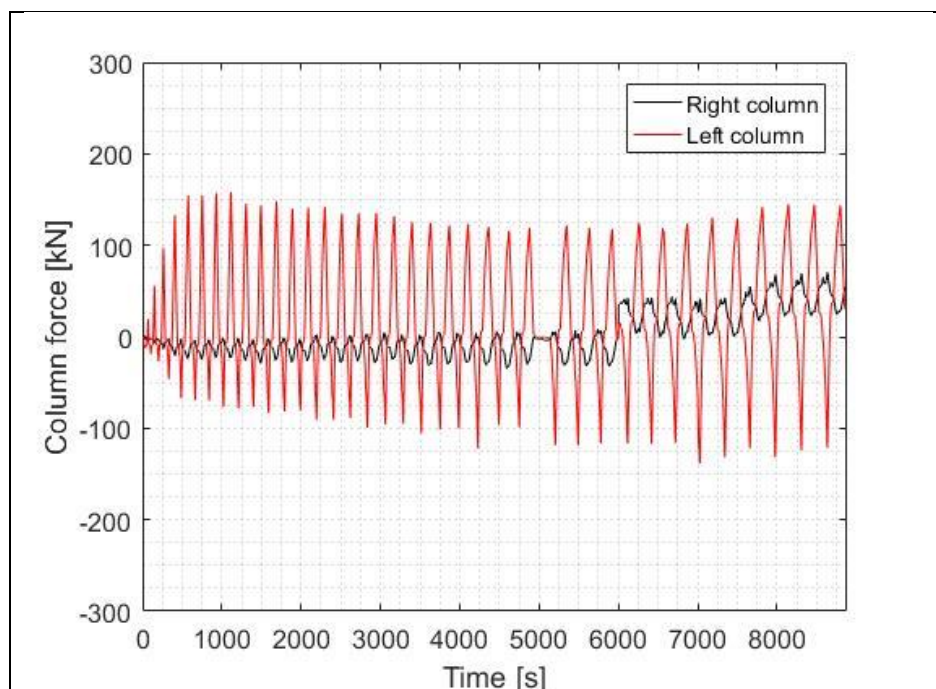


Figure 82. Load trend on columns

5.6.4. Bracings behaviour

Frame has disclosed elastic behaviour until the conclusion of ± 5 mm cycle (distinguishable also by force-drift ratio graph of *Figure 83a-b*). In-plane buckling occurred when frame was in tension, while continuous diagonal under compression. Plastic hinge started to form at mid-span of the brace. Therefore, continuous diagonal began to lose gradually bearing capacity in compression from about 245 kN to 100 kN, with a reduction of 59%. Last cycles have been performed with the purpose to lead the bracing in tension to yielding, even if it has not been joined. Interesting was the fact that it brought yet about 150 kN of loads during compression till tests end even after buckling. Total resistance of the brace during initial steps was +245 kN and -262 kN. Once it buckled, stiffness in compression has been compromised. Bearing capacity during last cycles reached no more than -100 kN in compression, with a reduction of 0.61%.

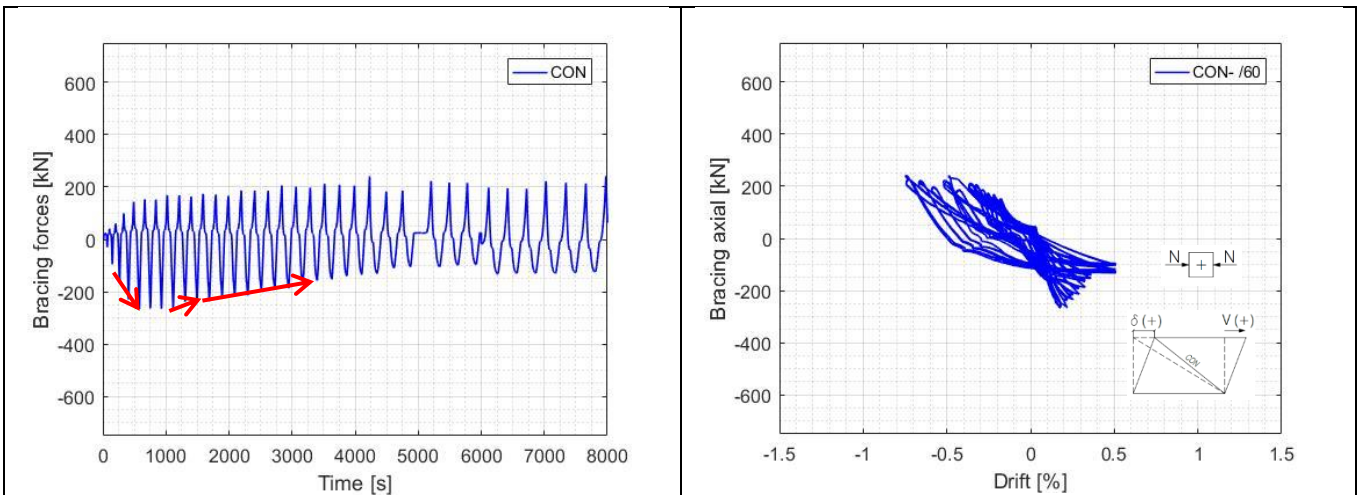


Figure 83. Load on bracings over time and displacement applied.

Brace buckling places large inelastic demands at the middle of the brace, as typically resulting in a plastic hinge at mid-span. Buckling occurred at first tension peak of ± 5 mm cycle. Before instability occurred, brace was bringing in compression about 75% of total load in frame. As diagonal has been losing bearing capacity, loads started to weight mainly on left column during compression phase. The opposite during tensile stresses phase in diagonal, during which rise in forces proceeded in brace and a reduction in the column. Numbers reported in the graph below identify the three trends of elements. Trend described is checked thanks to scheme proposed on the right of Figure 84.

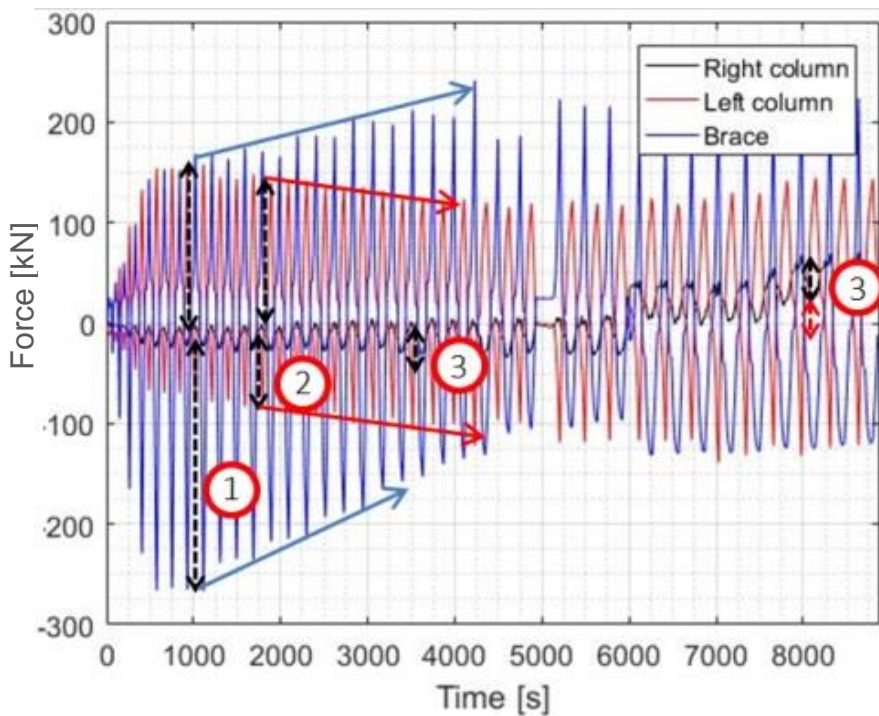
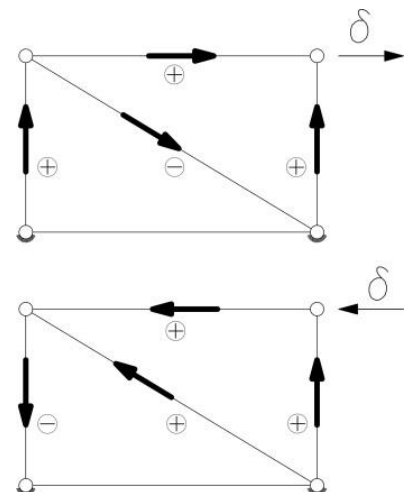


Figure 84. Trend of load on brace and columns. Comparison. Force distribution scheme



5.7. Test 5: X-shaped frame 2L70x7



Figure 85. Specimen on test bench

5.7.1. Loading history

Test 5 has been performed for 22 displacement cycles, pushing and pulling the frame by the actuator for an increasing drift up to a maximum value of 0.46 %. *Figure 86* shows loading history while *Table 16* provides the schedule of displacement cycles applied.

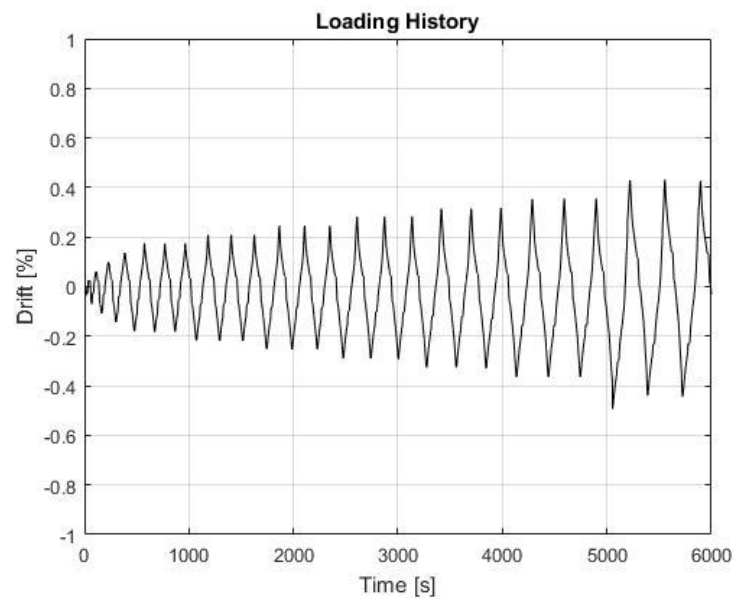


Figure 86. Test 5: loading history

Displacement step	Cycles	Cumulative n. of cycles	Displacement [mm]	Drift [%]
1	1	1	± 1	0.04
2	1	2	± 2	0.08
3	1	3	± 3	0.12
4	1	4	± 4	0.15
5	3	7	± 5	0.19
6	3	10	± 6	0.23
7	3	13	± 7	0.27
8	3	16	± 8	0.31
9	3	19	± 9	0.35
10	3	22	± 10	0.38
11	3	25	± 12	0.46

Table 16. Test 7: displacement cycles

5.7.2. Global overview

Test started applying negative lateral displacement to the frame. The continuous diagonal has been stressed by tension, while the discontinuous by compression. Global behaviour in terms of base shear-drift ratio has been reported in the graph of *Figure 87*.

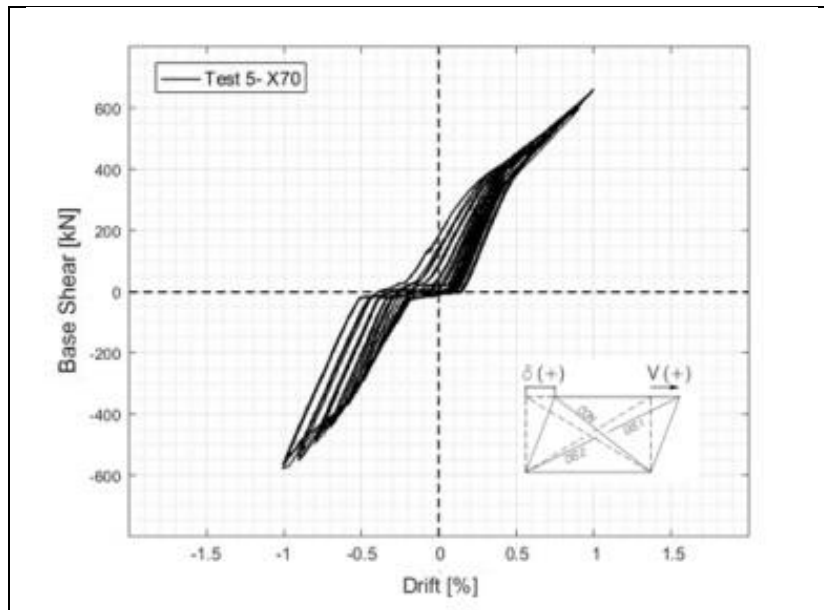


Figure 87. Test 5: global test hysteresis loops.

Higher resistance values were reached when discontinuous diagonal was loaded by tensile stresses, as shown in the asymmetric behaviour clear on *Figure 88a*. The maximum interstorey drift has not developed either buckling or ruptures on bracings. Even yielding has not occurred. Strain gauges data have verified that deformations have not reached values close to the yielding limit. Thus, the asymmetric trend could be recognised as effect of the following causes:

- asymmetrical geometry of the frame, due to presence of two different diagonals, continuous and discontinuous;

- lower compression resistance of diagonals DIS 1 and DIS 2, due to its particular geometrical imperfection;
- intrinsic geometrical imperfections of the frame, especially the non-complete adhesion at interface between the jack and the frame when load is applied;

Asymmetric behaviour is particular clear in last load cycle (drift of 0.38%): specimen has revealed resistances amounting at 565 kN and 665 kN, respectively for tension and compression. The difference reaches 100 kN, equal to 17.5 % in absolut value, between negative and positive displacement applied.

5.7.3. Bracings behaviour

Figure 88 shows the axial force trend in each one of the bracings as function of the lateral displacement applied. Axial force has been evaluated thanks to deformations data recorded by strain gauges on diagonals.

Axial load graph represents a symmetrical and linear progress. Higher values have been noticed comparing the tension resistance between continuous and discontinuous diagonals. Final cycle 0.38 % drift presents following characteristic values:

- axial load amounting at 351 kN in tension, and 354 kN in compression in CON diagonal;
- axial load amounting at 405 kN in tension, and 353 kN in compression in DIS1 diagonal;
- axial load amounting at 417 kN in tension, and 357 kN in compression in DIS2 diagonal;

Non-linearity, clear in the graph, could be probably connected to sliding phenomena happened at nodes bracings-frame.

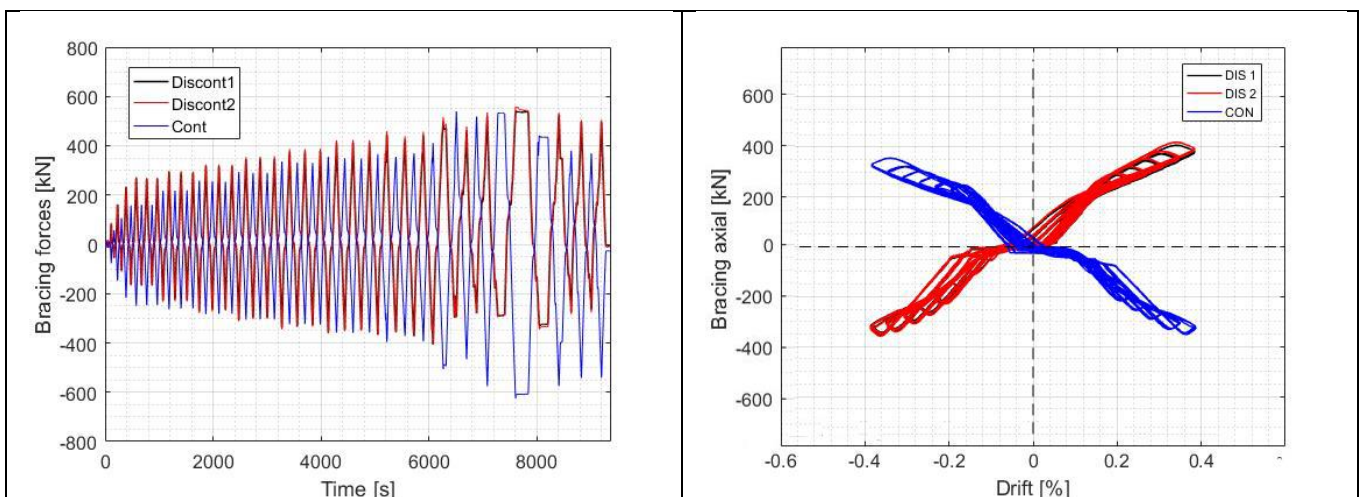


Figure 88. Test 5: axial load over time and displacement imposed (experimental results)

5.8. Test 7: Single diagonal frame 2L70x7

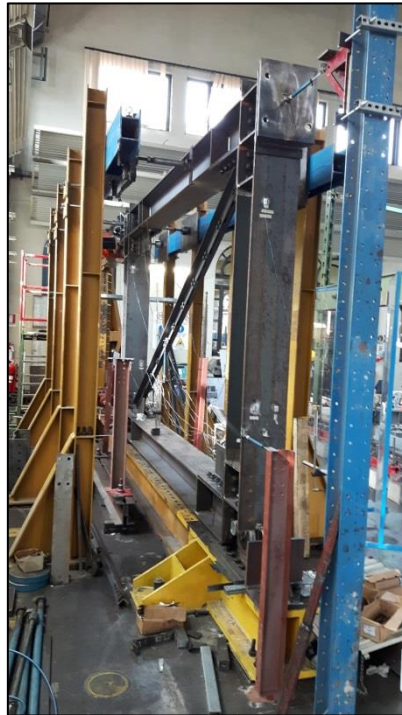


Figure 89. Test 7: Specimen on test bench before test initiation

5.8.1. Loading history

During test 2 frame has been loaded under displacement control for 31 cycles, up to maximum drift of 0.62%; first in-plane buckling of the bracing occurred during first loading cycle of 0.31% drift. Post-buckling behaviour of the diagonal has been better investigated through two additional cycles. A partial collapse of the angle profiles happened at 0.69% of drift. *Figure 90* shows loading history while *Table 17* provides the schedule of displacement cycles applied. *Figure 91* shows specimen before test initiation.

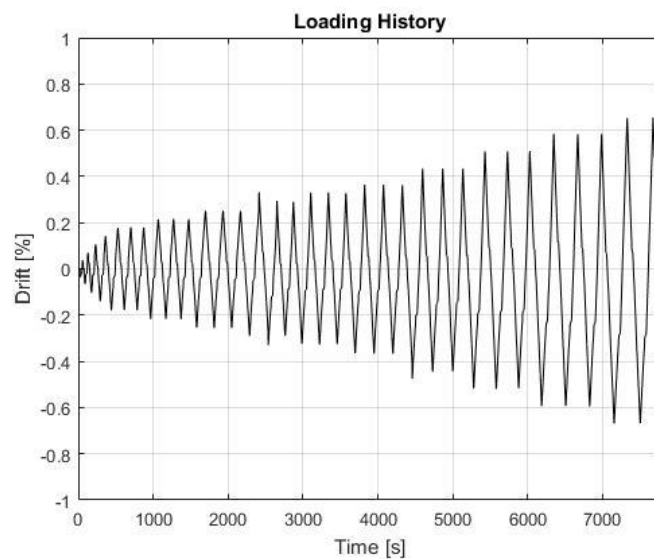


Figure 90 Test 7: loading history

Displacement step	Cycles	Cumulative n. of cycles	Displacement [mm]	Drift [%]
1	1	1	± 1	± 0.04
2	1	2	± 2	± 0.08
3	1	3	± 3	± 0.12
4	1	4	± 4	± 0.15
5	3	7	± 5	± 0.19
6	3	10	± 6	± 0.23
7	3	13	± 7	± 0.27
8	3	16	± 8	± 0.31
9	3	19	± 9	± 0.35
10	3	22	± 10	± 0.38
11	3	25	± 12	± 0.46
12	3	28	± 14	± 0.54
13	3	31	± 16	± 0.62
14	2	33	± 18	± 0.69

Table 17. Test 7: displacement cycles

5.8.2. Global behaviour

Test started applying first negative lateral displacement, putting diagonal bracing under tensile stress. Furthermore, *Figure 91* reports the hysteresis behaviour of specimen in a base shear-drift ratio graph.

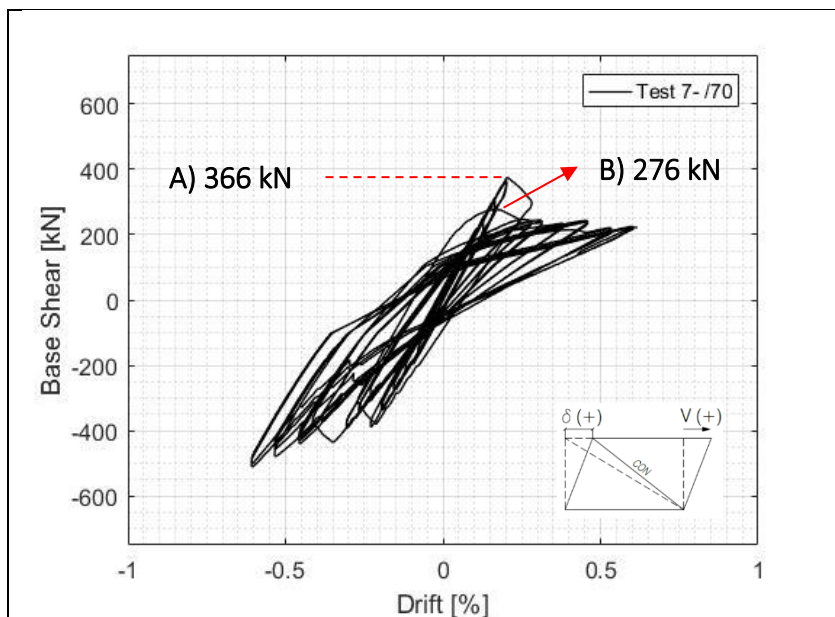


Figure 91. Test 7: Global test hysteresis loops

Frame has behaved completely elastic till ± 7 mm cycle (0.27% of drift). The response of frame was symmetrical, with equal resistance in both the lateral displacement direction. Last ± 7 mm cycle frame reached 337 kN and 366 kN, for compression and tension, respectively. Instability occurred first displacement peak ± 8 mm cycle (0.31% of drift), causing in-plane buckling in correspondence of mid-span of diagonal. Next ± 8 mm cycle, resistance of the frame was strongly reduced. The compression resistance decreased till 276 kN (point B), 26% lower than previous cycles.

Additional 5 incremental cycles was performed, till reaching 0.62% of drift. Geometrical inflexion of brace was continuously increased. Thus, during post-buckling phases, a plastic hinge was formed at mid-span of continuous brace. Moreover, plastic deformation has been observed at ends of the brace, in first bolts of connection with gusset plates. Evidences are reported by photos of *Figure 92* and *Figure 93*. Flexural stiffness of connection joints beam-column-brace become clear analysing *Figure 96*. Real behaviour is significantly different from the ideal hinge behaviour suggested by design phase. Even so at the end of 0.62% drift, brace was bearing 480 kN when undergone tensile stresses, while 220 kN during compression.



Figure 92. Test 7: plastic hinge during post-buckling phase (0.62% of drift)



Figure 93. Test 7: plasticization of diagonal edge (0.62% of drift)

Specimen has been submitted testing till displacement cycle of 0.69 % drift. Hence partial collapse of the diagonal occurred. *Figure 94* shows the brace at test ended, in which rupture is evident. Failure mechanism was developed into two different phases:

1. crack initiation on lower edge of both bracing vertical arms in compression, in correspondence of the hollow section accommodating the bolt;
2. crack propagation during tension stress phase in diagonal, towards perpendicular to stresses direction.

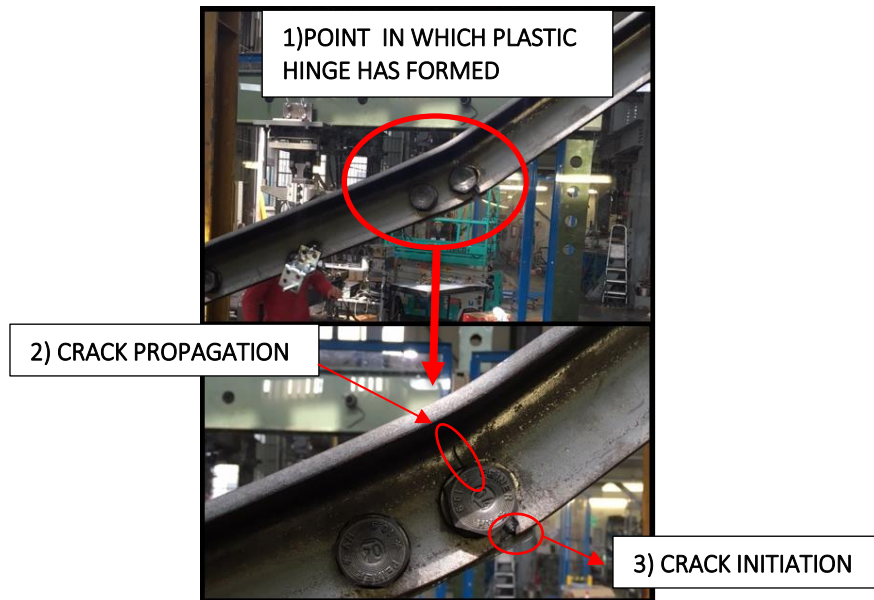


Figure 94. Test 7: collapse mechanism of brace (0.69% of drift)

5.8.3. Bracings behaviour

Observations done till now are detectable in graphs of *Figure 95a* and *Figure 95b*. They focus on axial load function of time and drift, respectively. Axial actions have been derived by strain gauges deformation data. Diagonal demonstrated linear and symmetrical trend till it has reached instability. After that, the capacity in compression was reduced of about 50%.

The drop increased gradually cycle by cycle, till the end of the test, without went to zero. Curves of axial forces function of drift show a flattening from initial to final steps, but despite the fact that diagonal was completely plasticized at mid-span, some residual resistance has been noticed. It carried again about 75 kN under compression.

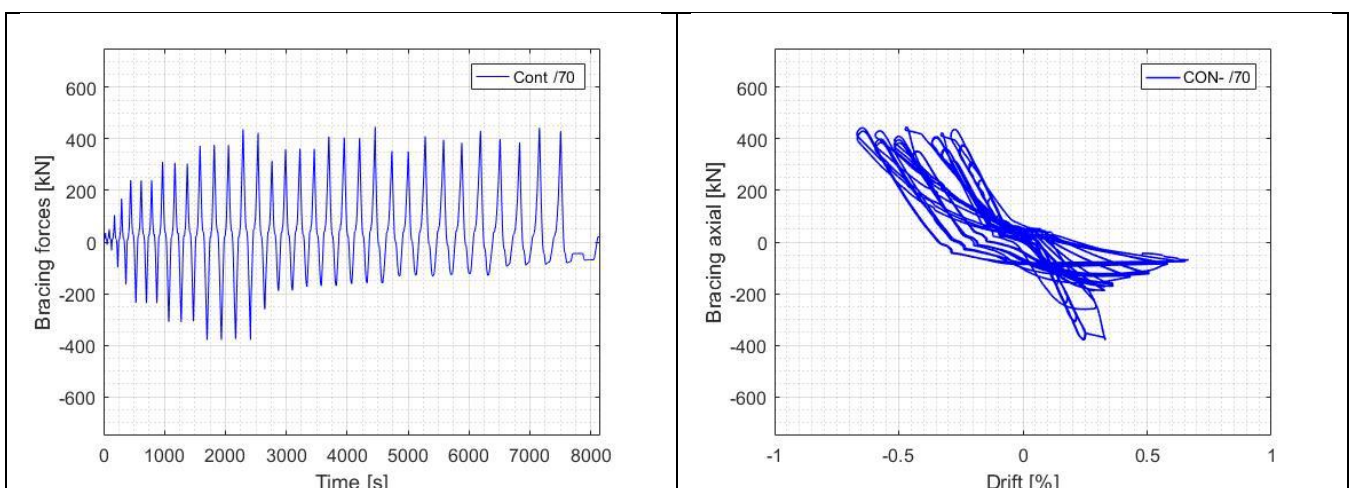


Figure 95. Test 7: diagonal axial load – displacement applied (experimental results)

5.9. Test 15: No-bracings and no-gussets frame



Figure 96. Specimen on test bench

5.9.1. Loading history

Structure without both gussets and bracings was loaded in test 15. Frame was only composed by structural elements columns and beams, and the connecting web angles that allowed relative rotation. Furthermore structure was tested beyond elastic limit of web angles. The 17 displacement cycles of test 15 are reported in *Figure 97* and *Table 18* with respective lateral drift values.

Loading history was modified from previous tests. Lateral drift imposed was characterized by single cycles increasing faster, since there were no needs to analyse incremental behaviour of diagonals.

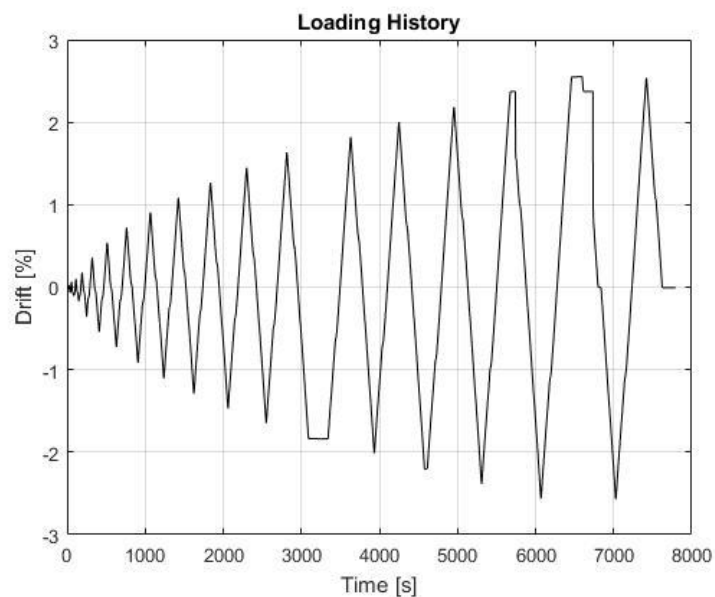


Figure 97. Test 15: loading history

Displacement step	Cycles	Cumulative n. of cycles	Displacement [mm]	Drift [%]
1	1	1	± 1	± 0.03
2	1	2	± 2	± 0.07
3	1	3	± 5	± 0.19
4	1	4	± 10	± 0.38
5	1	5	± 15	± 0.58
6	1	6	± 20	± 0.77
7	1	7	± 24	± 0.92
8	1	8	± 28	± 1.08
9	1	9	± 32	± 1.23
10	1	10	± 36	± 1.38
11	1	11	± 40	± 1.54
12	1	12	± 44	± 1.69
13	1	13	± 48	± 1.84
14	1	14	± 52	± 2.00
15	1	15	± 58	± 2.23
16	1	16	± 64	± 2.46
17	1	17	± 70	± 2.69

Table 18. Test 16: displacement cycles

5.9.2. Global overview

Comparing to frame with either both diagonal configuration or single diagonal, initial stiffness was widely reduced. Only web angles was contributing to oppose resistance to beam-column rotation. The value of initial stiffness derived from force-drift ratio graph of *Figure 98* amount at 2.3 kN/mm.

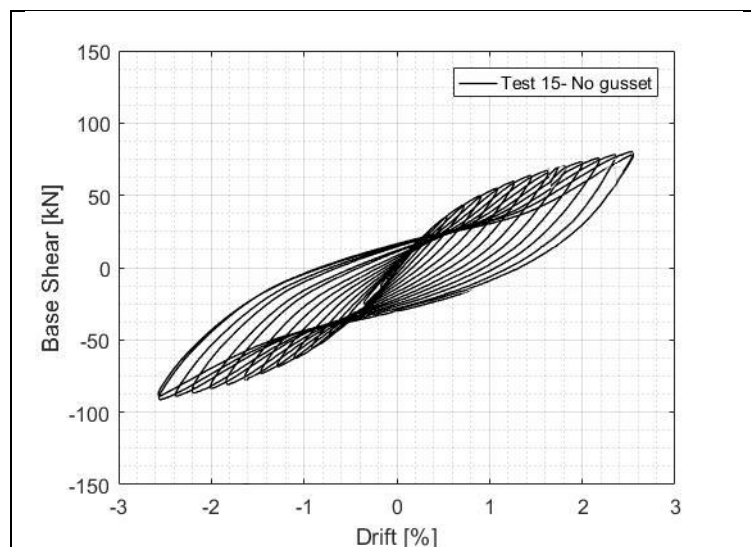


Figure 98. Global test hysteresis loops

Graph of *Figure 98* show complete hysteresis loops of test 15. The performance in stiffness decreased cycle by cycle. Deterioration was linked to yielding mechanism, followed by plasticization, at web angles. Without bulging or hairline cracking, as happened during previous test 14 where web angles was damaged up to open crack phase. In that case, web angles separated in two pieces along the heel between the two arms. Some more resistance was offered by compression contact of the two parts and friction in between. But the useful web angles gross-section resulted opened at the end of the test. The event of the cross-section breakage yet occurred because steel angles were already yielded

by cycles of all tests performed. Before test 15 web angles replaced, in order to test the frame without debilitation or any damages. Stiffness was deteriorating gradually, while the base shear grew up, even if slowly above ± 20 mm cycle. Furthermore, hysteresis plot stated the good ductility of the frame.

Photos of *Figure 99* demonstrates the different situation occurred to web angles during test 14 and test 15, at equal drift imposed. Even if also gusset plates was mounted in test 14, more hazardous damages came off into web angles, just because yet stressed and plasticized by previous tests. Also deformation of tee-section of web angles at column interface, resulting in the typical detachment of vertical heel, was greater. T-stub typical deformation are highlighted by photos of *Figure 99*. Test 15 maximum severance joined 8 mm versus 19 mm of test 14, before cracks opening.

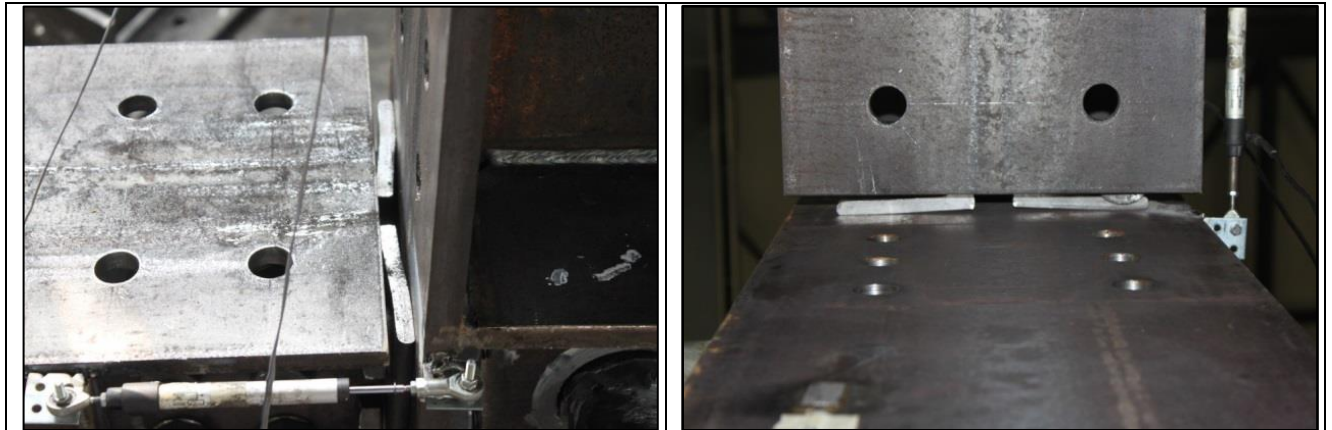


Figure 99. Web angles yielding

5.10. Test 16: No bracings frame

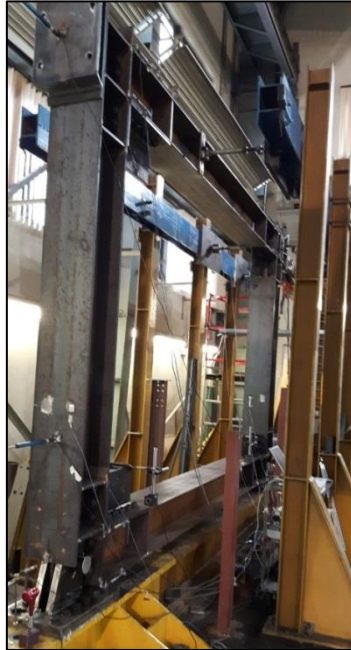


Figure 100. Test 16: specimen on test bench

5.10.1. Loading history

Aim of test 16 was to analyse the behaviour of the structure without the bracing system. Also test 14 was performed with similar configuration, but gusset plates were only kept mounted on the structure without replacing, so that it had all yielding effects collecting during previous tests. Therefore, unblemished gusset plates were installed during test 16. The addition of the gusset plate is theoretically assumed to strengthen the connection and thus the assembly is deemed to comply with the rigid-connection requirements. The 15 loading steps applied are reported in *Figure 101* and *Table 19* with respective lateral drift values. Loading history was different by previous tests. Lateral drift imposed was characterized by single cycle increasing faster, since there were no needs to analyse incremental behaviour of diagonals.

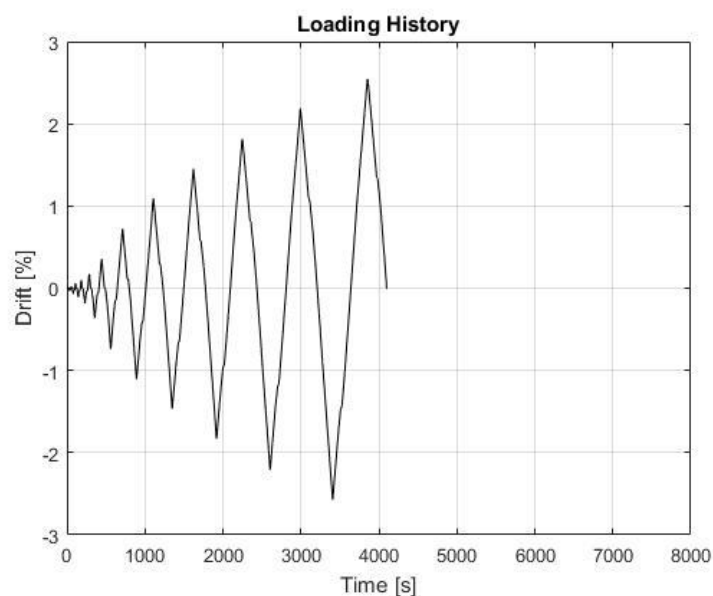


Figure 101. Test 16: loading history

Displacement step	Cycles	Cumulative n. of cycles	Displacement [mm]	Drift [%]
1	1	1	± 1	± 0.03
2	1	2	± 2	± 0.07
3	1	3	± 4	± 0.15
4	1	4	± 10	± 0.35
5	1	5	± 18	± 0.69
6	1	6	± 28	± 1.07
7	1	7	± 38	± 1.46
8	1	8	± 48	± 1.84
9	1	9	± 58	± 2.23
10	1	10	± 68	± 2.61

Table 19. Test 16: displacement cycles

5.10.2. Global behaviour

First negative displacement applied by the actuator to the structure lead the upper beam to move to the left and the columns counterclockwise rotation. *Figure 100* displays specimen on test bench before starting test. Stiffness of the structure was related to the only frame effect. As though rotational stiffness given by web angles and gusset plates. Initial stiffness of test 16 was given only by what is called “frame effect”, naturally existing in concentrically braced frames in the form of beam-to-column shear and gusset plate connections. Force-drift ratio graph of *Figure 102* explains the values that have been used for the calculation. 11,6 kN/mm was reached when frame was under tension and 10,1 kN/mm in compression. Asymmetrical trend is linked to the geometrical imperfections that caused a inhomogeneous application of the load.

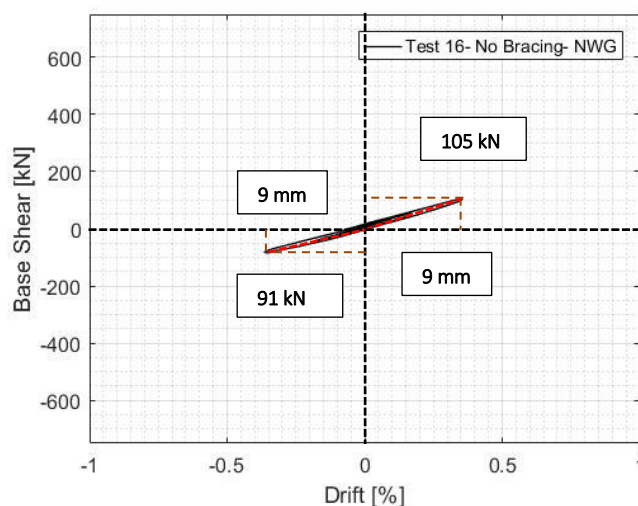


Figure 102. Initial stiffness

Graph of *Figure 103* explains the trend of base shear as function of imposed displacement. Huge differences became evident comparing stiffness of test 16 frame with braced frames of previous tests. Percentage of reduction in resistance reaches more than 50%.

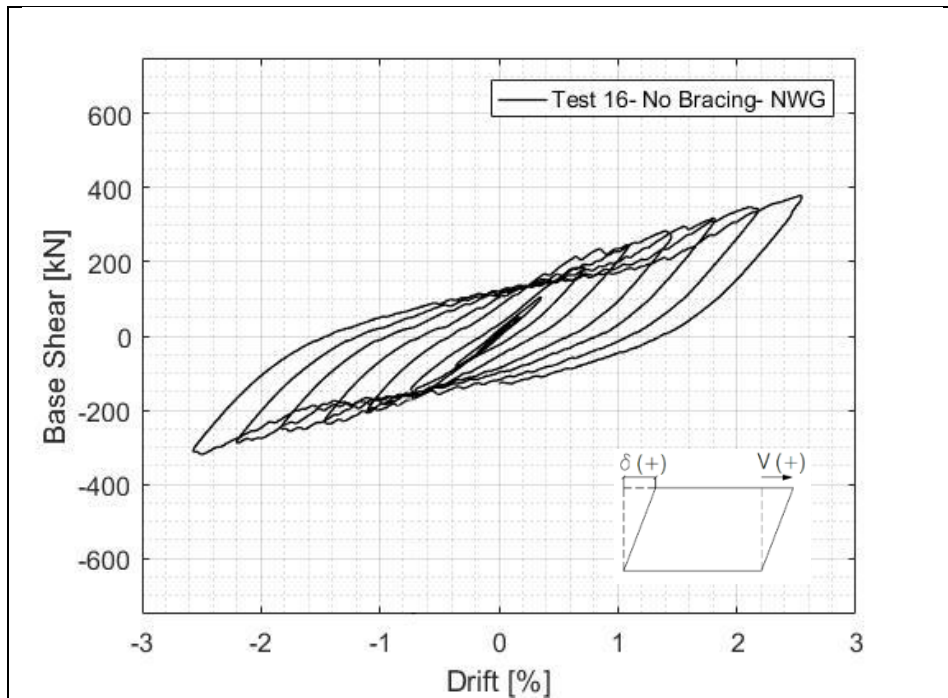


Figure 103. Global test hysteresis loops

Higher resistance has been developed by frame during positive displacement cycles, i.e. during $\pm 2.69\%$ drift cycle, load recorded reached $+379$ kN and -324 kN, for positive and negative displacement, respectively. Because of intrinsic geometrical imperfections of the frame, asymmetry clearly appeared in the hysteresis loops. They caused not uniform application of loads by the actuator. Test was stopped once 1.07% of drift was achieved. Once again at 2.23% drift. Visible deformations occurred into gusset plates at the interface bolted plate-column flanges. Photos in Figure 106, reported below, highlights critical deformations observed during test in the two different stopping times.

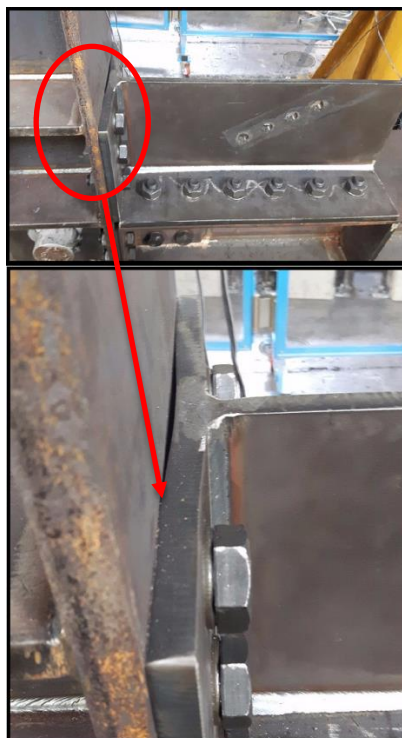


Figure 104. Test 16: gusset plates yielding. T-stub section.

Columns rotation, as well as whole frame displacement, became significant during last cycles applied. Yielding occurred in gusset plates in the mid point of vertical steel plate of the upper arm at interface with column. Globally, data about test performed results very useful. They will be analysed and discussed through Chapter 6, dealing with its benefits as source of reserve capacity provided to the overall structural system. Performances improve, providing extra stiffness and strength to the frame system. It couldn't be yet idealized as a pin. As we will demonstrate in Chapter 6, the detailed connection of bolted and welded plates of gussets designed for beam-column node results an additional safety system after bracings collapse.

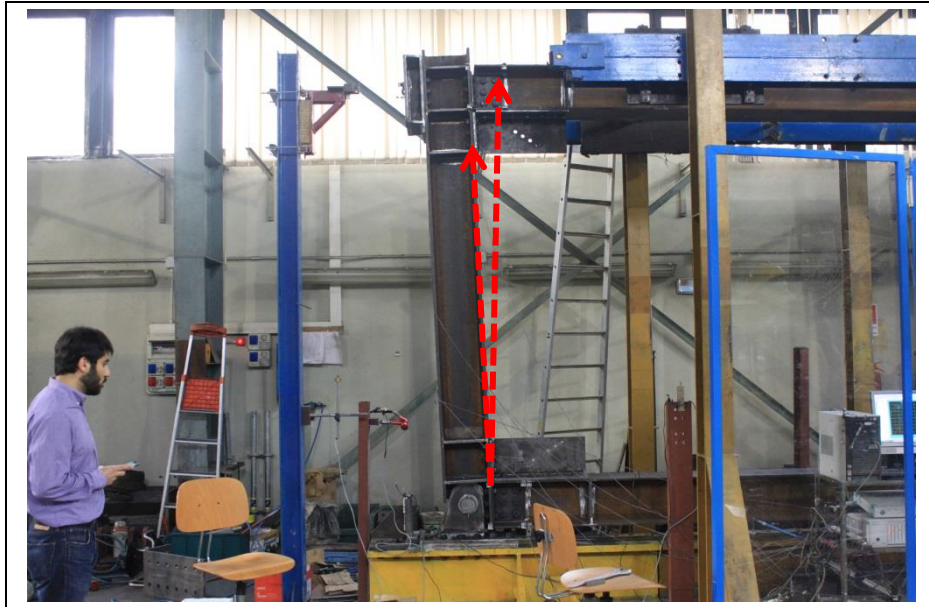


Figure 105. Beam-column node rotation

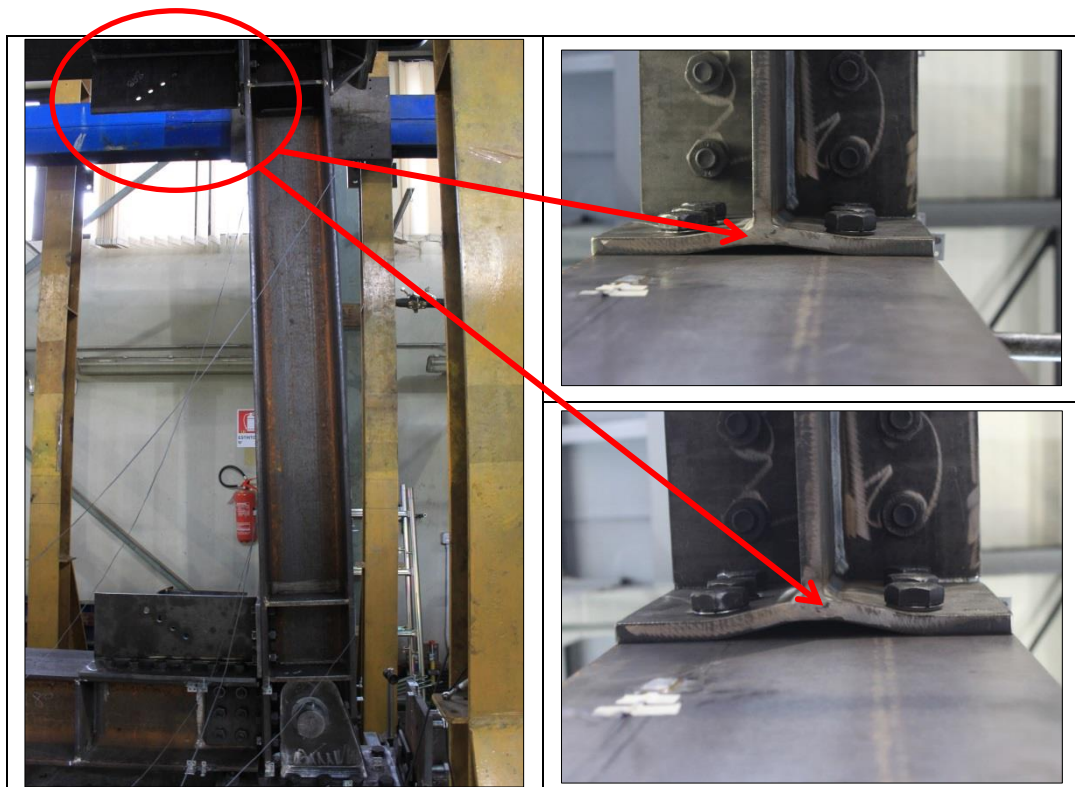


Figure 106. Yielding mechanism of the gusset plates

5.11. Test 13: X-braced frame 2L60x8

5.11.1. Loading history

2L60x8 MRF additional test was done in order to cover lacks of first test, specially checking bolts pre-tension and clearance in load transfer, so to reach more precise results. Thus, it allowed to investigate better the behaviour of the structure till overpassing the elastic limit state. Frame has been undergone up to 68 displacement control cycles, reaching a maximum value of 2,61% of drift. *Figure 107* shows the loading history while *Table 20* more in detail the displacement applied. Yielding, plasticization and bracings failure were reached during test. Post-buckling behaviour of bracings has been investigated in detail.

Bracings instability already occurred at 0.26% of drift. In spite of that, structure was able to recover bearing capacity and hardening cycle by cycle. The process went on till bracings failure, whereupon loads were brought mainly thanks to frame effect.

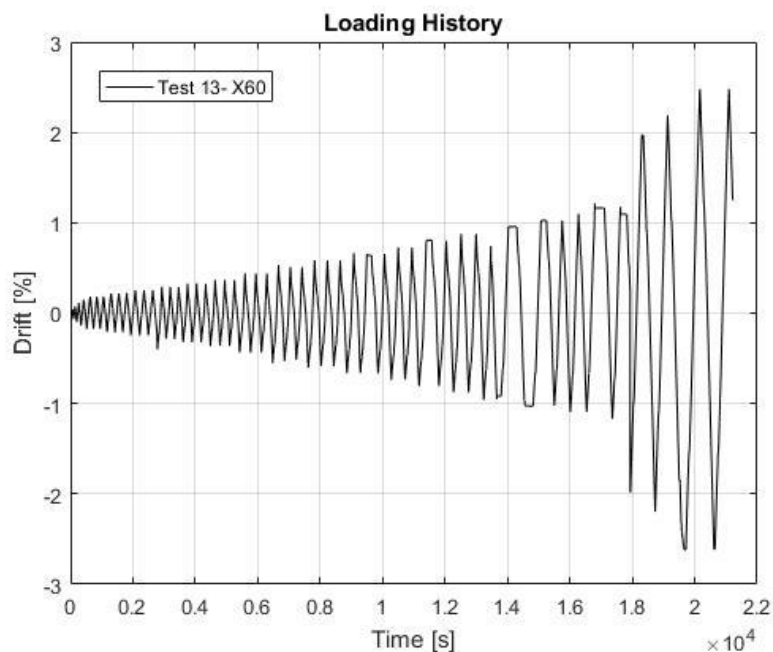


Figure 107. Test 13: loading history

N° of displacement cycle	N° of cycles	Cumulative number of cycles	Displacement [mm]	Drift [%]
1	1	1	± 1	± 0.04
2	1	2	± 2	± 0.08
3	1	3	± 3	± 0.12
4	1	4	± 4	± 0.15
5	3	7	± 5	± 0.19
6	3	10	± 6	± 0.23
7	3	13	± 7	± 0.27
8	3	16	± 8	± 0.31
9	3	19	± 9	± 0.35
10	3	22	± 10	± 0.38
11	3	25	± 12	± 0.46
12	3	28	± 14	± 0.54
13	3	31	± 16	± 0.62

14	2	34	± 18	± 0.69
15	2	37	± 20	± 0.77
16	2	40	± 22	± 0.85
17	2	43	± 24	± 0.92
18	2	46	± 26	± 1.00
19	2	49	± 28	± 1.08
20	2	52	± 30	± 1.15
21	2	54	± 32	± 1.23
22	2	56	± 34	± 1.30
23	2	58	± 36	± 1.38
24	2	60	± 38	± 1.46
25	2	62	± 40	± 1.54
26	2	64	± 42	± 1.61
27	2	66	± 44	± 1.69
28	2	68	± 46	± 1.77
29	2	70	± 48	± 1.85
30	2	72	± 50	± 1.92
31	2	74	+56 -52	+2.08 -2.00
32	2	76	+62 -58	+2.31 -2.23
33	2	78	+68 -64	+2.61 -2.46

Table 20. Test 13: displacement cycles

5.11.2. Global behaviour

Test started applying first negative displacement to the structure. Specimen was undergone compression, so that tensile stresses affected the continuous bracing. *Figure 108* shows the base shear-displacement relation during first loading cycles. Initial stiffness has carried out by calculating slope of the curves and highlighted in the plot, amounting at 88.5 kN/mm when frame was loaded in tension, and 103 kN/mm when undergone compression.

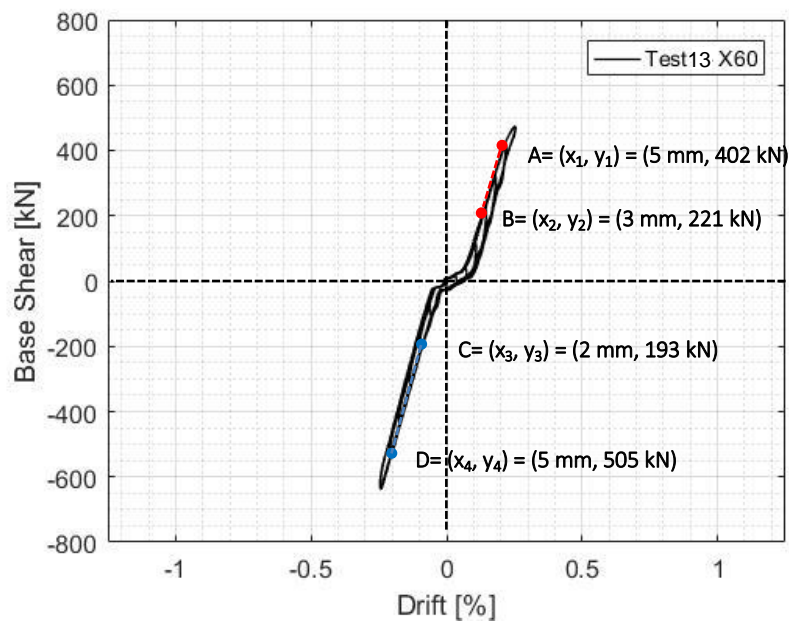


Figure 108. Initial stiffness (plot at first ±6 mm cycle)

Frame behaved as completely elastic up to ± 6mm cycles (0.23% drift), even if the structure didn't exhibit a symmetrical response with base shear values equal in both direction of lateral displacement. At the end of first ±6 mm cycle, frame resistance reached 650 kN when undergone to compression whilst about 500 kN during tension.

Curves of hysteresis loops started to expand in amplitude once first negative peak of ± 8 mm cycle. The curves seems just shifted, recovering its slope just above -450 kN during unloading phase. System dissipated energy in form of slip occurring at brace joints edges and at frame base. LVDT channels confirm that relative displacements have been recorded at several nodes. Both bracings axial load-drift ratio curves were affected by the friction resistance overcoming in correspondence of bolts, that slide into their holes till cover the clearance. Graphs of *Figure 109* show base-shear and bracing axial load over drift applied, plotted for 2800 s time step history.

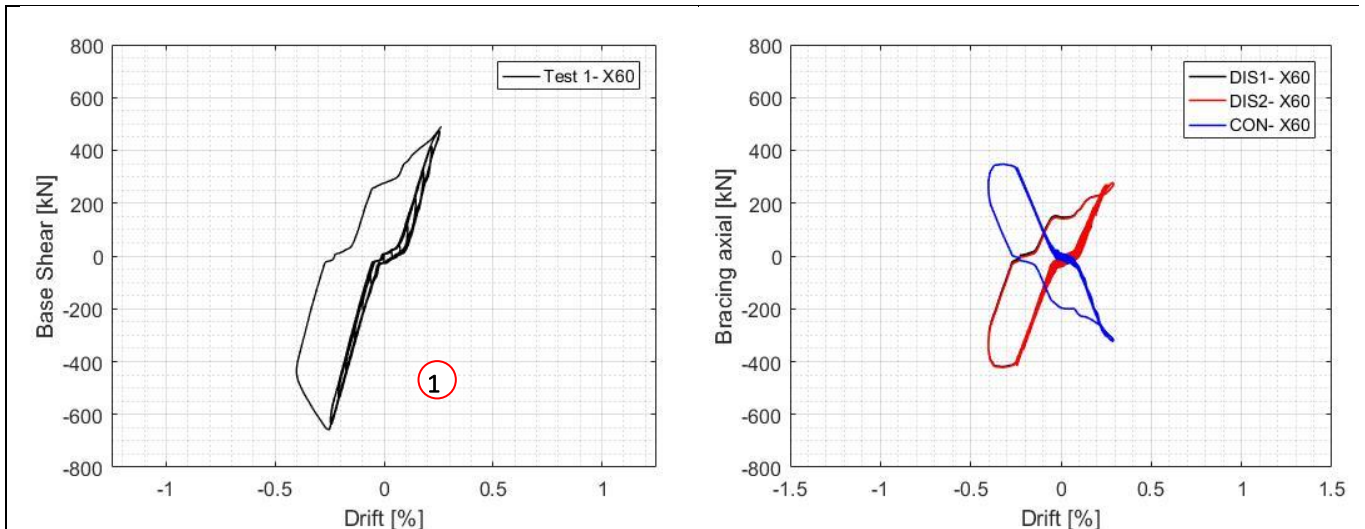


Figure 109. First slip occurred when frame under compression, force peak value 665 kN, drift -0,23% (plot at first compression peak of ± 8 mm cycle) (2800 s time step)

The bearing capacity of the overall structure was decreased of about 61% with respect to the previous cycle. Afterwards first hysteresis was produced resistance moved from 650 kN to 400 kN. Furthermore stiffness of the structure has been affected. Global base shear-drift ratio graph in *Figure 110* demonstrates how during jack compression phase, slope of the curve remains constant till about -300 kN when it decreases forming an horizontal segment that increases again till displacement peak. The trend is linked to the fact that since there is a clearance between the bolt and the hole in which it is fitted, the bearing stress is mobilised only after the plates slip relative to one another and start bearing on the bolt.

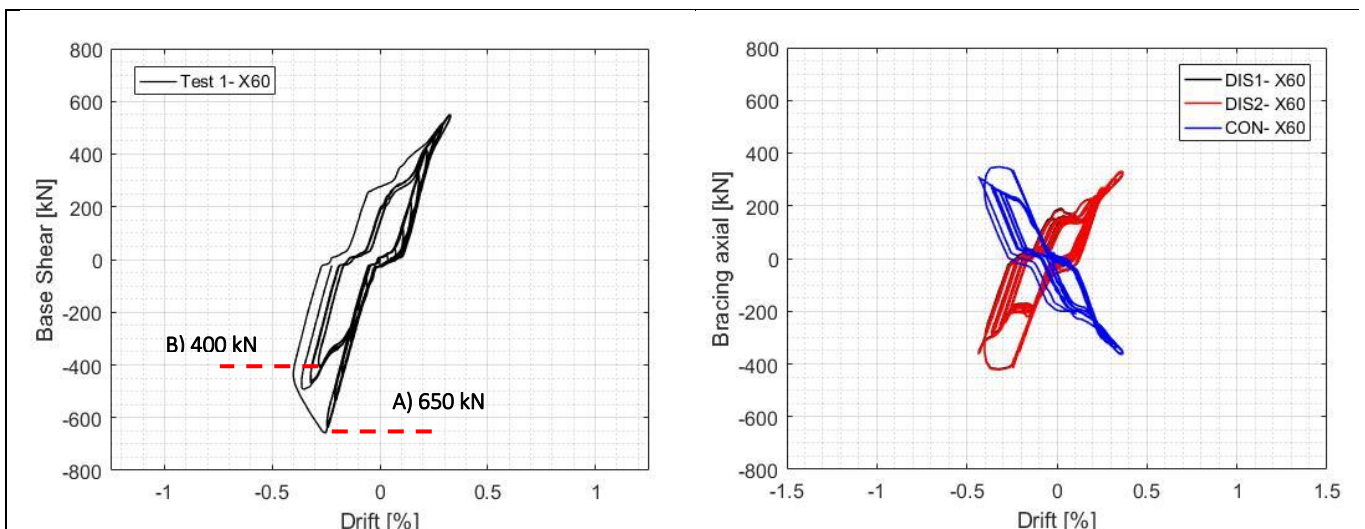


Figure 110. Bearing capacity reduction (plot at first compression peak of ± 8 mm cycle) (5550)

Structure regained strength cycle by cycle till go over maximum value recorded before first hysteresis occurred. Structure to recovered its resistance, as shown in *Figure 111*, and was again capable to support 675 kN of base shear force, before second hysteresis occurred at -0.46% drift. Curves again shifted as effect of bolts slip at connections of the frame elements.

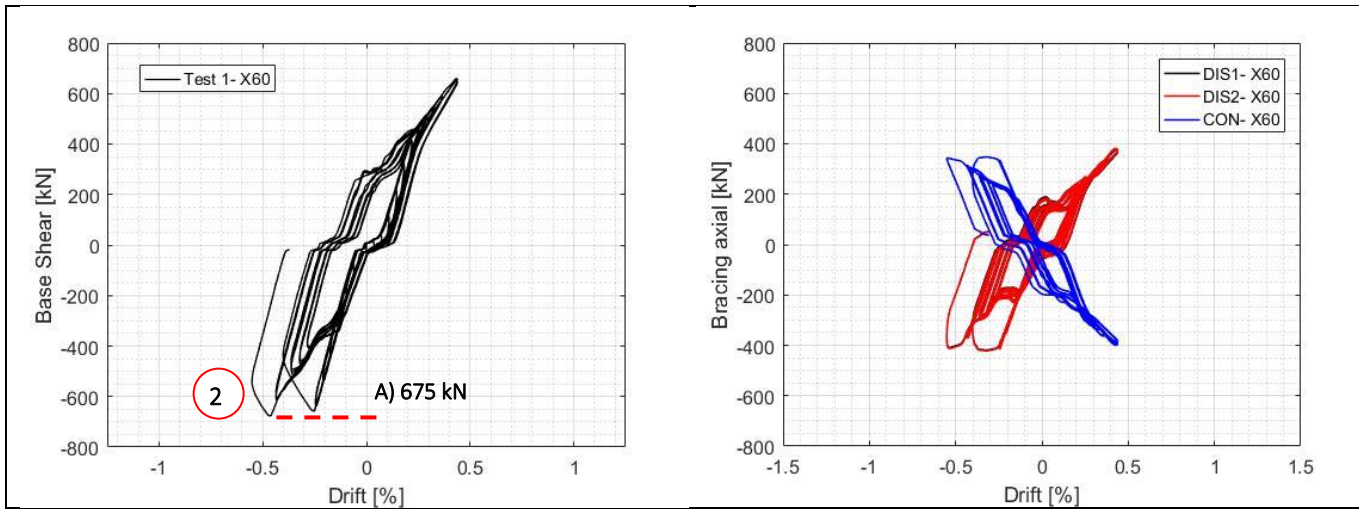


Figure 111. Second slip (plot at first compression peak of ± 12 mm cycle, drift -0,46 %, force peak value 675 kN) (6550 s time step)

First hysteresis while frame was under tension overcame at positive drift of +0.54%. Shifting of the curve is not yet linked to a buckling, but to additional slippage occurred at bracings bolts. Hypothesis has been confirmed by LVDT data.

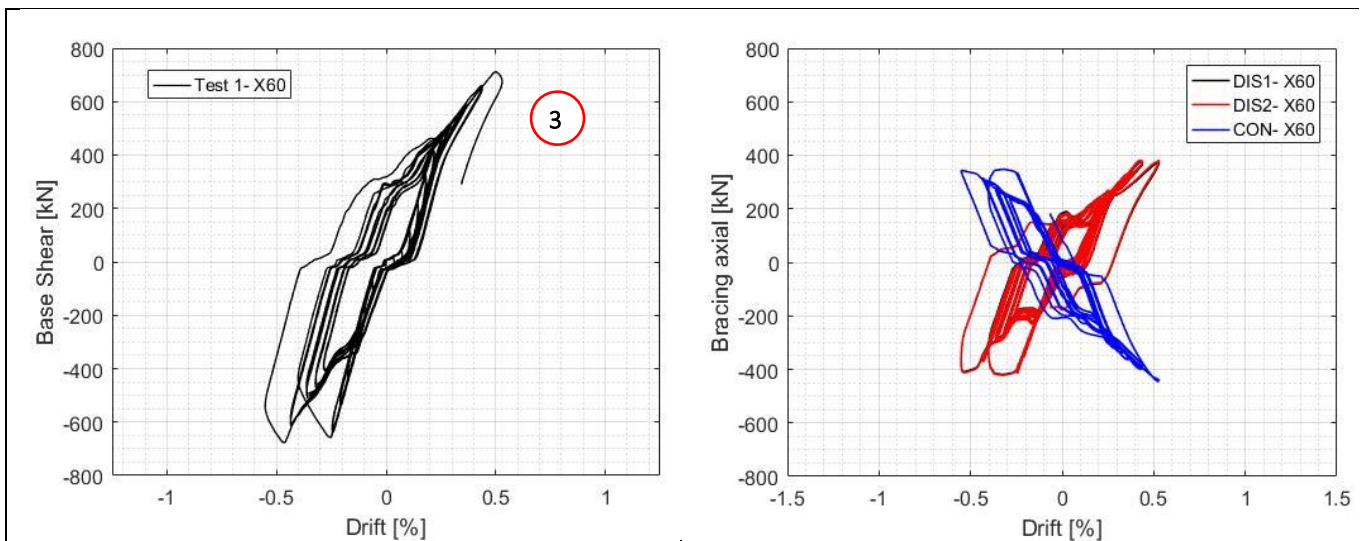


Figure 112. First slip occurred when structure under tension (plot at first tension peak of ± 13 mm cycle, drift +0.51 %, force peak value 703 kN) (6950 s time step)

In-plane buckling occurred at second tension peak of $\pm 0.59\%$ drift cycle (+15 mm). Continuous diagonal under compression buckled in-plane, developing plastic hinge at mid-span. Strength of the structure under tension fell down from 750 kN to 625 kN, with a reduction of 16%. Stiffness was also deteriorated, while frame started to lose bearing capacity for positive displacement applied. Graphs of *Figure 113* have been plotted at cycle after buckling.

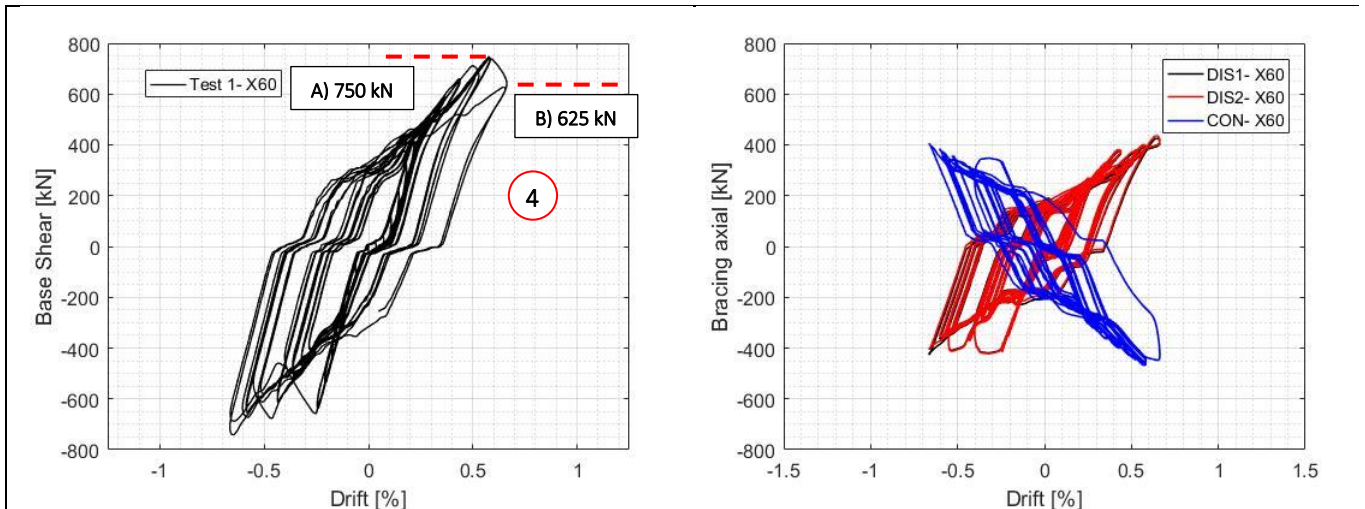


Figure 113. Continuous brace buckling, +0.59% (+15 mm) drift cycle, force peak value 750 kN (9850 s time step)

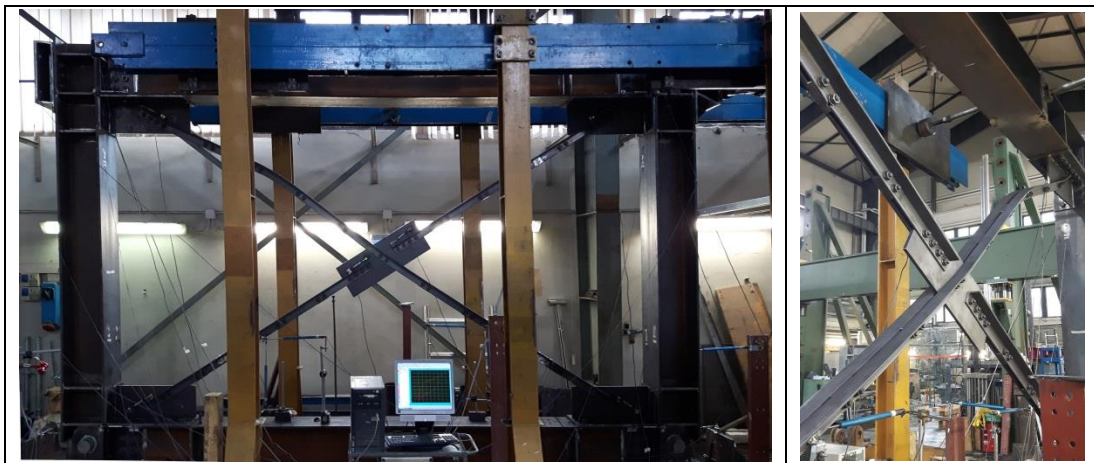


Figure 114. 4. plastic hinge is formed at mid-span of the north-west continuous diagonal

Instability of discontinuous brace occurred while reaching the first negative peak of ± 16 mm cycle. Plastic hinge formed along stitch plate at mid-span of north-east (NE) discontinuous diagonal. Frame lateral stiffness has been so reduced in both directions of loading. Photos below show curvature of the diagonal after buckling.



Figure 115. 5. Plastic hinge formed after first in-plane buckling on mid-span of NE diagonal

Additional loading cycles have been done in order to investigate in deep post-buckling behaviour of the frame. Low cycle fatigue to which frame was undergoing went on plasticizing several frame nodes. Performances continued to degrade cycle after cycle, so that steel frame lose gradually stiffness (slope is highlighted by idealization line in base shear-drift ratio graph of *Figure 116*). Post-buckling phase was characterized by subsequent buckling and plastic hinges formation at several nodes of the structure, among which NE, NW and SW braces joint ends, first connecting bolt of SW brace-mid-plate, and the upper connecting bolt of the continuous diagonal with mid-plate.

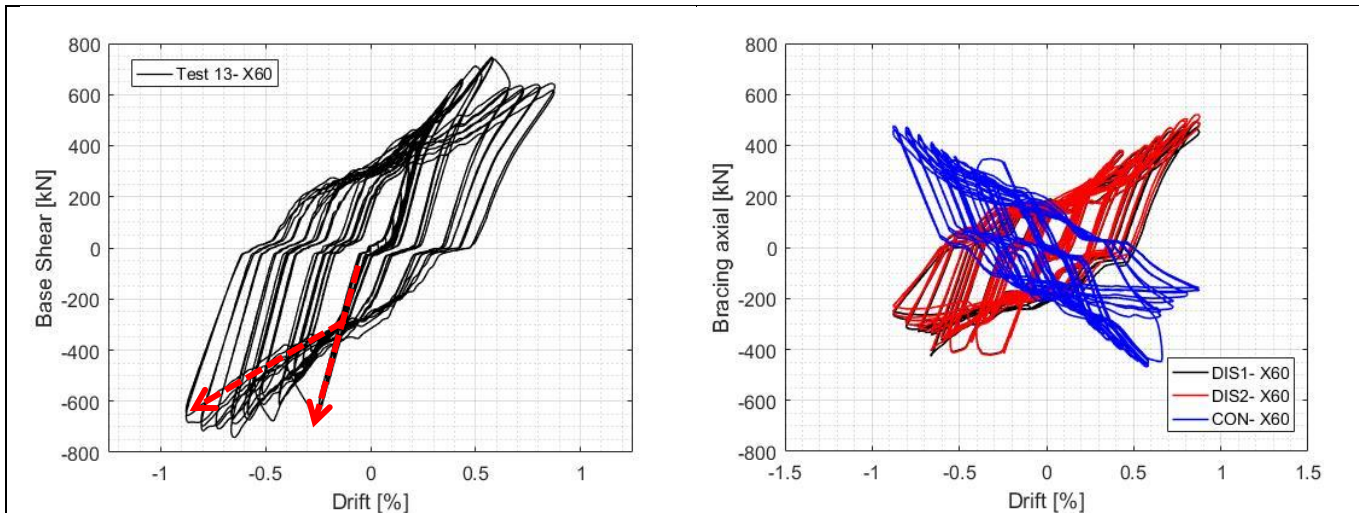


Figure 116. Global behaviour. Stiffness deterioration. (13080 s time step)

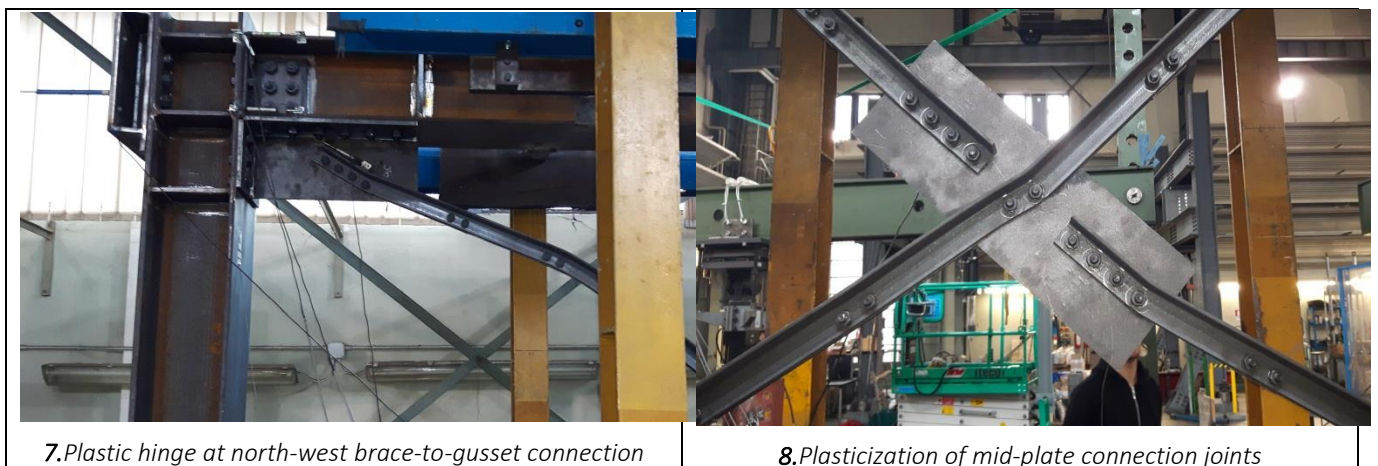


Figure 117. Plasticization of frame nodes

Besides, tension stresses cyclically alternating on diagonals went on deteriorating plastic hinges causing crack initiation and subsequent opening and propagation along gross-section. First crack developed at mid-span of NE discontinuous diagonal. Relative opening was visually clear starting from +20 mm cycle (+0.76% drift) while tension stresses affected discontinuous diagonal, causing crack opening.

From the beginning of ± 20 mm cycle to the end of first tension peak of ± 30 mm cycle, crack, initiated after tearing, propagated under tension peaks till affecting the whole gross-section. It start on the lower edge in form of an hairline formation, then reaching the upper horizontal flanges before causing failure.



11. Crack opening at bolt of stitch plate of the NE discontinuous diagonal (first tension peak of ± 20 mm).



18. Crack propagation reaches horizontal flanges of the NE discontinuous diagonal (first tension peak of ± 30 mm).

Figure 118. Plasticization, cracks opening and propagation at NW discontinuous diagonal

Instance at which graphs of Figure 119 have been plotted, highlights a cycle loop at which strength of the frame was strongly reduced. An abrupt drop in strength occurred while frame was being pulled by the actuator. Reduction in frame strength resulted as effect of plasticization of SW brace joint end and bolts connections at mid-plate. Overall lateral resistance was decreased.

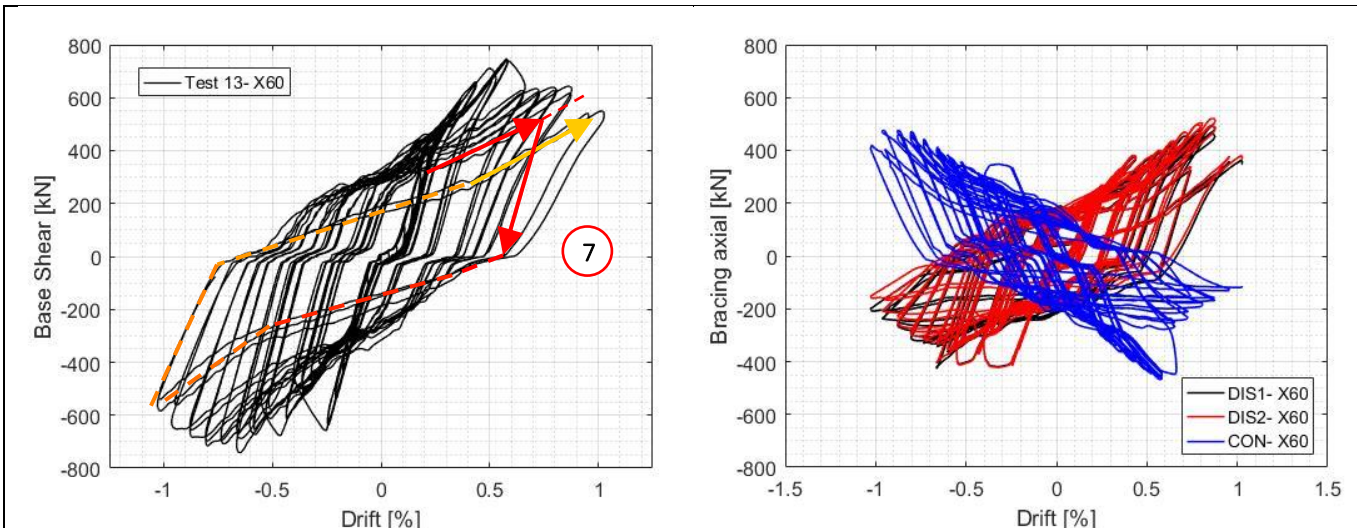


Figure 119. Global behaviour. Brace axial load-drift ratio. (15150 s time step)

Photos reported below show main nodes affected by open crack, mainly in correspondence of bolts, in which section results weaker. During post-elastic phase, plastic hinges, presented at several nodes of the frame, continued to be still impaired, evolving in preferential point of subsequent crack openings since areas of stresses concentration for inelastic demand.



Figure 120. Crack opening at plastic hinges yet presented at frame nodes

Worst situation developed at NE diagonal where crack propagated among the bracing, affecting the whole cross-section, from web to flange. At the end of first tension peak of ± 30 mm cycle, crack reached horizontal flanges. While, during second tension peak of ± 30 mm cycle ($+1.15\%$ of drift) applied to the structure, failure occurred at mid-span of north east discontinuous brace (DIS2), in correspondence of the mid-span stitch plate. Fracture divided the diagonal gross-section into two separated segments. The abrupt failure of NE discontinuous diagonal resulted in crack propagation among bracings gross-section in correspondence of first bolts connecting NW and SW brace joints ends to respective gusset plates. Figure 121 represents base shear-displacement graph after second cycle of ± 30 mm.

Point A in the graph represents first reference cycle peak at which rupture occurred. Point B is the maximum resistance reached at second peak of the same cycle. Resistance was reduced of about 50%, falling down from 450 kN to 225 kN, taking as reference range of positive drift. It means almost no more contribution from diagonals. Stiffness was provided by practically only semi-rigid beam-to-column connections. On negative displacement field, structure was even able to bear up to 500 kN. Point C represents maximum of first compression peak of ± 32 mm drift cycle imposed.

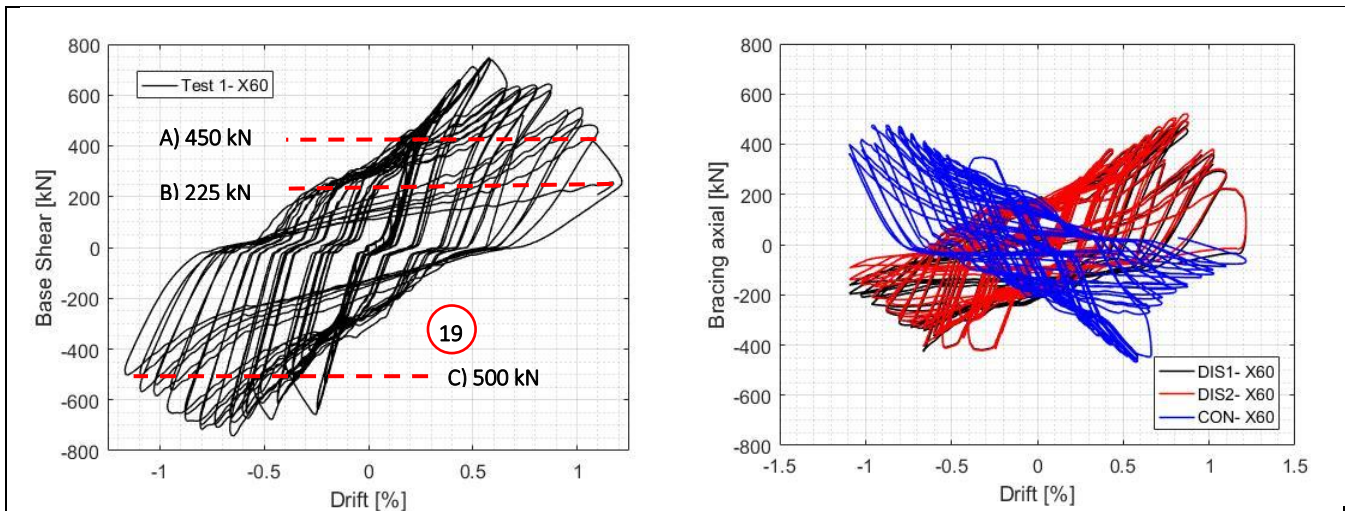


Figure 121. Global behaviour (17150 s time step)



Figure 122. Failure along the stitch plate bolts in mid-span of the north-east discontinuous diagonal. (second frame tension peak of ± 30 mm). Gross-section separation at mid-span of NE discontinuous brace. Cracks, initiated after plastic hinge formation, propagate.

Instance at which frame hysteresis loops is plotted in base shear-drift ratio graph of following Figure 123, wants to highlight the abrupt reduction in strength and stiffness of the structure after discontinuous brace gross-section failure. Although, even if brace failed, it could still reengage forces under compression thanks to crack closure, providing a residual resistance. Overall bearing capacity of the frame is given mainly by tension diagonal and frame effect of semi-rigid beam-to-column connection.

Failure of continuous brace occurred at first negative peak of ± 38 mm cycle (1.46% of drift). Data are not detectable by the following graphs since control unit has not recorded for few minutes, so informations about have been lost. What it is possible to carry out is the fact that frame, after both diagonals failure, continued to provide relative strength, and a valuable amount of ductility. Gusset plates at nodes significantly strengthen the structure, providing residual lateral stiffness.

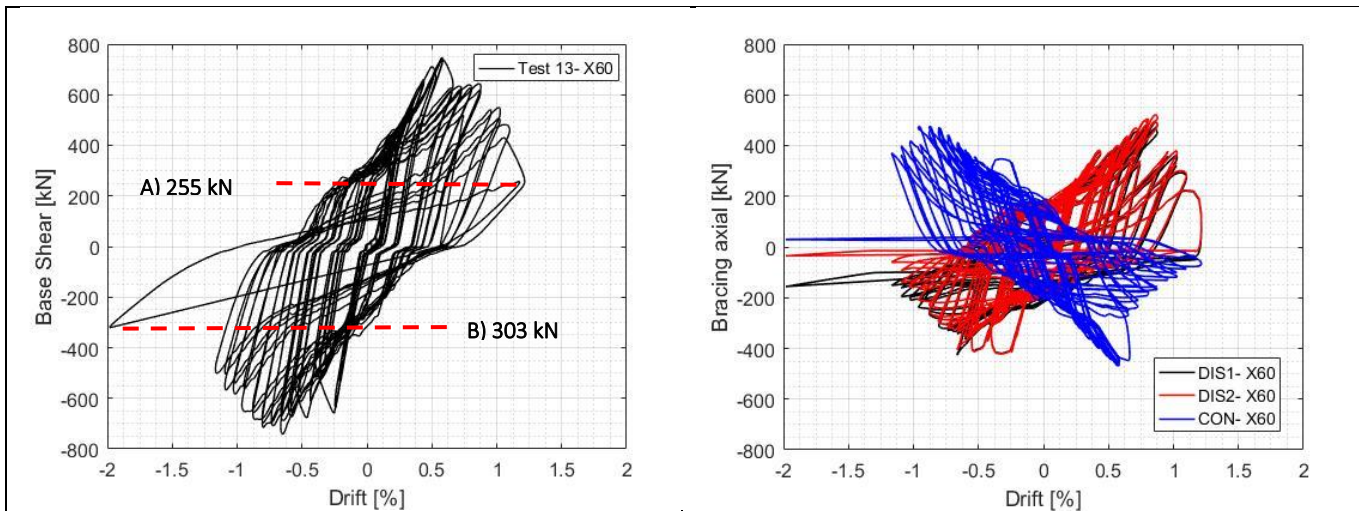


Figure 123. Global behaviour (18150 s time step)



Figure 124. Failure at mid-span of the north-west continuous diagonal (first frame compression peak of ± 38 mm cycle).

Plots reported in Figure 125 described trend in base shear and bracing axial load during last test cycle. Strength and stiffness of the structure is provided mainly by what is called “frame effect”. Curves became similar to which observed later, performing test 16, where only frame without bracings was tested. No more lateral resistance was offered by bracings. Contribution in strength and stiffness is provided by gusset plates, which constitute the semi-rigid beam-to-column connection.

Thus, bearing capacity of failed braces was seriously compromised, achieving values oscillating between no more than +35 kN and -35 kN, representative of a residual capacity derived by the two parts of the broken sections that were returning cyclically in contact. Discontinuous brace 1, that remained undamaged till test end, carried more than 150 kN.

Interestingly, peaks of curves in the negative drift field, show clearly the yielding mechanism occurred at gusset plates. Vertical plate surface yielded and deformed in typical T-stub strain, highlighted in photo of Figure 126.

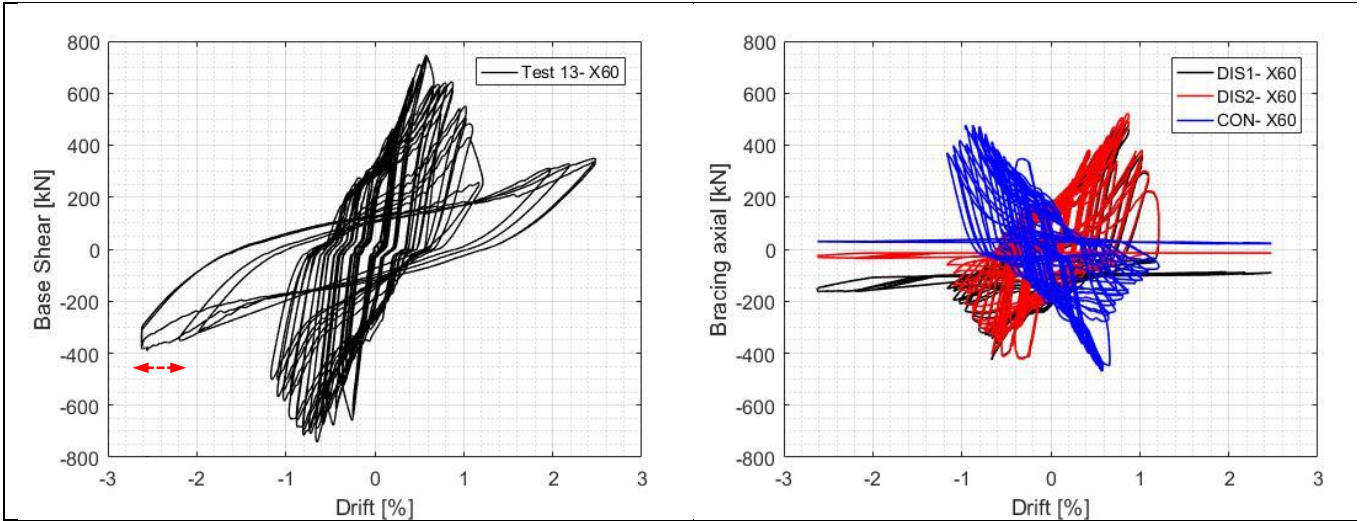


Figure 125. Global behaviour (20200s time step).



Figure 126. Frame at test end; yielding at gusset.

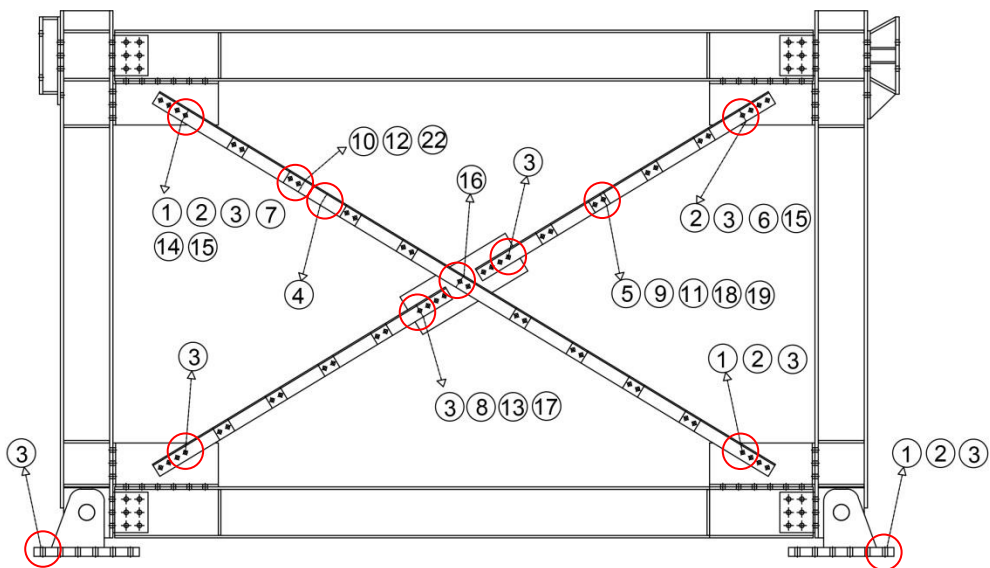


Figure 127. Main phases on a drawing

Main phases of the test are schematized and located on a front view of the frame, reported in *Figure 127*. Sequence of number is chronological. Test 13 could be summarized through following phases:

1. First slip occurred when frame under compression, force peak value 665 kN, drift -0,23% (-8 mm).
2. Second slip occurred when frame under compression, force peak value 675 kN, drift -0,46 % (-12 mm).
3. Slip of bolts at connection nodes when frame under tension, force peak value 703 kN, drift +0.51% (+13 mm);
4. Buckling of continuous diagonal CON. Plastic hinge is formed at mid-span of the north-west continuous diagonal, force peak value 750 kN, drift +0.58 % (+15 mm).
5. Buckling of discontinuous diagonal DIS2. Plastic hinge is formed in corresponding of the mid-span stitch plate of the north-east discontinuous diagonal, force peak value 742 kN, drift -0,61% (-16 mm).
6. Plasticization of discontinuous diagonal DIS2. Plastic hinge is formed at first connecting bolt north-east discontinuous diagonal-gusset, force peak value 650 kN, drift -0,69 % (-18 mm).
7. Plasticization of continuous diagonal CON. Plastic hinge is formed at first connecting bolt north-west discontinuous diagonal to semi-rigid beam-to-column connection, third tension peak of ± 18 mm cycle, 0.69% drift.
8. Plasticization of discontinuous diagonal DIS1. Plastic hinge is formed at first connecting bolt south-west discontinuous diagonal to mid-plate, at -0,84 % of drift applied (-22 mm).
9. Crack initiation (hairline-crack formation) along bolts in stitch plate bolt of the north-east discontinuous diagonal, (+22 mm).
10. Crack initiation (hairline-crack formation) along bolts in stitch plate of the north-west continuous diagonal
11. Crack opening along bolts in stitch plate of the north-east discontinuous diagonal
12. Crack opening along bolts in stitch plate of the north-west continuous diagonal
13. Crack initiation (hairline-crack formation) along bolts in first connecting bolt south-west brace-mid plate (first frame tension peak of ± 28 mm, 1.07% of drift).
14. Crack initiation (hairline-crack formation) along first bolt in connection CON/North-West gusset plate
15. Crack opening in first connecting bolt of north-west and north-east braces joints ends to beam-to-column gusset plates.
16. Crack opening in first connecting upper bolt continuous brace-mid plate.
17. Crack opening in first connecting bolt south-west brace-mid plate.
18. Crack propagation reaches the horizontal flanges at the north-east discontinuous diagonal (first frame tension peak of ± 30 mm, DIS in tension, CON in compression).
19. Failure along the stitch plate bolt at mid-span of the north-east discontinuous diagonal. (second frame tension peak of ± 30 mm, DIS in tension, CON in compression).
20. ± 32 mm cycle: even if discontinuous diagonal rupture occurred, continuous diagonal works in tension up to overall 500 kN of base shear reaction. While having continuous in compression the frame reach a maximum resistance amounting at 250 kN
21. ± 34 mm cycle: with discontinuous diagonal rupture, continuous work in tension up to overall 480 kN of base shear reaction.
22. failure at mid-span of the north-west continuous diagonal (first frame compression peak of ± 38 mm cycle, so when tensile stress into diagonal), till previous ± 38 mm cycle it bring 480 kN in tension).

5.11.3. Column and beams

Column force over time graph is reported in *Figure 128*. Values fluctuated between +225 kN and -250 kN decreasing during last cycles. Columns forces trend is quite similar to that in bracings. Drops in forces peaks result in cycles after braces buckled or plastic hinge formed. Moreover, once north-east diagonal failure occurred, forces went on to increase in columns only in case of compression stresses (negative values).

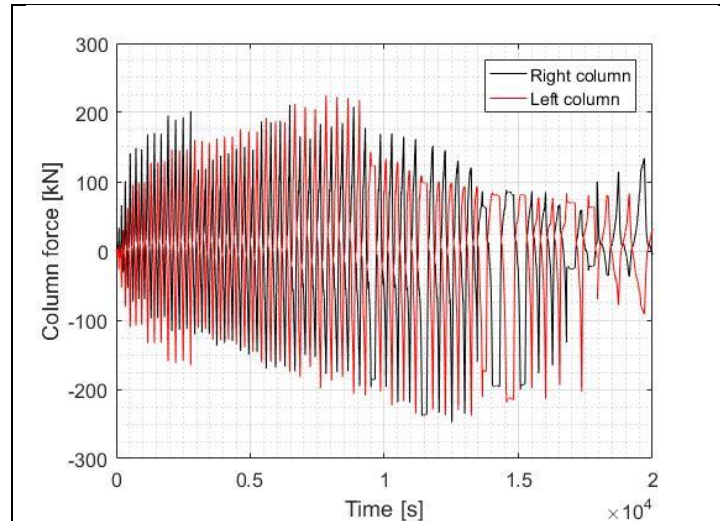


Figure 128. Load trend on beams

5.11.4. Bracings behaviour

Aspects about bracings behaviour during cyclic test 13 have been yet discussed through detailed chronological description about shear force-drift ratio and bracings axial-drift graphs reported in paragraph 5.11.2.

Main conclusion, besides performance states degradation already presented, could be observed in the capacity of the bracings to provide resistance also after failure. The surfaces of the two parts of opened gross-section, separated while bracings are pulled in traction, reverted in contact under compression, so that to supply a residual bearing capacity. This is highlighted from forces trend of last cycles (began at 1.5×10^4 s time step) reported in graphs of *Figure 129*. The phenomenon, neglected by standards, can be a valuable source of over-resistance of a system designed for low and medium magnitude seismic events.

Generally, till bracings behaved elastically, up to first peak of ± 16 mm displacement cycle, compression and tension peaks resulted symmetrical. Discontinuous diagonal 2 reached first instability, once outmatched 400 kN. Effects hit also continuous diagonal resistance, due to instantaneous release of load from DIS2 and the system that revealed less rigid. Next cycle, compression resistance of DIS2 reached no more than 215 kN, with a reduction of 46%.

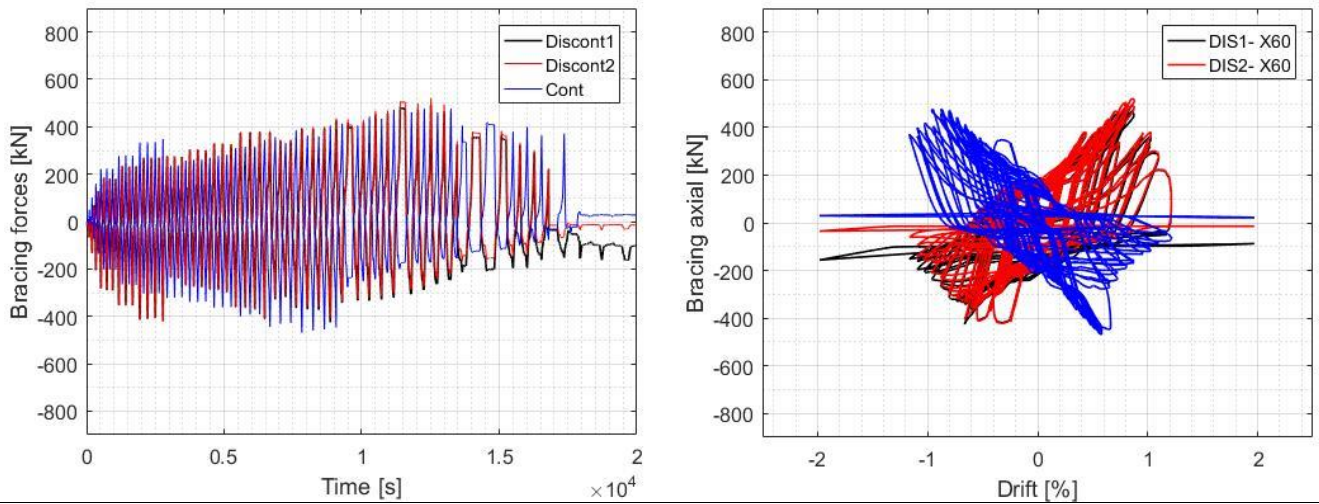


Figure 129. Axial load of bracings over time and displacement applied

5.11.5. Energy dissipation

The area inside ingoing and returning curves describes the amount of energy dissipated during each cycle. It has been calculated using trapezoids method multiplying each dF (force differential) per each dx (displacement increment), then subtracting integrals of ingoing less returning curves for each hysteresis loop. *Figure 130* reports a scheme about calculation performed.

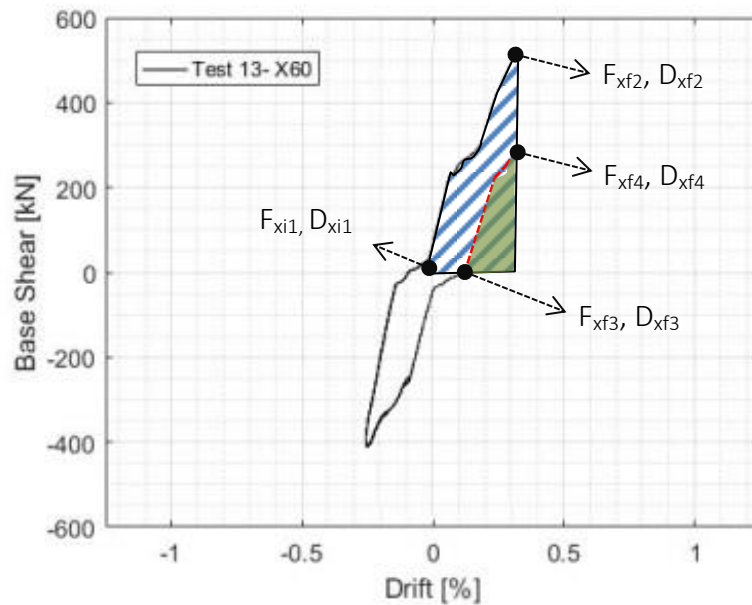


Figure 130. Calculation scheme hysteresis loop area

According to the scheme, following equation have been used:

$$AREA_{loop} = \int_{D_{x1}}^{D_{x2}} dF_i \cdot dD_i - \int_{D_{x3}}^{D_{x4}} dF_j \cdot dD_j$$

Curve of *Figure 131* reports values of the areas of hysteresis loop of the entire test. Trend is characterized by a polynomial grow with peaks in correspondence of main phenomena of energy dissipation. First peak recorded correspond to slip of the structure, that dissipate energy by friction , generating heat. Checking LVDT data, slip occurred at bolts of brace joints ends of continuous diagonal and at east base plate. This latter displaced of about 5 mm, while SE and NW CON-brace joints about 3

mm each one. Thus, first rise in energy dissipation, amounting at 2286,91 kN.mm, was linked to slip. It has to be noticed that base plate slip is not to be taken into account, so that only 1247,4 kN.mm results effective energy dissipated. The value has been derived by splitting in percentage by total each millimetre recorded at pots of frame nodes. A scheme is reported in graph of *Figure 131*.

Next peaks are caused by additional slips occurred at remaining connection nodes, buckling of diagonal under compression stresses, plastic hinges development and failure of bracings.

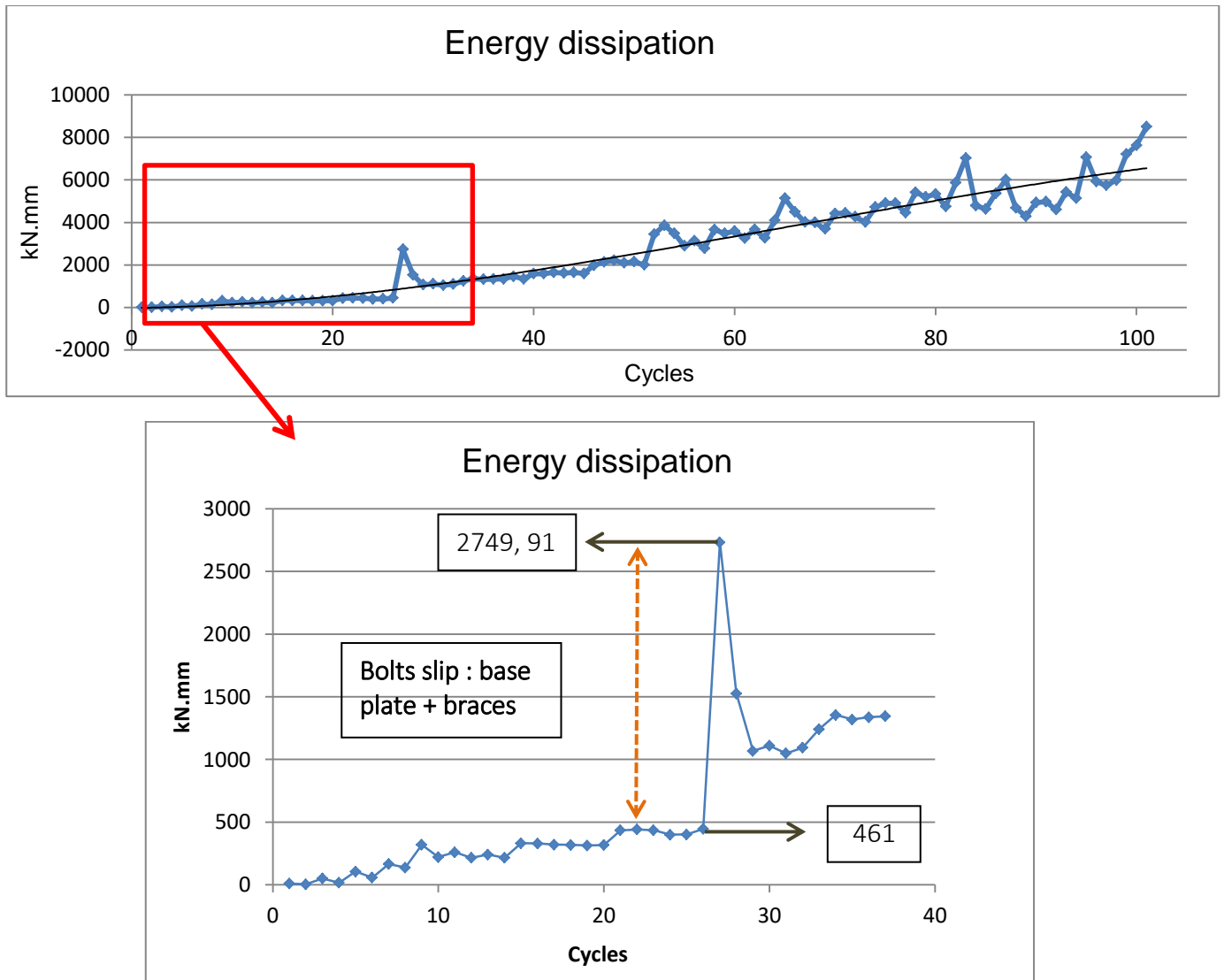


Figure 131. Energy dissipation for each cycle

It follows a list of energy dissipation sources of the frame tested during test 13. For each one it is given a general view starting from the notion. Energy dissipation is given by:

1. Bolt slip, where energy is dissipated due to friction in form of heat. This phenomenon takes place at brace joints connections and base plate. This latter has been evaluated to be about 1% of the overall energy dissipated, so that it could be negligible.
2. Local buckling, that is an extremely important aspect of steel sections on account of the fact that very thin elements used will invariably buckle before yielding. Concept has been schematized by picture of *Figure 132*. Plates elements (flanges and webs of bracings) buckled locally before brace developed fully plastic section. These members failed before the full strength of the member was realized because more slender element buckled first. In local buckling, the axis of the member is not distorted, but the strength of the cross section is

compromised by the buckling of a component of the cross section. Furthermore in some cases, local failure may cause the failure of the whole structural member.

3. Ovalization of bolts holes. After connection slip occurred, bolts bear on the bolt holes at large storey drifts, causing localized plastic deformations around the bolt hole and gradually worsened pinched response.
4. Global buckling, characterized by the sudden sideways failure of a structural member subjected to compressive stress. As an applied load is increased on the thin member, such as the brace, it will ultimately become large enough to cause the member to become unstable. Further load will cause significant and somewhat unpredictable deformations, leading to complete loss of the member's load-carrying capacity.

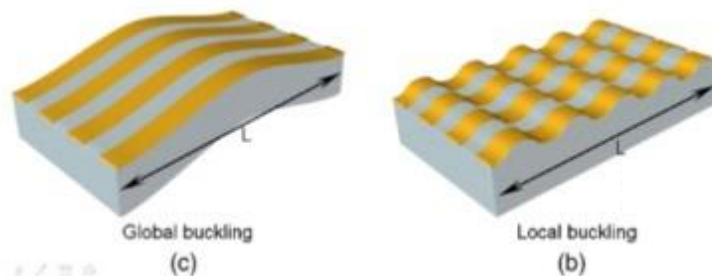


Figure 132. Scheme of global (a) and local (b) buckling mechanism

5. Yielding of gusset plates, which develop typical T-stub deformation

Thus, graph reported in *Figure 133* represents the cumulative dissipated energy cycle by cycle till test end. It is possible to recognize different main trends punctuated by different phenomena occurred during test. We have supposed local buckling phenomena starting increasing energy dissipation between bolts slip and global buckling even if they have not been observed by naked eyes.

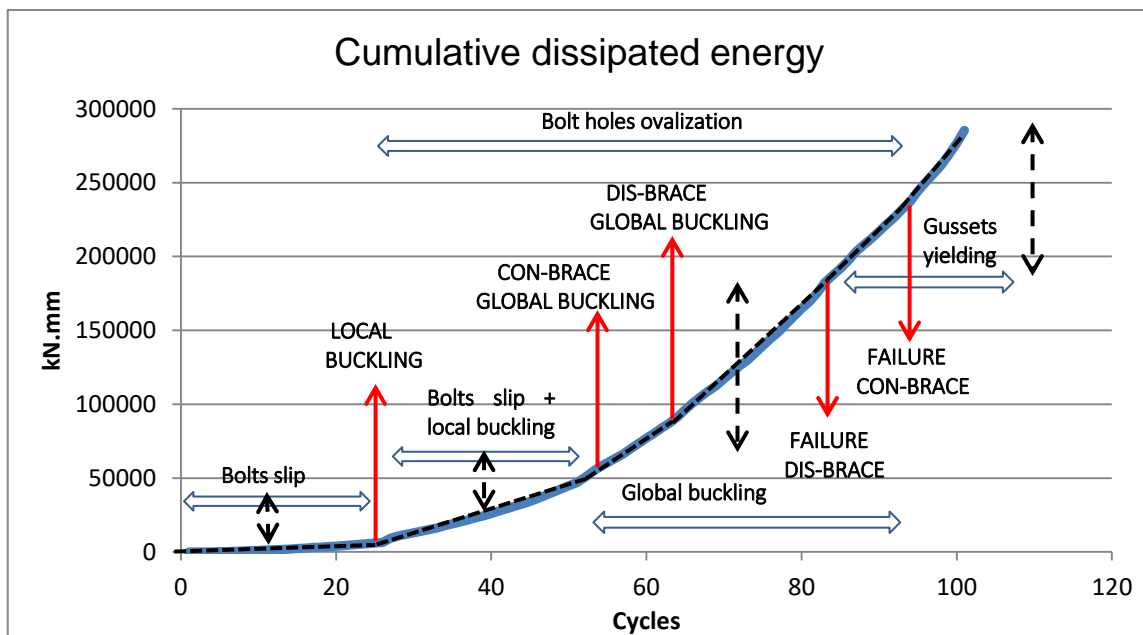


Figure 133. Curve of cumulative energy dissipated during test 13.

Table 21 summarizes results highlighted by graph explaining in terms of percentage, the contribution of each event to overall energy dissipation. Bolts ovalization contribution has been evaluated taking care of last segment of each cycle, when bearing capacity of the whole structure does not yet increased while drift is growing.

Event	Partial Energy [kN.mm]	Overall Energy [kN.mm]	Percentage
Bolts slip	6.064,52	285.267,1	2,1 %
Local buckling	51.483,82	285.267,1	18 %
Global buckling	124.836,93	285.267,1	43,7 %
Gussets yielding	77.401,63	285.267,1	27,1 %
Bolt holes ovalization	25.959,30	285.267,1	9,1 %

Table 21. Percentage of contribution in energy dissipation

Increasing of plastic deformations was observed during the test, producing a progressive reduction of the absorbed energy. Buckling represents main phenomenon of energy dissipation. In points in which plastic hinges formed, high inelastic demand was placed, resulting in plastic deformations and consequent energy release. Thermography photos show concentration of energy and increase in temperature at plastic hinges and brace joints connections in which slip occurred.

More than 10 % of total energy has been dispersed by bolts slip and bolt holes ovalization. Relevant is also the contribution of gusset plates, once bracings were both failed. They provide additional devices to energy dispersal and ductility. The progressive reduction of the absorbed energy, goes on till complete failure of both diagonals. Once bracings didn't give yet lateral resistance, gusset plates were activated, restarting energy dissipation to grow. Next graph compare test 13 with test 16, performed testing the frame without bracings system, but with complete semi-rigid beam-to-column connection composed by gussets plus double web angles. Bars represents a percentage calculated as following:

$$\% = \frac{E_{test_13} - E_{test_16}}{E_{test_13}} \cdot 100$$

Where E is the energy dissipated at the relative displacement applied.

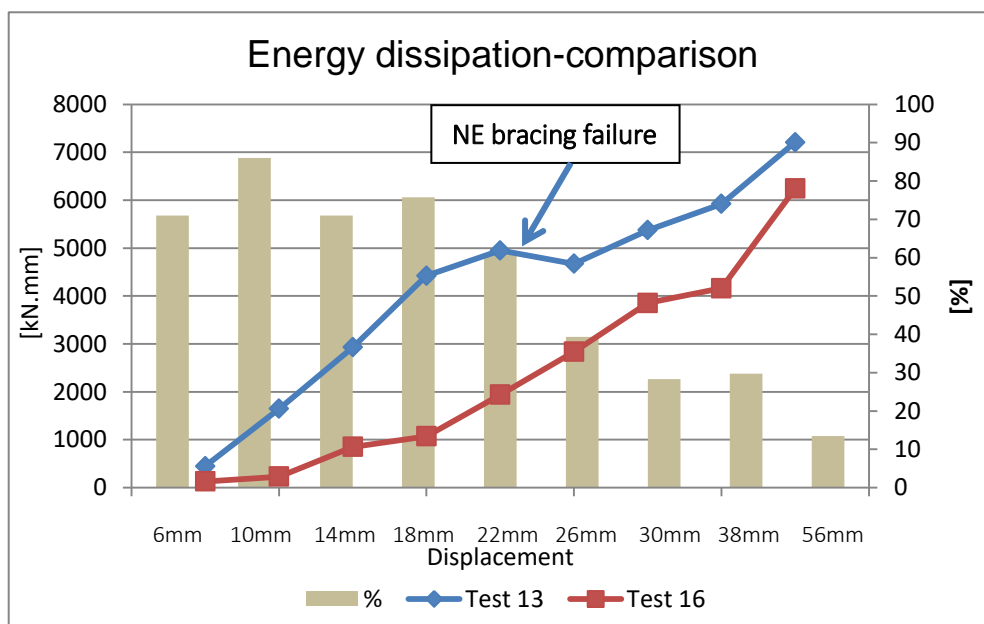


Figure 134. Compare cumulate the energy dissipation comparison. Test 13 vs Test 16

Additional comparison has been done in order to evaluate the contribution of compression diagonal in terms of energy dissipation. Graph of *Figure 135* shows cumulative energy dissipation of test 13 and test 3, for what regarding positive displacement applied. Single diagonal configuration frame behaved more dissipative than cross-configuration frame during initial loading cycles, till buckling occurred in test 3 (point 14 in the graph, corresponding at 0.19% drift cycle, 5 mm). *Table 22* demonstrates in terms of percentage, the evolution of energy ratio between test3 and test13 as cycles increase.

Cycles	1	5	10	15	20	25	30	35
Displacement	1	5	6	8	10	12	16	20
Test 13/Test3	1.03	0.92	0.62	0.89	1.25	1.60	2.06	2.52

Table 22. Ratio about energy dissipation

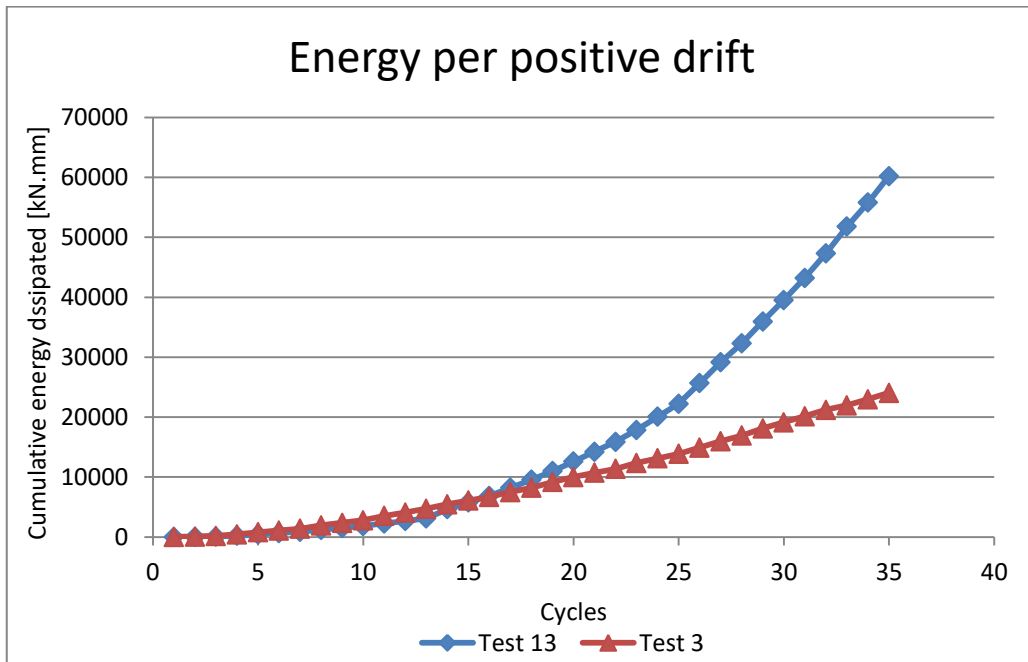


Figure 135. Cumulative energy dissipation of positive displacement loops

Using the scheme of *Figure 136*, percentage of overall cumulative energy about compression diagonal contribution in dissipation has been also calculated and compared energy of negative displacement hysteresis loops. In order to have a coherent comparison, only cycles having equal values of displacement applied have been taken into account.

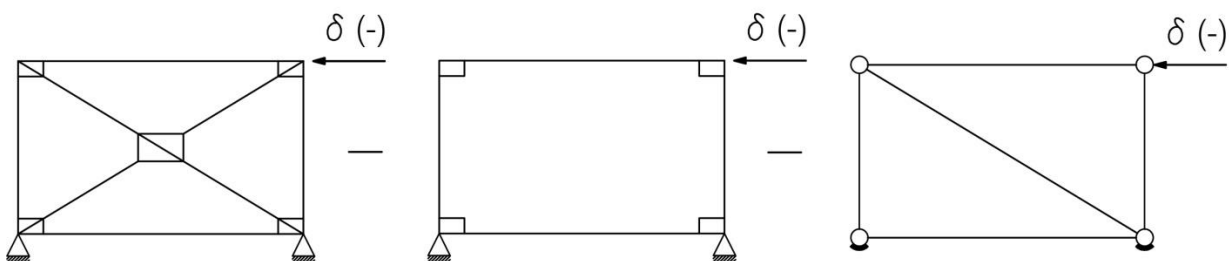


Figure 136. Calculation scheme

Cumulative Energy	Test 13	Test 16	Test 23	Unit
Positive Cycles	32302,43	7958,58	1613,641	kN.mm
Negative Cycles	31274,49	7640,236	3913,962	kN.mm
Total	63576,92	15598,82	7772,601	kN.mm

Table 23. Energy dissipation comparison

$$E_{compr.diagonal} = E_{test\ 13} - E_{test\ 16} - E_{test\ 23}$$

$$\% = \frac{E_{test\ 13} - E_{compr.diagonal}}{E_{test\ 13}} \cdot 100$$

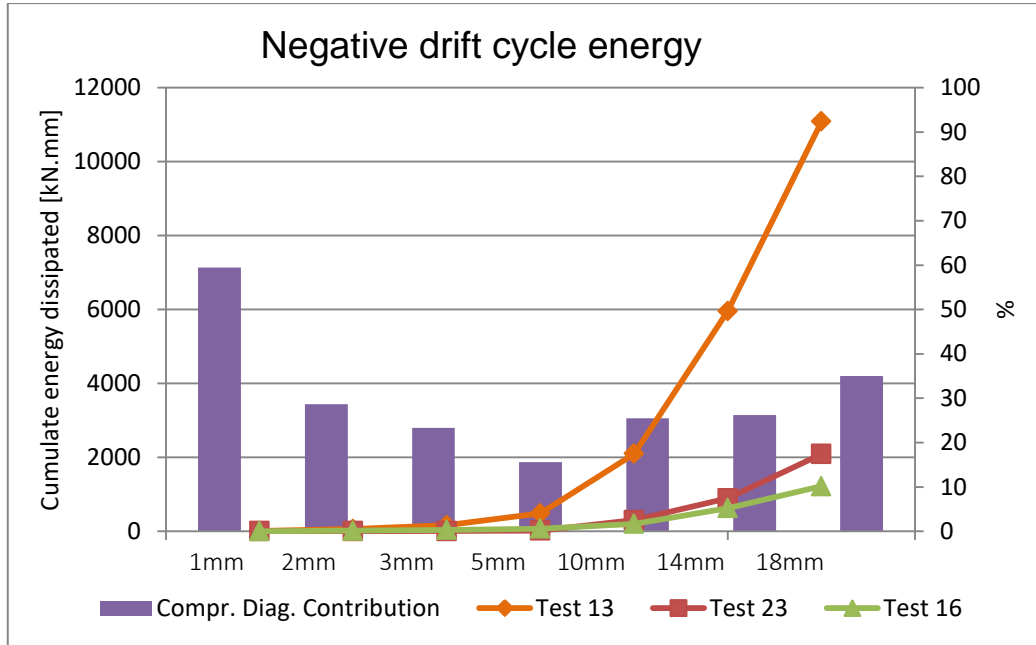


Figure 137. Cumulative energy of negative drift cycle loops

Displacement applied mm	Cumulate Energy Negative Cycles			Unit
	Test 16	Test 13	Test 23	
1	3,62	9,407787	1,97725	kN.mm
2	16,02071	60,13717	4,112264	kN.mm
3	36,38475	165,7301	8,38535	kN.mm
5	72,75573	485,2262	21,9045	kN.mm
10	204,5728	2100,353	301,4304	kN.mm
14	625,2458	5957,629	891,1689	kN.mm
18	1219,395	11084,98	2091,72	kN.mm

Table 24. Cumulate energy dissipated

Extra way to evaluate how the presence of compression diagonal weight on overall energy dissipation has been followed. Cumulative energy for negative and positive cycles have been calculated. Formulation used is the following:

$$E_{tension\ diagonal} = E_{test\ 3} - E_{test\ 16}$$

$$E_{compr.diagonal} = E_{test\ 13} - E_{tension\ diagonal} - E_{test\ 16}$$

$$\% = \frac{E_{compr.diagonal}}{E_{test\ 13}}$$

	Test 13	Test 3	Test 16	E_{tension}	$E_{\text{compression}}$	%	Unit
Positive Cycles	32302,43	16934,21	7958,58	8975,63	15728,822	0.48	kN.mm
Negative Cycles	31274,49	9304,804	7640,236	1664,568	21969,94	0.70	kN.mm
Total	63576,92	26239,01	15598,82	10640,19	37337,91	0.58	kN.mm

Table 25. Comparison of energy dissipation between tests (13vs3vs16)

Test 3 energy dissipation was also investigated. Graph of *Figure 138* shows the cumulative energy dissipation, split in positive and negative displacement cycles. During positive displacement cycles, more energy has been dissipated. This is mainly linked to the presence of diagonal under compression that buckled placing large inelastic demand at mid-span. Most of energy dispersal under tension is instead dissipated by frictional phenomena of bolts slip and ovalization of the holes. Globally, negative displacement cycles was 46% less dissipative than positive loading cycles applied. *Figure 138* demonstrates how capacity design rules could be reviewed taking care about compression diagonal contribution in global performances of the frame.

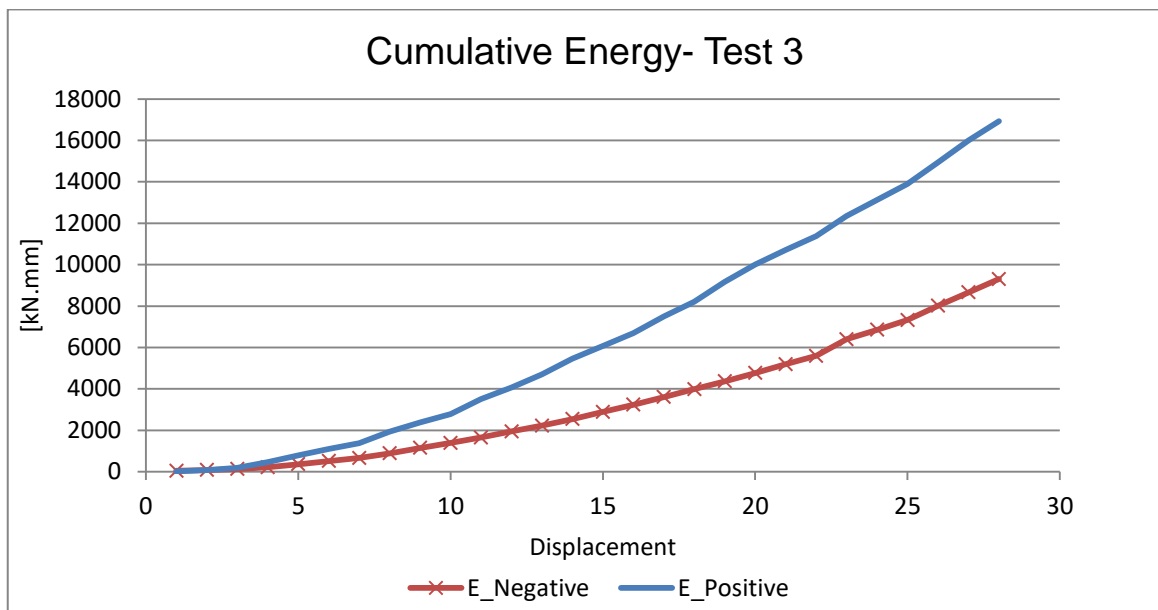


Figure 138. Cumulate energy dissipation during positive drift cycle vs negative drift cycle loops

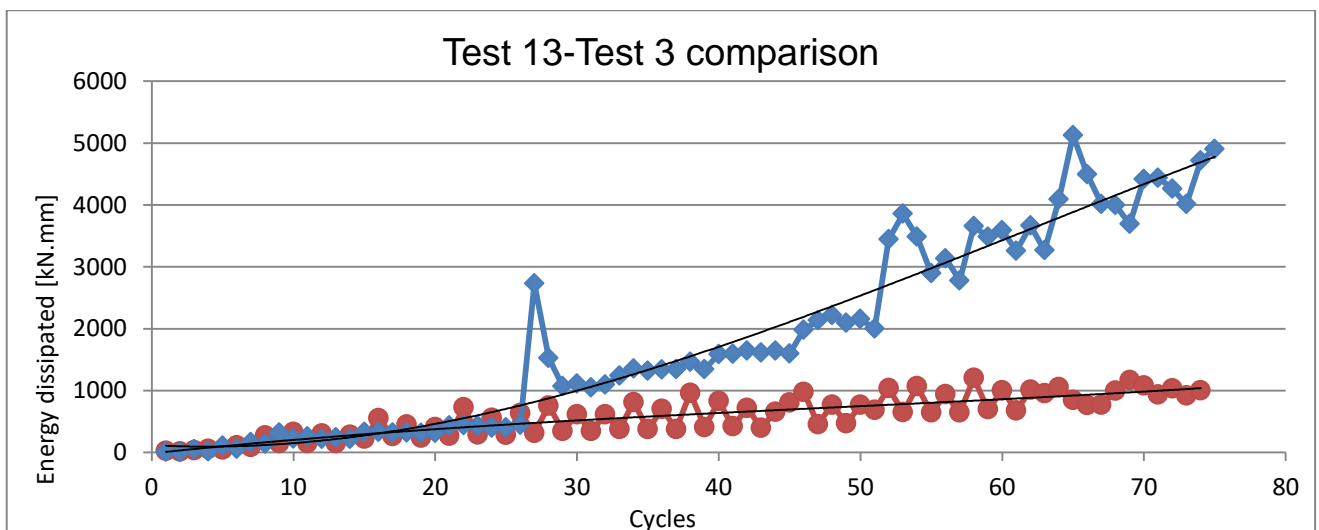


Figure 139. Energy dissipation for each cycle (Test13 vs Test3)

5.12. Test 17: Pinned X-braced frame 2L60x8



Figure 140. Specimen on test bench

5.12.1. Loading history

Frame has been loaded under displacement control for 12 cycles, up to a maximum drift of 0.54%. *Figure 141* shows loading history while *Table 26* provides the schedule of displacement cycles applied.

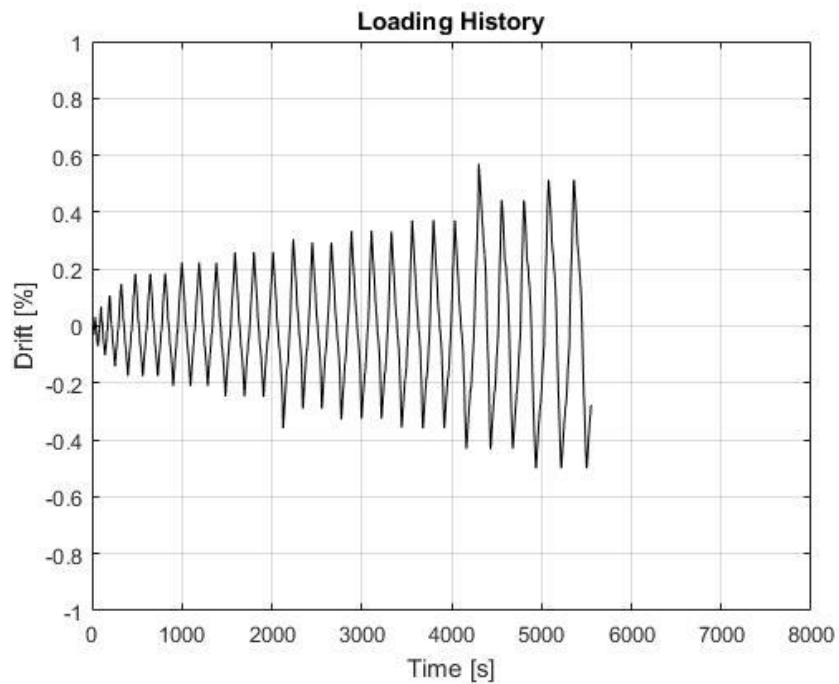


Figure 141. Loading history

Displacement step	Cycles	Cumulative n. of cycles	Displacement [mm]	Drift [%]
1	1	1	± 1	± 0.04
2	1	2	± 2	± 0.08
3	1	3	± 3	± 0.12
4	1	4	± 4	± 0.15
5	3	7	± 5	± 0.19
6	3	10	± 6	± 0.23
7	3	13	± 7	± 0.27
8	3	16	± 8	± 0.31
9	3	19	± 9	± 0.35
10	3	22	± 10	± 0.38
11	3	25	± 12	± 0.46
12	3	28	± 14	± 0.54

Table 26. Displacement cycles

5.12.2. Global overview

Frame behaved completely elastic during initial steps of test 17. Idealization line of the stiffness is simply to state by force-drift ratio graph of *Figure 142*. Thus, initial stiffness amounted at 75 kN/mm. The trend is almost symmetrical, even if it reaches 300 kN in compression and about 325 kN in tension, with a difference of 7%.

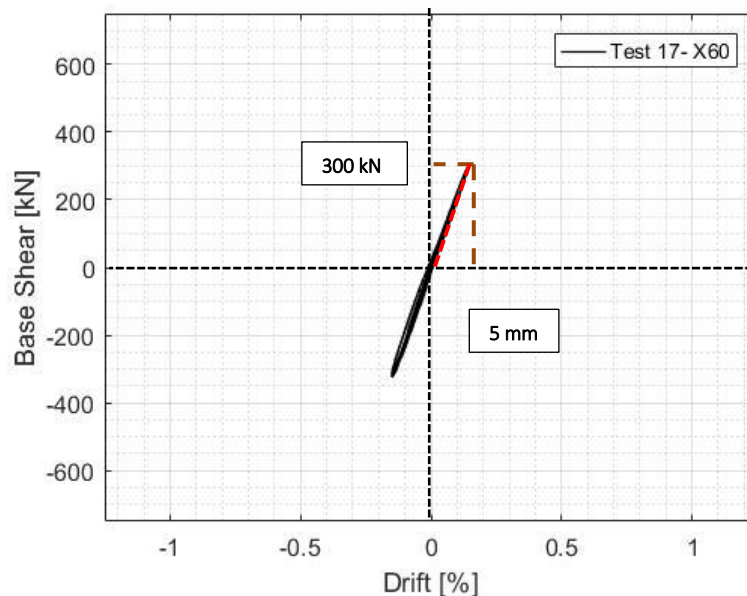


Figure 142. Initial stiffness

Energy dissipation, is explained by curves of force-drift ratio graph of *Figure 143*. Plastic deformation occurred just at $\pm 0.19\%$ of drift. The problem was linked to a bad design done for the connection angle brace-column-beam made data useless for any observation, except about initial stiffness. The steel plate that had to rotate, met resistance along its stroke, embedding either beam or column whichever counterclock or clock wise rotation occurred. Data recorded after plasticization on attack section of the brace will be neglected since they are useless. Maximum resistance reached before ± 5 mm displacement cycle, was 350 kN for both tension and compression stresses.

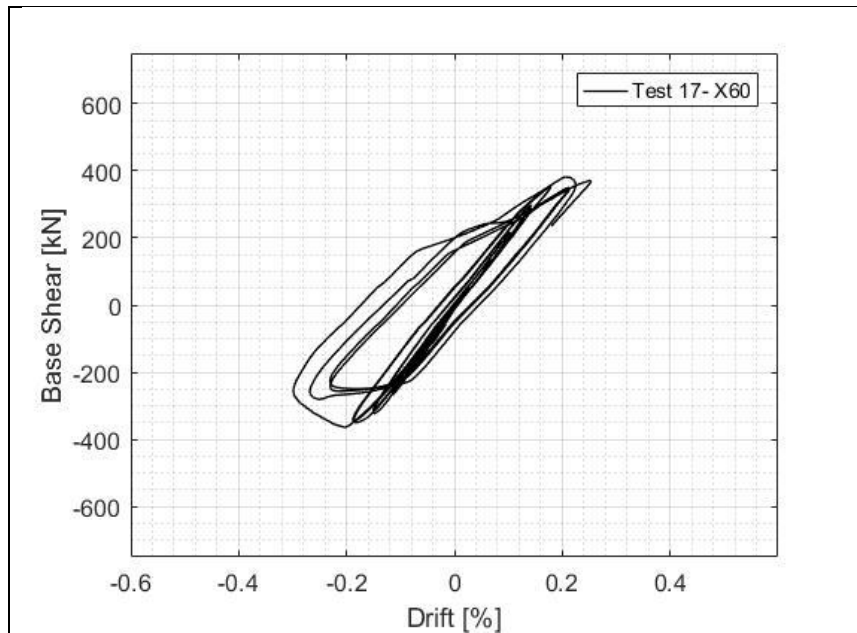


Figure 143. Global test hysteresis loops



Figure 144. Buckling mechanism of the system. Brace touched the beam..

5.12.3. Column and beams

Strain gauges were not installed into beams for pinned frame tests. No data about them are available. Instead, columns have been detected. The trend of forces in right and left column remained symmetrical till plasticization of the brace at north-east node.

Main observations that could be done about test 17, refer to pre-buckling phase. Informations recorded after plastic buckling (curves after 2048 s time step in graph of *Figure 145*) are inconsistent. Thus, till brace behaved elastically, columns forces grew up symmetrically, even if a certain discrepancy during pre-buckling cycle is noticed:

- right columns forces reached -365 kN under compression and +276 kN under tension
- left columns forces restrained between -318 kN during compression and +279 kN in tension

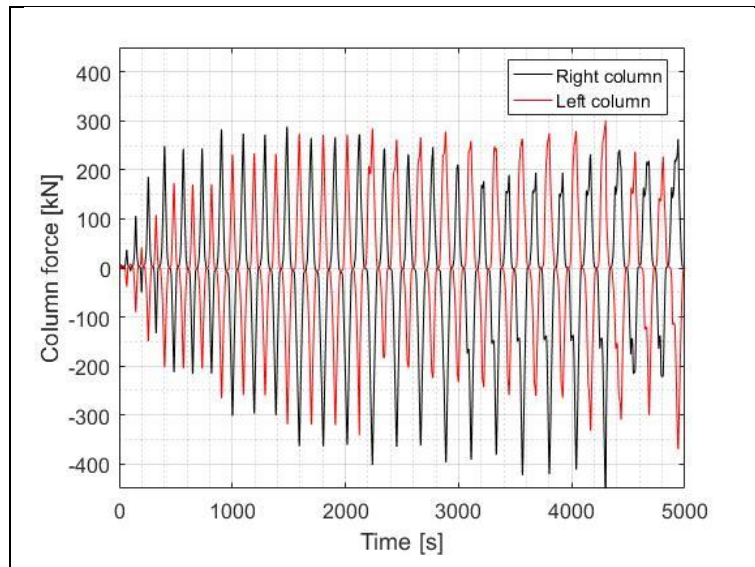


Figure 145. Load trend on columns

5.12.4. Bracings behaviour

Lateral stiffness of the structure in a pinned frame is offered by bracings system. Otherwise it could be able to displace horizontally, making columns and beams to rotate freely. Thus, bracings contained movement of the structure during test till plasticization of their section. Before plastic hinge was formed, diagonals axial force trend was symmetrical and completely elastic. During first loading peak of $\pm 0.19\%$ drift cycle the bearing capacity of continuous diagonals reached +250 kN in tension and -175 kN during compression. Discontinuous bracings behaved as little bit more resistive in compression up to -200 kN for DIS2 and -225 kN for DIS1. Bracings axial forces-drift ratio graphs is reported in Figure 146.

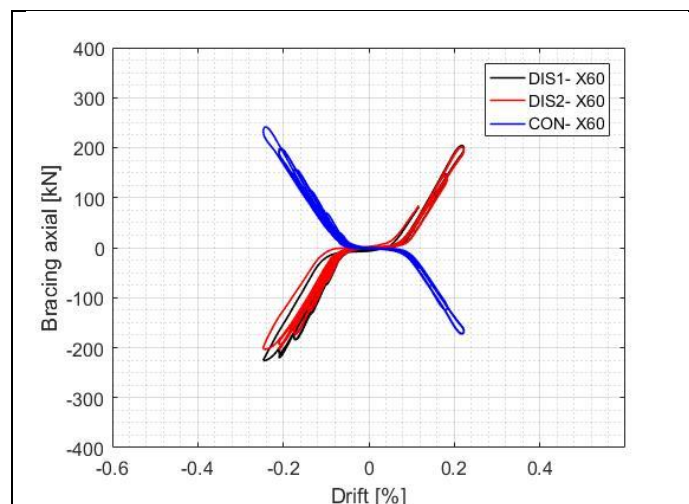


Figure 146. Pre-buckling phase axial loops in bracings

Higher values have been noticed comparing tension resistance values of continuous and discontinuous diagonals. Post-buckling data were inconsistent to derive conclusions, since buckling occurred due to design bugs. The maximum bearing capacity of the each brace for what regarding the first initial steps within the elastic range, is described by following characteristic values:

- Axial load amounting at 250 kN in tension, and 175 kN in compression in CON diagonal;
- Axial load amounting at 215 kN in tension, and 225 kN in compression in DIS1 diagonal;
- Axial load amounting at 215 kN in tension, and 200 kN in compression in DIS2 diagonal;

5.13. Test 18: Pinned X-braced frame 2L70x7



Figure 147. Specimen on test bench

5.13.1. Loading history

Rotational problems noticed during previous cycle, were avoided modifying the modular steel plate used for the connection column-beam-brace. A part of the section has been removed, trimming the element slanting on the shorter longitudinal upper side of 5 cm. Additional precaution has been adopted curving the corner formed by intersection of the cutting lines, in order to avoid points of load concentration and possible crack initiation. After that, cyclic increasing stepwise amplitude test has been performed for 15 cycles under displacement control. The loading history is reported in *Figure 148* while displacement cycles is listed in *Table 27*.

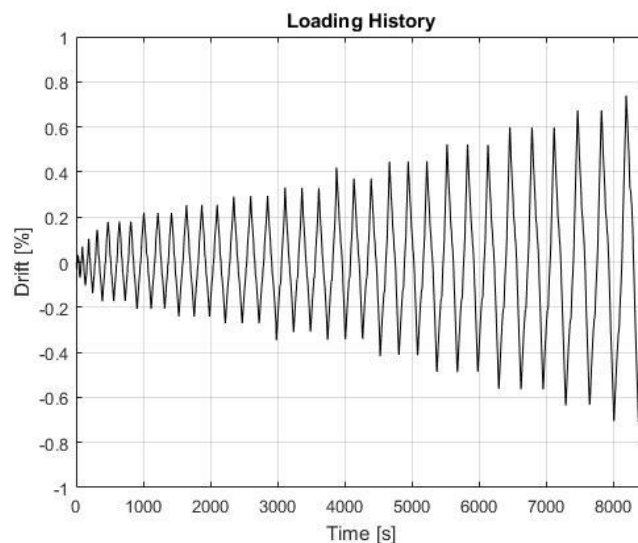


Figure 148. Loading history

Displacement step	Cycles	Cumulative n. of cycles	Displacement [mm]	Drift [%]
1	1	1	± 1	± 0.04
2	1	2	± 2	± 0.08
3	1	3	± 3	± 0.12
4	1	4	± 4	± 0.15
5	3	7	± 5	± 0.19
6	3	10	± 6	± 0.23
7	3	13	± 7	± 0.27
8	3	16	± 8	± 0.31
9	3	19	± 9	± 0.35
10	3	22	± 10	± 0.38
11	3	25	± 12	± 0.46
12	3	28	± 14	± 0.54
13	3	31	± 16	± 0.61
14	3	34	± 18	± 0.69
15	2	36	± 20	± 0.76

Table 27 Test 18: displacement cycles

5.13.2. Global overview

Initial steps of the test were performed in fully elastic regime. The curve in force-drift ratio shows how the frame completely recovers deformation after being loaded. Initial stiffness, derived by idealization line due to the fact that curves are perfectly straight, reached 82 kN/mm when frame undergone tension, and 97.25 kN/mm under compression. Curve during compression resulted more slope. At an equal drift of +4 mm, the structure achieved a bearing capacity of 328 kN and 389 kN, for tension and compression, respectively.

Hysteresis loops are described by force-drift ratio graph of *Figure 149*. In-plane buckling occurred during first compression peak of ±0.19% drift cycle. Beam-column-bracings connection steel plate didn't get in contact with the upper beam, so that not precluding its rotation along its stroke as during previous test. Situation just after instability is reported in *Figure 149*. Energy dissipated is individuated by area of the curve performed after buckling while returning to zero force. Stiffness changed, as well as the bearing capacity of the frame. Cycle after in-plane sway of the brace, the resistance was reduced of 25%, from 565 kN to 425kN. A second instability, is highlighted, carrying out during tension peak of ±0.23% drift cycle. Therefore, plastic deformation brought to a significant decrement of the curves slope. Even if, cycle by cycle, frame regained bearing capacity up to reach a base shear value of 525 kN during last displacement cycles. The so called hardening process took place.

Asymmetrical behaviour has been performed. Referring to ±0.46% drift cycle, specimen has revealed resistances amounting at 450 kN and 550 kN, respectively for tension and compression. The difference reaches 100 kN, equal to 18 % in absolut value, between negative and positive displacement applied. Also sliding effects are detectable by graph. They are represented by the horizontal segment of the line, when it pass around drift 0 during post-buckling phase.

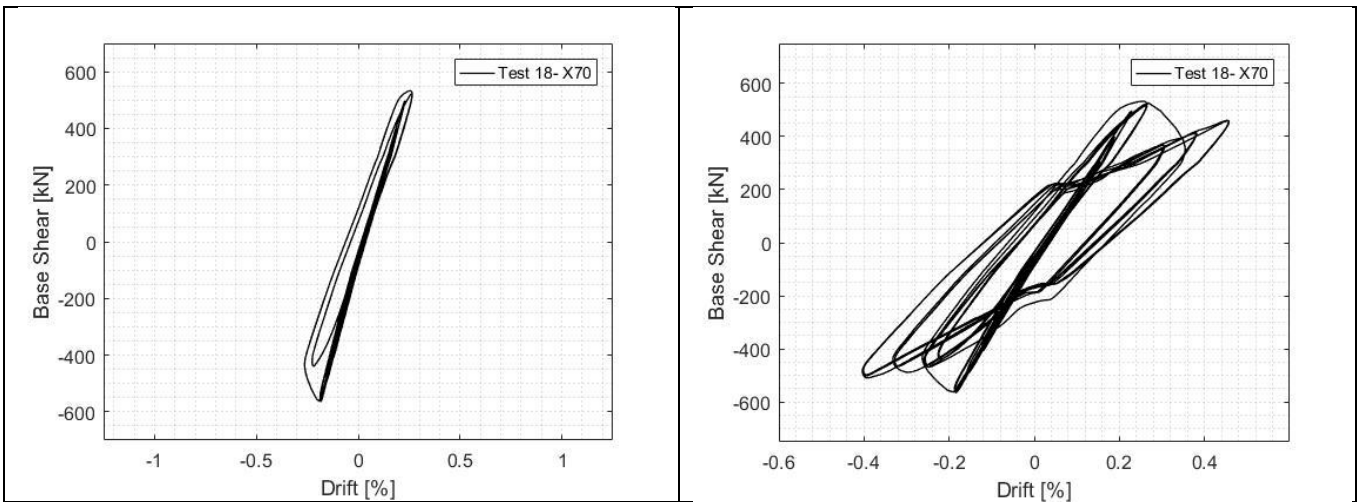


Figure 149. Initial step and global test hysteresis loops

5.13.3. Columns

Figure 150 shows trend of loads on columns during test 18. As for test 17, strain gauges were not installed into beams for pinned frame tests. Columns loads have instead been detected. The trend of forces in right and left column was not symmetrical even during initial steps elastic phase.

North-east bracing buckled at 3000 second time step (+10 mm of displacement applied), after which its bearing capacity was reduced of about 36%, from 550 kN to 350 kN. Generally, about maximum values recorded:

- right columns forces reached -500 kN under compression and +500 kN under tension
- left columns forces restrained between -443 kN during compression and +350 kN in tension

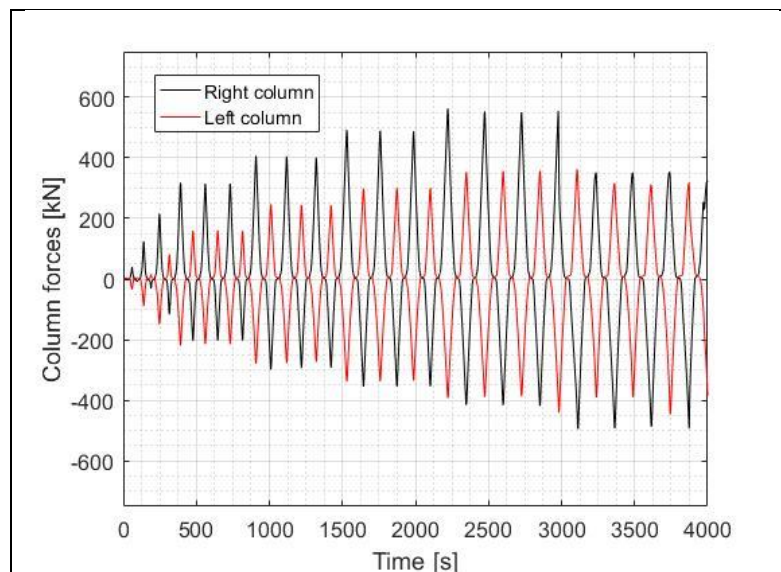


Figure 150. Load trend on columns

5.13.4. Bracings behaviour

Referring to graphs of *Figure 151*, -0.19% interstorey drift has developed first buckling on DIS2 bracing. Strain gauges data have verified that deformations have never reached values close to the yielding limit in both diagonals. The asymmetric trend could be recognised as effect of the same causes yet individuated during semi-rigid frame tests, such as asymmetry in diagonals geometry and imperfection in the loading transfer by the actuator at right column upper edge.

DIS2 and CON bracings behaved more symmetrical than DIS1 diagonal. During cycle of $\pm 0.43\%$ drift cycle DIS1 diagonal was loaded by higher compression stresses than DIS2, with a difference of 50%. This is connected to the fact that DIS2 diagonal buckled during first steps, losing bearing capacity. Maximum resistance values of diagonals were:

- axial load amounting at 420 kN in tension, and 225 kN in compression in CON diagonal;
- axial load amounting at 312 kN in tension, and 410 kN in compression in DIS1 diagonal;
- axial load amounting at 375 kN in tension, and 382 kN in compression in DIS2 diagonal;

Non-linearity is also connected to sliding phenomena occurred between braces and gusset plates.

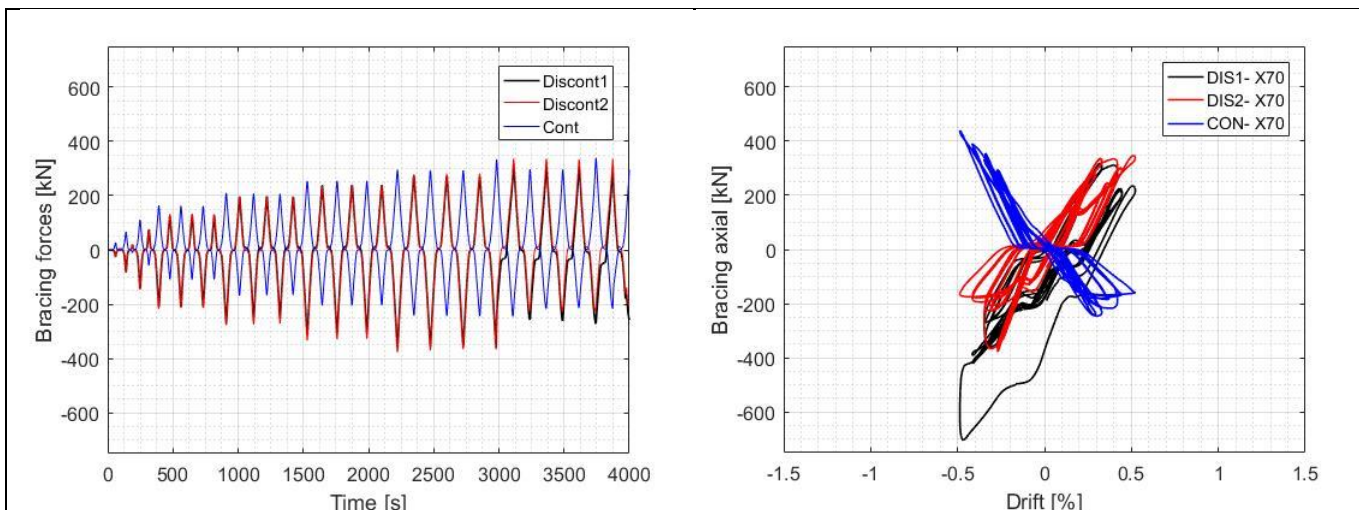


Figure 151. Bracing axial load over time and displacement applied



Figure 152. Detail of plastic hinge on continuous brace.

5.14. Test 19: Pinned single diagonal frame 2L70x7

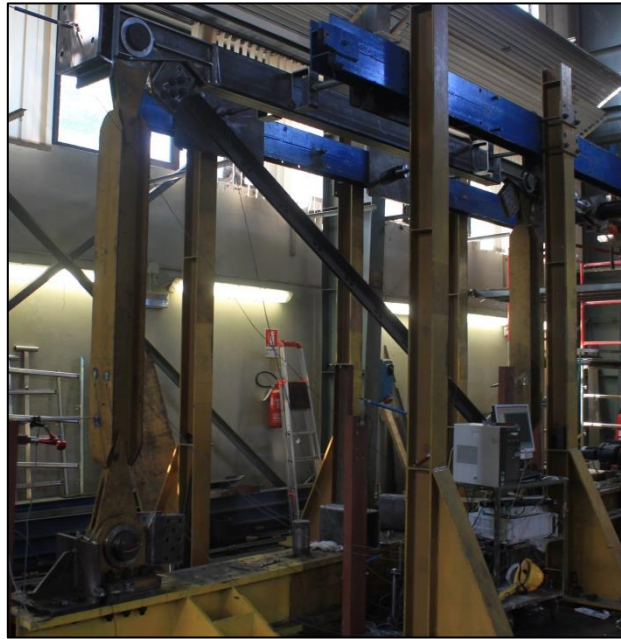


Figure 153. Specimen on test bench

5.14.1. Loading history

Test 19 has been performed for 14th displacement control loading cycles. On the contrary of other single diagonal frame test, drift values imposed to structure, have been increased for both tension and compression till last cycles. Loading history and displacement cycles are reported in *Figure 154* and *Table 28*, respectively. Frame was undergone testing up to a maximum drift of 0.69%.

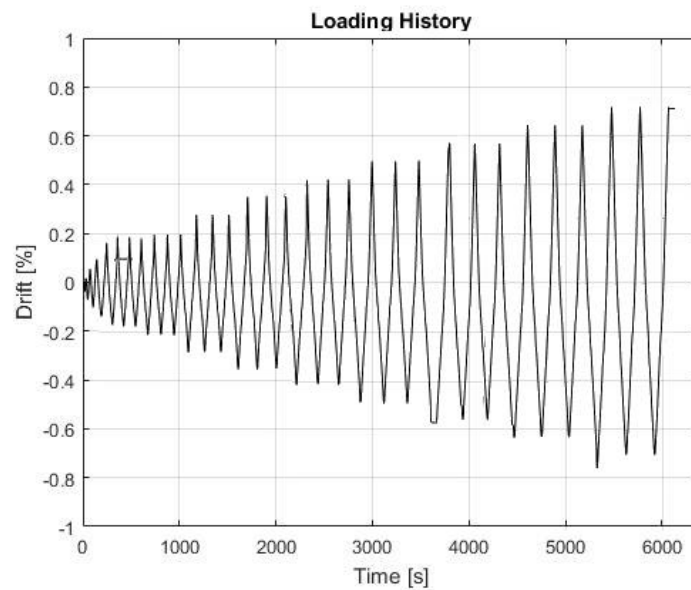


Figure 154. Loading history

Displacement step	Cycles	Cumulative n. of cycles	Displacement [mm]	Drift [%]
1	1	1	± 1	± 0.04
2	1	2	± 2	± 0.08
3	1	3	± 3	± 0.12
4	1	4	± 4	± 0.15
5	3	7	± 5	± 0.19
6	3	10	± 6	± 0.23
7	3	13	± 7	± 0.27
8	3	16	± 8	± 0.31
9	3	19	± 9	± 0.35
10	3	22	± 10	± 0.38
11	3	25	± 12	± 0.46
12	3	28	± 14	± 0.54
13	3	31	± 16	± 0.61
14	3	34	± 18	± 0.69

Table 28. Test 19: displacement applied

5.14.2. Global overview

Structure behaved elastic up to 0.23% drift cycle. While frame was undergoing tension, diagonal started developing compression stresses. When the displacement peak was reached, in-plane buckling occurred. Initial stiffness derived from slope of shear-drift ratio curves about initial steps before 6th cycle. It is equal to about 50 kN/mm for both the loading direction.

Base shear-drift ratio curves are shown in *Figure 155*. Hysteresis that came out, results the combination effect of brace buckling, slippage, ovalization and crack opening that occurred during test. Plastic hinge was formed in the mid-span of the continuous diagonal. Total resistance of the frame was +186 kN and -325 kN. Difference in bearing capacity results from asymmetry of single diagonal frame configuration, resulting weaker in tension loading direction (diagonal under compression). Buckling of the brace occurred during first compression peak ± 5 mm. After that no more resistance to horizontal displacement was offered when frame undergone positive displacement. Photo of *Figure 155b* provides a view about buckling mode of test 23. Furthermore, no plastic deformation was observed in columns and beams. Slippage and ovalization of bolts and brace yielding are the ones to provide ductility.

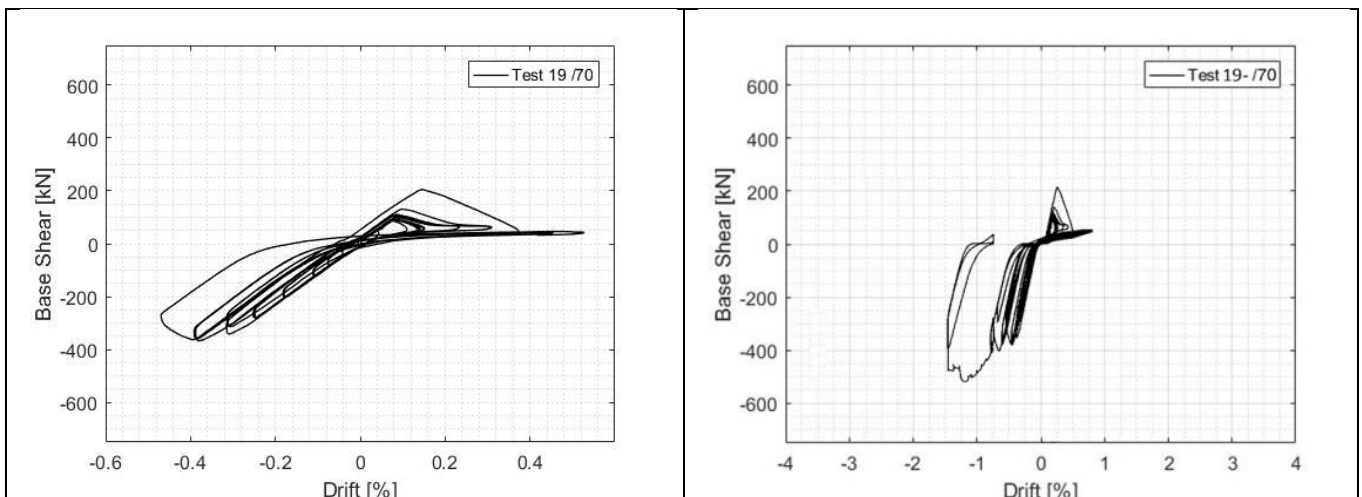


Figure 155. Hysteresis loops after buckling and at test end.

5.14.3. Column and beams

Forces trend among the frame follows the forces distribution scheme reported in *Figure 156*, together with the column force distribution over time. Data from right column strain gauges result useless. Whereas loads on left column follows the correct distribution of theoretical scheme. Meanwhile tension was applied to frame during post-buckling phase, bracing had no more resistance to horizontal displacement. Column, free to rotate and displace not developed high stresses. Forces in column oscillated between:

- 200 kN for compression and 125 kN for tension during pre-buckling phase
- 220 kN for compression and 38 kN for tension during post-buckling phase

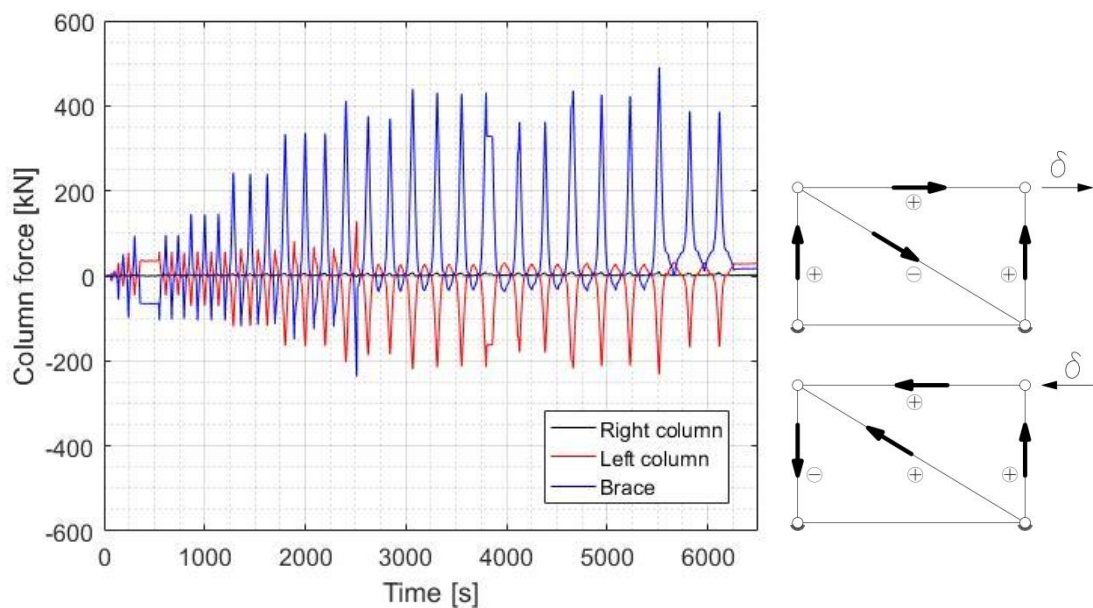


Figure 156. Trend of load on brace and columns. Comparison. Force distribution scheme.

5.14.4. Bracings behaviour

Single diagonal configuration exploits the good performance given by diagonal under tension. While during compression the slenderness of the element makes it weak. This is also deducible by graphs of *Figure 157*. Once diagonal buckled, its resistance to compression became almost negligible. Instability occurred when compression stresses went up to 215 kN, while imposing ± 5 mm cycle. Dealing with brace under tension, the bearing capacity has not been reduced. Last cycles tensile stresses reached yet 500 kN.

Furthermore, frame was not being loaded whilst imposed drift was returning to zero. On the other hand, at corresponding zero force, some deformations were stored, after plastic hinge was formed. Besides plastic deformation at mid-span of diagonal, slippage and ovalization of bolts holes were significant.

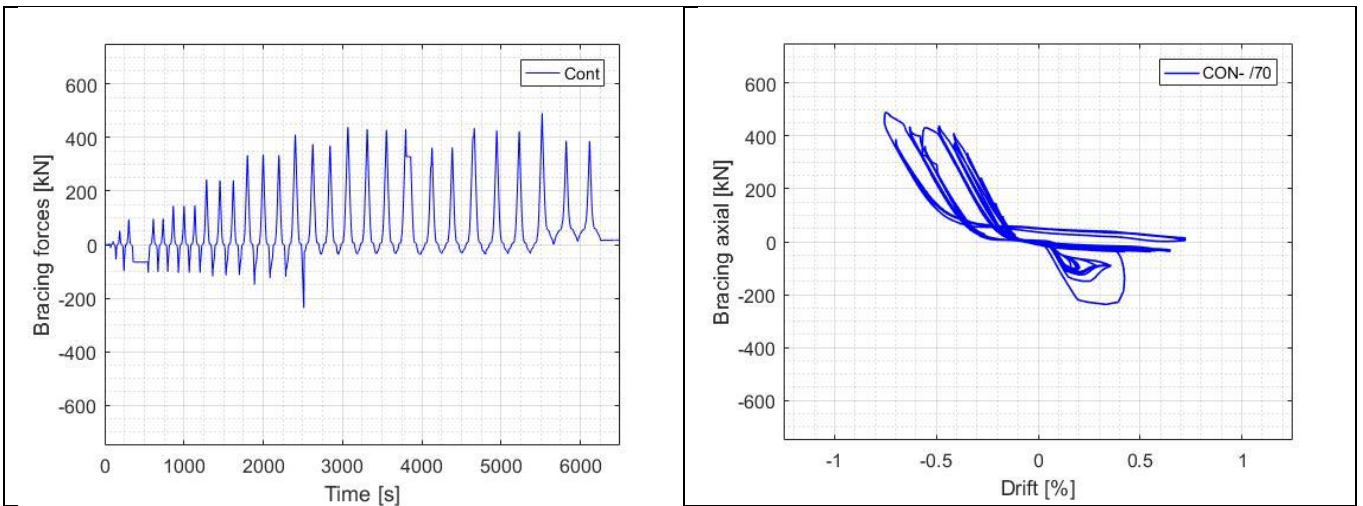


Figure 157. Bracings axial load over time and displacement applied

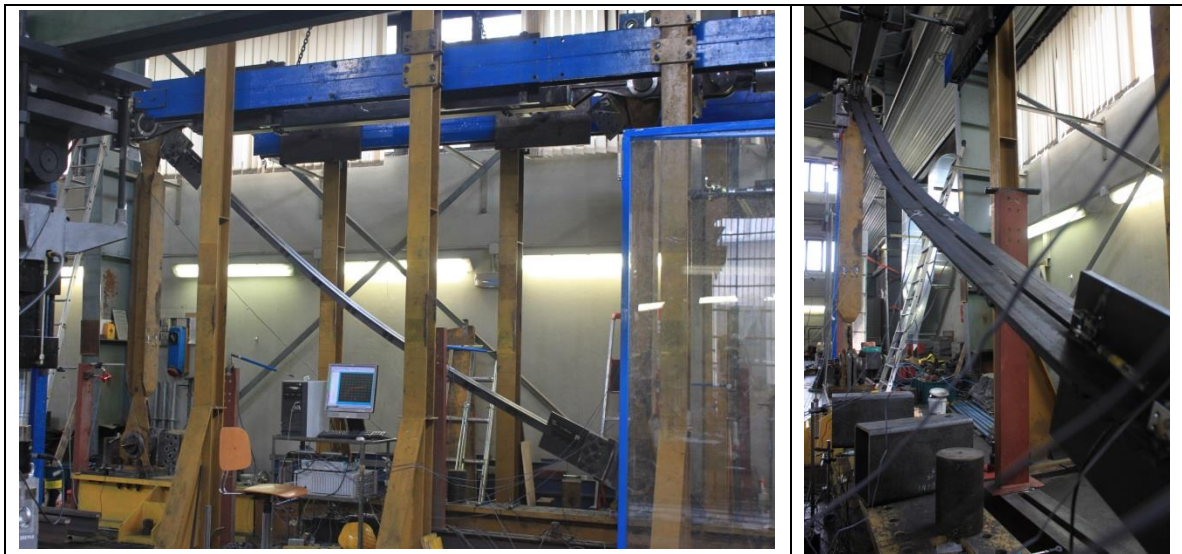


Figure 158. Buckling of diagonal (+0.19% drift applied)

5.15. Test 23: Single diagonal pinned frame 2L60x8



Figure 159. Specimen on test bench

5.15.1. Loading history

2L60x8 pinned frame with tension diagonal was tested under displacement control loading protocol reported in *Figure 160*. Standard protocol was followed until 10th cycle. From 11th to 20th cycle only negative displacement has been increased, till reaching -2.50% drift. In-plane buckling of the brace occurred during first loading cycle of 0.19% drift. Post-buckling phase has been then investigated through four additional cycles. *Figure 160* shows loading history while *Table 29* provides the schedule of displacement cycles applied.

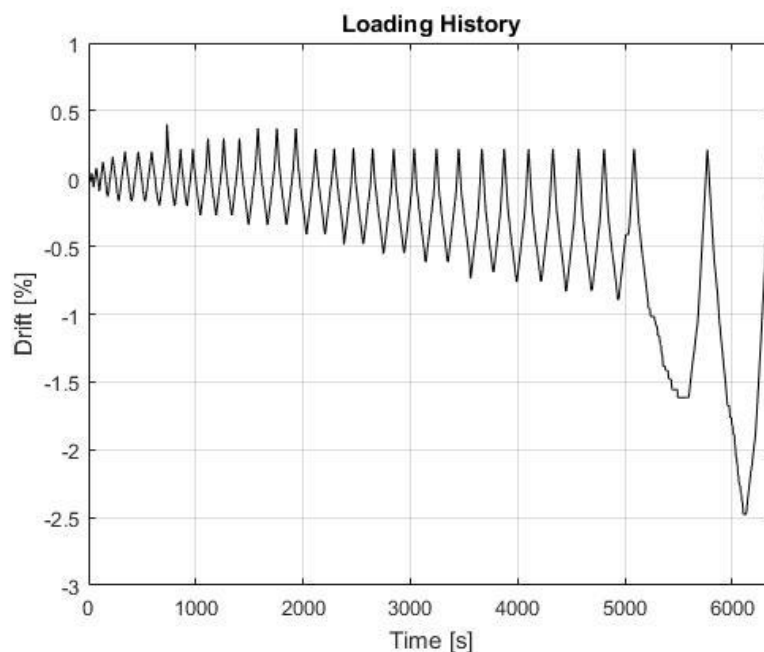


Figure 160. Loading history

Displacement step	Cycles	Cumulative n. of cycles	Displacement [mm]	Drift [%]
1	1	1	± 1	± 0.04
2	1	2	± 2	± 0.08
3	1	3	± 3	± 0.12
4	1	4	± 4	± 0.15
5	3	7	± 5	± 0.19
6	3	10	± 6	± 0.23
7	3	13	± 7	± 0.27
8	3	16	± 8	± 0.31
9	3	19	± 9	± 0.35
10	3	22	± 10	± 0.38
11	2	24	+6 -12	+0.23 -0.46
12	2	26	+6 -14	+0.23 -0.54
13	2	28	+6 -16	+0.23 -0.61
14	2	30	+6 -18	+0.23 -0.69
15	2	32	+6 -20	+0.23 -0.77
16	2	34	+6 -22	+0.23 -0.84
17	2	36	+6 -24	+0.23 -0.92
18	2	38	+6 -26	+0.23 -1.00
19	1	39	+6 -30	+0.23 -1.15
20	1	40	+6 -65	+0.23 -2.50

Table 29. Test 23: displacement cycles

5.15.2. Global overview

Initial stiffness of single diagonal 2L60x8 has been derived from force-drift ratio. The value amounts at 34.8 kN/mm (174 kN at 5 mm displacement applied). Configuration of tension diagonal frame make the structure weaker when tension is applied to frame, since compression stresses develop into diagonal. Slender profiles are low resistive to buckle.

Global force-drift ratio graph has been plotted and reported in *Figure 161*. Hysteresis loops reflects the inelastic deformation behaviour. Total resistance of the frame was +186 kN and -325 kN. Difference in bearing capacity results from asymmetry of single diagonal frame configuration, resulting weaker in tension loading direction (diagonal under compression). Buckling of the brace occurred during first compression peak ± 5 mm. After that no more resistance to horizontal displacement was offered when frame under tension. Photo of *Figure 164* provides a view about buckling mode of test 23.

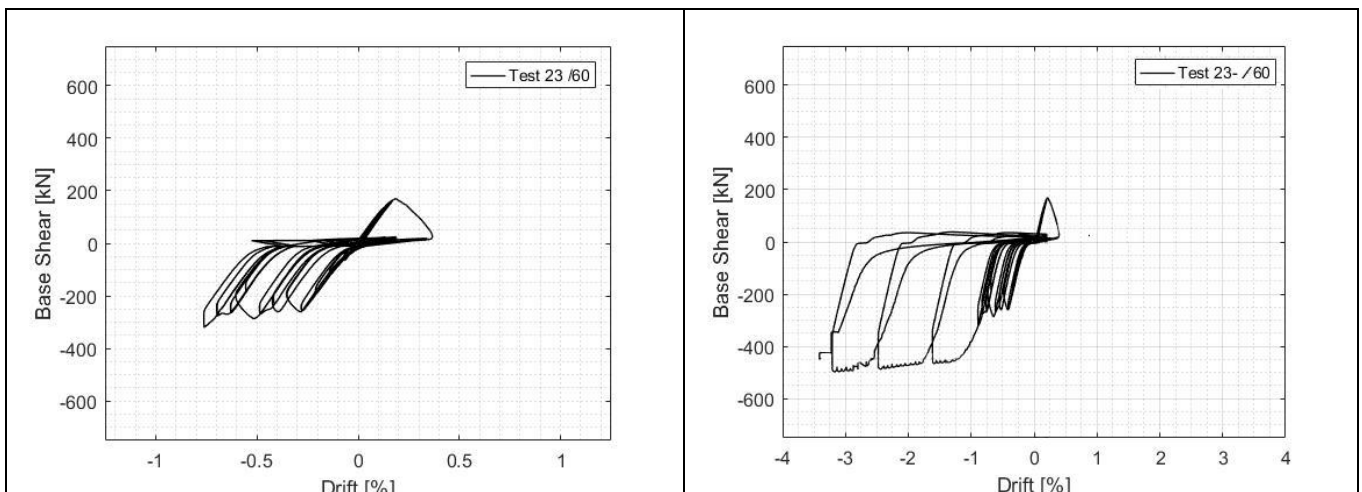


Figure 161. Global hysteresis loops pre-yielding and after yielding of the brace

Furthermore, no plastic deformation was observed in columns and beams, designed to remain elastic. Therefore, slippage and ovalization of bolts are the only ones to provide ductility. Test specimen until the joint fracture never reached tensile yielding of gross section due to the fact that their connections have not been designed according to capacity design rules.

5.15.3. Columns and beams

Forces data about right column are not relevant, since strain gauges were damaged. While loads on left column increased till buckling occurred in brace. After that, column was being loading only when frame was undergoing compression. Meanwhile tension was applied to frame during post-buckling phase, bracing buckled so to not be able to oppose resistance to horizontal displacement. Column became free to move on the right, rotating. In this situation, no stresses was developed into column gross section. Conversely, when frame were being pushing, tensile stresses were evolving in continuous diagonal and compression in the right column. Forces distribution on columns have been reported in *Figure 162*. Loads was shared 30% on column and 70% on brace. Forces in column oscillated between:

- 100 kN for compression and 32 kN for tension during pre-buckling phase
- 15 kN for compression and 200 kN for tension during post-buckling phase

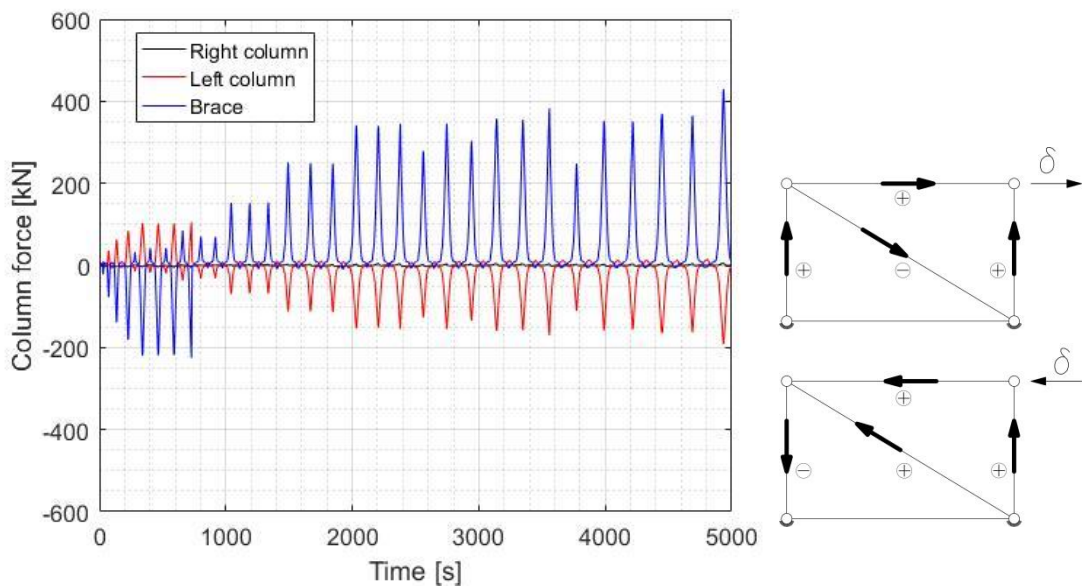


Figure 162. Trend of load on brace and columns. Comparison. Force distribution scheme.

5.15.4. Bracings behaviour

The rotation demand of beam-to-column connections has introduced a bending moment into the brace in case of moment resisting frame. Since bracing ends were hinged in the pinned frame, no moment was transferred to brace. Thus, brace buckling occurred due to pure compression load. Elastic buckling occurred during first compression peak of ± 5 mm cycle while axial loads on brace reached 218 kN. Plastic hinge was formed, so that no more resistance was offered next cycle. Dealing hand with diagonal under tension, resistance kept on achieving more than 400 kN, until yielding occurred at 1.12% drift.

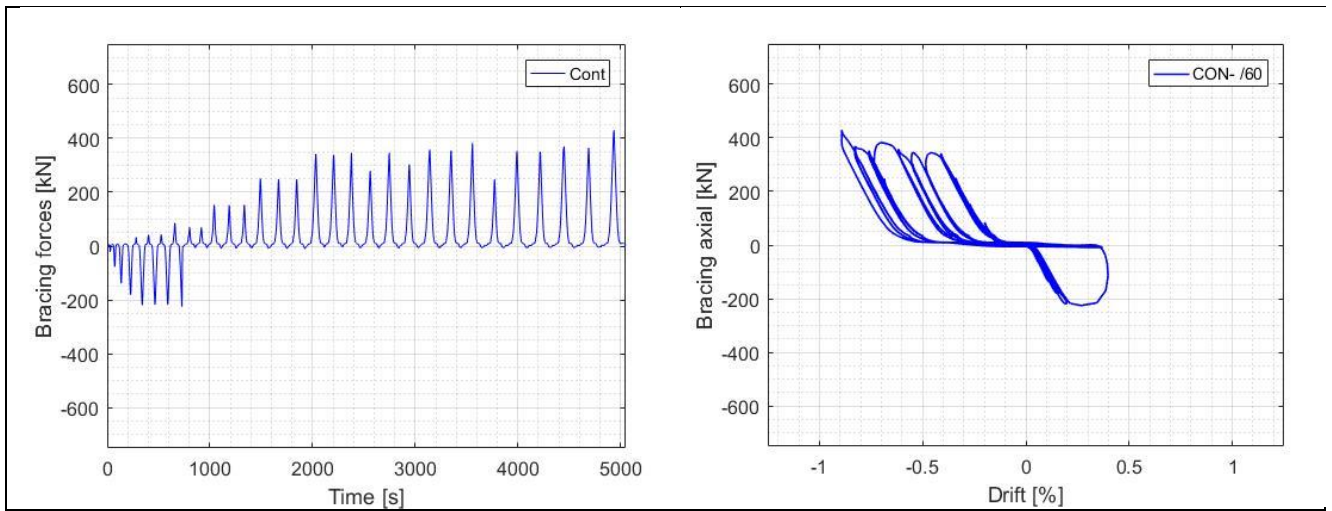


Figure 163. Bracings axial load over time and displacement applied



Figure 164. Buckling of diagonal. (+0.19% drift applied)

6. Analysis of test results

In this chapter it will be analysed in depth the results obtained during tests. Following paragraphs deal with main topics investigated such as energy dissipation, ductility and stiffness, and how configuration and elements of the frame contribute to improve performances. A detailed overview is carried out, in which main focus has been performed on slip and ovalization phenomena, that result to give a valuable contribution to frame in terms of ductility, so that to overall energy dissipation. Additional deep investigation has been presented about gusset plates, liable of many effects to global efficiency of the analysed systems.

6.1. Energy dissipation

6.1.1. Bolts slip and ovalization

Trend of shear about test 5 has been reported as function of drift in graph of *Figure 165*. It has been chosen since frame never passed beyond the elastic limit, so it best represents energy dissipation not connected to plasticization of bracings. Black curves demonstrate behaviour till 0.15% drift cycle. Their reduced amplitude are expounded by the fact that energy brought to the frame, was completely released during unloading phase. While red characterizes curves from 0.19% to 0.38% drift cycles. Within this range, hysteresis became significant. The amplitude of curves gradually increased, so that a part of the energy loaded in frame has been not released, but dissipated.

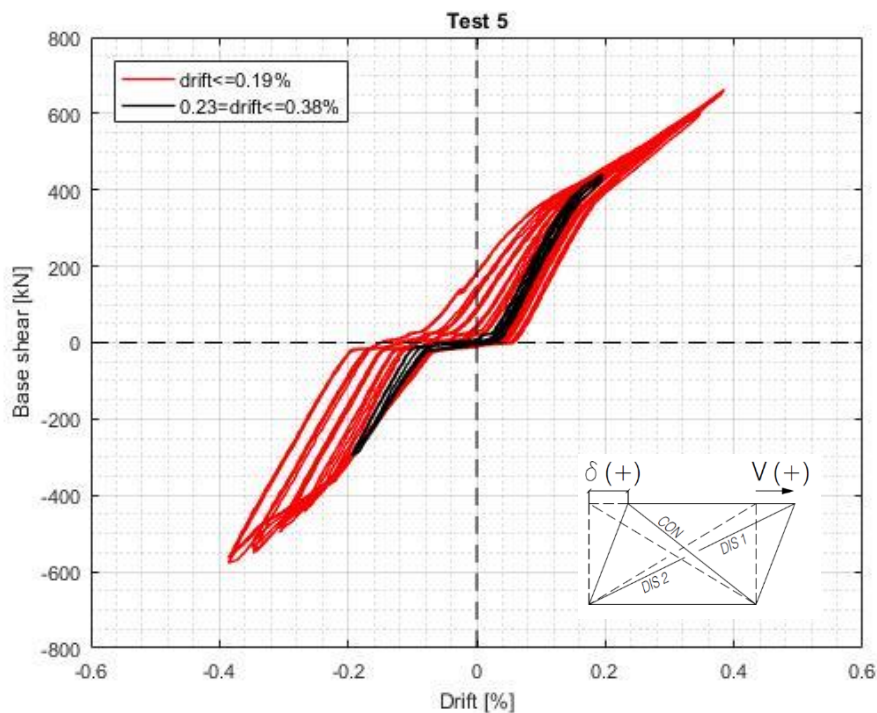


Figure 165. Test 5: base shear – drift

Either yielding or plastic deformation have not been observed on structural elements of the frame. Besides bracings and gussets have not yielded or plasticized. Thus, energy dissipation highlighted by hysteresis loops was not linked to post-elastic deformation, but to slippage at braces ends and ovalization of bolts holes.

Slip mechanisms are common in bolted connected steel frame. Since there is a clearance between the bolt and the hole in which it is fitted, the bearing stress is mobilised only after the plates slip relative to one another and start bearing on the bolt. Pretension in the bolt causes clamping forces between the plates even before the external load is applied. When the external load is applied, the tendency of two plates to slip against one another is resisted by the friction between the plates. The frictional resistance is equal to the coefficient of friction multiplied by the normal clamping force between the plates. Until the externally applied force exceeds this frictional resistance the relative slip between the plates is prevented. When the external force exceeds the frictional resistance the plates slip until the bolts come into contact with the plate and start bearing against the hole. Beyond this point the external force is resisted by the combined action of the frictional resistance and the bearing resistance. Slip data from LVDT at brace joints nodes are reported in Appendix F.

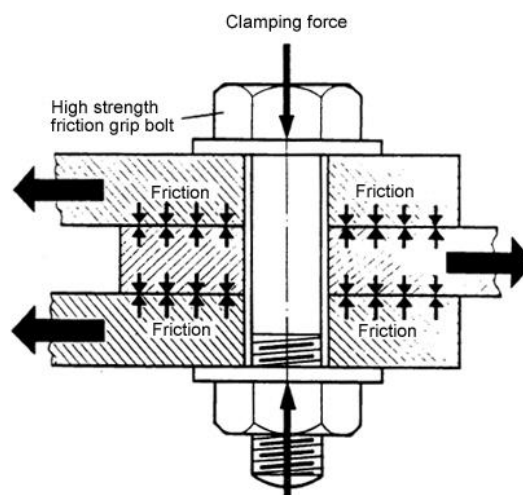


Figure 166. Scheme of involved force at bolt connection

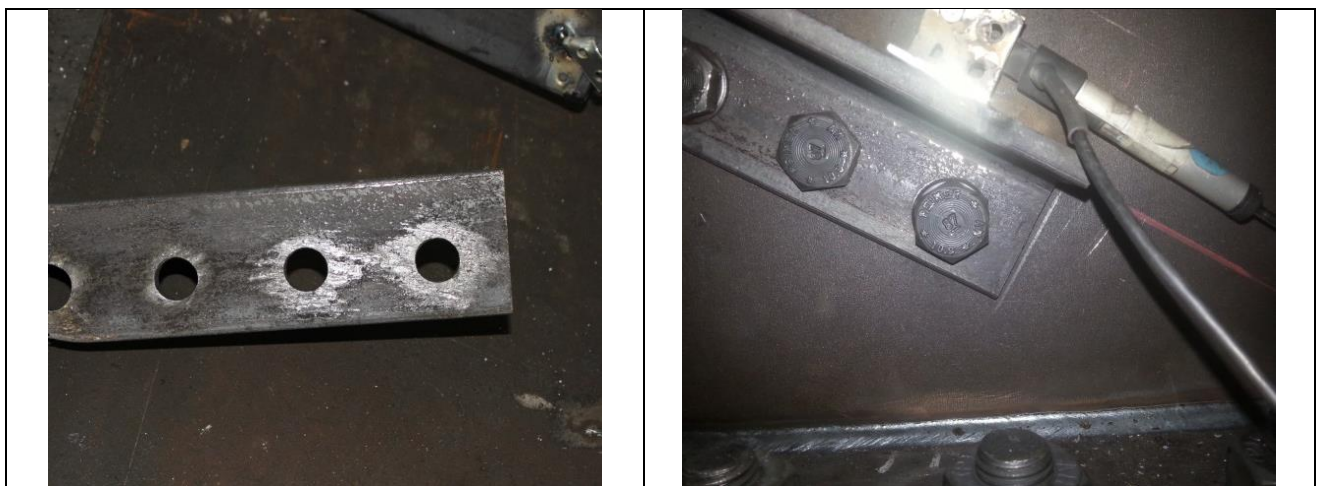


Figure 167. Slip and its effects on internal surface of brace at connection to gusset

As shown by force-drift ratio graphs previous reported for each test, two well defined stages termed pre-sliding and sliding can be observed. In the pre-sliding stage the hysteresis loop adopts a very steep stiffness tendency interrupted by a zone with very low stiffness where the bolts are laterally loaded due to the bolt hole tolerance. This stage represents the case before the sliding mechanism of the slotted plate is fully activated. In the sliding stage where the sliding mechanism of the slotted plate is fully activated and the slotted plate slides for a given distance the hysteresis loop adopts a very low stiffness.

Bolts ovalization also contributed to energy dissipation. This phenomenon mainly occurred at bolts holes of node boom hook of brace ends. Normally, hole is slightly larger than the fastener and the fastener is loosely placed in hole. After connection slip occurs, the bolts bear on the bolt holes at large storey drifts, causing localized plastic deformations around the bolt hole and gradually worsened pinched response. Slippage occurred due to ovalization and ovalization increased slippage. This ovalization results in an increasing “slack” in the system around the point of zero force. Hence, the experimental curves, typical of bolted connections, shows pinched hysteresis loops with a large slip plateau (very low slope of the experimental curve) and subsequent sudden stiffening.

To prevent excessive deformation of the hole, an upper limit is placed on the bearing load. This upper limit is proportional to the fracture stress times the projected bearing area:

$$R_n = C \cdot F_u \cdot \text{Bearing Area} = C \cdot F_u \cdot d_b \cdot t$$

If deformation is not a concern then $C = 3$;

If deformation is a concern then $C=2.4$ ($C = 2.4$ corresponds to a deformation of 6.35 mm).

So, the equation for the bearing strength of a single bolts is ϕR_n where, $\phi=0.75$ and

$$R_n = 1.2 \cdot L_c \cdot t \cdot F_u < 2.4 \cdot F_u \cdot d_b \cdot t \cdot F_u$$

L_c is the clear distance in the load direction, from the edge of the bolt hole to the edge of the adjacent hole or to the edge of the material. The relationship can be simplified as follows:

The upper limit will become effective when $1.2 \cdot L_c \cdot t \cdot F_u = 2.4 \cdot F_u \cdot d_b \cdot t \cdot F_u$

i.e., the upper limit will become effective when $L_c = 2 \cdot d_b$

Thus, braces bolts holes have been snapped every time a test ended. As well as diameter variation has been documented and reported in a table. An overview about slippage and ovalization are outlined below through photos. Detailed data about radius length variation of the bolt holes in bracings, gusset plates and mid-plate, measured after every test have been reported in Appendix K.

Table 30 shows different plastic mechanisms observed in the specimens. All the single diagonal specimens first entered the post-elastic regime at the mid-length of the bracing, after which a significant loss of stiffness and resistance has been observed. After plastic buckling at a larger drift, a significant slip occurred in the bracing connections, which had a positive impact on the quantity of global energy dissipation.

Frame configuration	Bracing configuration	Plastic buckling on bracing		Bolt slip at bracing joints	
		Base shear [kN]	Drift [%]	Base shear [kN]	Drift [%]
MRF	60X	448	0.58	740	-0.30
	60S	226	0.19	243	-0.43
	70X	-	-	538	-0.71
	70S	380	0.26	437	-0.41
PF	60X	-	-	324	-0.38
	60S	183	0.19	256	-0.29
	70X	582	0.19	472	-0.43
	70S	202	0.19	293	-0.27

Table 30. Numerical values obtained for various inelastic mechanisms



Figure 168. Bolt holes ovalization at brace joints ends

6.1.2. Bracings buckling

Buckling load of continuous brace could be evaluated, for what regarding tension diagonal configuration frame, starting from base shear, applying the principle of effects super-imposition, according to the scheme of *Figure 169*. Particularly:

- scheme a) represents tests 3, 7, 19 and 23, in which lateral displacement imposed (+8 mm) is highlighted as well as the correspondent value of base shear (376 kN), liable of brace instability;
- scheme b) represents frame during test 16, in which the load value indicated stands for that recorded for a displacement imposed of +8 mm: resistance of this specimen configuration is provided by the only semi-rigid beam-to-column connection;
- scheme c) has been obtained subtracting scheme b) from scheme a): base shear value that is deduced explains the resistance provided by brace, that in case of test 7 amounts at 291 kN.
- compression axial load on diagonal could be therefore derived by using the equation:

$$N_{2L60x8} = \frac{V}{\cos \theta} = \frac{199.2}{\cos 30^\circ} = 230 \text{ kN}$$

$$N_{2L70x7} = \frac{V}{\cos \theta} = \frac{291}{\cos 30^\circ} = 336 \text{ kN}$$

Hence, compression axial loads obtained (i.e. 336 kN), confirm the axial load values derived by strain gauges deformations data (the corresponding one for test 5 is 340 kN).

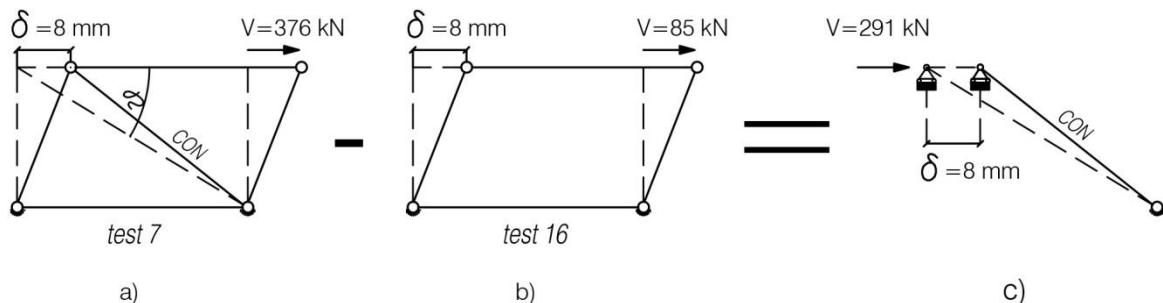


Figure 169. Test 3-7-18-23. Evaluation of axial buckling load of brace through base shear (values about test 5)

Conclusions about axial load trend in bracings are proved by graphs of *Figure 170* representing axial action over in-plane inflexion of the brace, measured by potentiometer assigned to channel 10 of control unit. Curves have been highlighted by means of two distinct colours:

- a pre-buckling phase emphasized using black colour; in case of 2L60x8 bracings profiles up to a maximum drift of 0.19%, while 0.27% for 2L70x7 gross-section profiles. During elastic phase, inflexion oscillated between either 1 mm and 2.5 mm in S60 MRF or 1 mm and 5 mm in S70 MRF, under tension and compression, respectively;
- post-buckling phase noted by red colour; reference cycles included drift from 0.19% to 0.54% for 2L60x8, while from 0.31% to 0.35% for 2L70x7. Profiles of test 3, reached plastic deformation just behind first compression peak of 0.19% drift cycle, when compression stresses reached 226 kN. Besides buckling of 70 mm profiles occurred during 0.31% cycle while continuous diagonal was loaded up to 340 kN, involving an inflexion of 36.86 mm.

- after tests ended, and pots removed, residual deformation of diagonals amounted at 57.13 mm in 2L60x8 and 29.54 mm in 2L70x7.

Data about inflexion of tension diagonal pinned frame have not been reported since pots probably didn't work. Data resulted inconsistent.

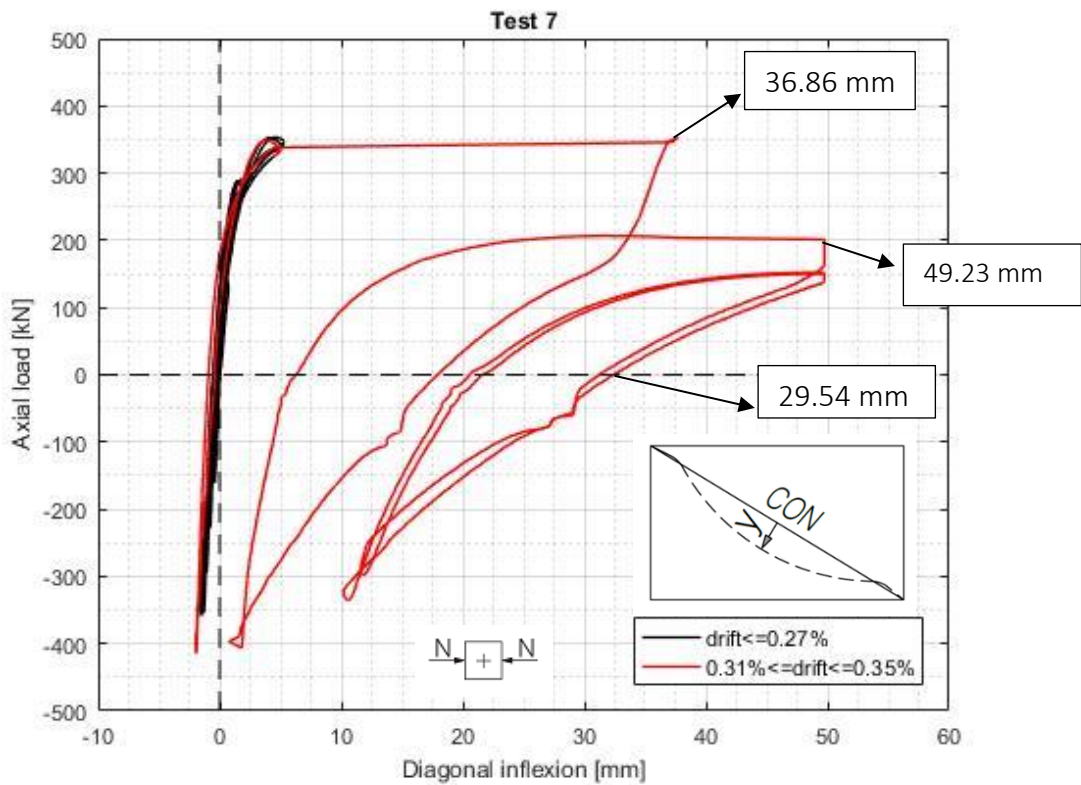
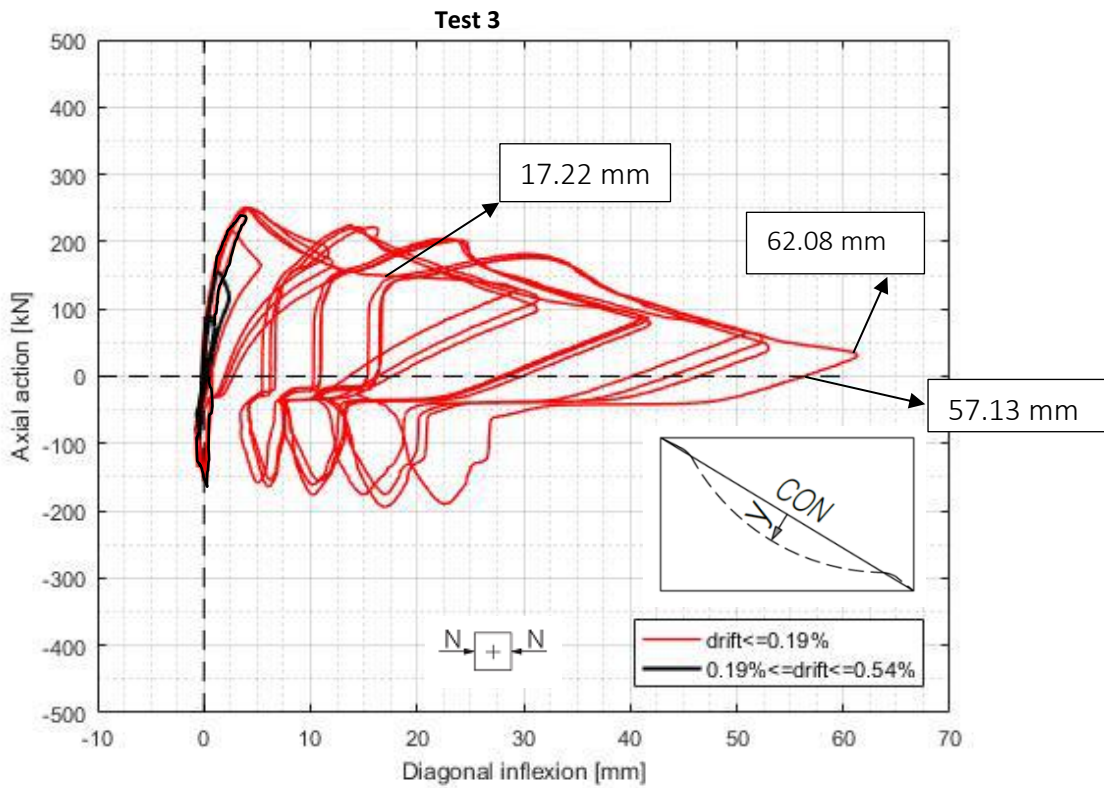


Figure 170. Diagonal inflexion over axial load in bracings

Table 31 provides a comparison between forces that generate buckling into compression diagonal. Collation has been done in order to highlight differences between EC3 obtaining values and those derived by experimental tests. Besides, to more understand the gap in-between, it has been performed EC3 calculation using yielding and rupture stresses values from laboratory tensile tests using a safety coefficient equal to 1.

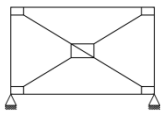
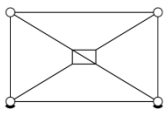
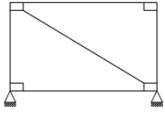
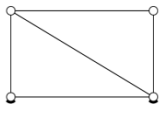
TEST TYPOLOGY	DIAGONAL SECTION	EC3 DESIGN VALUE	EC3 DESIGN VALUES (safety coefficient = 1 yielding stress and rupture from tensile specimens test)	EXPERIMENTAL VALUES	RATIO EXP. DATA/EC3
		$N_{b,Rd,x}$	$N_{b,Rd,x,REAL}$	$N_{b,Rd,x,TEST}$	
		[kN]	[kN]	[kN]	
1) 	2L60x8 (Test 01)	188.81	202.51	300.00	1.59
	2L60x8 (Test 13)			402.00	2.12
	2L70x7 (Test 05)	235.01	265.08	buckling not reached; max compression load recorded: 357 kN	-
2) 	2L60x8 (Test 17)	188.81	202.51	-	-
	2L70x7 (Test 18)	235.01	265.08	-	-
3) 	2L60x8 (Test 03)	57.33	61.48	245.00	3.98
	2L70x7 (Test 07)	80.16	86.09	340.00	4.24
4) 	2L60x8 (Test 23)	57.33	61.48	218.00	3.80
	2L70x7 (Test 19)	80.16	86.09	225.00	2.81

Table 31. Comparison between design and experimental values about buckling axial load in compression diagonal

Data of test 17 about instability are not reported because useless, since sway occurred due to bad design of the beam-brace-column connection geometry. Nevertheless, all other values of $N_{b,Rd,x}$ became significant. Buckling axial loads resulted much more higher than those indicated for design by EC3 in every case. During test 5, instability didn't occur even if axial load in diagonal overtaken the standards limit by 34%: at 357 kN buckling was not reached yet.

The effect of pre-tension of bolts and a well assessment of the loading system, resulted evident comparing test 1 with test 13. Though both tests deal with cross-configuration frame with 2L60x8 diagonal section, the in-plane buckling axial load occurred at 100 kN higher in test 13, with a difference of 25%. Comparing to EC3 values, the gap increases more, reaching 33% and 50%, for test 1 and test 13, respectively. More evident discrepancy resulted by test done on single diagonal configuration frame. In case of moment resisting frame with tension diagonal, experimental values are 4 times higher than those derived by EC3 prescriptions. Furthermore, $N_{b,Rd,x}$ recorded during single diagonal pinned frame tests results either 3.5 or 2.5 times more, for 2L60x8 and 2L70x7, respectively.

Therefore it could be argued that EC3 overly underestimates bearing capacity of the compression diagonal, at least as regards the tested profiles. Underestimation is mainly linked to:

- overestimation of the free-length inflexion of the compressed rod, equal either to half of the continuous diagonal length cross-configuration frame (both diagonals are considered as active) or to the total length of continuous diagonal in case of single bracing frame;
- overestimation of the parameter α , representing the imperfection coefficient assigned for the stability curve of hot-rolled double angle profiles.

Thus, the reduction coefficient for the relative buckling mode χ results as underrate. Therefore, first consequence is that bearing capacity of the compressed rod arises as evaluated too much on safety side.

6.1.3. Idealization of the brace

Experimental results, especially those regarding stiffness, real behaviour of the diagonal under compression stresses has been summarized by schematic rods shown in *Figure 171*:

- stiffness of brace in the elastic field is exclusively guaranteed by brace extensional stiffness;
- during post-buckling phase, after plastic hinge development, stiffness of the brace is given by contribution of both mid-span and diagonal edges springs, molding the connection constraint to main members;
- after failure stiffness of the braces has just given by spring at its ends.

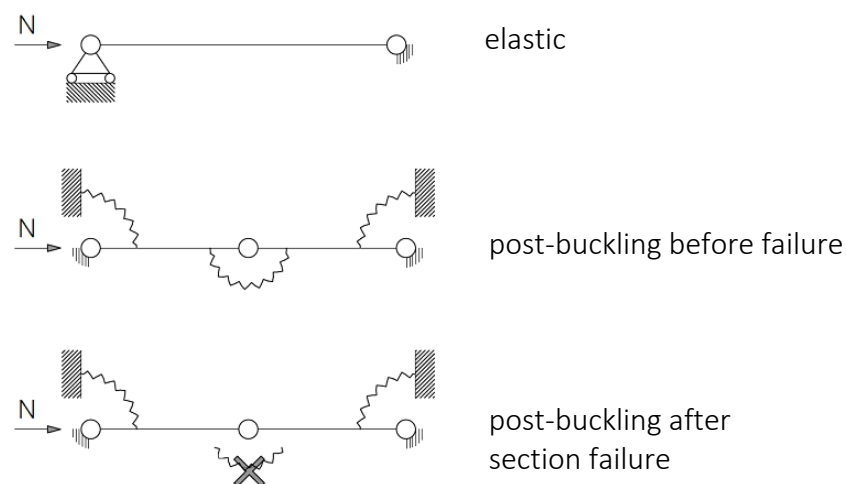


Figure 171. Test 3-7-19-23: bracing behaviour idealization

6.1.4. Strength and stiffness comparison

Resistance and stiffness values are summarized in *Table 32*. Stiffness has been derived by base shear-drift ratio graph for each test performed. Besides resistances adopted have been evaluated in correspondence of +5 mm (0.19% of drift) positive displacement applied, in fully elastic field.

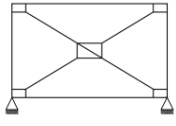
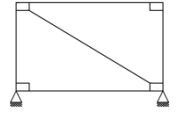
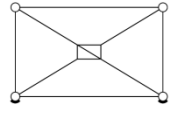
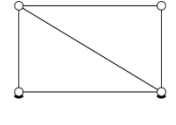
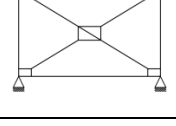
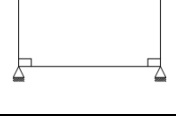
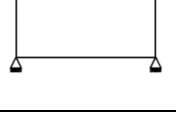
TEST TYPE	DIAGONAL SECTION	k_{el}	k_{pl}	R_{5mm}
		kN/mm	kN/mm	kN
1) 	2L60x8	58.84	20.55	294.23
	2L70x7	73.90	NA	369.50
2) 	2L60x8	51.25	-3.50	256.25
	2L70x7	55.92	-7.38	279.63
3) 	2L60x8	50.12	NA	250.60
	2L70x7	51.52	NA	257.46
4) 	2L60x8	32.40	0.00	162.00
	2L70x7	18.50	0.00	92.46
5) 	2L60x8	70.83	-56.25	354.18
6) 	ONLY GUSSET	13.36	NA	66.83
7) 	NO GUSSET	2.30	NA	11.50

Table 32. Stiffness and strength tests comparison

Stiffness of different configuration frames has been evaluated in both elastic and plastic field. The calculation scheme has been reported in graph of *Figure 172*:

- stiffness in the elastic field is equal to the slope of the red dot line passing through the origin of axes and for the point at which the frame has reached the maximum resistance before continuous brace instability (point A);
- hardness during plastic phase is equal to the slope of the blue dot line passing through the point at which the frame has reached the maximum resistance during cycle after buckling (point B) and the point in which has been measured the resistance peak during last cycle before crack formation (point C)

Frame types with and without gussets show instead a symmetrical trend, developing same stiffness in both loading direction. Their elastic stiffness amount at 13.36 kN/mm and 2.30 kN/mm, respectively.

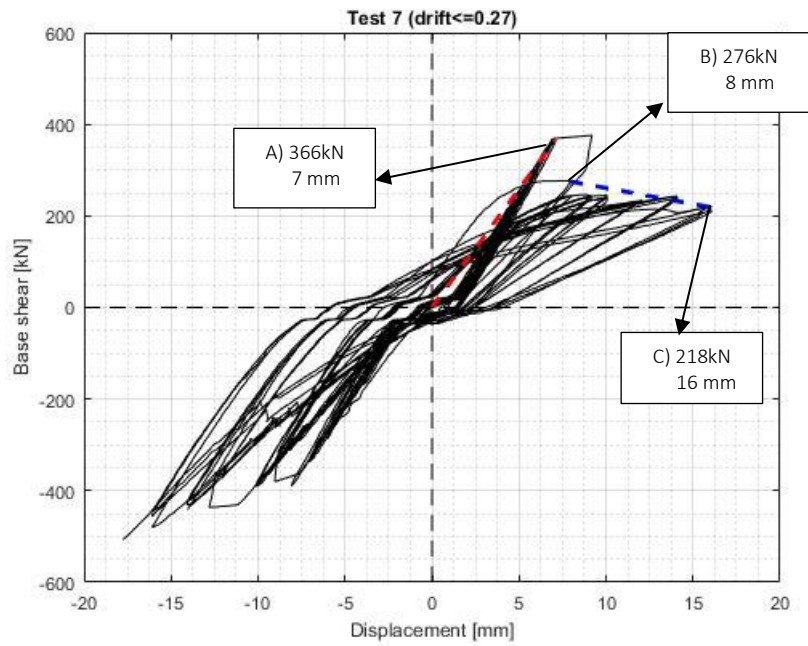


Figure 172. Test 7: calculation scheme of frame global stiffness

6.1.5. Overstrength from compression diagonal

Past experience and observations of building behaviour following severe earthquakes has shown that structural overstrength plays a very important role in protecting buildings from collapse [1, 2]. This is explained by the presence of such structures with significant reserve strength not accounted for in design. In the literature, several studies have been carried out in order to evaluate the effect of the overstrength on the seismic response of steel moment-resisting framed buildings [1-3].

In the case of concentrically-braced frames, EC8 assumes that only tension diagonals participate in the lateral resistance of earthquake-induced loading, and hence, in these structures dissipative zones are mainly located in the tension diagonals. EC8 approach is different from that followed in other seismic codes. Thus, this research performed through previous presented tests, concludes that, also if slightly underestimated, compression diagonal made differences in prediction of the variation in lateral resistance of frame. Test results illustrate that the design approach adopted in European provisions whereby the lateral frame resistance is only based on the tension diagonals could provide a reasonable representation of the behaviour within practical ranges of brace slenderness. However, in terms of satisfying the objectives of capacity design, it is important that additional checks are considered to account for possible adverse effects caused by the contribution of the braces in compression.

Discontinuous diagonal under compression provided overstrength in global resistance of the frame. This evidence is clearly highlighted by graphs of *Figure 173* reported below. Both active bracings frame response is compared through global force-drift ratio and initial stiffness with correspondent one of tension diagonal configuration.

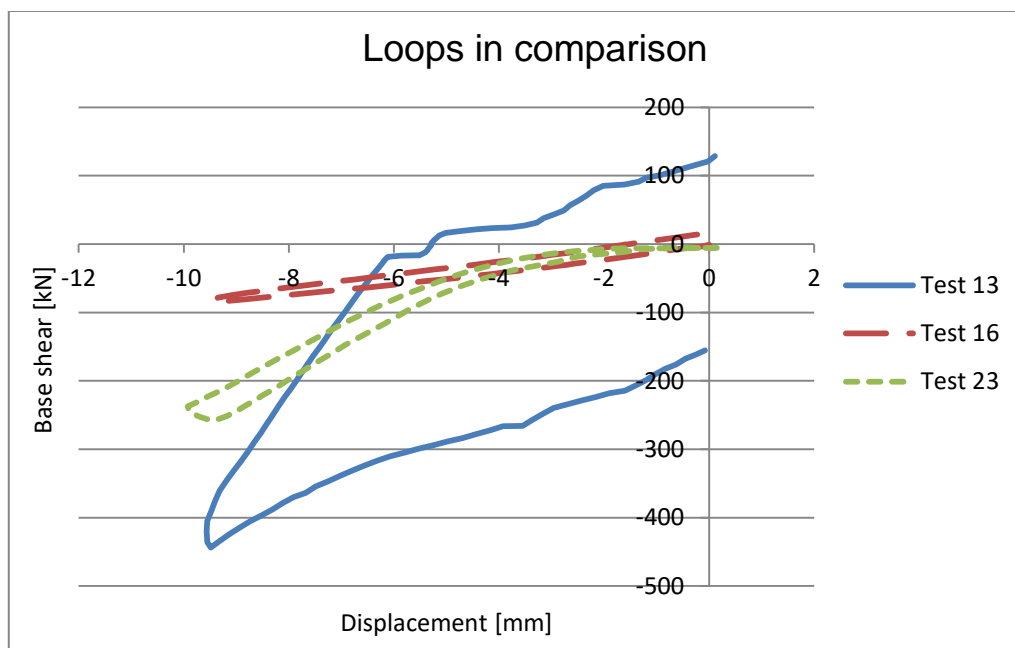


Figure 173. Hysteresis loops comparison

Overstrength must be only evaluated for what regarding negative displacement, when continuous brace is stressed by tension. For instance, at equal drift value, i.e. -7 mm applied to 2L70x7 moment resisting frame, tension diagonal configuration reached a resistance of 333 kN while both active bracings frame achieved 431 kN. Thus, overstrength tendered by compression discontinuous diagonal amounts at 29%.

Compression bracing significantly influences as well the initial stiffness of X-braced frames which is an aspect that is normally neglected during the analysis stage in current design practice. *Figure 174* highlights this evidence. Overall behavior of the frames with and without compression diagonal is significantly different.

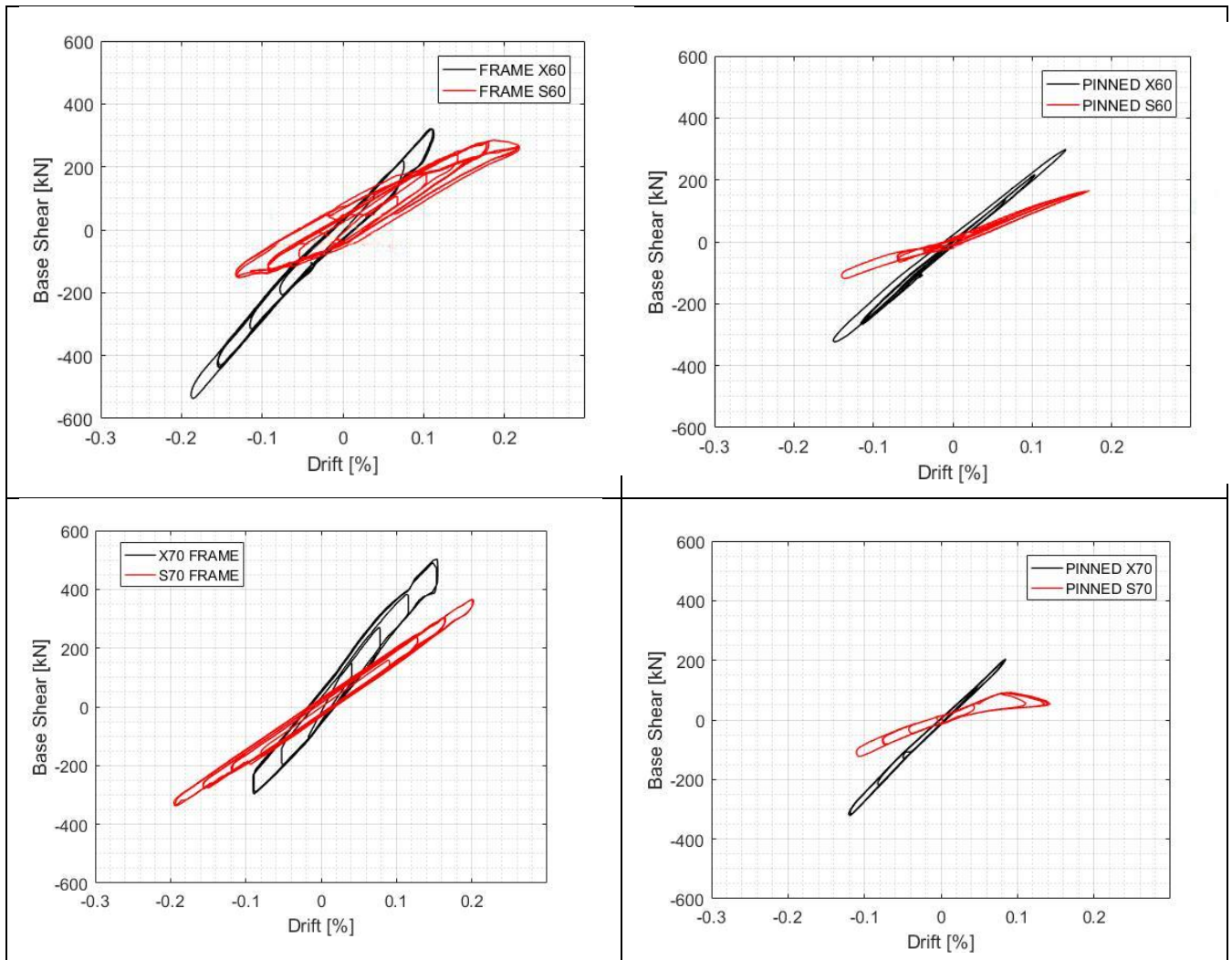


Figure 174. X-braced vs Single diagonal frame - initial stiffness

Contribution of the compression diagonal is not limited only to the initial stiffness of the structure. As confirmed by graphs of *Figure 175*, the global resistance of the braced frame is also completely different when the compression diagonal is taken into account. X-braced specimen exhibited also higher energy dissipation due to extra post-buckling and bolt-slip dissipations. Furthermore, during post-buckling phase, even after joints were fractured, compression bracings provided a moderate amount of strength both under tensile and compression forces. The separated surfaces returns in contact when undergone compression, providing residual resistance.

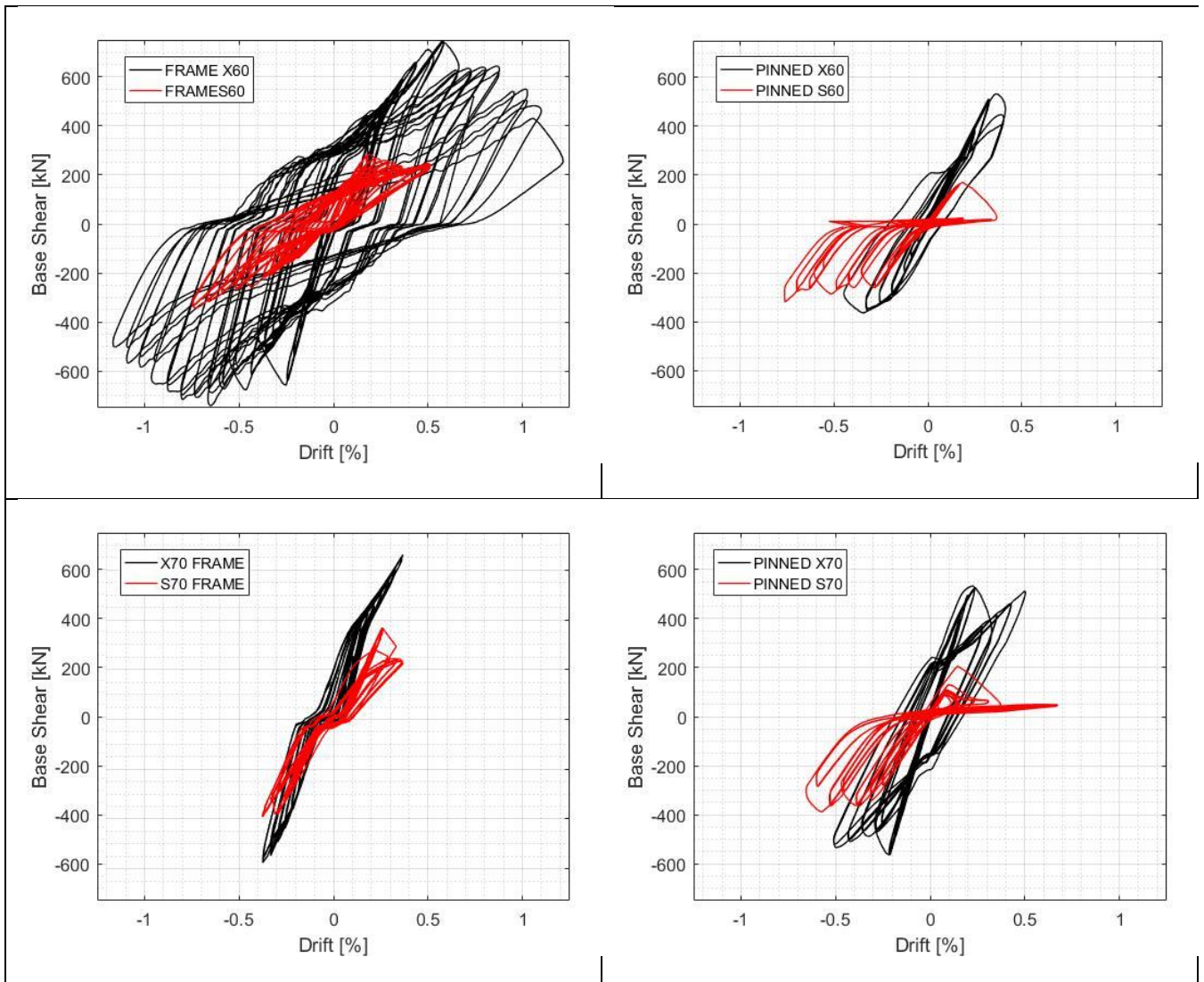


Figure 175. X-braced vs Single diagonal frame - global behaviour

The effects of bracing configurations were not studied beyond elastic response as presented here. Depending on concept, seismic design codes provide various response modification factors (R) for different types of lateral load bearing systems but configuration of these systems are often ignored in the proposed values.

Computation of R can be carried out using the following method but there are some essential values which should be derived first. These values include: yield and ultimate displacements, respectively Δ_y and Δ_u ; also yield force and elastic strength demand force which would be presented by F_y and F_{Ed} , notations respectively. R estimation can be carried out by defining two factors: strength demand reduction factor due to ductility, R_d and overstrength factor, Ω . Equation 4 shows parameter derived for evaluation of R-values (Uang, 1991, Behbahani, 1996,).

$$R_d = \frac{\text{Elastic Strength Demand}}{\text{Real Strength}}$$

$$\Omega = \frac{\text{Real Strength}}{\text{Design Strength}}$$

$$R = R_d \Omega$$

6.1.6. Pinned vs moment resisting frame

The global behaviour of pinned and moment resisting frames have been compared through graphs of *Figure 176*. Strength and stiffness amplification of the specimens is linked to frame effect, so that partial strength gusset plate beam-to-column connections really improved resistance and stiffness. Additional further effect, in case of a semi-rigid frame, was given by the reduced effective slenderness of the bracings due to semi-rigid beam ends. In the pinned case the slenderness of the bracings is higher due to the larger effective length.

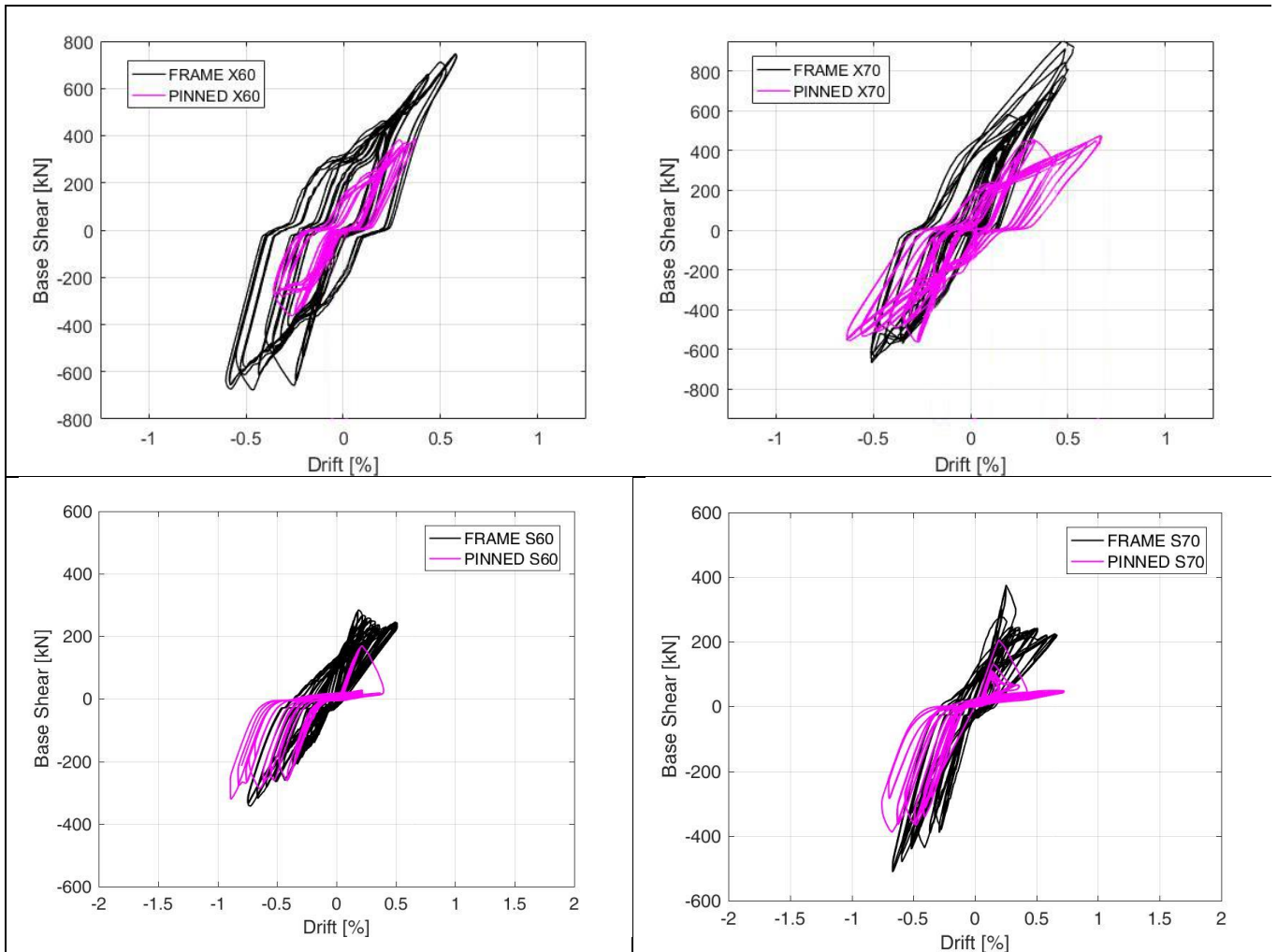


Figure 176. Global behaviour semi-rigid vs pinned frame

Frame effect contributed actively to rise up resistance of the system in both stresses situations of tension and compression. Looking at single diagonal configuration frames, buckling in moment resisting frames was reached at values almost 2 time higher than those in the pinned configuration, considering towards weaker direction, so when continuous brace was under compression. The same applies to cross configuration frames, in which evident improvement in stiffness and resistance performances are noticed.

6.1.7. Gusset plate

Frame action, discussed through previous chapters, derived mainly from beam-to-column gusset-plate connection. *Figure 177*, where the global base shear-drift behavior of the frame with and without gusset plates have been compared, shows the capacity of the semi-rigid connection with respect to only web angles. As result, 75% percent of the elastic stiffness and 79% of the ultimate resistance (at 2% drift) are provided by the gusset plate connections. Rotational stiffness of both subsystems of beam-to-column connection, has been evaluated and reported in detail through next chapter.

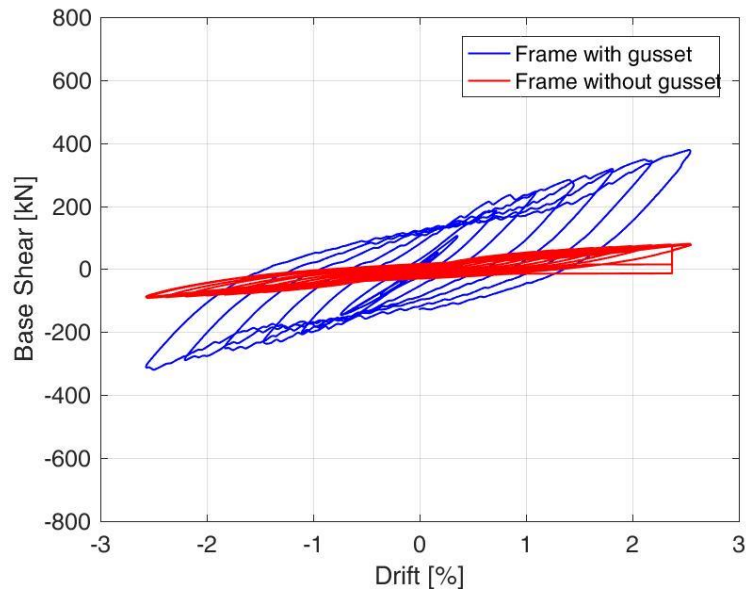


Figure 177. Global base shear-drift behaviour of the frame with and without gusset plate connections

First effect in performances improvement provided by gusset plates is given in initial stiffness of the frame. The slope of the curve increases clearly in case of moment resisting frame, compared with the corresponding configuration of the pinned frame. Gusset plate connection contributes to stiffness from initial to final steps. *Figure 179* and *Figure 180* report idealization line derived by interpolation of data: base-shear force (y-axis) and displacement applied (x-axis). Both slope and resistance peak value are higher for the case of a moment resisting frame. Thus, gusset plates connections behaved somehow different from the fully pinned connection proposed by standards for extracting and evaluate design data. Boundary conditions could be improved by taking into account additional performances, normally neglected, provided by gusset plates connection. Reserve capacity of these connection devices permits to have overall performance of the frame improved and an additional source for structural elements to stand also after bracings collapse.

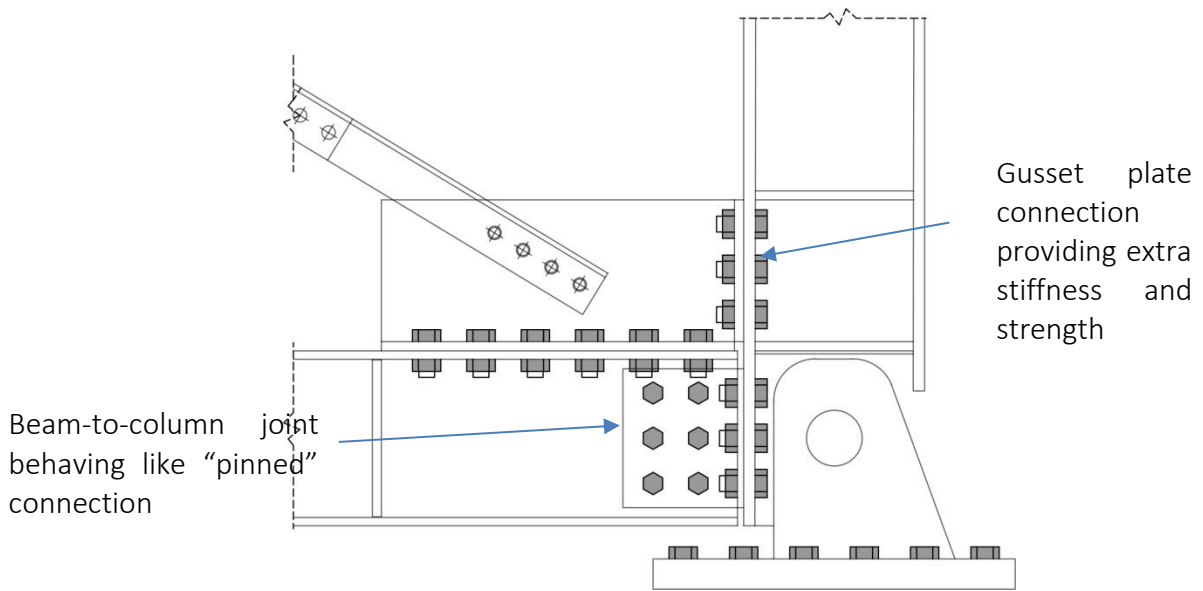


Figure 178. Geometry of beam-to-column connection

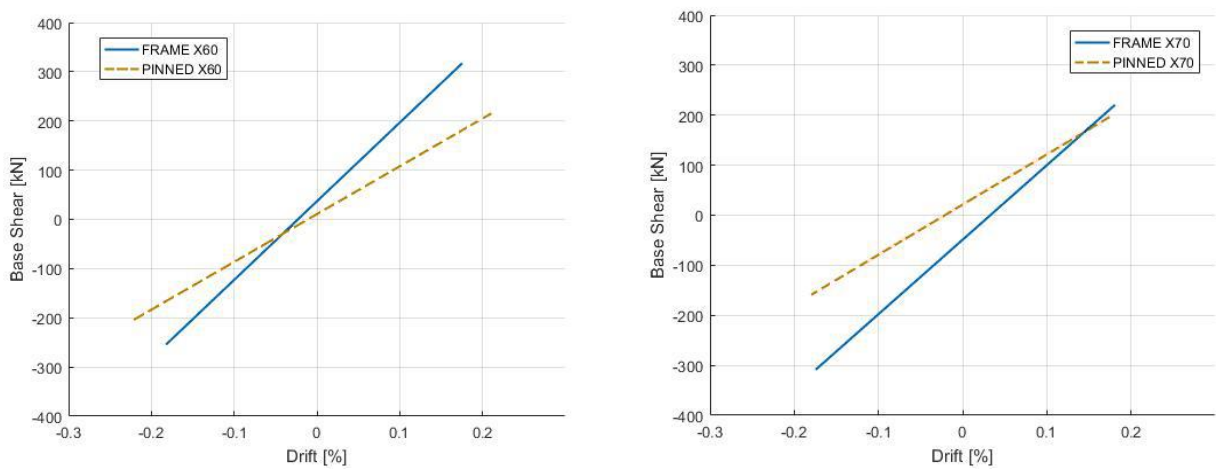


Figure 179. Initial stiffness comparisons of X-braced semi-rigid and pinned frames

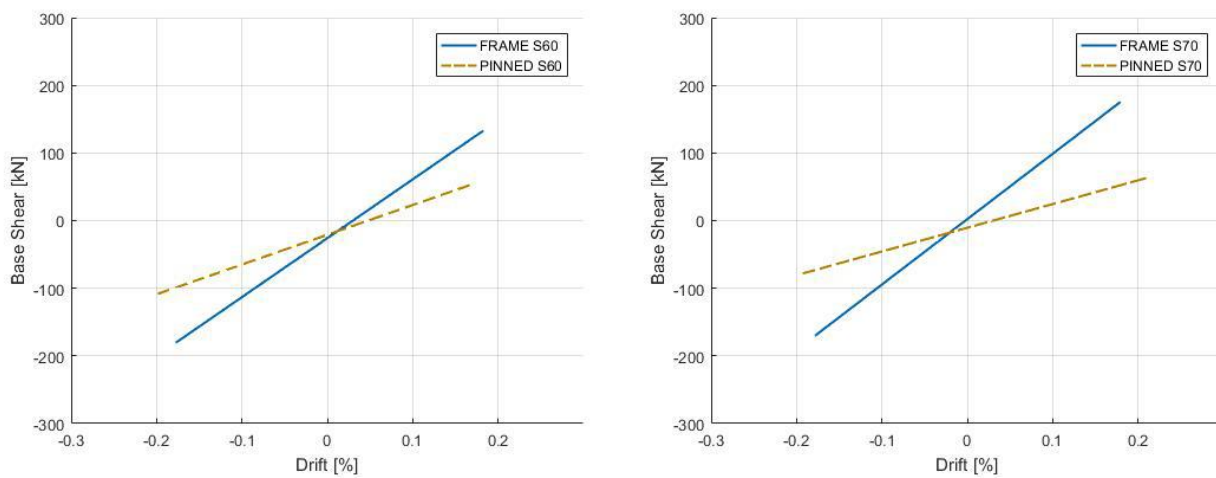


Figure 180. Initial stiffness comparisons of semi-rigid and pinned frames

6.1.8. Reserve ductility of the frame

Studies have shown in their globality that the overstrength depends on different factors which the most important of them is member ductility factor. One term used to categorize a steel frame is ductility, or the ability to deform after one or several of its members and/or connections become fully yielded. Higher ductility steel frames are typically used in areas that experience high seismic activity, whereas lower ductility steel frames are typically used in areas with low or moderate seismic activity. One aspect that influences the ductility of such steel frames is the type of connections at joints. In high seismic regions, these connections are designed to provide moment resistance; in regions with lower seismic demands however, these connections are considered pins in design and are thus assumed to provide zero moment resistance. Using highly ductile frames is not economical in low to moderate seismic regions because of the greater costs associated with implementing the anchored (moment resisting) connections that are only necessary for high seismic activity.

Gusset plates semi-rigid connections could be a valuable resource to prevent collapse, providing a certain degree of stiffness and strength after bracing failure. This reserve effect has been quantified among full-scale tests performed with several configurations, and its potential to improve seismic performance of concentrically braced frames in moderate seismic actions are reported. Semi-rigid beam-to-column connections provided a “reserve” capacity to the steel frame after bracing’s post buckling failure thanks mainly to gussets. Black hysteresis curve shows the global force-displacement behavior of the braced frame with single diagonal, drawn until bracing failure, while the blue hysteresis curve shows the global force-displacement behavior of the empty frame without bracings. The frame without bracings has been pushed until large drifts to show how much the steel frame with no bracings would deform with increasing base shear. It should be noted that the frame action could sustain a significant portion of the peak base shear. The capacity of each specimen following failure of the bracing systems (single or cross-bracing) is reported in *Figure 181*, where:

V_b : Peak base shear when bracing is under compression

V_t : Peak base shear when bracing is under tension

V_{fb} : Peak base shear of frame in the same direction with V_b

V_{ft} : Peak base shear of frame in the same direction with V_t

	V_b (KN)	V_t (KN)	V_{fb}/V_b	V_{ft}/V_t
60X	747	-742	0.42	0.35
60S	285	-343	1.11	0.75
70X	854	-505	0.39	0.51
70S	376	-511	1.02	0.50
V_{fb} (KN)	316			
V_{ft} (KN)		-258		

Figure 181. Peak base shear reached in the tests

After plastic buckling occurred, additional load cycles have been imposed to the specimens until failure of the bracing joint. During this post-buckling phase, both under tension and compression cycles, the specimens continued to have significant strength and stiffness. With reference to *Figure 182* and *Figure 183*, first plastic buckling occurred at point A, then failure at the net section occurred in the bracing joint at point C (B for S60); the frame with fractured bracings has been pushed and pulled until point E. The values beyond point D on graphs show the base shear carried only by frame action with the corresponding drift value. The numerical values are summarized in table of *Figure 184*.

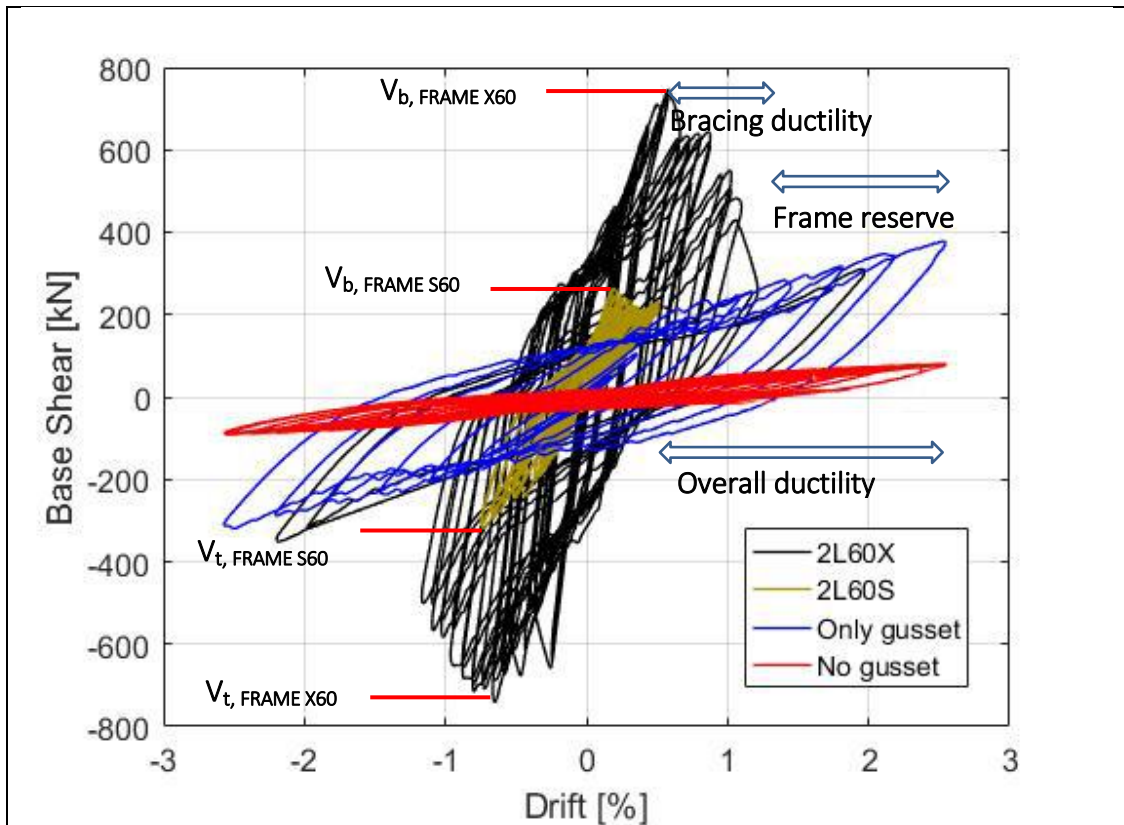


Figure 182. Ductility resources of the 2L60x8 braced frame

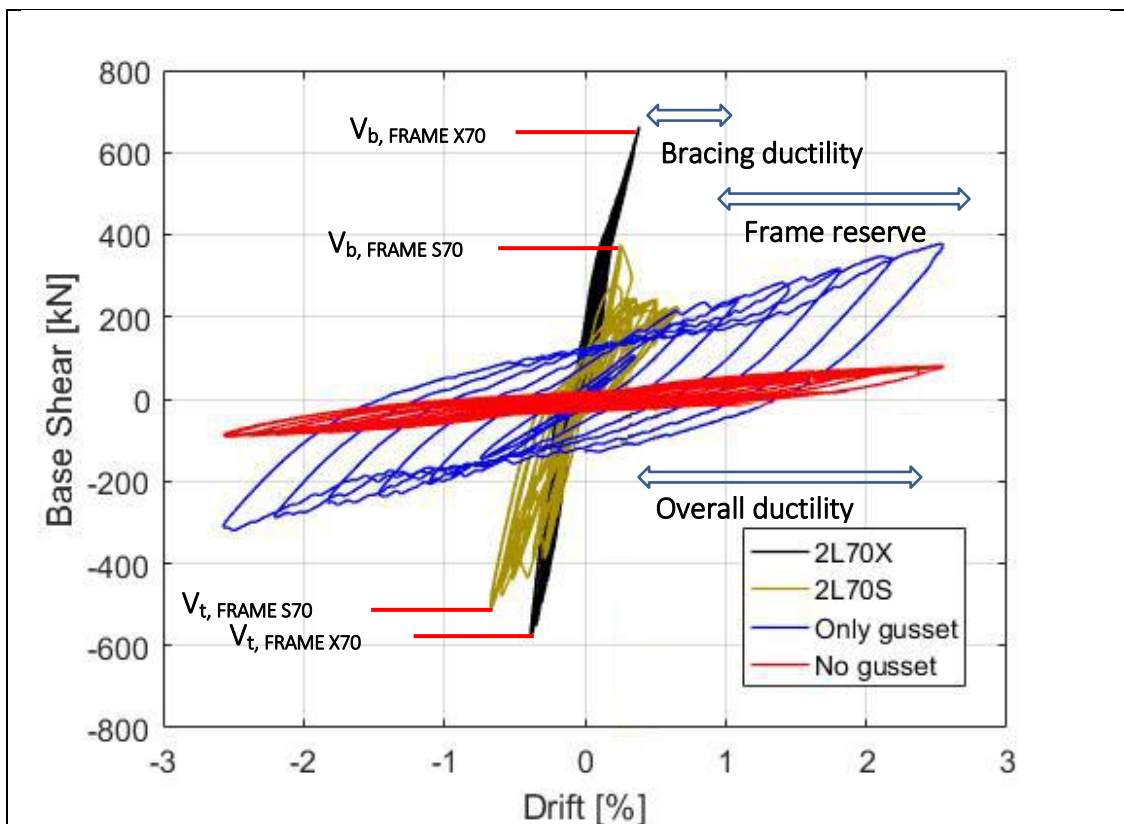


Figure 183 Ductility resources of the 2L70x7 braced frame

The figures show how the overall ductility of the frame with bracings increases when the frame ductility is taken into account. The frame continued to offer extra ductility also after the bracing failure. In the first case presented, having the weakest diagonal (2L60x8) the overall ductility is even more than three times looking globally performances. Stronger the diagonal (2L70x7), more the braced frame takes advantage of the frame effect even before the bracing post buckling failure.

Frame	Bracings	A		B		C		D		E	
		Base shear [kN]	Drift [%]	Base shear [kN]	Drift [%]	Base shear [kN]	Drift [%]	Base shear [kN]	Drift [%]	Base shear [kN]	Drift [%]
MRF	60X	506	0.27	747	0.58	430	1.16	247	1.19	350	2.54
	60S	285	0.19	207	0.37	225	0.51	173	0.51	295	1.81
	70X	-	-	-	-	-	-	-	-	-	-
	70S	376	0.27	242	0.33	222	0.67	197	0.67	295	1.81

Figure 184. Base shear and Drift values at various instances (A, B, C, D, E)

Empirical evidence indicates that analysed steel braced frames possess appreciable reserve capacity – in the form of gravity framing and gusset plate connections. These partially restrained connection elements form a “reserve” moment frame system that can prevent sidesway collapse even when the primary lateral force resisting system (LFRS) is significantly damaged due to brace fracture. When required, reserve capacity can be enhanced without significant expense. As summarized by Hines et al. (2009), collapse performance of CBF systems that possess limited ductility appears to be impacted less by a system’s strength than by its reserve capacity. Thanks to this frame action, specimen continued to deform reaching large drifts (around 2%) with not too large but remarkable resistance and stiffness. At point C, after bracing fracture, additional resistance was provided by combining frame action and residual resistance of the fractured bracing. Additional contribution was provided by the two surfaces of open-cracks section, returns in contact during compression at brace. Figure 185 shows different moments about test 13, that results complete of data for the whole duration of elastic and plastic phases, till both bracings failure and frame effect of gussets activation. This latter improves very well the system in terms of overall ductility, showing its benefit as reserve source for preventing collapse.



a. During post-buckling



b. After both bracings completely fractured

Figure 185. Specimen X60 during post buckling and after bracings’ complete failure

7. Initial connection stiffness

Stiffness of semi-rigid connection composed by double web angles and bolted gusset plate has been calculated splitting the two components. Each one following a different approach in order to reach more reasonable values coherent with experimental recorded data and numerical simulation, performed and presented by Alper Kanyilmaz Doctor Document (2016). Double web angles contribution has been evaluated following the formulations indicated in the document “Moment-rotation relationship of semi-rigid connections with web angles”, developed by N.Kishi and Wai-Fah Chen, ASCE members. Gusset plate rigidity has been evaluated according to C.Stoakes Degree of Doctor Document prescriptions. Results have then been validated by data of experimental tests.

Web Angles

N.Kishi and Wai-Fah Chen (ASCE28, 1990) presented a semi-analytical procedure in order to predict the moment-rotations characteristics of a semi-rigid connections. The model is based on three parameter, elastic-plastic, stress-strain model proposed previously by Richard (1961) and can be easily applied to the second-order frame analysis with semi-rigid connection¹.

The geometry of the angle web designed for the beam-column connection is shown in *Figure 186*.

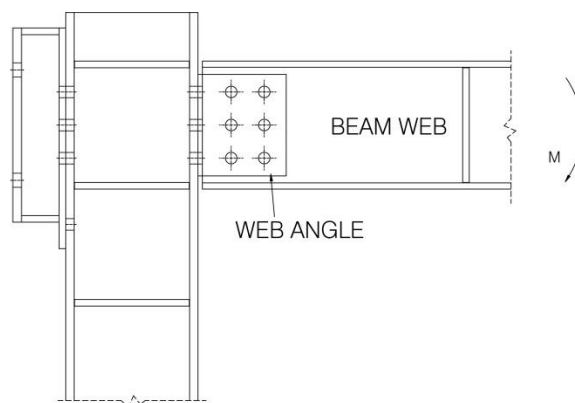


Figure 186. Semi-rigid beam-to-column connection

Driving assumptions driving the analytical formulation of Kishi and Chen et al. (1987):

- Effect of shear force on connection deformation is ignored
- Part of angle connected to the column behaves linearly elastic
- Part of angle connected to the beam behaves as a rigid body. Deformations are very small.
- Part of the angle fastened to the column flange acts as a moderately thick plate, in which the fixed support is assumed to be at the fastener-nut edge close to the beam web, and the concentrated torsional moment is in equilibrium with the connection moment acting at free edge (*Figure 187*)

¹ Reported from part of Journal of Structural Engineering Vol. 116, No. 7, July 1990. Downloaded from ascelibrary.org by Li. Co.Sa 8181901/mi/155985 on 05/26/16. Copyright ASCE.

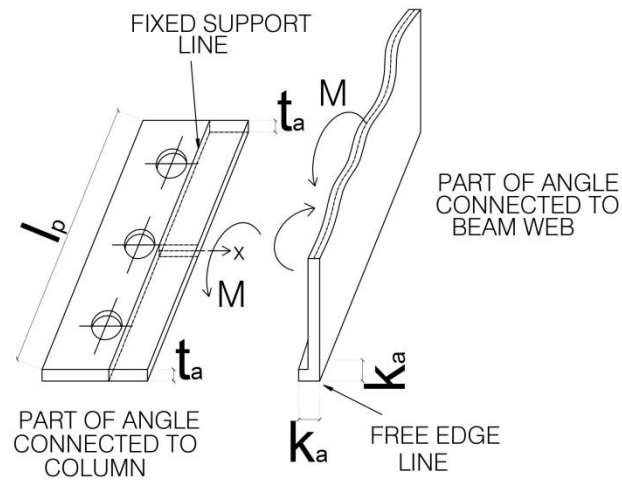


Figure 187. Geometrical scheme for deriving parameters

Using bending torsional theory, the governing differential equation is:

$$EC_w \frac{d^4 \phi}{dx^4} - GJ \frac{d^2 \phi}{dx^2} = m_t$$

In which:

- E is the Young Modulus
- C_w is warping constant
- ϕ is the angle rotation
- G is the Shear Modulus
- J is uniform torsion constant
- m_t is distributed torsional moment (here assumed $m_t = 0$)

Starting from the eq.1 and imposing the boundary conditions at free and fixed edges, Kishi and Chen, has developed a relation between connection moment and rotation, setting θ_r to ϕ :

$$M = R_{ki} \theta_r$$

where:

$$R_{ki} = G \frac{t_a^3}{3} \frac{\alpha \cosh(\alpha \beta)}{(\alpha \beta) \cosh(\alpha \beta) - \sinh(\alpha \beta)}$$

$$\beta = \frac{g_1}{l_p}$$

$$g_1 = g_c - k_a - \frac{w}{2}$$

In which:

- t_a is the thickness of web angle
- $\alpha = 4,2967$ (with Poisson number equal to 0,3)
- l_p is the length of web angle
- g_1 is the gauge distance from the fixed support line to the free edge line
- g_c is the gauge distance from angle heel to center of bolt near the beam web adjacent to the column
- k_a distance from angle heel to the toe of the fillet

w is the width of fastener's nut
 R_{ki} is the initial connection stiffness

For a double web-angle connection initial rotational stiffness is equal to $2 \cdot R_{ki}$.

Connection stiffness-double web angle		
Parameter	Value	Unit
g_c	60,75	mm
k_a	47,25	mm
g_1	2,5	mm
w	32	mm
t_a	10	mm
α	4,2967	-
l_b	200	mm
β	0,0125	-
G	79,3	GPa
R_{ki}	2,2E+09	Nmm/rad
R_{ki}	4,4E+09	Nmm/rad

Table 33. Rotational stiffness of web angles connection

Gusset Plate

Christopher D. Stoakes Degree of Doctor Document² has been chosen as reference for calculation of initial stiffness connection of the gusset plate.

The gusset plate is divided into segments of length equal to the spacing of the connection bolts. Each segment acts as a linear spring. Out-of-plane legs of the gusset plate are assumed acting as cantilever beams subjected to a point load at the free end. The geometry of the connection detail is reported in *Figure 188*, reference for formulation adopted.

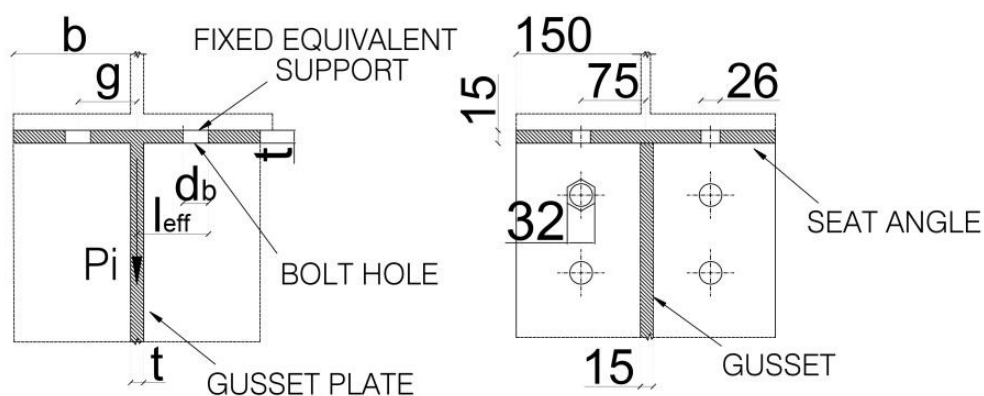


Figure 188. Angle and gusset cross-section for stiffness estimation

² Title of the reference book is "BEAM-COLUMN CONNECTION FLEXURAL BEHAVIOR AND SEISMIC COLLAPSE PERFORMANCE OF CONCENTRICALLY BRACED FRAMES Submitted in partial fulfilment of the requirements for the degree of Doctor of Philosophy in Civil Engineering in the Graduate College of the University of Illinois at Urbana-Champaign, 2012

In which:

- g is the gage distance from the heel of the angle to the centerline of the bolt hole
- L_{eff} is the effective length of the cantilever beam model of the out-of-plane angle leg
- t is the plate thickness
- P_i is the point load applied to the free end of the cantilever

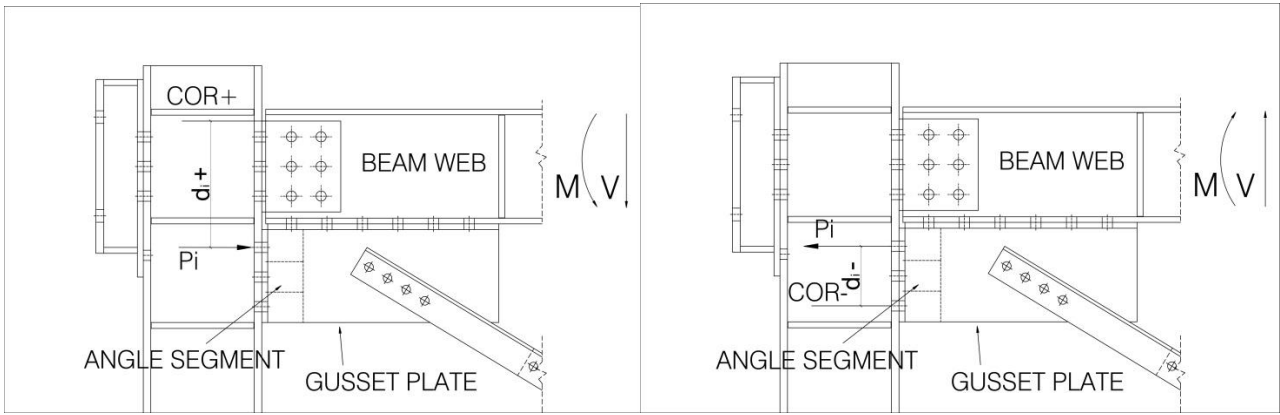


Figure 189. Connection geometry for estimation of connection stiffness: (a) positive bending; (b) negative bending.

The stiffness of each segment has been evaluated using the following formula, considering flexural and shear deformations:

$$k_i = \frac{P_i}{\Delta_i} = \left(\frac{L_{eff}^3}{3EI} + \frac{L_{eff}}{GA_s} \right)$$

Where:

- Δ_i is the displacement corresponding to P_i
- A_s is the shear area
- E is the elastic modulus
- I is the moment of inertia
- G is the shear modulus

The section properties, I and A_s , should be based on a rectangular section having thickness t and width b_{net} which is computed from:

$$b_{net} = b - d_b$$

Where:

- b is the width of the angle segment
- d_b is the nominal bolt diameter

Since the critical section is rectangular, A_s should be taken as 5/6 of the gross area $A = b_{net}t$. Based on the experimental and numerical results of Stoakes experience, L_{eff} is computed as:

$$L_{eff} = 4t + \frac{g}{4}$$

While, thanks to post-processing of strain gauges data and validation through a numerical model, the equation has been modified to:

$$L_{eff} = 4t + \frac{g}{11}$$

Initial stiffness of gusset plate is finally determined through the following formula:

$$K_{conn} = \sum_1^{N_b} k_i d_i^2$$

In which:

d_i is the distance from the centroid of the angle segment to the center of rotation
 N_b is the number of bolts

The center of rotation, is the bottom of the beam web angles for positive bending and the top bolt row for negative bending. It should be noted that d_i for positive bending will be different than d_i for negative bending.

Connection stiffness - gusset plate		
Parameter	Value	Unit
g	75	mm
l_{eff}	66,8	mm
t	15	mm
G	79300	MPa
E	210000	MPa
d_b	26	mm
b	150	mm
b_{net}	124	mm
A	1860	mm ²
$A_{s,net}$	1550,0	mm
I	34875	mm ⁴
k_i	70814,47	N/mm

Table 34. Segment stiffness derivation

N_b			
3			
Lever arm	Positive	Negative	Unit
d_1	320	75	mm
d_2	395	150	mm
d_3	470	-	mm
K_{conn}	3,39E+10	1,99E+09	Nmm/rad

Table 35. Global rotational stiffness derived by gusset plates

Once both stiffness contribution of web angles and gusset plate have been evaluated, resulting values of initial rotational stiffness are reported in the following summary *Table 37*.

-	Positive	Negative	Unit
Web Angle	4,40E+09	4,40E+09	Nmm/rad
Gusset	3,39E+10	1,99E+09	Nmm/rad
Total	3,83E+10	6,40E+09	Nmm/rad

Table 36. Summary of rotational stiffness

Ultimate Moment Strength

Following Stoakes indications, angles have been again divided into segments based on bolt spacings. Plastic hinges are assumed to form in both legs of the angles. *Figure 190* shows the reference connection geometry used for moment strength calculation.

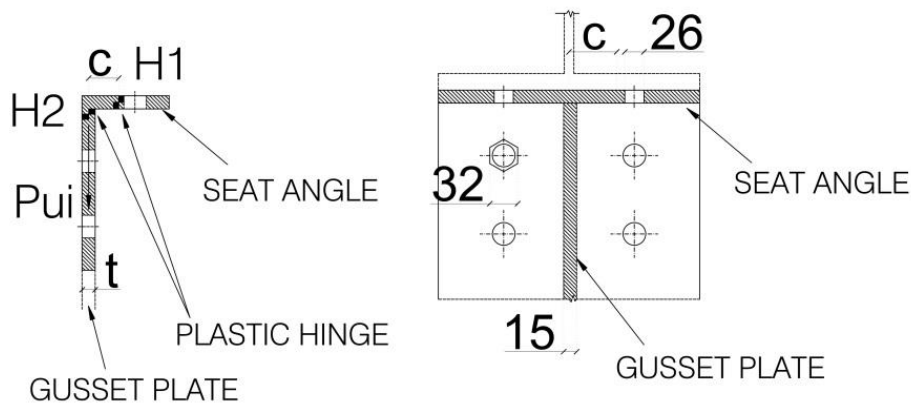


Figure 190. Web angles and gusset cross-section for moment strength estimation

Referring to the figure above:

- H1* is the plastic hinges in the out-of-plane leg
- H2* is the plastic hinges in the in-plane leg
- c* is the distance between the plastic hinges
- P_{ui} is the applied load corresponding to formation of *H1* and *H2*

Taking a free body diagram of the angle between the two plastic hinges yields the expression for P_{ui}

$$P_{ui} = \frac{M_{p1} + M_{p2}}{c}$$

in terms of the plastic moment strength M_{p1} , of *H1*, and M_{p2} , of *H2*. M_{p1} and M_{p2} are calculated from

$$M_{pa} = F_u Z_{xa}$$

Where:

- F_u is the ultimate tensile strength of the angles
- Z_{xa} is the plastic section modulus that corresponds to plastic hinge H_α

Z_{x1} is computed using b_{net} and Z_{x2} is computed using b , which were defined in the section of Stoakes initial stiffness calculation. The tensile strength is used in the plastic hinge calculation to recognize that strain hardening of the angle material results in higher moment strengths for cyclic loading than would be realized under monotonic loading. In addition, the ultimate moment strength corresponds to fracture initiation in the gusset plate and web angles. Fracture limit states are typically approximated using F_u in the AISC *Specification* (2005b).

The distance between the plastic hinges, c , is computed using:

$$c = L_{eff} - \frac{t}{2} - \frac{W}{2}$$

Where:

t is the angle thickness

W is the width of the head of the bolt corresponding to the angle segment, which can be found in AISC *Steel Construction Manual* (2005c).

L_{eff} is defined in the initial stiffness section

Once P_{ui} is known for each angle segment, the connection moment strength M_{conn} is found from

$$M_{conn} = \sum_1^{N_b} P_{ui} d_{ui}$$

where d_{ui} is the distance from the centroid of the angle segment, or centerline of the bolts in the seat angle-gusset plate, to the location of the contact force F_c .

Figure 191 shows d_{ui} and the location of F_c for positive bending and negative bending. Like d_i for the initial stiffness calculation, d_{ui} is different for positive and negative bending. F_c is located at the bottom of the web angle, or heel of the seat angle when it is present, for positive bending.

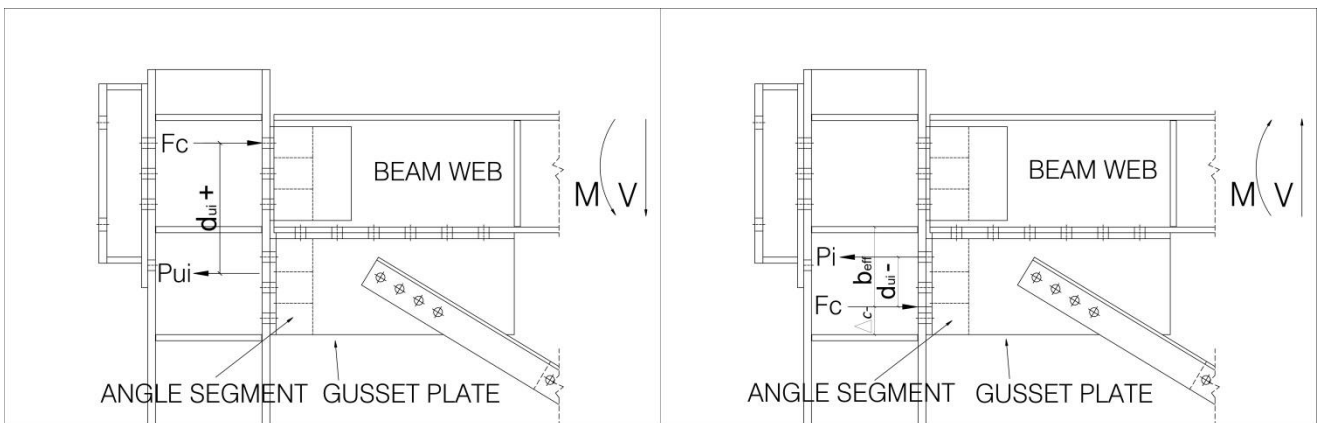


Figure 191. Connection geometry for estimation of connection strength: (a) positive bending; (b) negative bending.

In negative bending, the location of F_c varies with angle thickness and beam depth according to

$$\Delta_c^- = 0.5d_{beam} - 28t + 203$$

where Δ_c^- is the distance, in mm, from the top of the gusset plate angle to F_c for negative bending, shown in Figure 4, and d is the beam depth. Δ_c^- is greater than or equal to the edge distance to the first bolt row, P_{ui} , so that all bolts of this row have been excluded when calculating M_{conn} .

Based on the recommendations of the commentary to Chapter B of the AISC *Specification* (2005b), the rotation capacity for braced frame connections used in reserve LFRSs should be limited to 0.03 rad. Thus, a limit has to be placed on the rotation capacity of braced frame connections used for reserve capacity. Since Stoakes experimental program considered only one beam depth, and the finite element models did not model propagation of damage, there is insufficient data to make a recommendation based on the results presented in this study³.

Ultimate Moment Strength			
	Web angle	Gusset plate	Unit
N_b	6	6	n. of bolts
b	100	300	mm
b_{net}	74	248	mm
l_{eff}	55,1875	78,75	mm
t	10	15	mm
$Z_{1, web\ angle}$	1850	13950	mm ³
$Z_{2, web\ angle}$	2500	16875	mm ³
$F_{u, web\ angle}$	489,67	517,0	MPa
M_{p1}	905889,5	7212150	Nmm
M_{p2}	1224175	8724375	Nmm
c	34,1875	55,25	mm
W	32	32	mm
P_{ui}	62305,3	288443,9	N

Table 37. Evaluation of P_{ui} load generating plastic hinges.

Positive bending			Negative bending		
Parameter	Value	Unit	Parameter	Value	Unit
d_{u1}	40	mm	d_{u1}	62	mm
d_{u2}	115	mm	d_{u2}	193	mm
d_{u3}	190	mm	d_{u3}	268	mm
d_{u4}	320	mm	d_{u4}	243	mm
d_{u5}	395	mm	d	290	mm
d_{u6}	470	mm	Δ_c	68	mm
M_{conn}	363301360,6	Nmm	M_{conn}	61746495	Nmm
M_{conn}	363,3	kNm	M_{conn}	61,7	kNm

Table 38. Ultimate moment strength for rotational directions

³ Beam-column connection flexural behaviour and seismic collapse performance of concentrically braced frames by C. Stoakes, pag 122.

8. Conclusions. Future research.

Concentrically-braced frames (CBFs) are used extensively in moderate seismic regions, and they are almost always designed without ductile detailing or capacity design requirements. Thus, brittle limit states are expected under design-level demands and there is no assurance that the overall system response will be acceptable. However, these systems do possess reserve capacity, and it may be a useful tool for preventing collapse under large seismic demands. This research program has investigated all sources of reserve capacity in low-ductility CBFs with the objective of developing a rational design philosophy that will be economical for moderate seismic regions where high-cost ductile detailing and capacity design are not feasible. This thesis provides an overview of in-progress work to evaluate potential low-ductility limit states in braced frames, quantify potential sources of reserve capacity, determine the effect of the reserve capacity sources on seismic response and develop a seismic design approach that employs reserve capacity.

Braced frames can be an effective system for seismic retrofit due to their high stiffness and because they can be assembled from pieces of relatively small size and weight. Braced frames are most effective at the building perimeter, where they can control the building's torsional response. ASCE 7 allows buildings to be considered sufficiently redundant (and thus avoid a penalty factor) with two braced bays on each of the presumed four outer lines (assuming a rectangular layout). Such a layout is good for torsion control as well. In mid-rise or high-rise buildings, CBFs are often used in the core of the structure, with a perimeter moment frame used to provide additional torsional resistance. The design of elements interconnecting these frames is critical to ensure that brace ductility remains the primary source of inelastic drift.

CBFs are designed using capacity design procedures, with the braces serving as the fuses of the system. Optimal design of CBFs entails careful selection and proportioning of braces so as to provide limited overstrength and avoid a concentration of inelastic demands. Designers should strive for a small range of brace demand-to-capacity ratios so that the resulting system is proportioned to spread yielding over multiple stories rather than concentrating it at a single location. Overstrength can be beneficial, but care should be taken to maintain a well-proportioned design in order to avoid concentration of ductility demands.

Presented work, dealing with the experimental study of concentrically X-braced full-scale frame realized using as diagonal profiles equilateral variable section angles coupled together by means of stitch plates. The braced frame was representative of the bracing system of a steel multi-storey building designed according to EC8 in low ductility class with low dissipative behavior. This option, recommended only for low-moderate seismicity areas, provides the structural element design based only on resistance, without any requirement about ductility. Comparing the experimental results about tests has confirmed that high stiffness is provided by bracing to the whole structure. Therefore, introducing concentric bracing in a frame allows to limit the horizontal displacement of the entire structure so as to reduce the resistant section of the profiles used for the main structural members.

Important conclusions deals with main topics presented in Chapter 6. Compression diagonal was observed producing benefits, increasing initial stiffness and in the global strength of both configuration of frame (single diagonal and cross configuration). This means also that in the phase of elastic field, compression diagonals influence the global behavior of the structure in terms of frequency and vibration modes. Thus, design seismic actions should be evaluated considering both the diagonals contribution in tension and compression. Boundary conditions of the compression diagonals could be also reviewed and represented in a more matter-of-fact way.

Analyzed configurations, shown in *Figure 192*, correspond to X-configuration frame (Tests 1-2-5-17-18; $\bar{\lambda} = 1.11$), tension diagonal configuration (Tests 3-7-19-23; $\bar{\lambda} = 2.22$) and no-diagonal frame with only gusset plates at beam-to-column nodes. (Test 4-8-12-16).

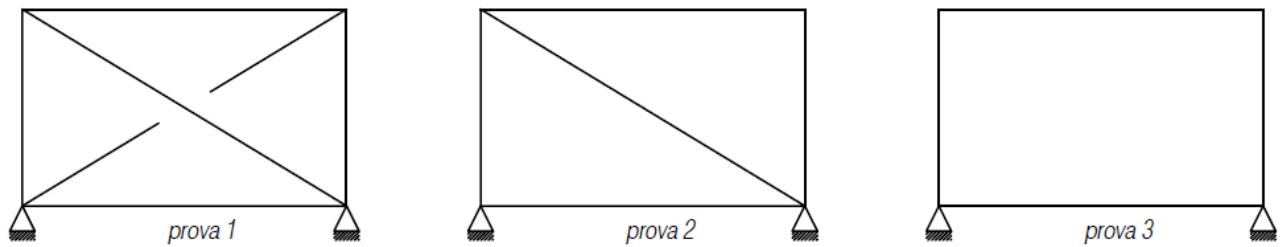


Figure 192. Configurations of braced frame tested

Tests have shown how compression axial load that has generated buckling, was 4 times higher than bearing capacity evaluated following EC3. Thus, regarding at analysed profile types, it is possible to confirm that EC3 prescriptions underestimate excessively the bearing capacity of the compression diagonal .

Also overall overstrength and ductility could be carefully designed taking into account about phenomena normally neglected by standards. As well as bolts holes ovalization and bolts slip that represent 10% of the overall energy dissipation devices of the system. Ovalization also contribute in increase ductility of the system, coupled in parallel with frame effects provided by gusset plates. It has been shown how seismic performance could be improved taking into account about frame reserve capacity. Comparing hysteresis loops of braced-frame tests with only no braced frame, showed that the braced system, also after brace failure, had a reserve ductility due to the frame action gusset plates. Corner gussets plates could be used as reserve devices to prevent collapse after diagonals failure. Additionally, the error of evaluating beam-end as pinned, could bring to wrong assessment of global stiffness and strength of the structure.

Results obtained from the entire experimental survey planned by MEAKADO project, of which this work is part, are fundamental to validate a numerical model for analyzing the instability of plastic and hysteretic behavior of concentrically braced-frames.

APPENDIX A – Lab report about specimens monoaxial tensile tests

Pag. 1/2

POLITECNICO DI MILANO
SISTEMA QUALITÀ
LABORATORIO PROVE MATERIALI

MODULO DI REGISTRAZIONE – PROVA DI TRAZIONE SU provette rettangolari (UNI EN 6892-1)

Commessa/Ingresso				
Richiedente/Cod. Cliente	ALPER			
Data prova	20/01/2016 - 27/01/2016			
Macchina utilizzata	100 kN	200 kN	300 kN	500 kN
Materiale	"L"			

Campione N°	Spessore mm	Larghezza mm	Sezione mm ²	Snervamento Rp _{0,2}		Rottura Rm		A ₅₀ %	A _{5,65/5*} %	L ₀
				daN	MPa	daN	MPa			
11A-1	7,92	20,16	159,70		339		462		35,71	70
11A-2	7,94	20,01	158,90		366		457		34,26	70
11A-3	7,94	18,65	148,10		342		468		35,00	70
11B-1	6,98	19,83	138,40		341		482		27,14	70
11B-2	7,03	20,65	145,20		328		475		21,43	70
11B-3	6,99	19,57	136,80		340		479		22,86	70
11C-1	7,90	20,23	159,80		337		464		37,14	70
11C-2	7,96	20,27	161,30		343		471		37,14	70
11C-3	8,06	19,63	158,20		340		460		32,86	70
1B-1	13,38	19,97	267,20		374		549	35,00	33,33	90
1B-2	13,55	19,92	269,90		375		544	33,75	32,22	90
1B-3	13,42	20,19	270,90		375		548	35,00	32,22	90
3L-1	10,30	19,86	204,60		363		491		30,00	80
3L-2	10,52	20,57	212,30		368		492		30,00	80
3L-3	10,25	21,03	215,60		363		486		31,25	80

Figure 193. Values of lab tensile test of specimens

POLITECNICO DI MILANO							
SISTEMA QUALITÀ							
LABORATORIO PROVE MATERIALI							
DIPARTIMENTO DI INGEGNERIA STRUTTURALE							
MODULO DI REGISTRAZIONE – PROVA DI TRAZIONE SU PROVETTE CILINDRICHE (UNI EN 10002-1)							
Commessa/Ingresso							
Richiedente/Cod. Cliente		ALPER					
Data prova		29/01/2016					
Macchina utilizzata		100 kN	200 kN	300 kN	500 kN		
Materiale							
Campione	Diametro (Ø)	Sezione	Snervamento	Rottura	A ₈₀	A _{5,65·s⁻¹}	L ₀
N°	mm	mm ²	MPa daN	MPa daN	%	%	
2C-1	10,00	78,5	357	561		34,00	50
2C-2	10,00	78,5	344	535		30,00	50
2C-3	10,00	78,5	389	582		28,00	50

Figure 194. Values of lab tensile test of specimens

POLITECNICO DI MILANO										
SISTEMA QUALITÀ										
LABORATORIO PROVE MATERIALI										
MODULO DI REGISTRAZIONE – PROVA DI TRAZIONE SU provette rettangolari (UNI EN 6892-1)										
Commessa/Ingresso		2016/								
Richiedente/Cod. Cliente		ALPER								
Data prova		27/01/2016								
Macchina utilizzata		100 kN	200 kN	300 kN	500 kN					
Materiale										
Campione	Spessore	Larghezza	Sezione	Snervamento	Rottura	A ₈₀	A _{5,65·s⁻¹}	L ₀		
N°	mm	mm	mm ²	daN	MPa	daN	MPa	%	%	
BAB1-1	16,16	21,33	344,70		385		513		27,00	100
BAB1-2	15,98	20,50	327,60		384		515		31,00	100
BAB1-3	15,87	20,20	320,60		393		523		23,00	100

Figure 195. Values of lab tensile test of specimens

APPENDIX B – Complete bill of materials and design papers

Both complete bill of materials and drawings used for production and assembly of the whole frame is reported below. Parameters have been used by production company.

Bill of materials

COMPLETE PIECES BILL- MOMENT RESISTING FRAME				
ID	NAME	QUANTITY	STEEL TYPE	DESCRIPTION
1	HEA300 Length: 3980mm	2	S355JR	<i>beams</i>
2	HEB 300 Length: 3000mm	2		<i>columns</i>
3	L200x100x10x230	8		<i>L-profile of web angles connection</i>
4	LAM 180x210x10	8		<i>stiffening plates of beam connection</i>
5	LAM 260x140x15	28		<i>stiffening plates of beam and column connection</i>
6	LAM 300x235x15	4	S275JR	<i>connection plates columns to bracings</i>
7	LAM 585x300x15	4		<i>connection plates beams to bracings</i>
8	LAM 585x235x15	2		<i>upper bracings angular plates</i>
9	LAM 585x235x15	2		<i>lower bracings angular plates</i>
10	L 70x7x1950	4		<i>profiles for "short" diagonals</i>
11	L 70x7x4100	2		<i>profiles for "long" diagonals</i>
12	LAM 700x250x15	1		<i>mid-plate for bracings connection</i>
13	LAM 100x70x15	16		<i>plates for bracings padding</i>
14	HINGE LATERAL PLATE	4	S355JR	-
15	HINGE STRENGHTENING PLATE	4		<i>to weld on columns webs</i>
16	LAM 600x360x50	2		<i>base plates</i>
17	PIN	2		-
18	LAM 310x500x15	1		<i>connection plate column-jack</i>
19	LAM 165.6x365x15	2		<i>stiffening plates jack node</i>
20	LAM 145x175x10	4		
21	LAM 145x220x15	1		
22	LAM 145x405.9x15	1		
23	LAM 365x440x20	1		<i>frame end plate</i>
24	LAM 310x500x15	1	<i>plate for jack connection</i>	
25	LAM 85x365x15	2	<i>left frame node</i>	
26	LAM 85x410x15	1		
27	LAM 365x440x20	1		
TOTAL		110		

Table 39. List of steel elements for moment resisting frame assembly

COMPLETE BILL OF MATERIAL - PINNED FRAME					
ID	NAME	QUANTITY	STEEL TYPE	NOTES	
1	HOT-ROLLED FORMED HOLLOW PROFILES 50x250x8 Length: 3210mm	1	S355JR	<i>beam</i>	
2	LAM 700x250x18	4		<i>connection plates beam node</i>	
3 A B	LAM 450x260x15	24	S275JR	<i>steel plate for bracings type A and B</i>	
3 C	LAM 450x260x15	12		<i>steel plate for bracings type C</i>	
4+5	LAM 215x260x20/15	8	S355JR	<i>external steel plates for bracing connection node</i>	
6	LAM 440x300x26	4		<i>internal steel plates for bracing connection node</i>	
7	LAM 167.50x145x18	4		<i>stiffening steel plates</i>	
8	LAM 150x250x20	2		<i>connection steel plated beam- corner plates</i>	
9	LAM 310x340x20	2		<i>steel plate for jack anchorage</i>	
10	LAM 405x64x10	2		<i>internal steel stiffeners</i>	
11	LAM 60x64x10	2		<i>external steel stiffeners</i>	
12	LAM 700x25x10	4			
13	LAM 145x25x10	4			
14	LAM 405x25x10	4			
TOTAL		77			

Table 40. List of steel elements for pinned frame assembly

Bill of fasteners

BILL OF BOLTS - PINNED FRAME			
BOLTS ACCORDING TO EN14399/4			
DESCRIPTION	QUANTITY	CLASS O RESISTANCE	NOTES
M-24-95-56	64	10.9-HV	
TOTAL	64		

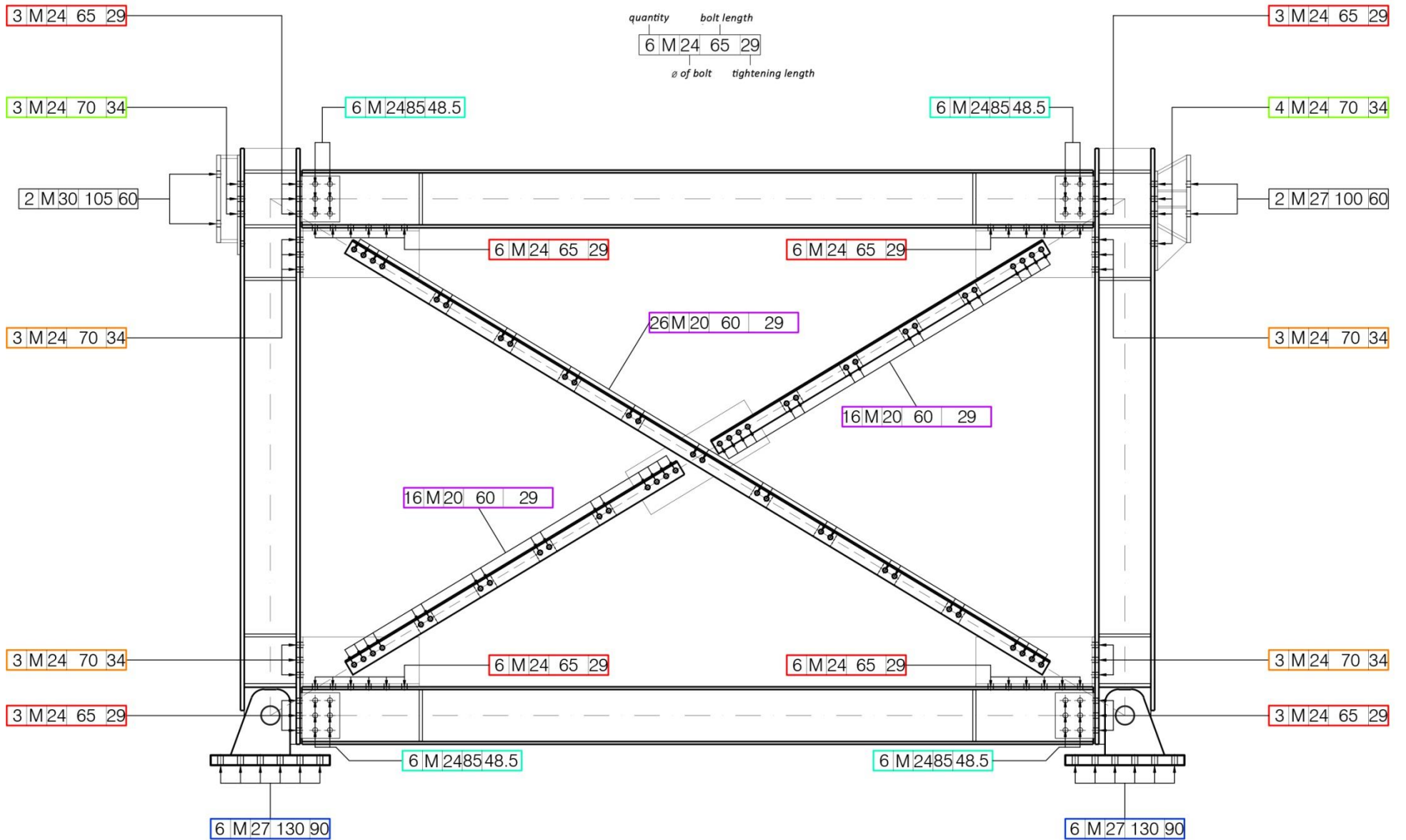
BILL OF BOLTS- MOMENT RESISTING FRAME			
BOLTS ACCORDING TO EN14399/4			
DESCRIPTION	QUANTITY	CLASS OF RESISTANCE	NOTES
M-20-60-31	58	10.9- HV SISTEM	
M-24-65-29	72		
M-24-70-34	38		
M-24-85-48.5	24		
M-27-130-90	24		<i>base plates anchorage</i>
M-27-100-60	4		<i>jack plates</i>
TOTALE	220		

NUTS ACCORDING TO EN14399/4			
DESCRIPTION	QUANTITY	CLASS OF RESISTANCE	NOTES
M20	58	10.9- HV SISTEM	
M24	134		
M27	28		
TOTALE	220		
WASHERS ACCORDING TO EN14399/4			
DESCRIPTION	QUANTITY	CLASS OF RESISTANCE	NOTES
φ21	116	10.9- HV SISTEM	<i>for screws M20</i>
φ25	268		<i>for screws M24</i>
φ28	56		<i>for screws M27</i>
TOTAL	440		

Graphic charts

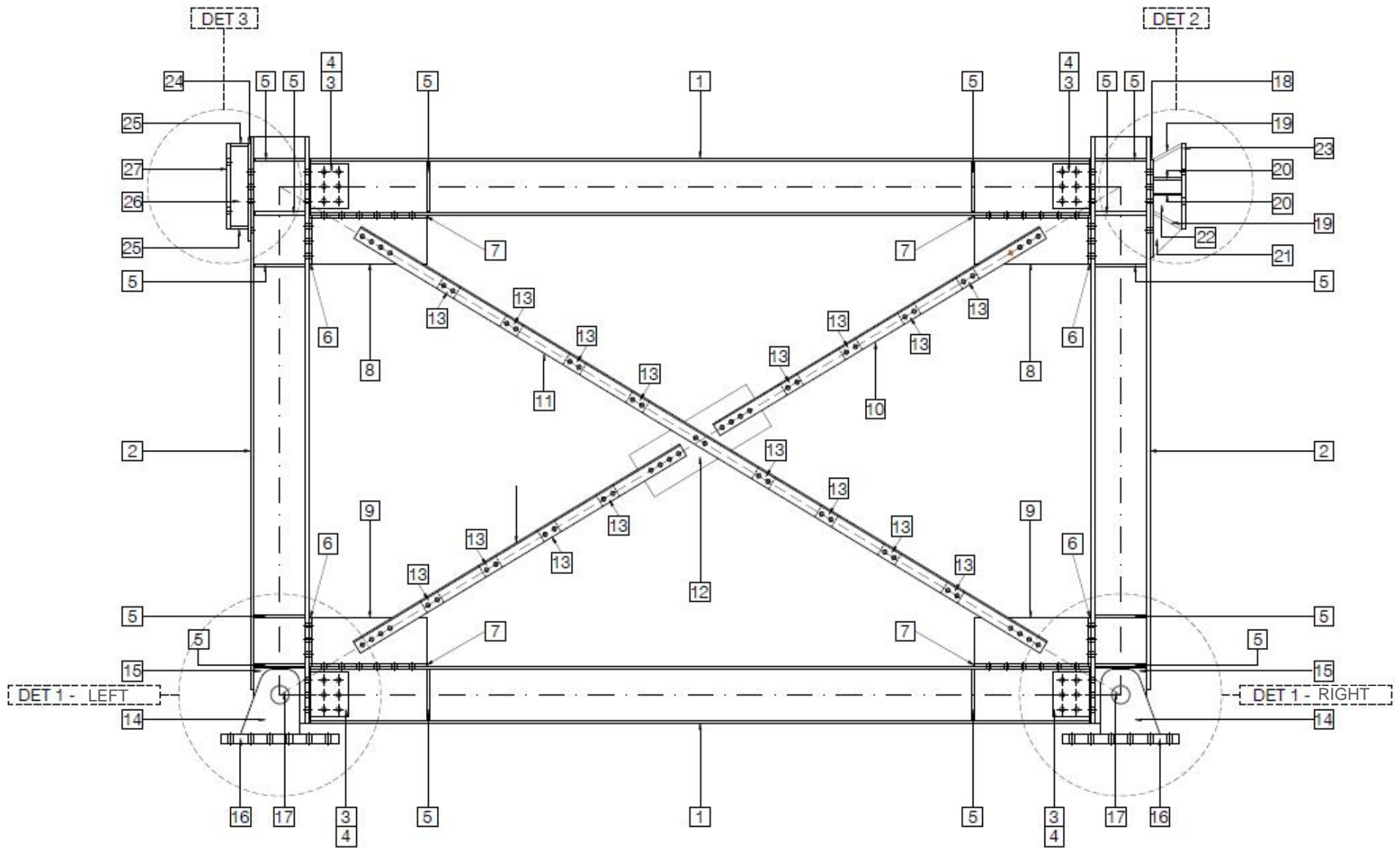
Graphic papers are composed by:

- back and front view of the whole frame with indication of notation given to each piece;
- back and front view of the whole frame with indication about bolts used;
- construction details of frame nodes;
- drawing paper for each piece used and assembled in frame.



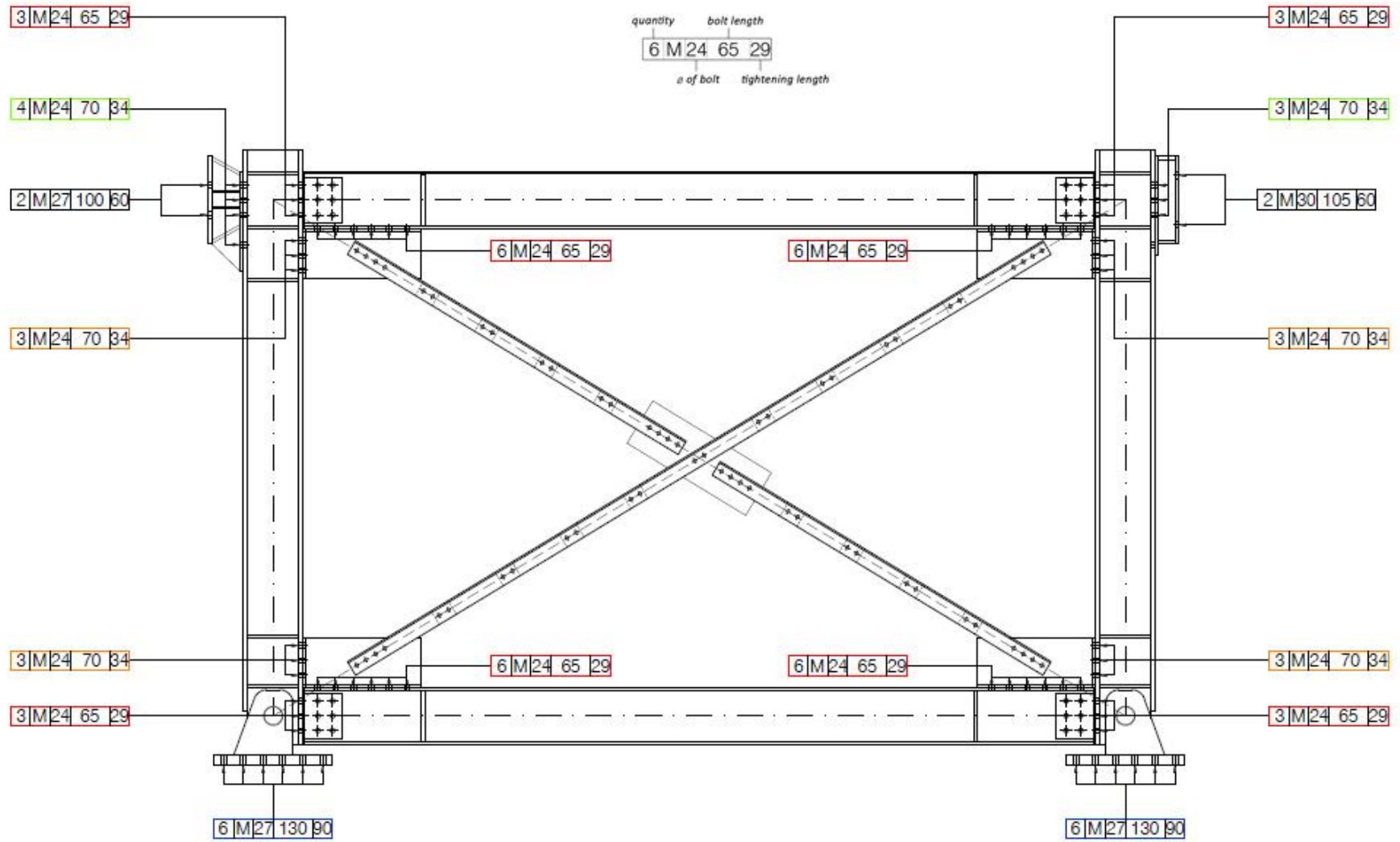
FRONT VIEW- BOLTS IDENTIFICATION

SCALE 1:20



FRONT VIEW- NUMBER OF PIECES

SCALE 1:20

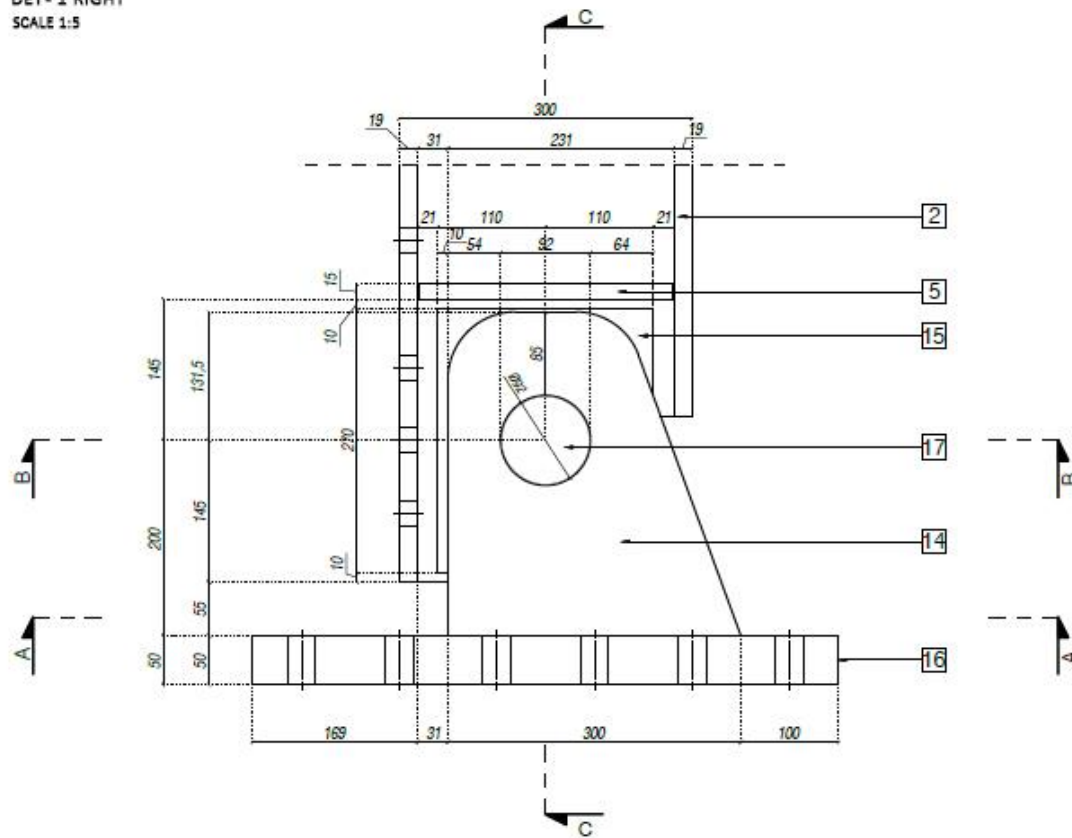


BACK VIEW- BOLTS IDENTIFICATION

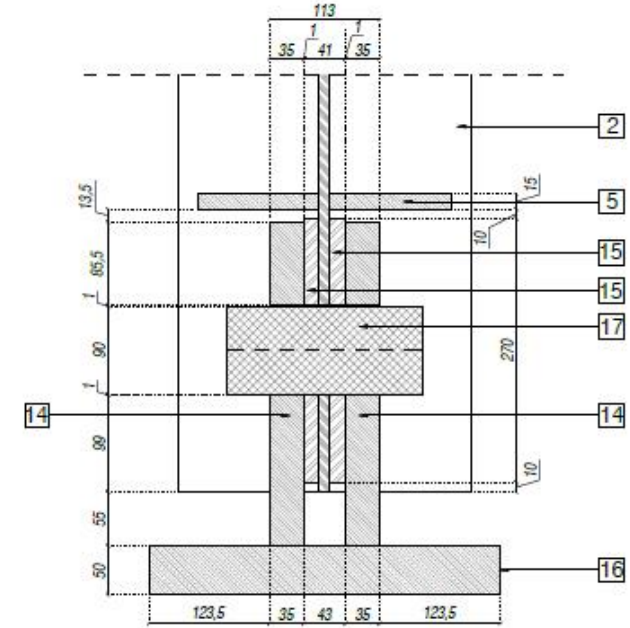
SCALE 1:20

DET- 1 RIGHT
SCALE 1:5

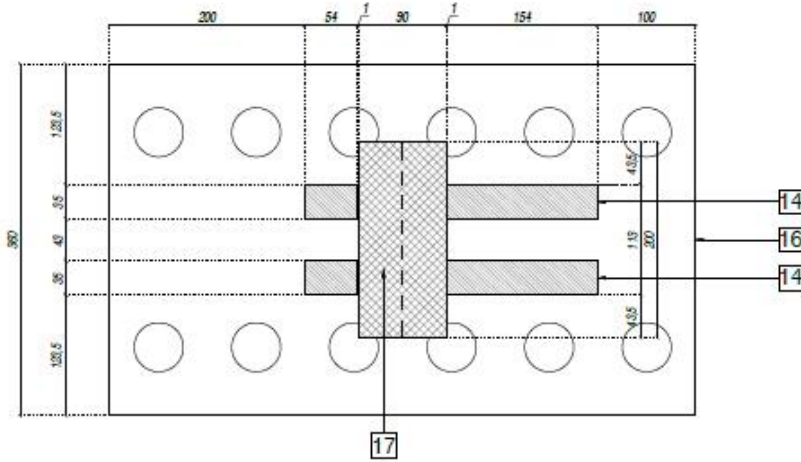
FRONT VIEW



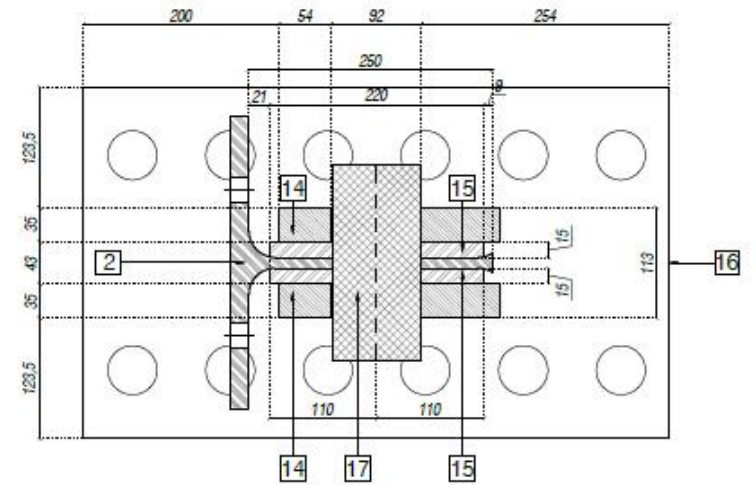
SECTION C-C



SECTION A-A

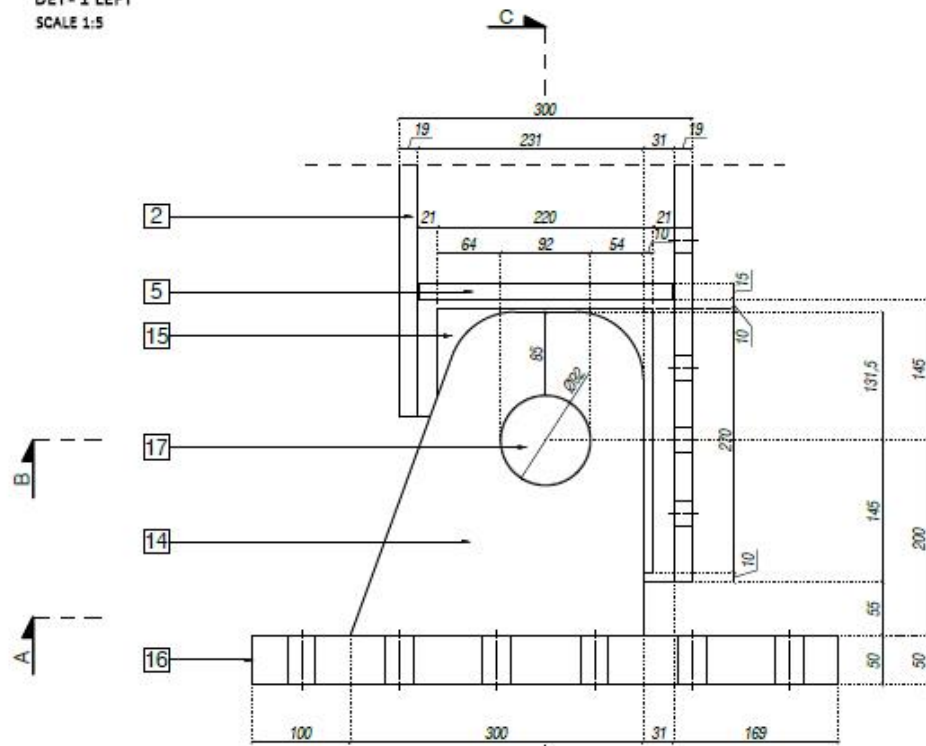


SECTION B-B

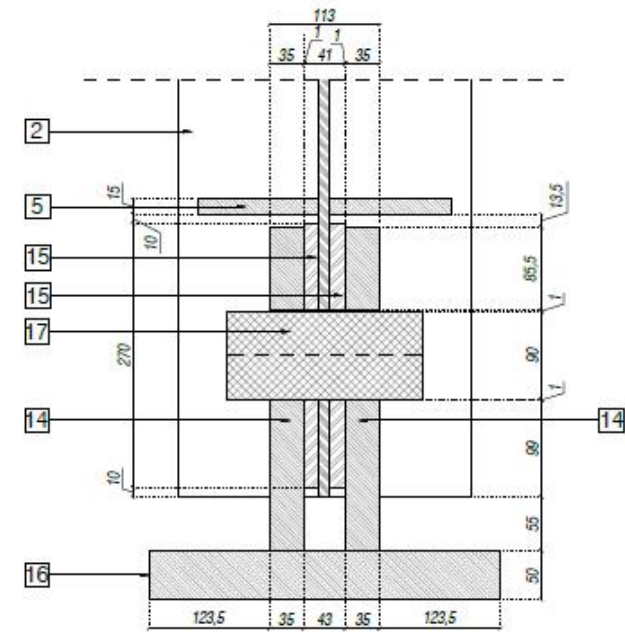


DET - 1 LEFT
SCALE 1:5

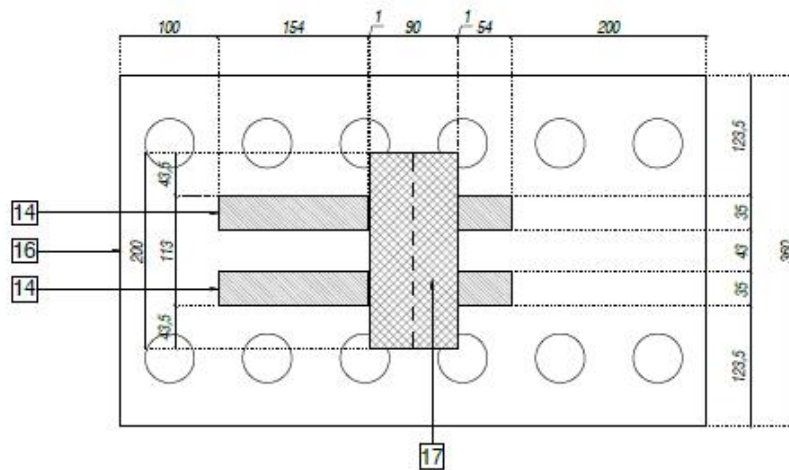
FRONT VIEW



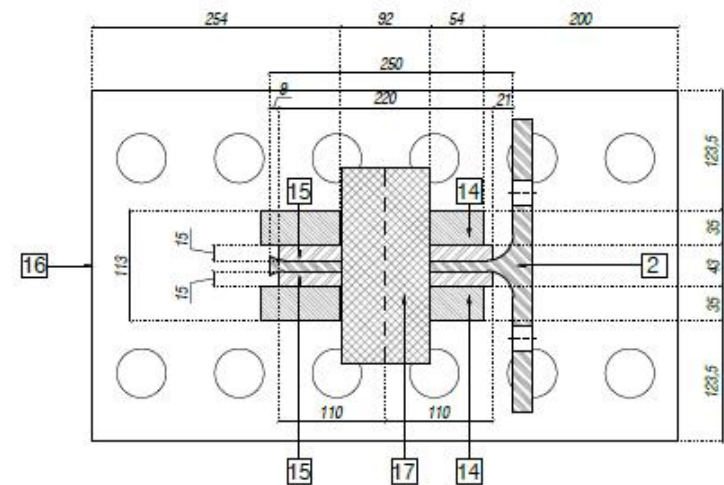
SECTION C-C

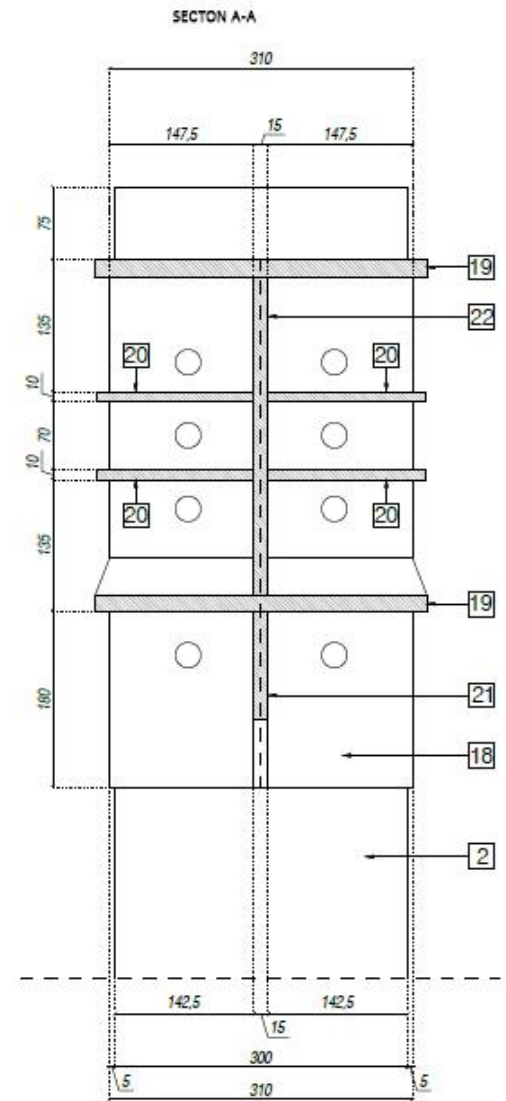
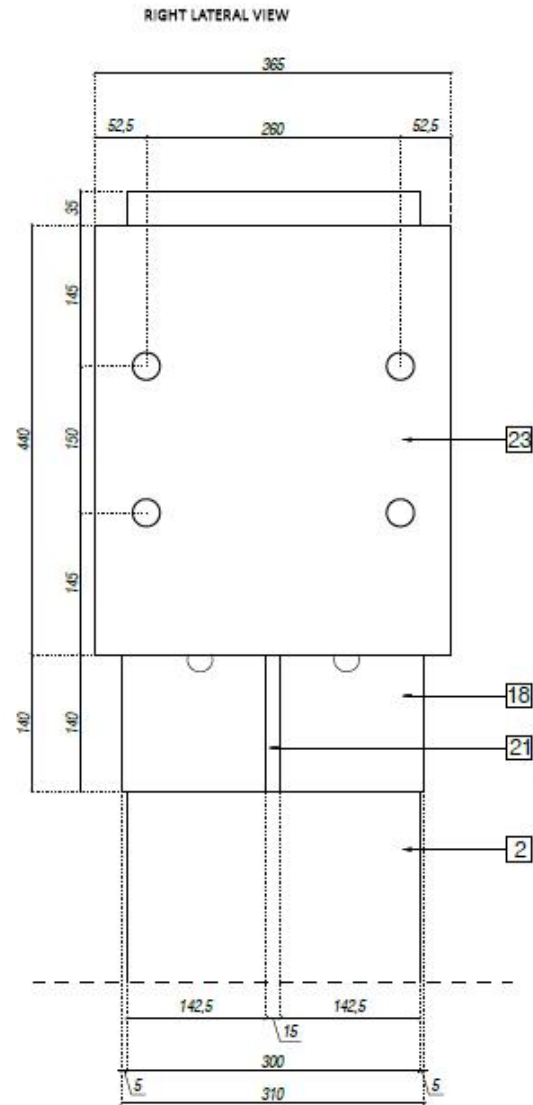
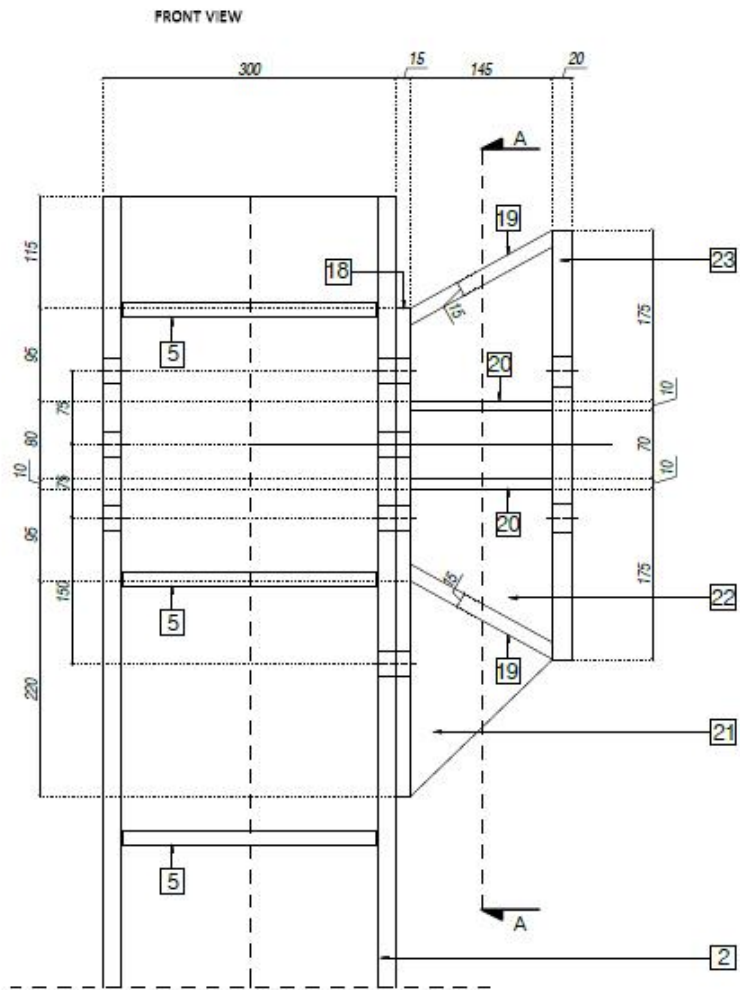


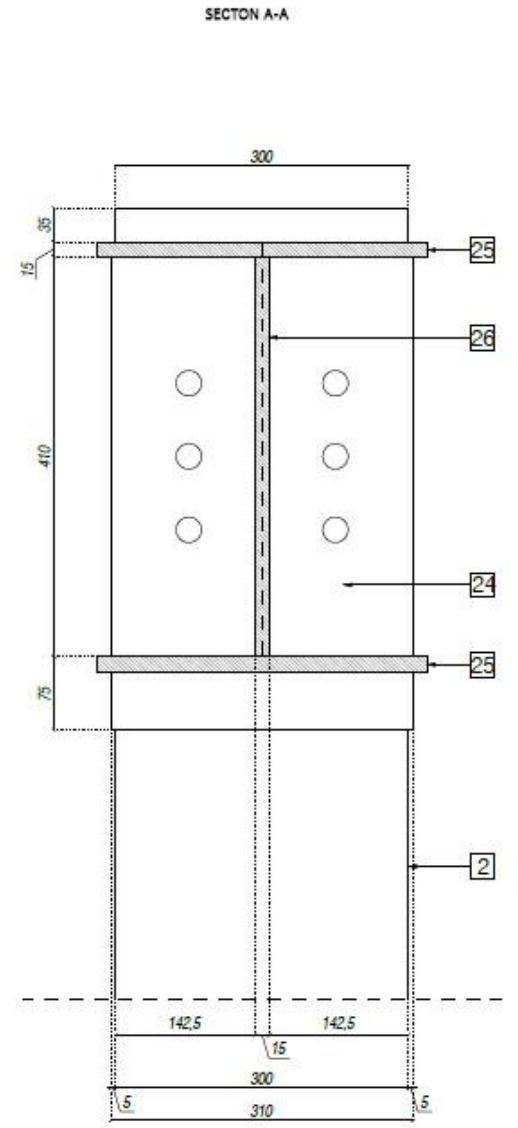
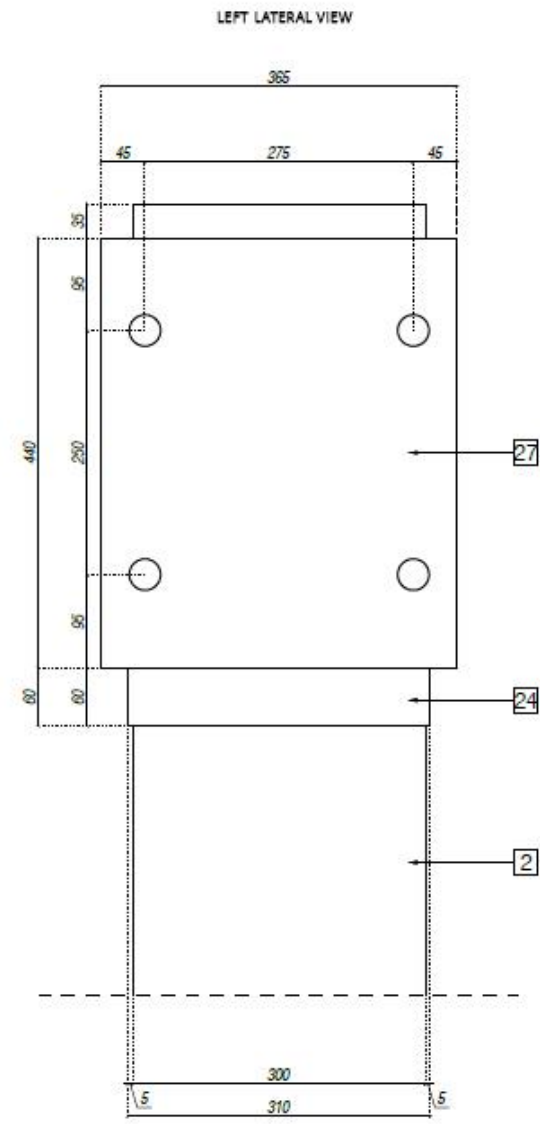
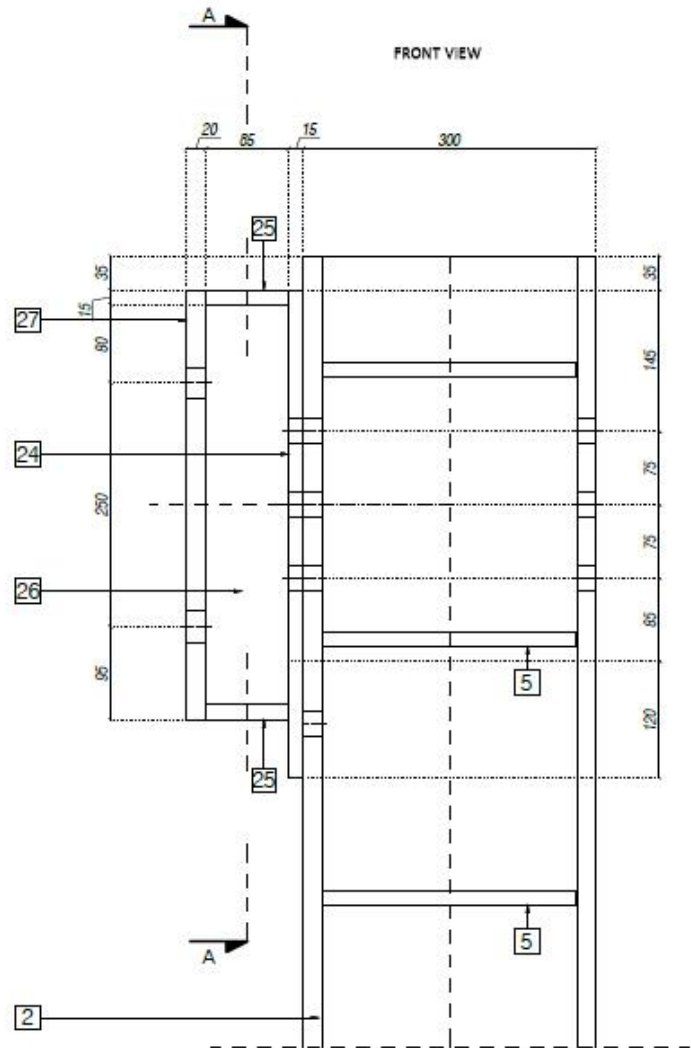
SECTION A-A



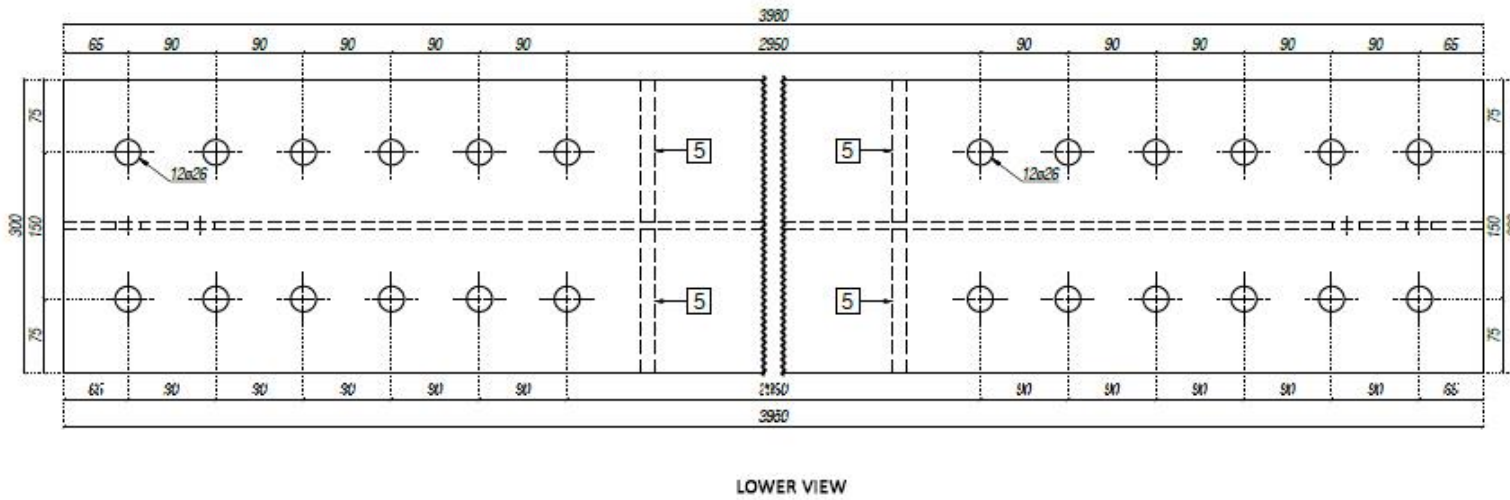
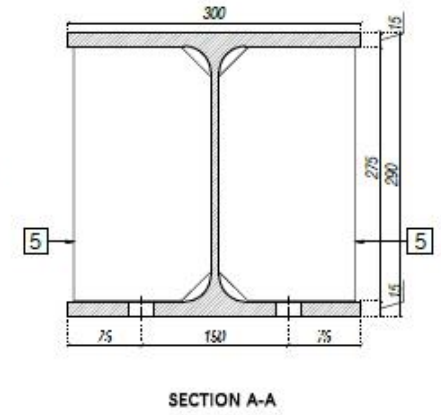
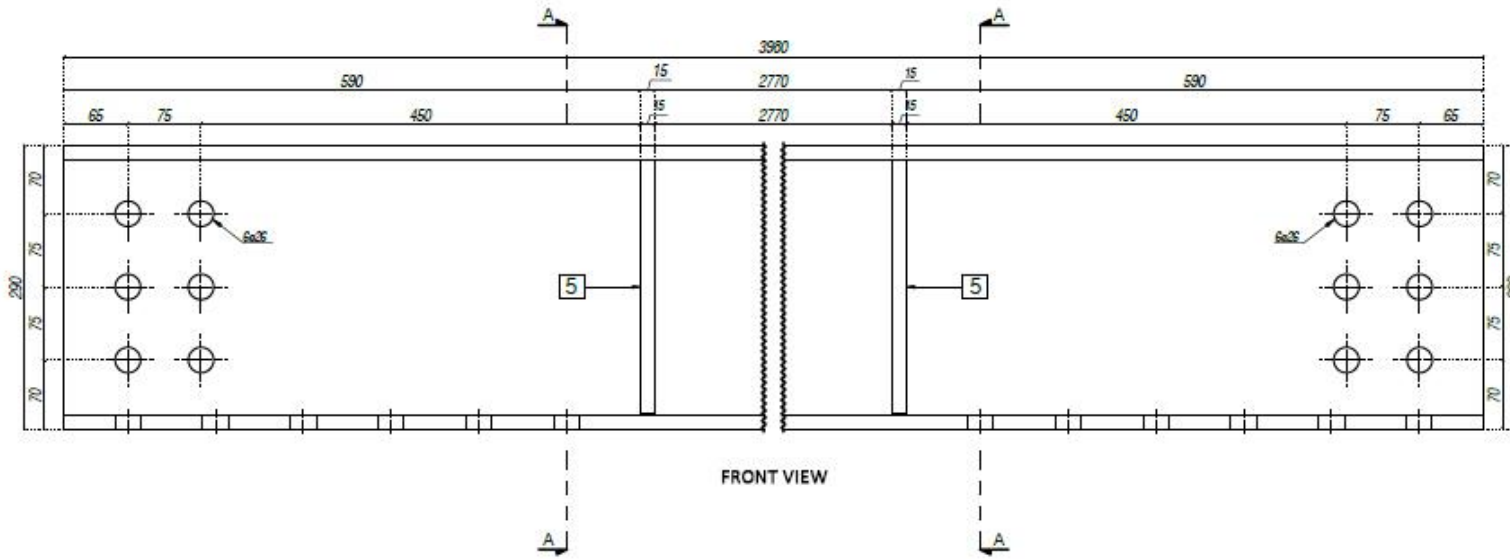
SECTION B-B

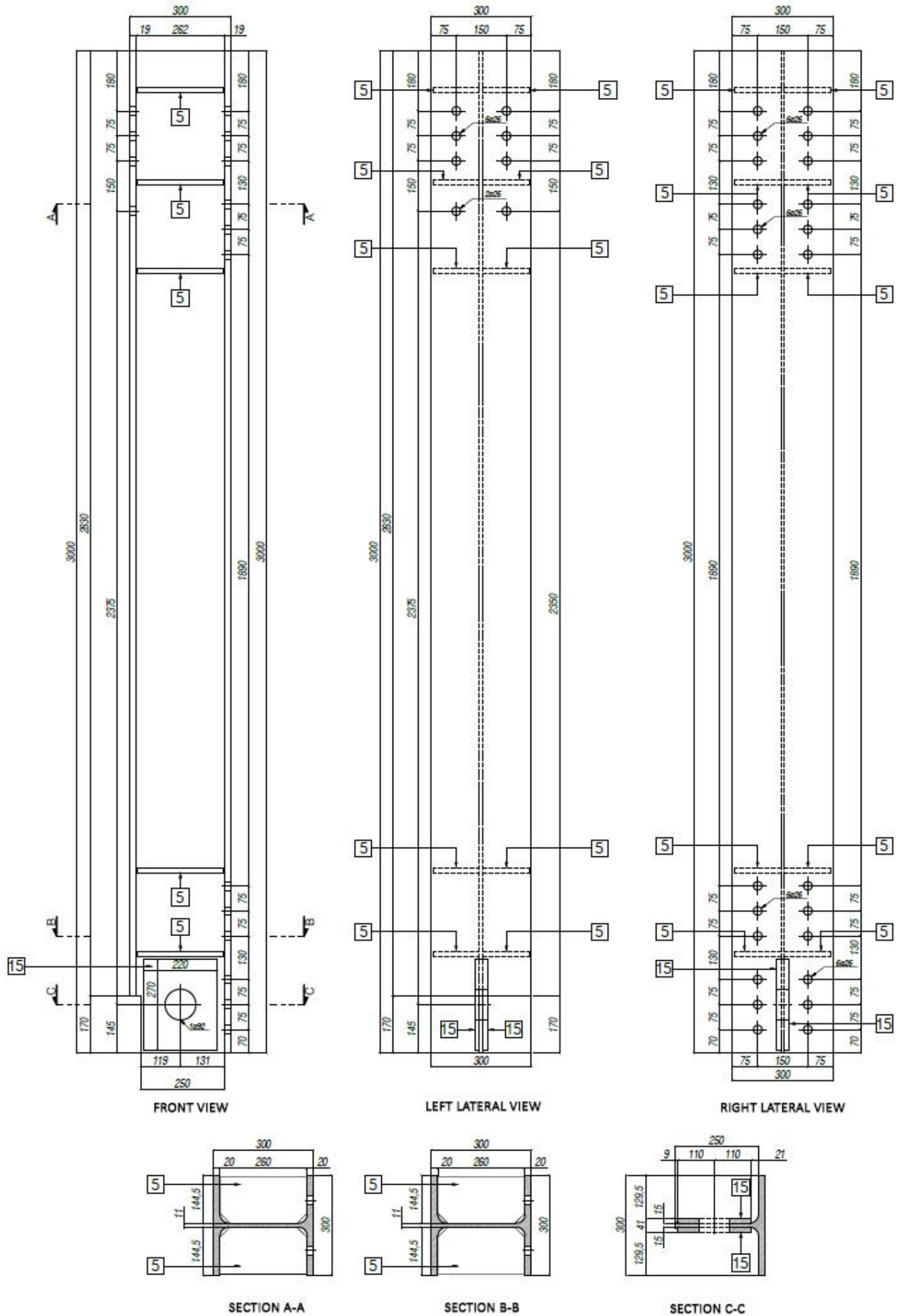




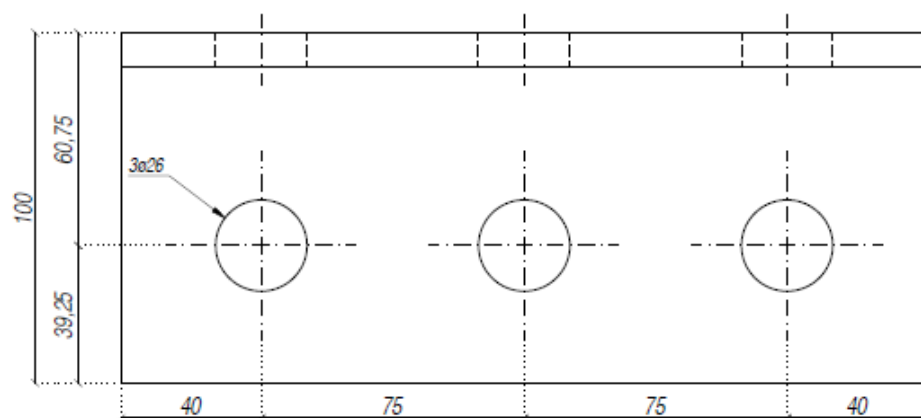
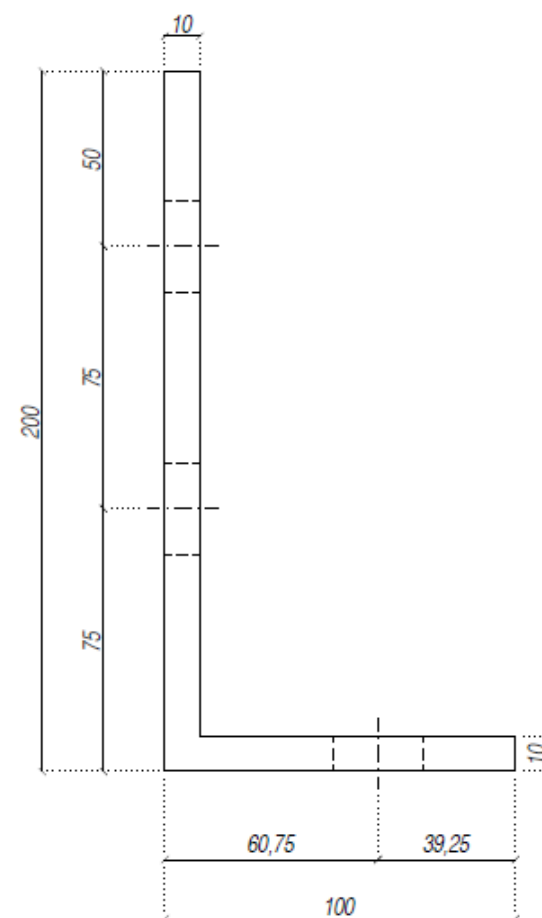
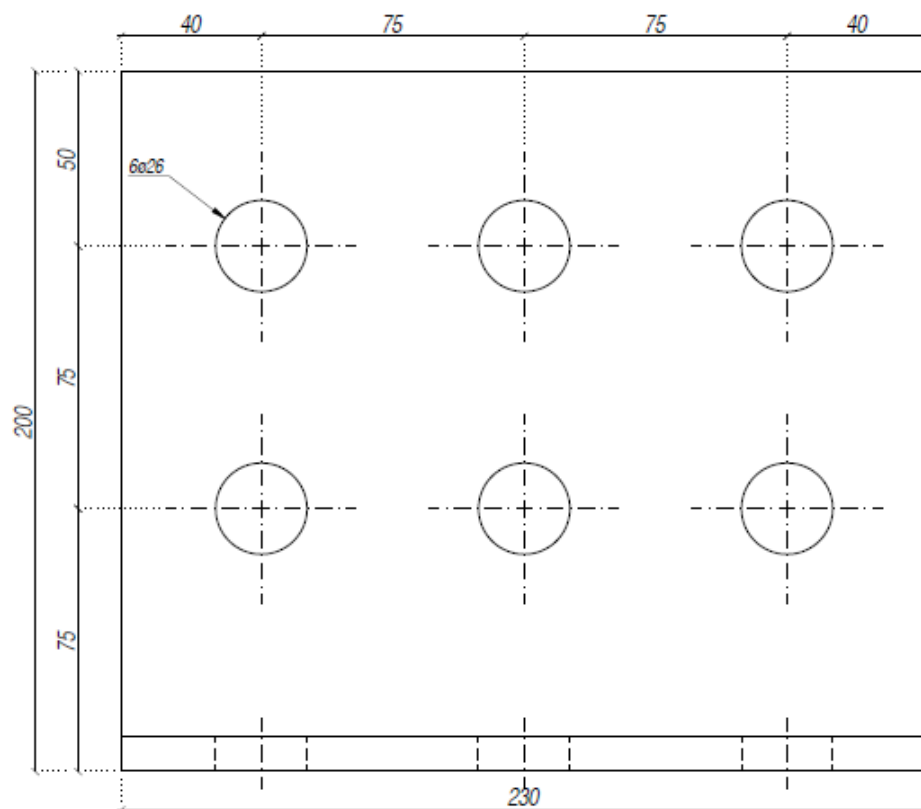


1 2x HEA300
S355JR

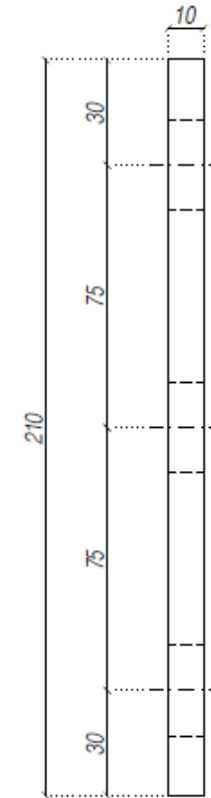
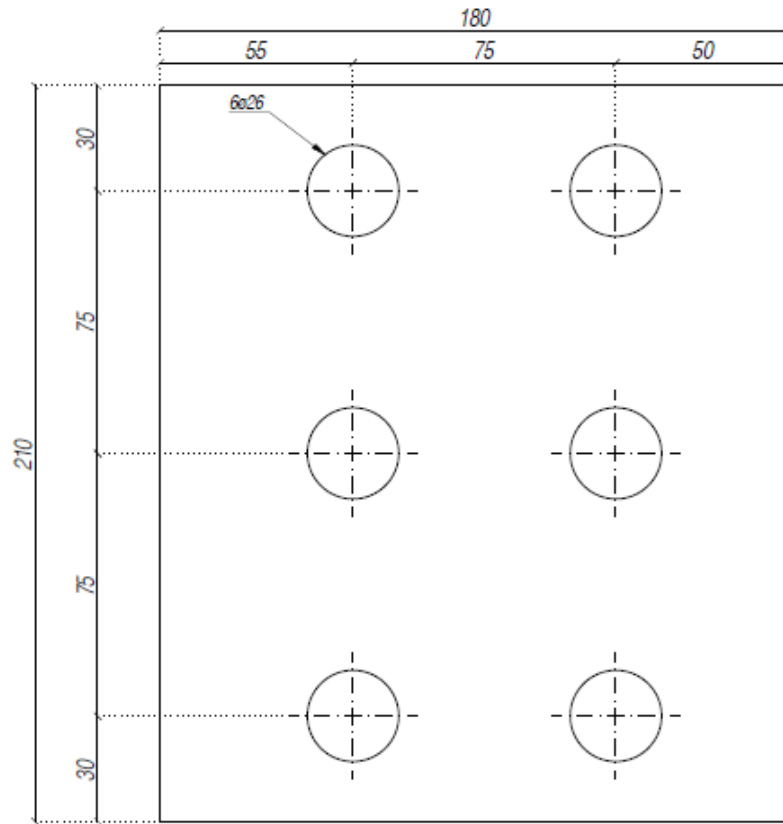




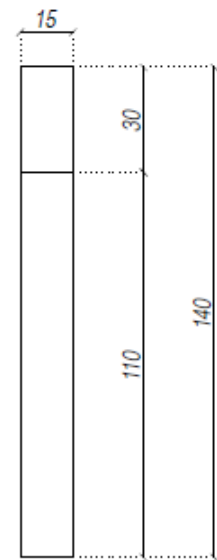
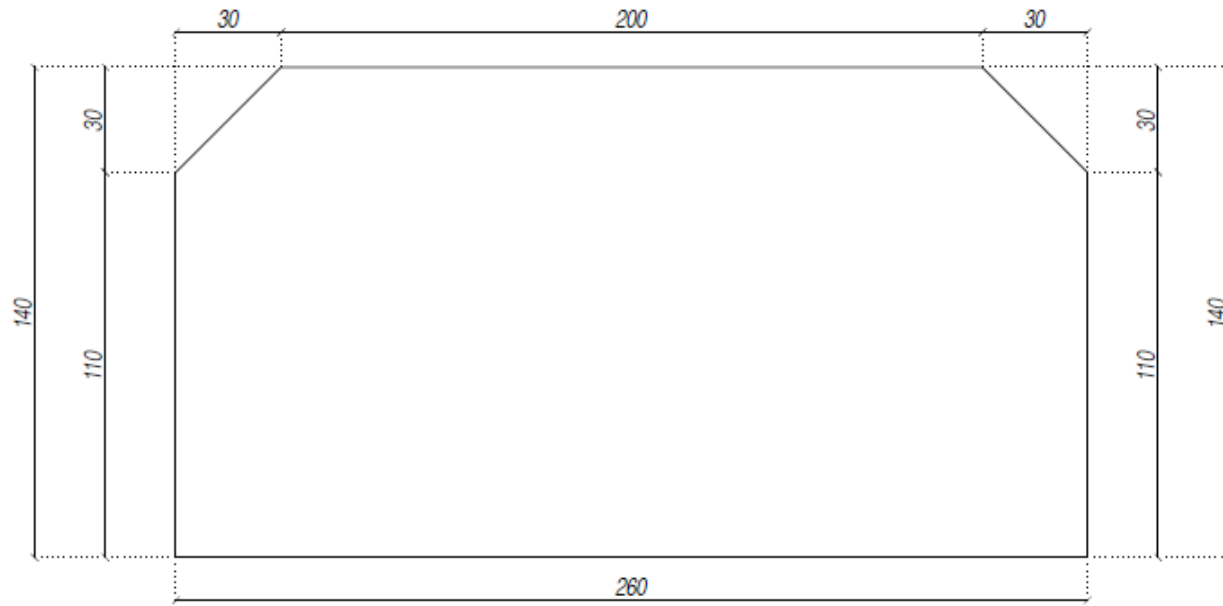
3 8x L 200x100x10x230
S275JR



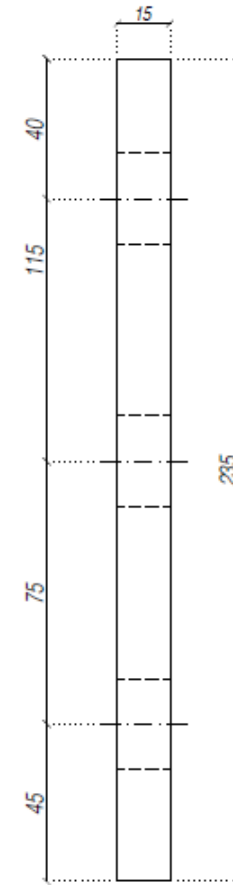
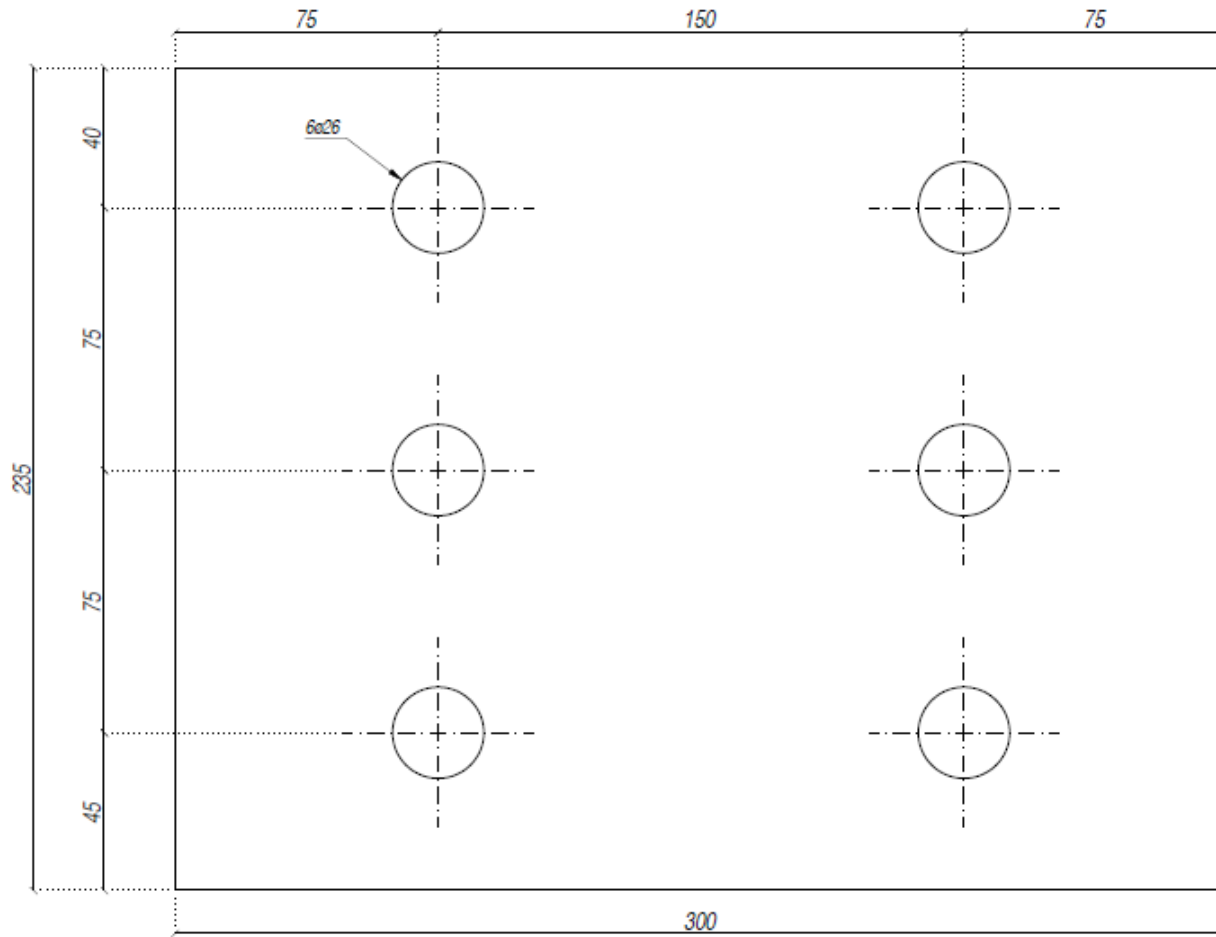
4 8x LAM 180x210x10
S355JR



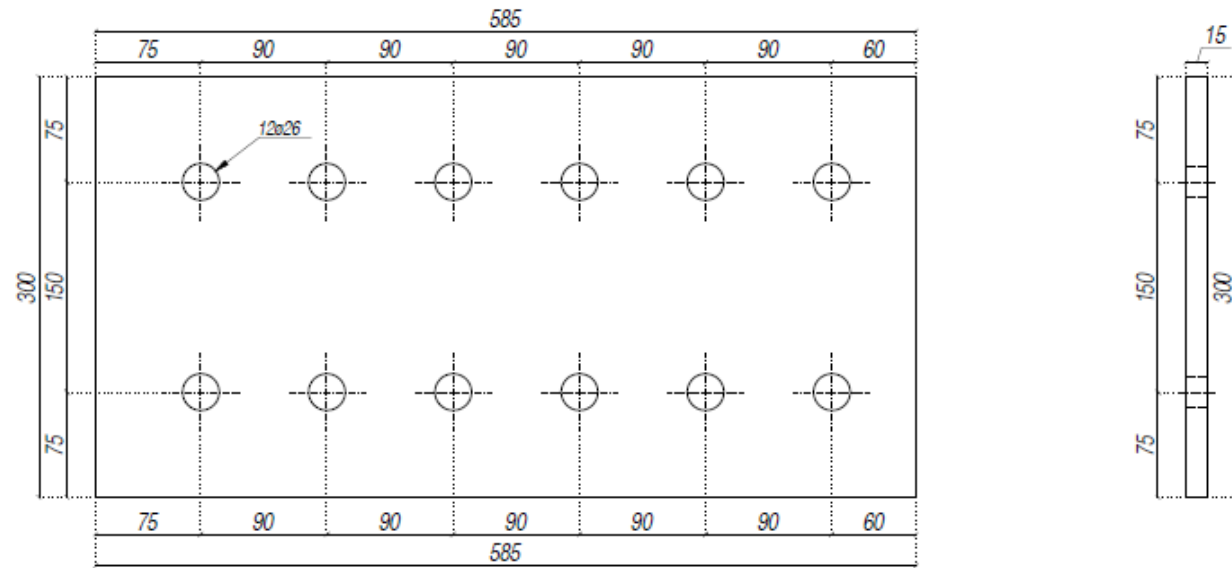
5 28x LAM 260x140x15
S355JR

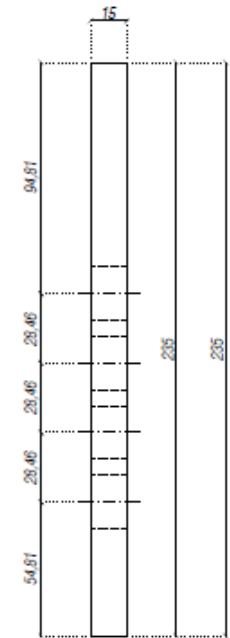
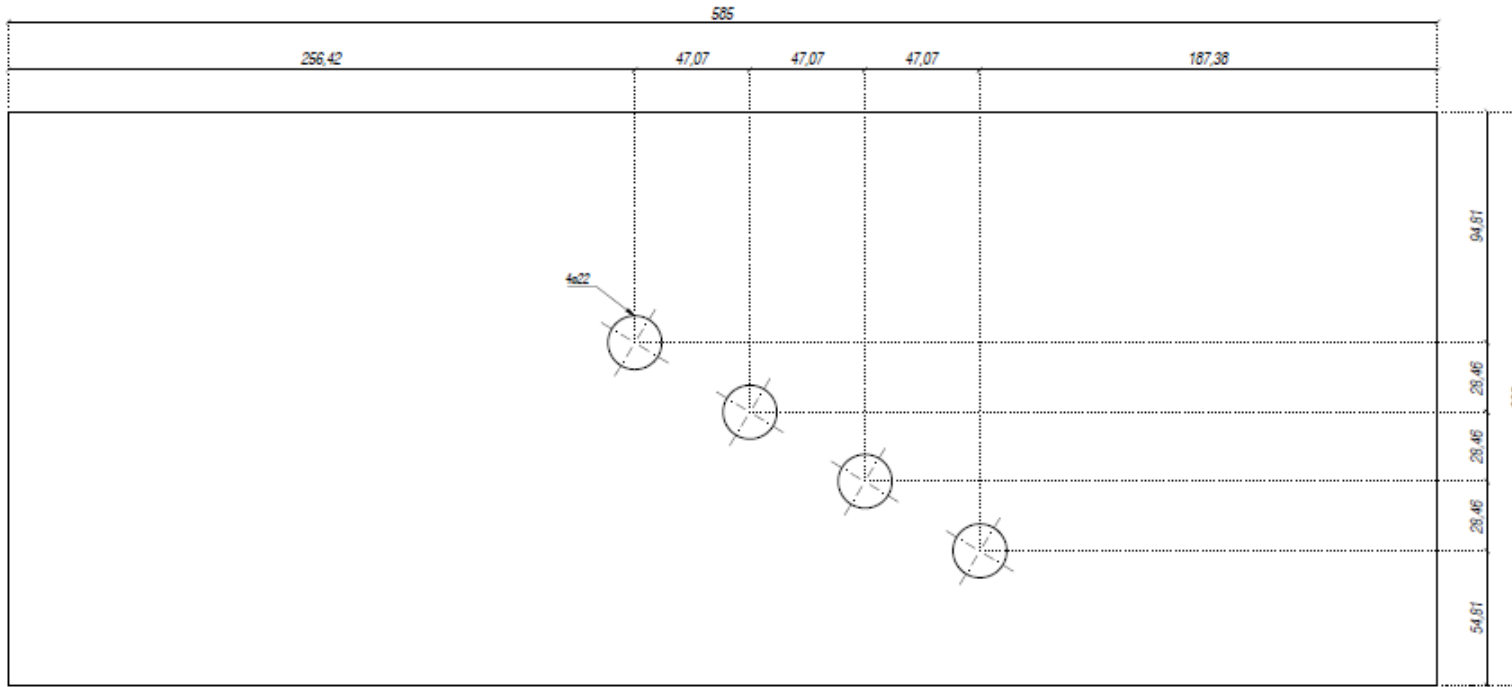


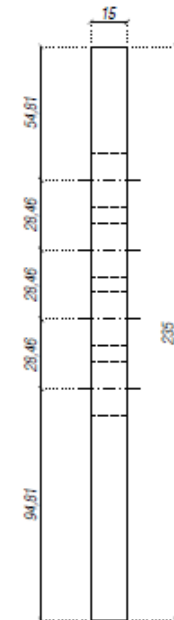
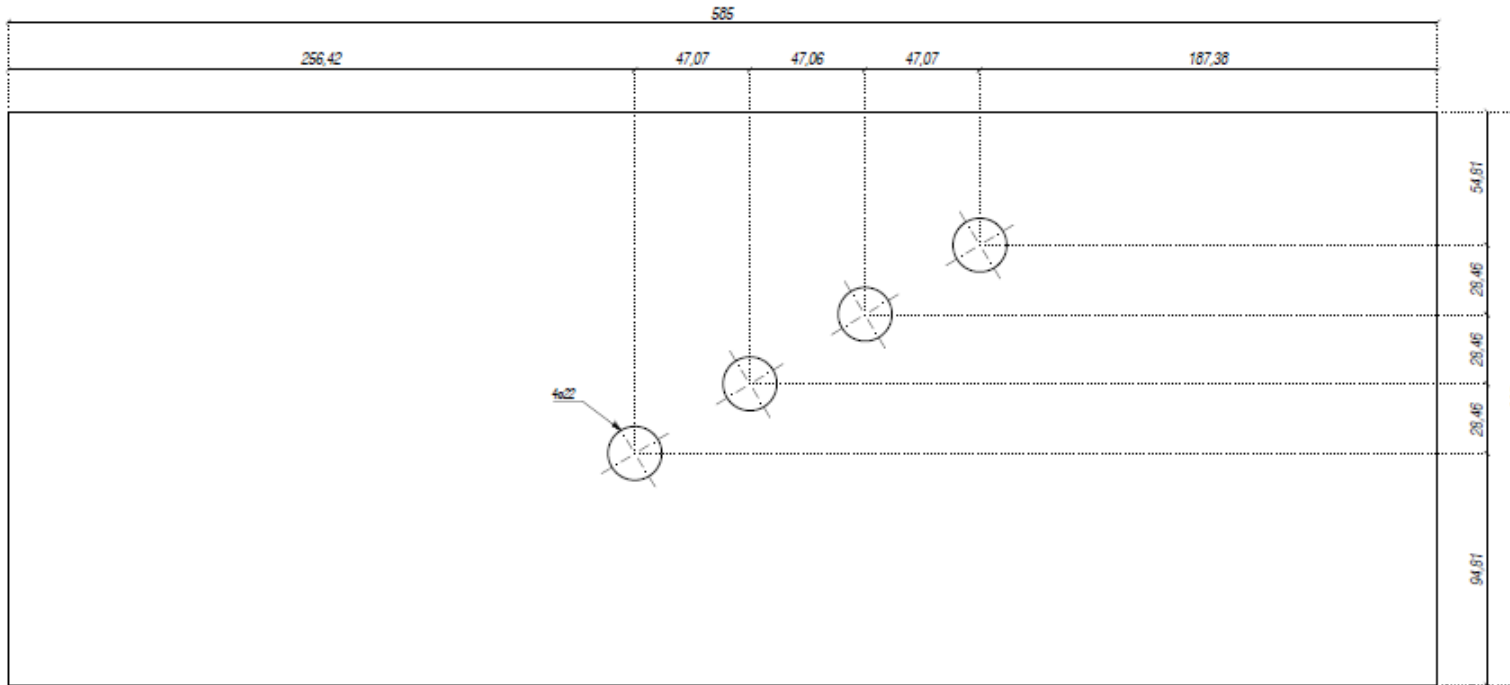
6 4x LAM 300x235x15
S275JR



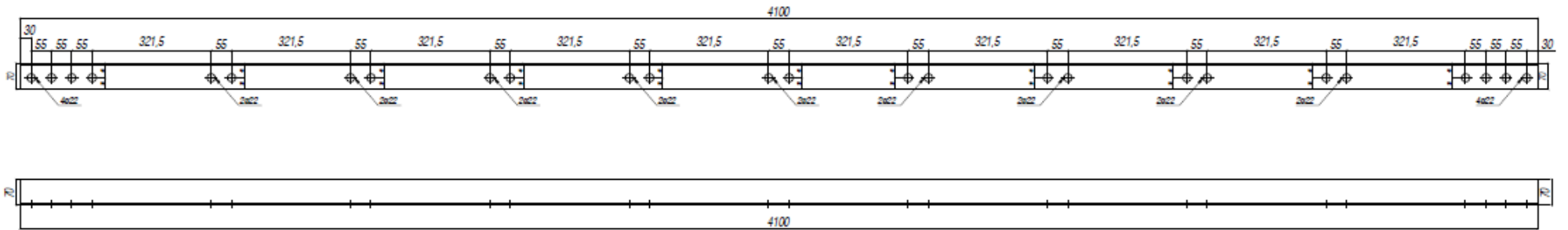
7 4x LAM 585x300x15
S275JR



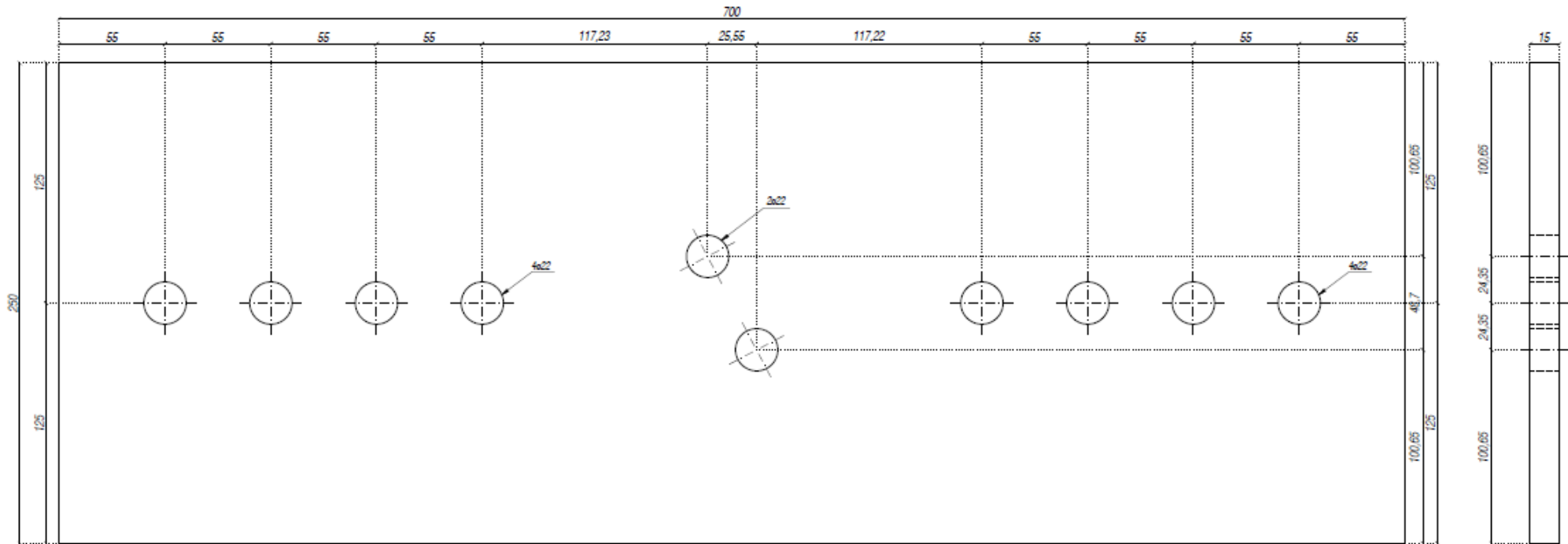




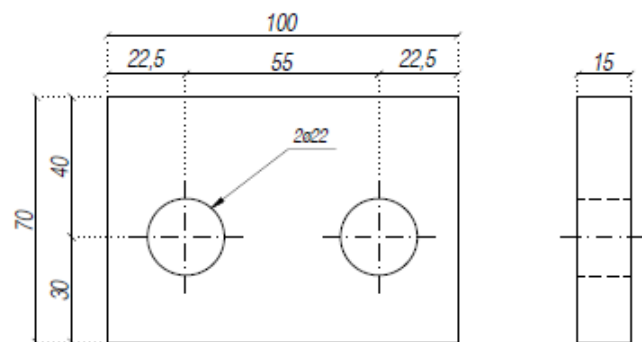
11 2x L 70x7x1950
S275JR



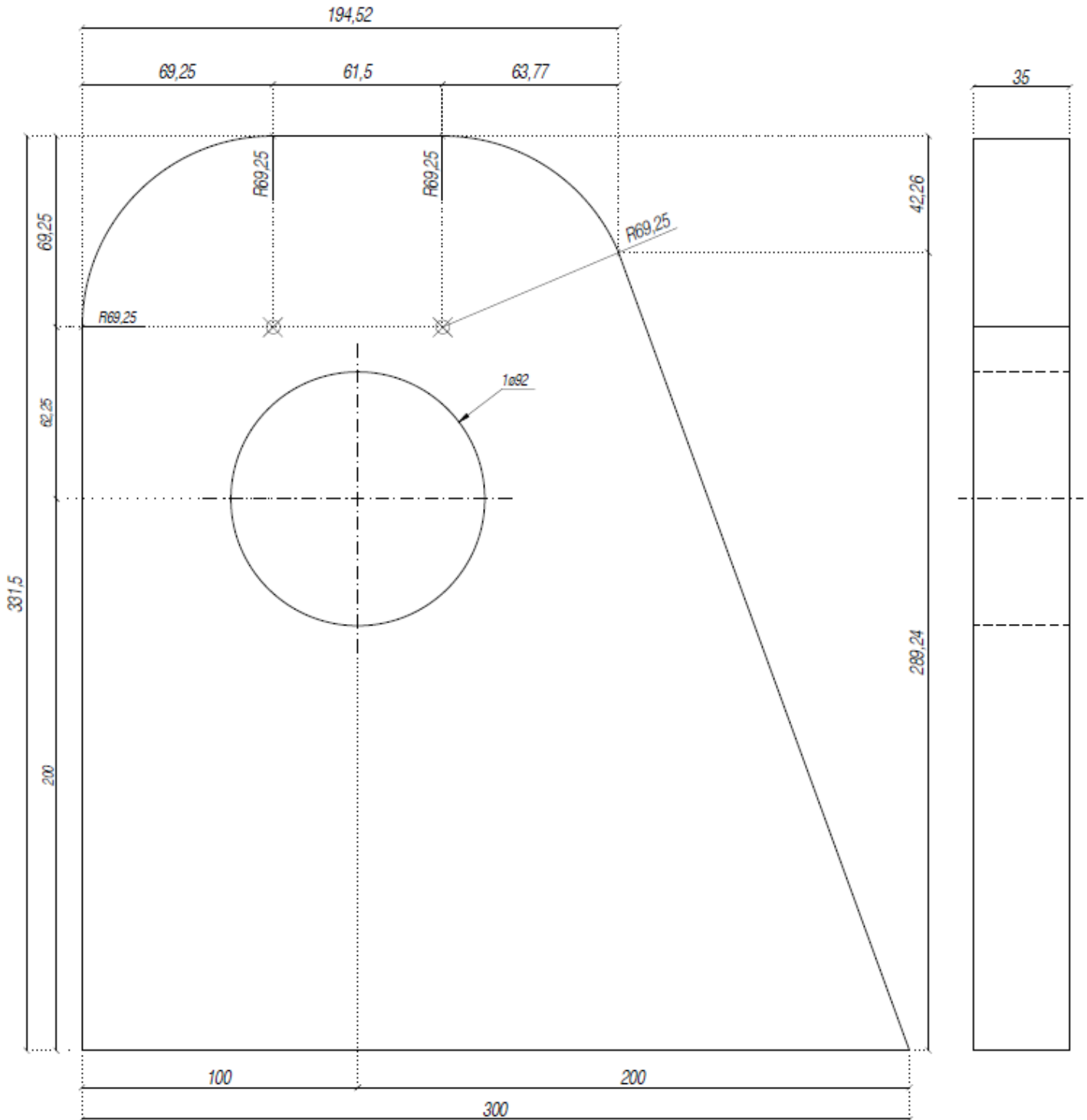
12 1x LAM 700x250x15
S275JR



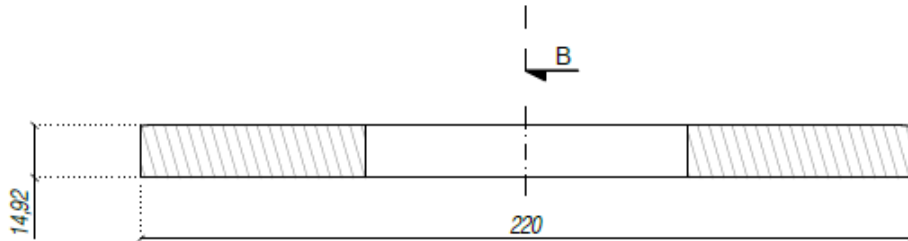
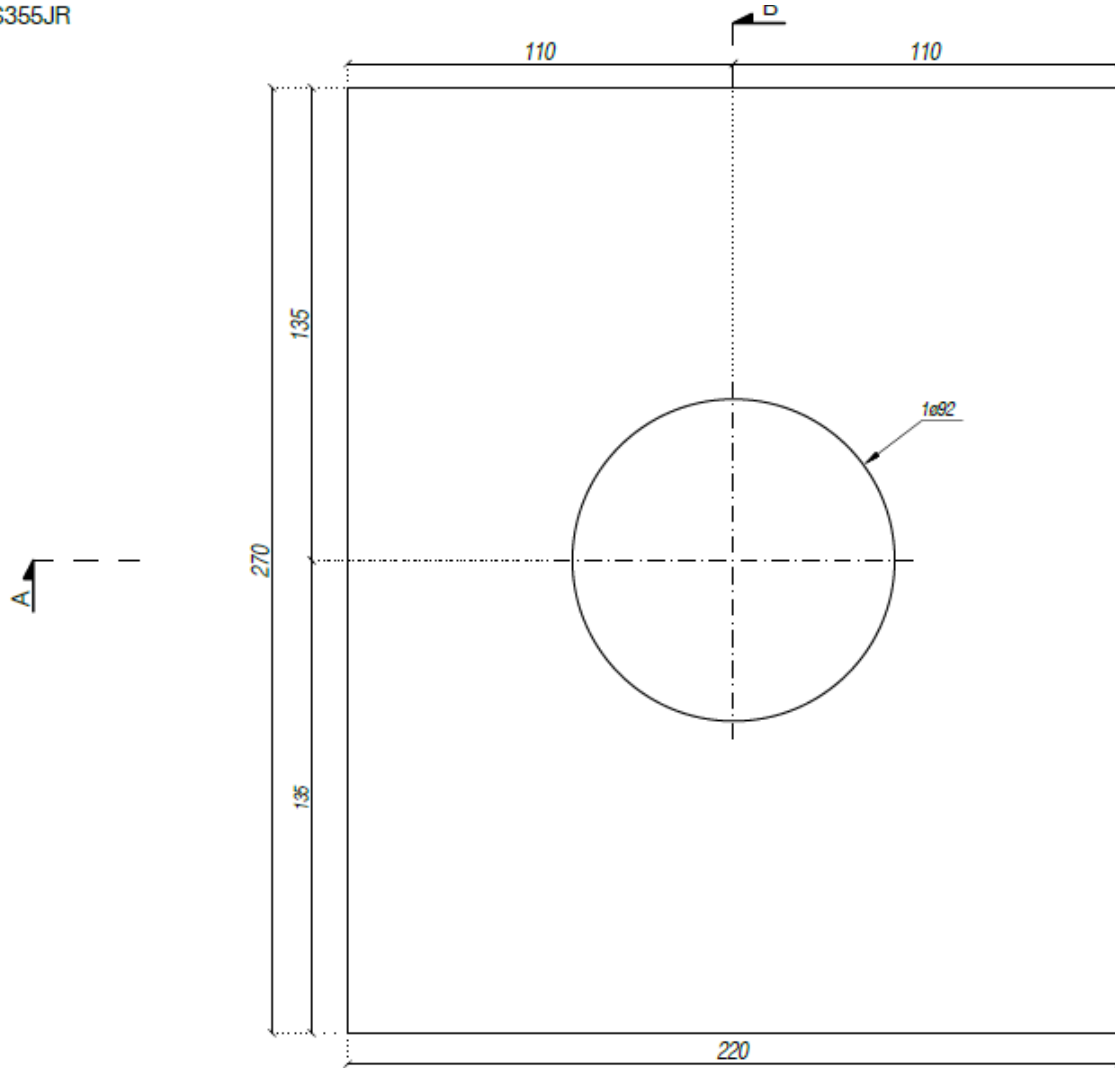
13 16x LAM 100x70x15
S275JR



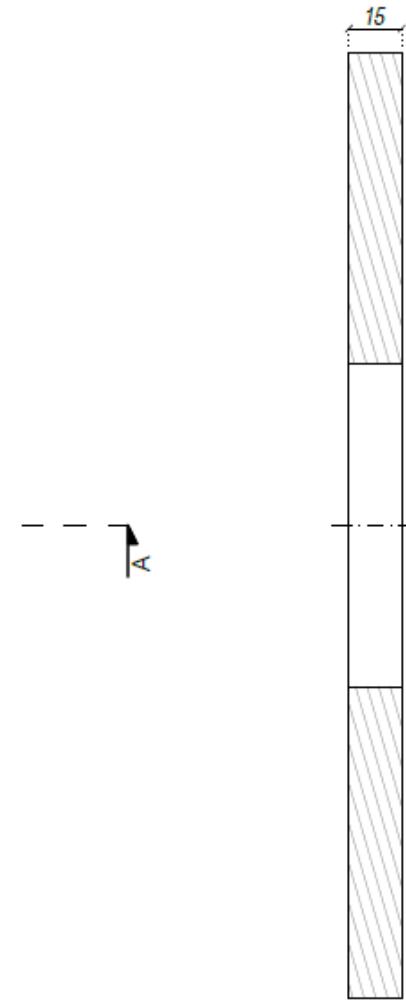
14 LATERAL STEEL PLATE OF THE HINGE
S355JR



15 4x HINGE STIFFENERS – TO WELD ON COLUMN WEBS
S355JR

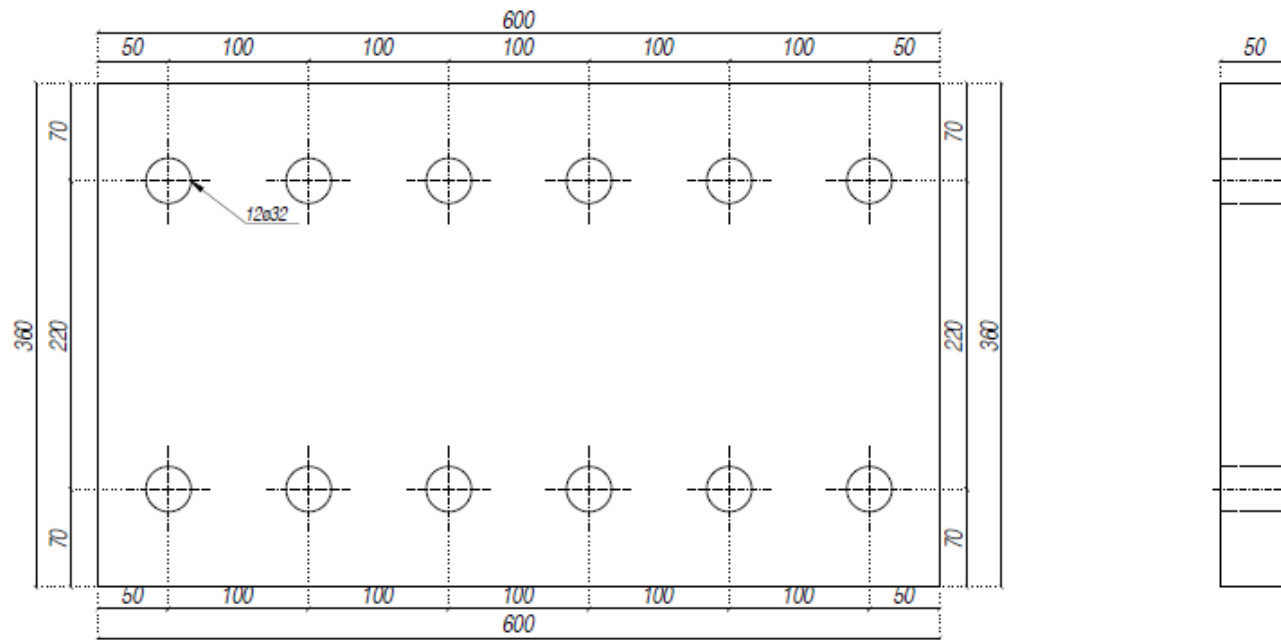


SECTION A-A

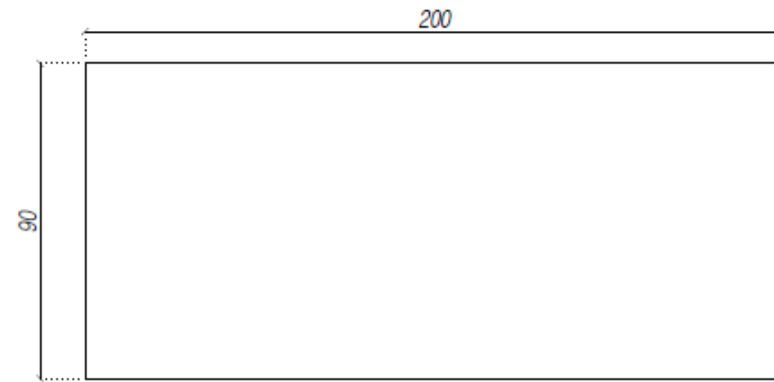
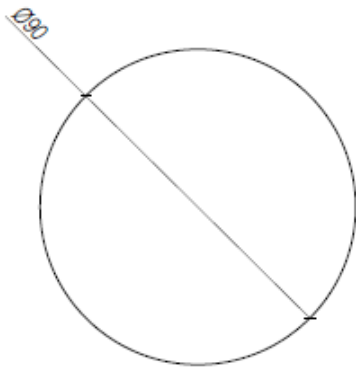


SECTION B-B

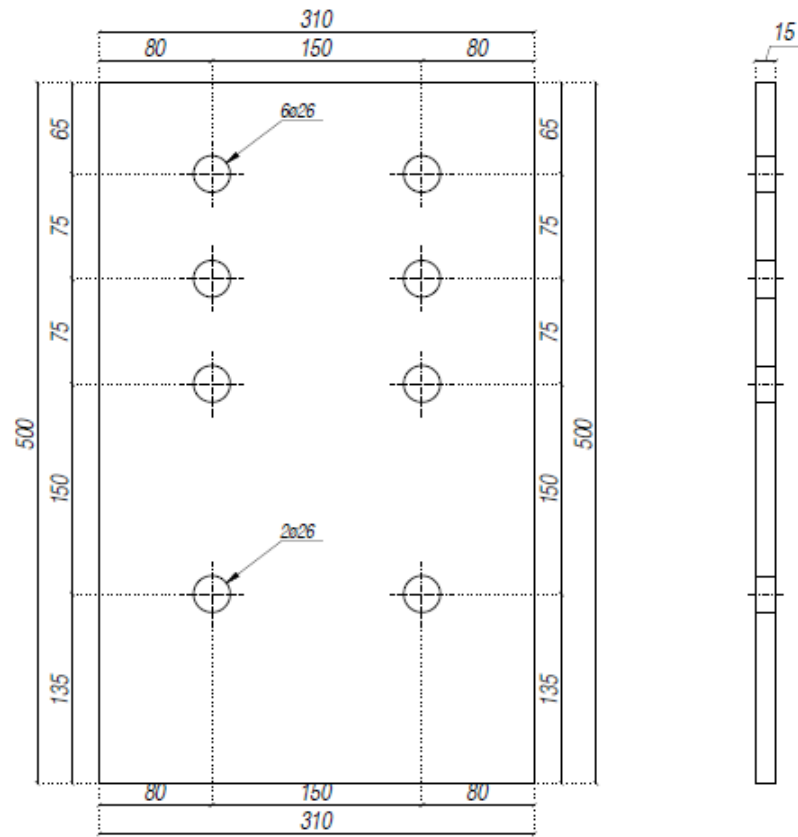
16 2x LAM 600x360x50
S355JR



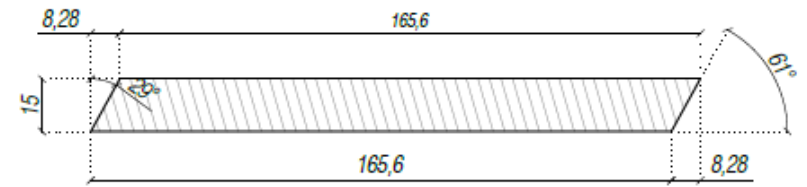
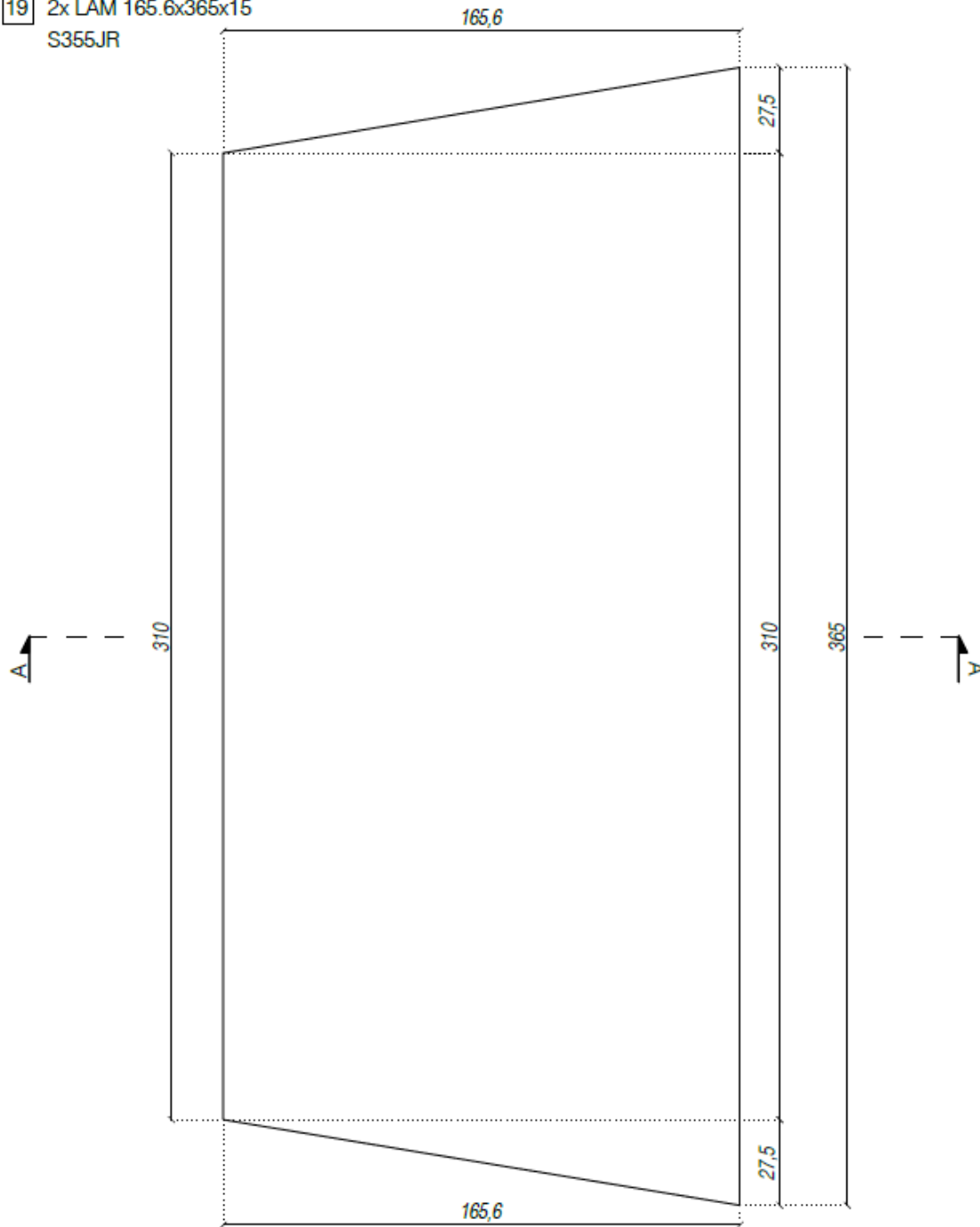
17 2x PERNO \varnothing 90
S355JR



18 1x LAM 310x500x15
S355JR

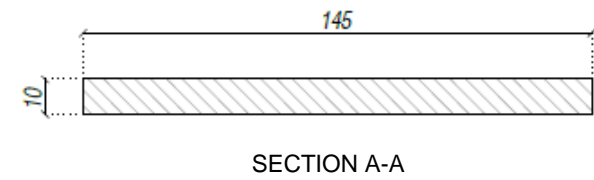
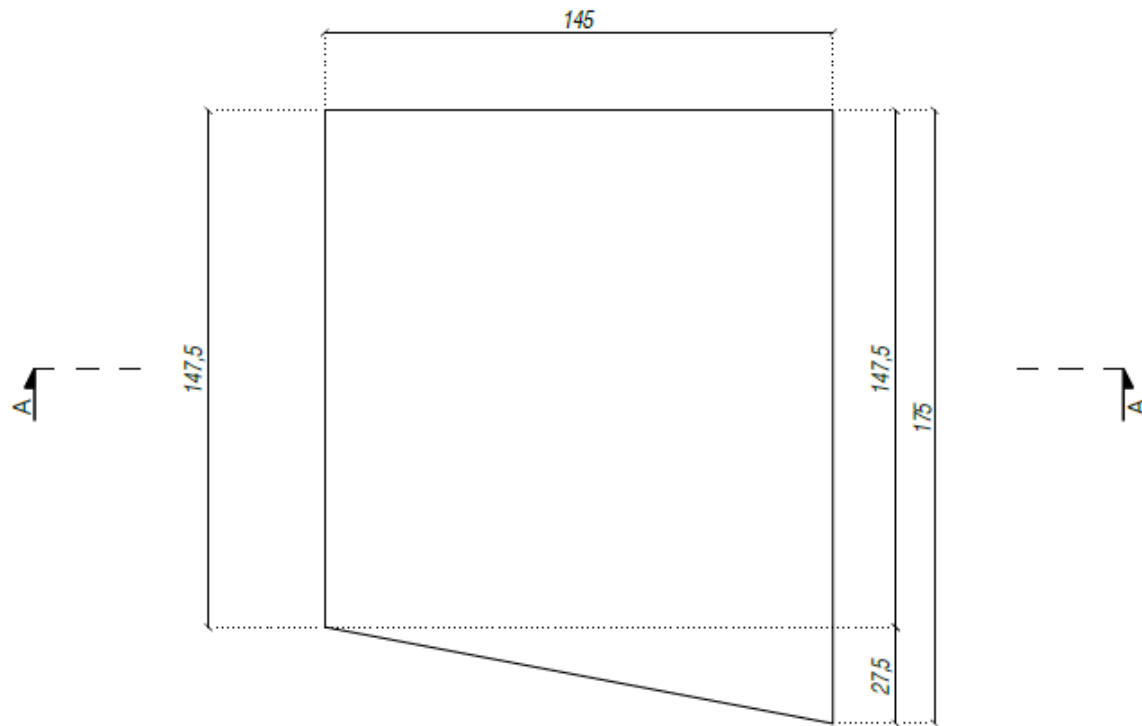


19 2x LAM 165.6x365x15
S355JR

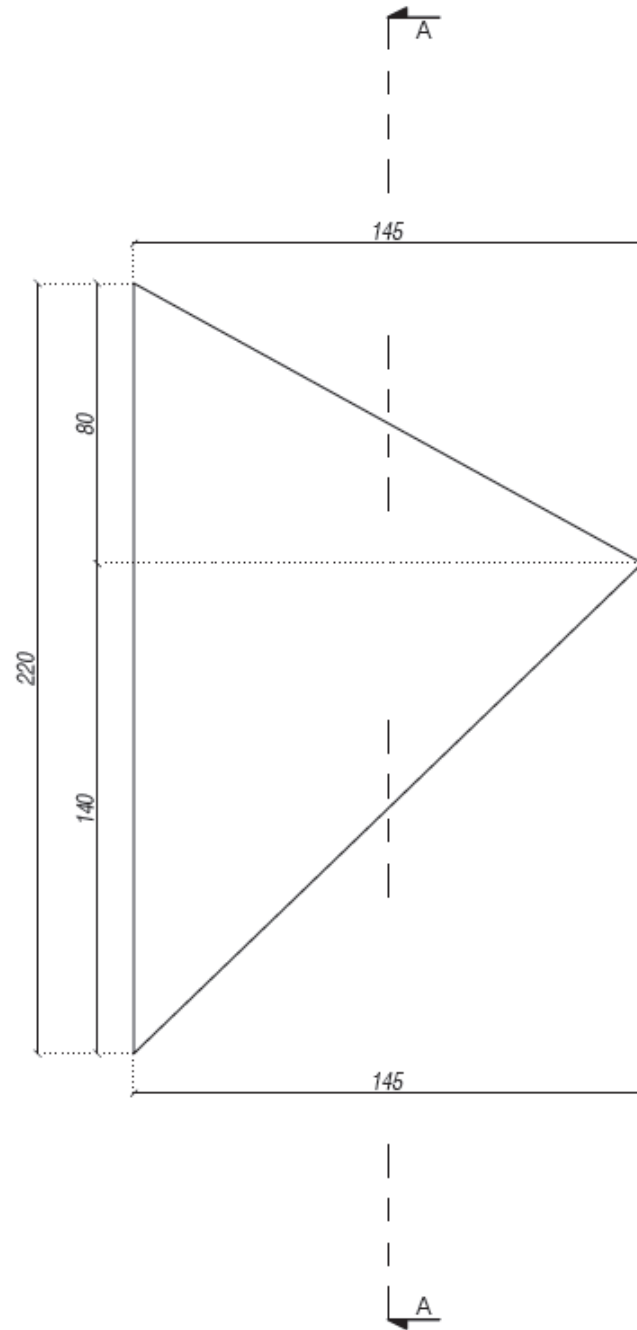


SECTION A-A

20 4x LAM 145x175x10
S355JR

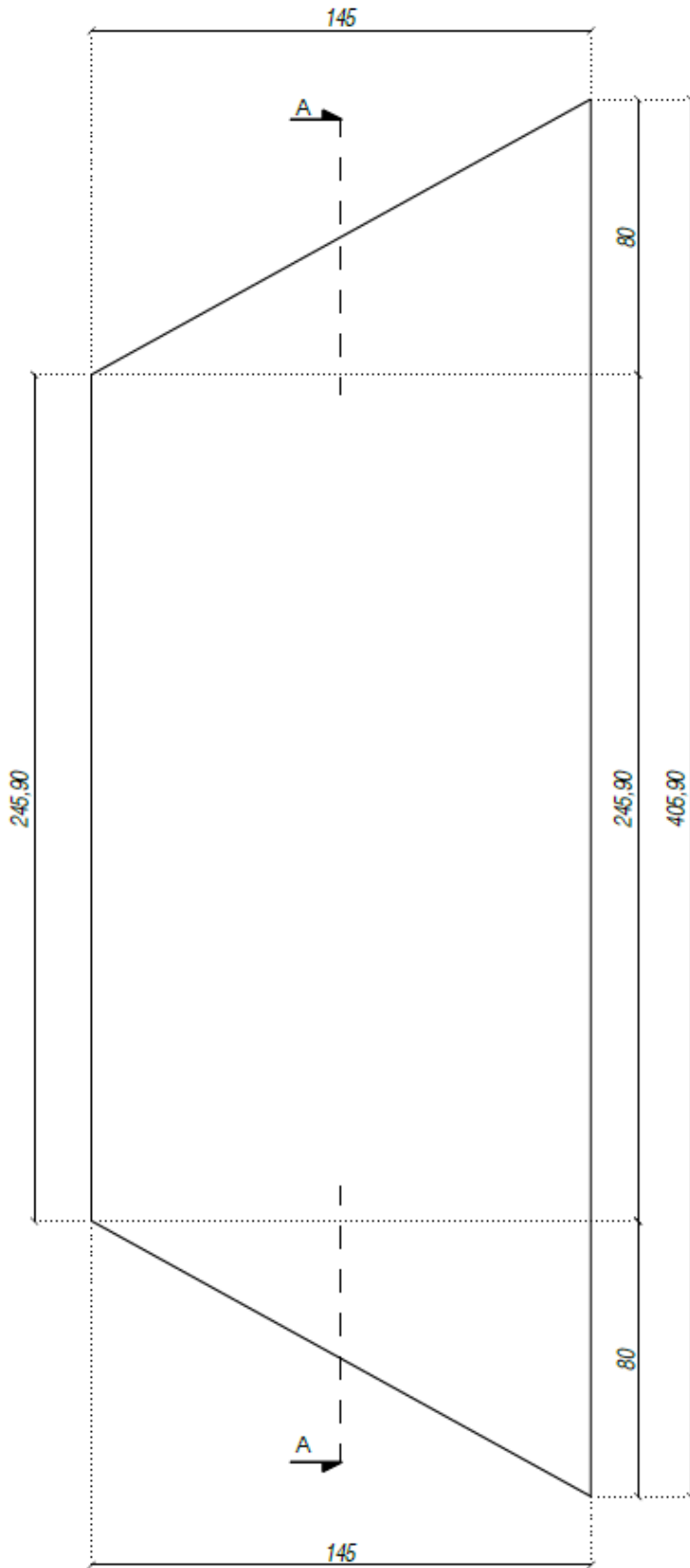


21 1x LAM 145x220x15
S355JR



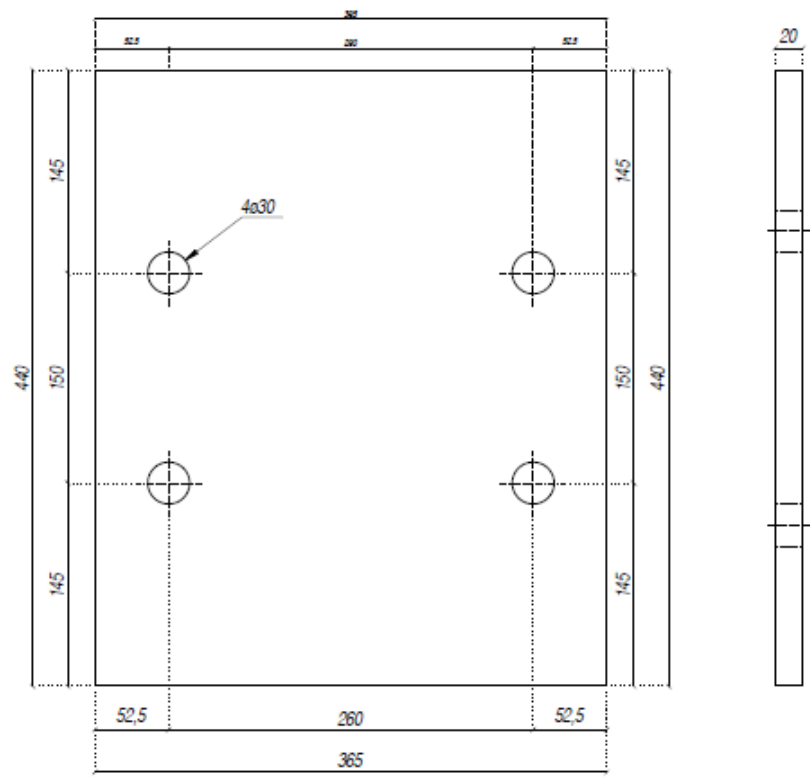
SECTION A-A

22 1x LAM 145x405.9x15
S355JR

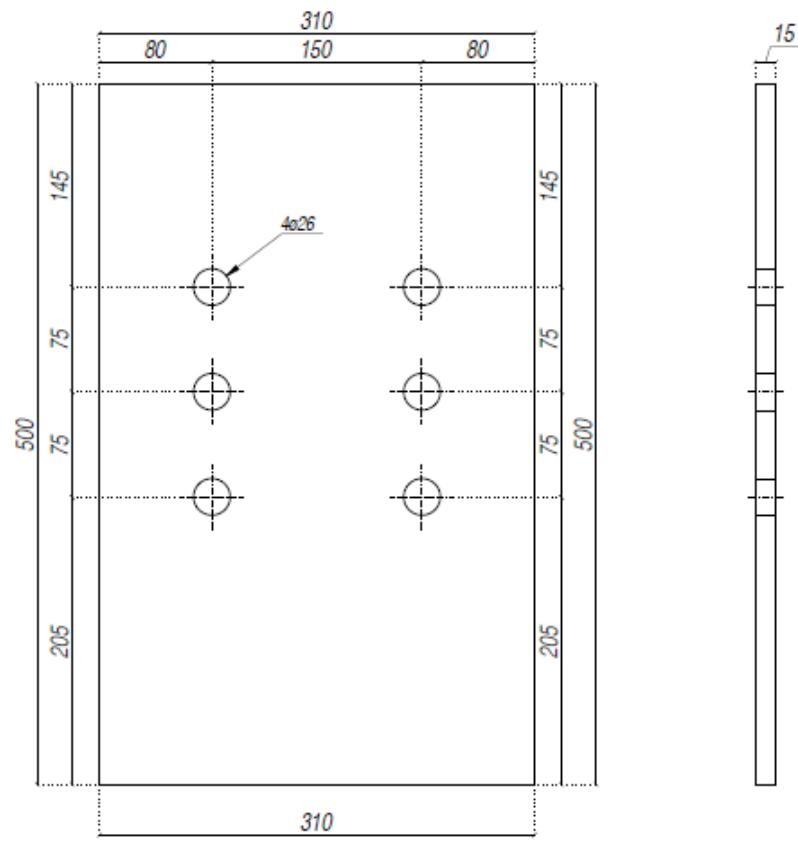


SECTION A-A

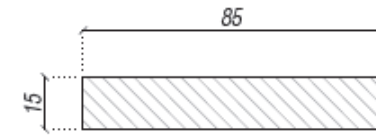
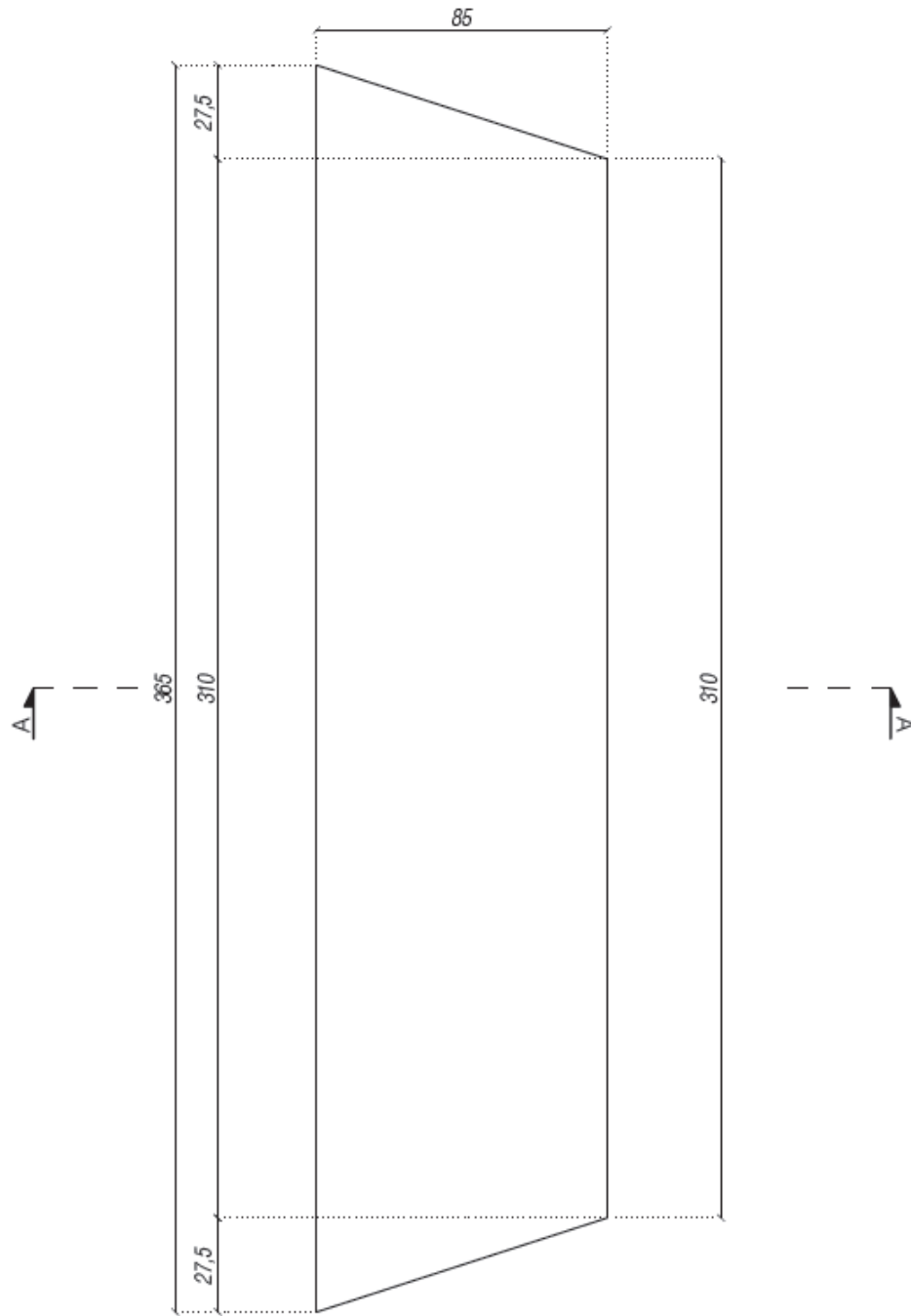
23 1x LAM 365x440x20
S355JR



24 1x LAM 310x500x15
S355JR

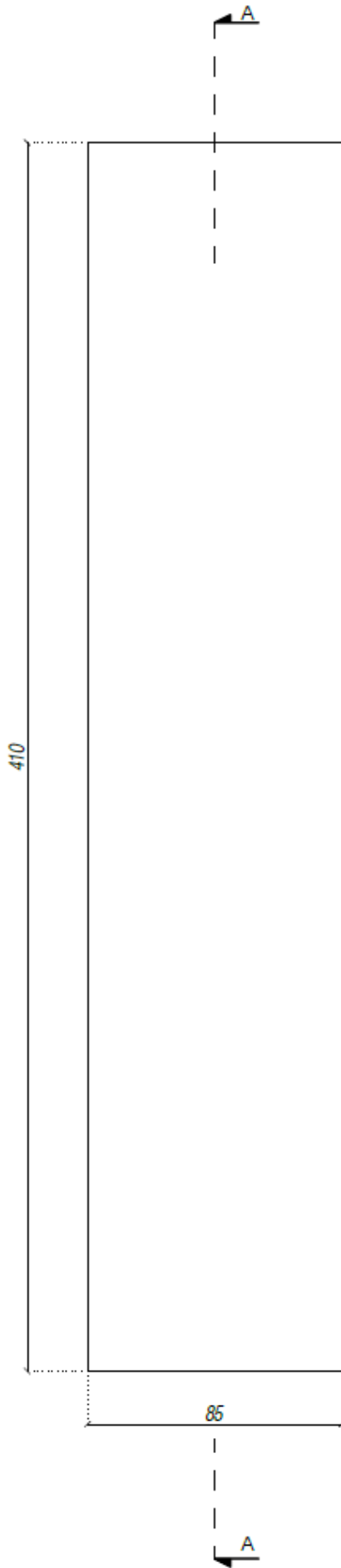


25 2x LAM 85x365x15
S355JR



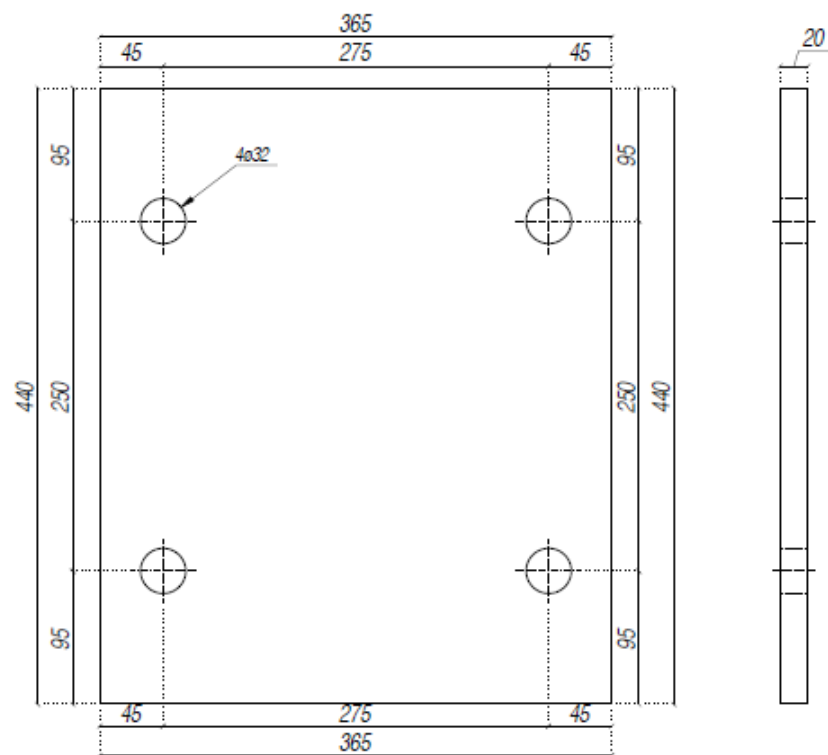
SECTION A-A

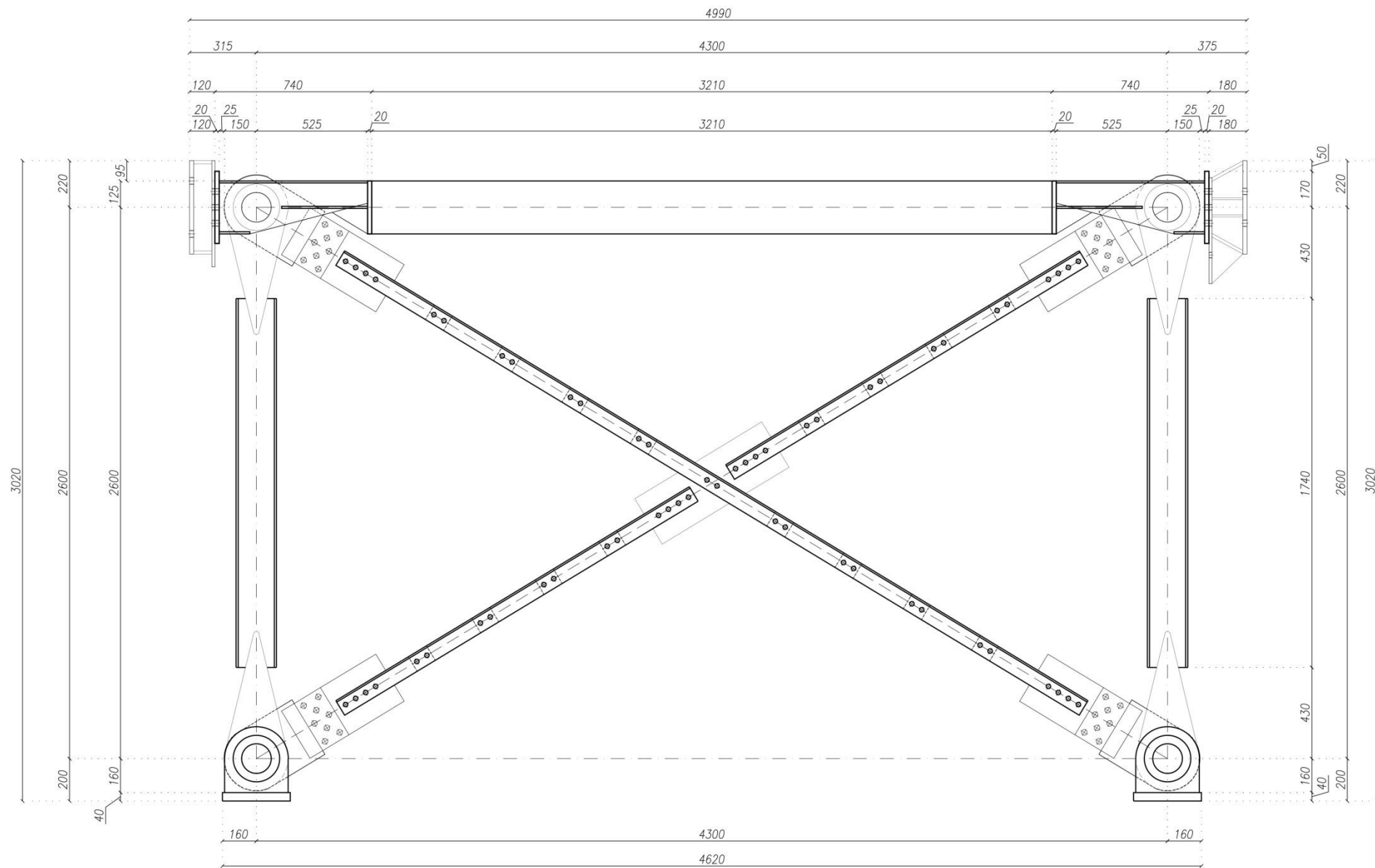
26 1x LAM 85x410x15
S355JR



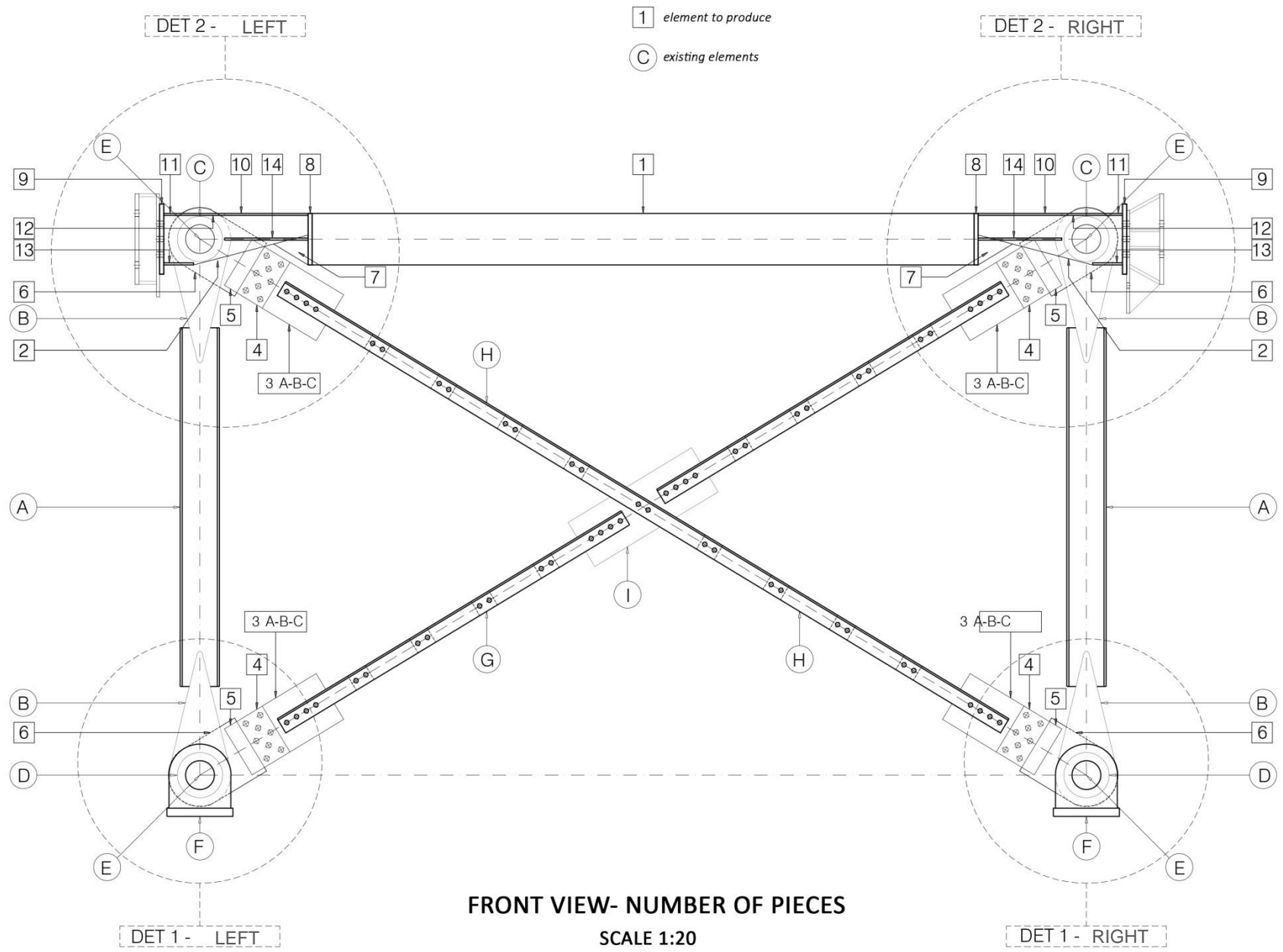
SECTION A-A

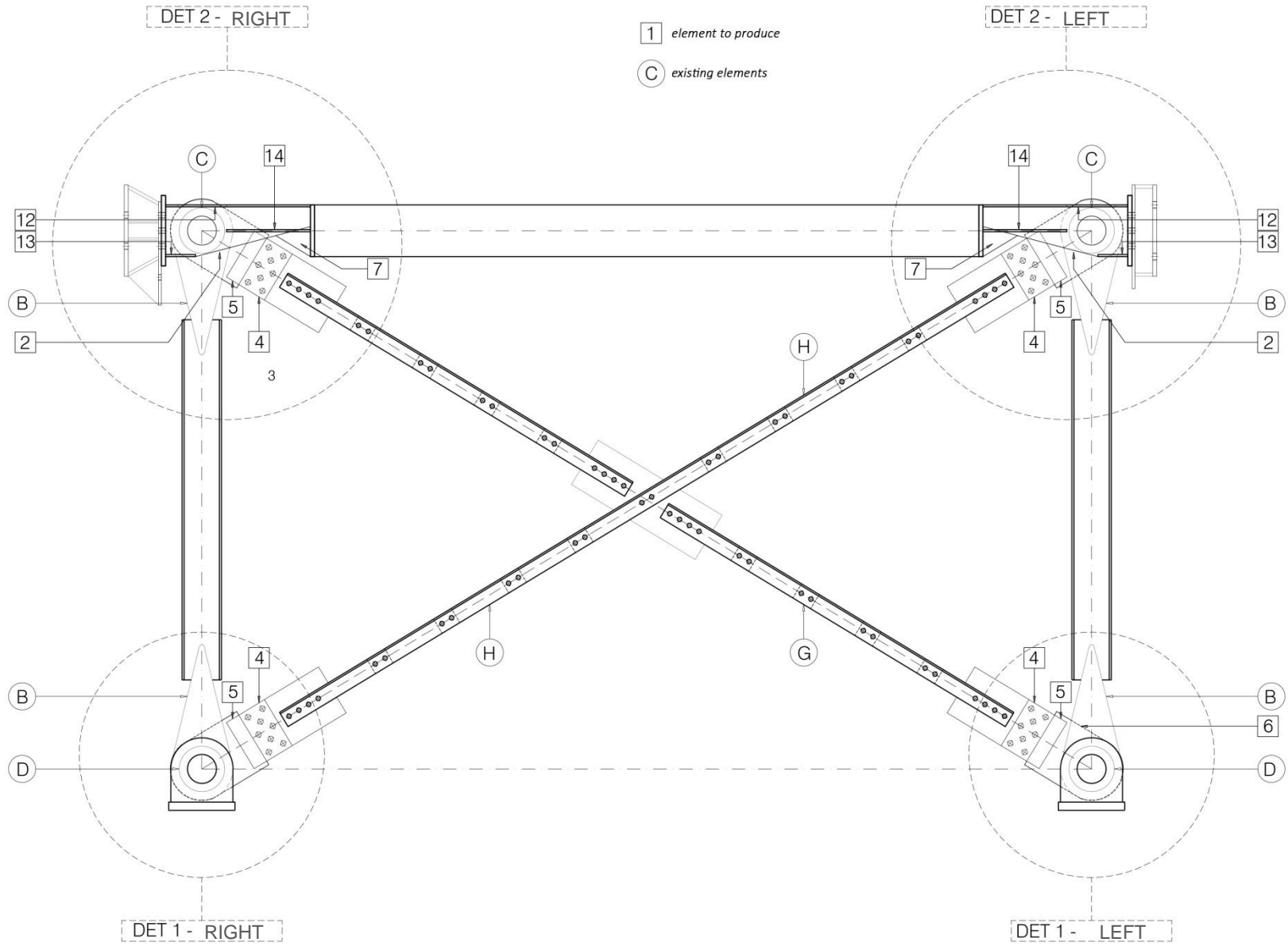
27 1x LAM 365x440x20
S355JR





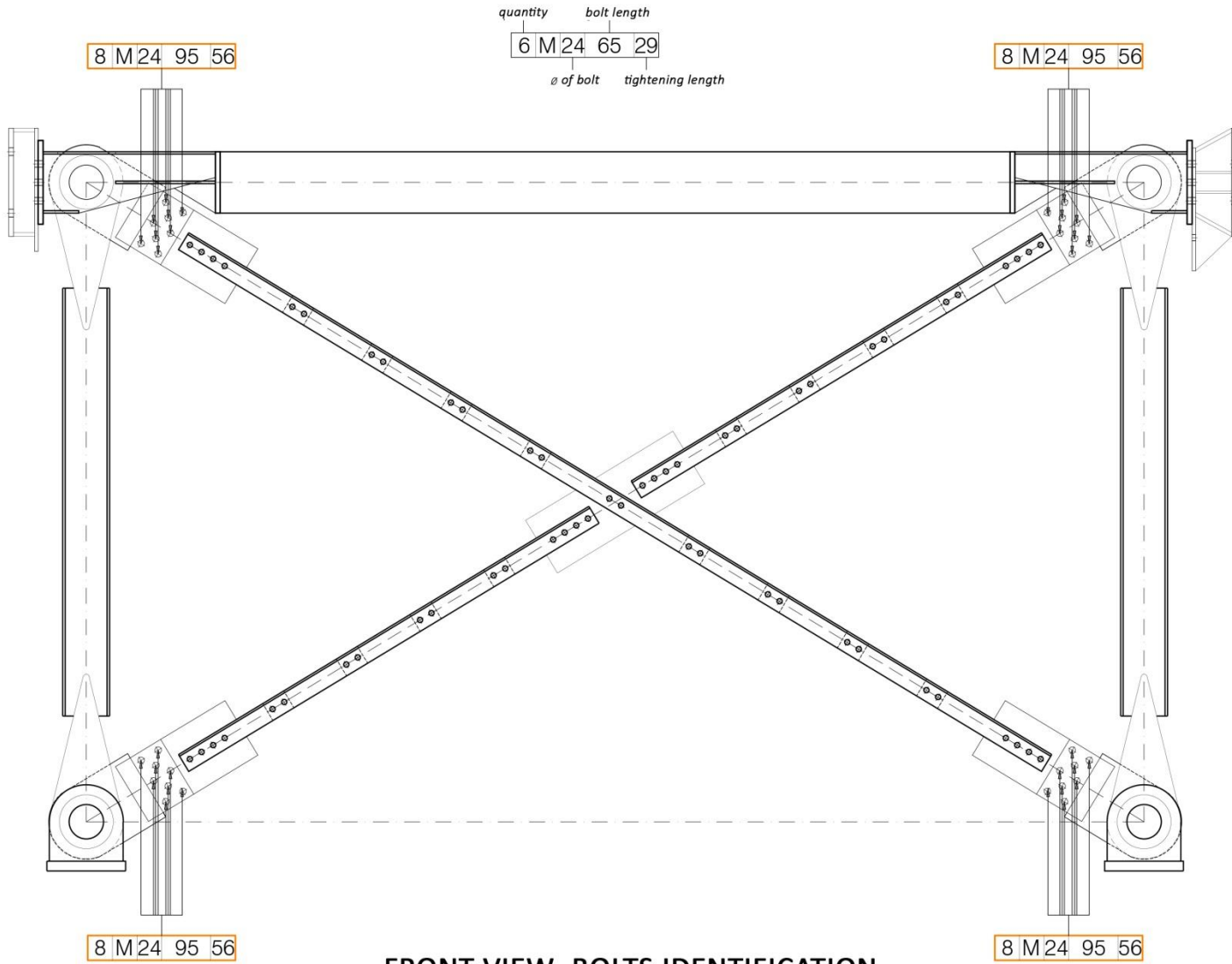
FRONT VIEW
SCALE 1:20





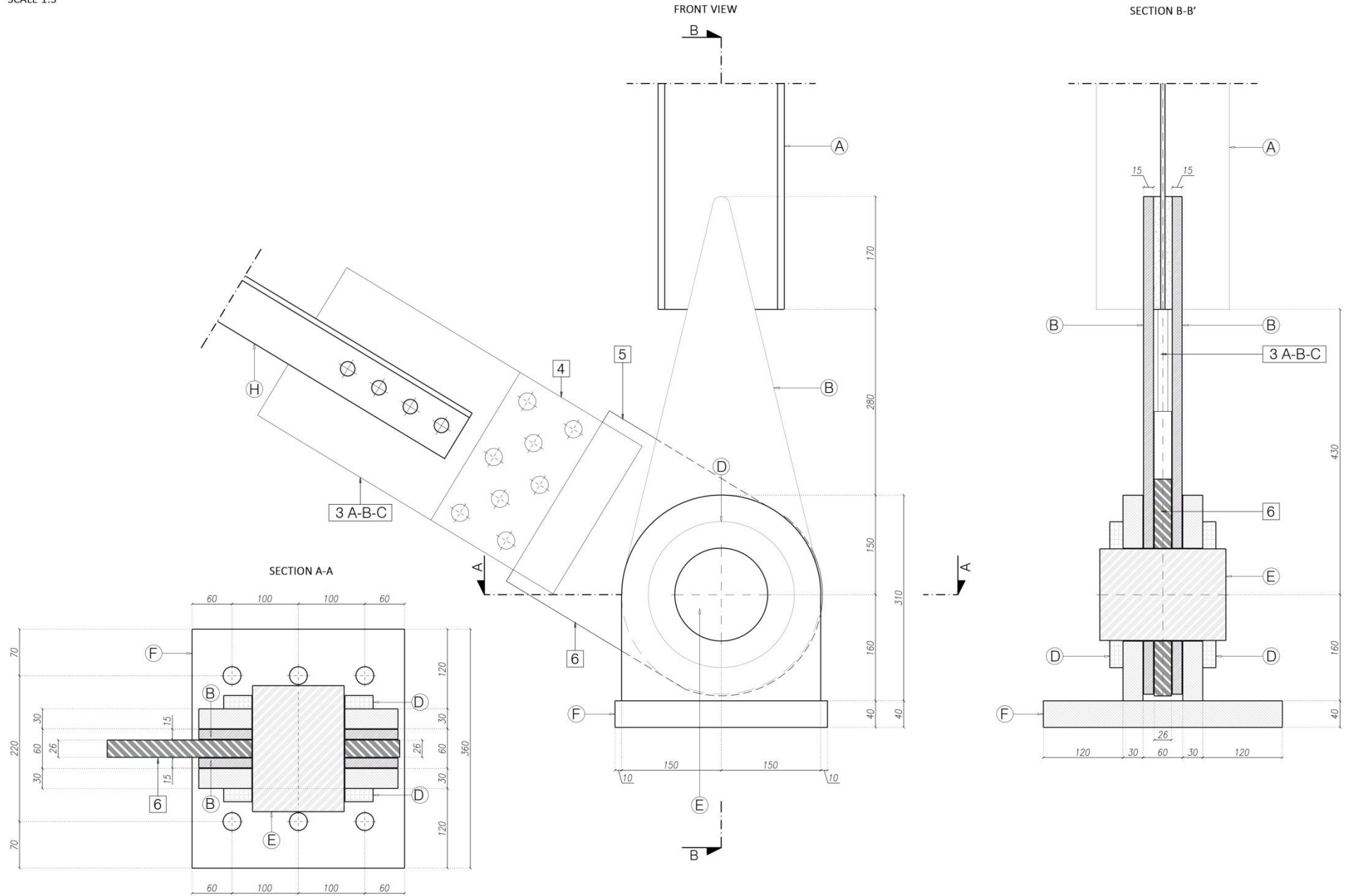
BACK VIEW- NUMBER OF PIECES

SCALE 1:20

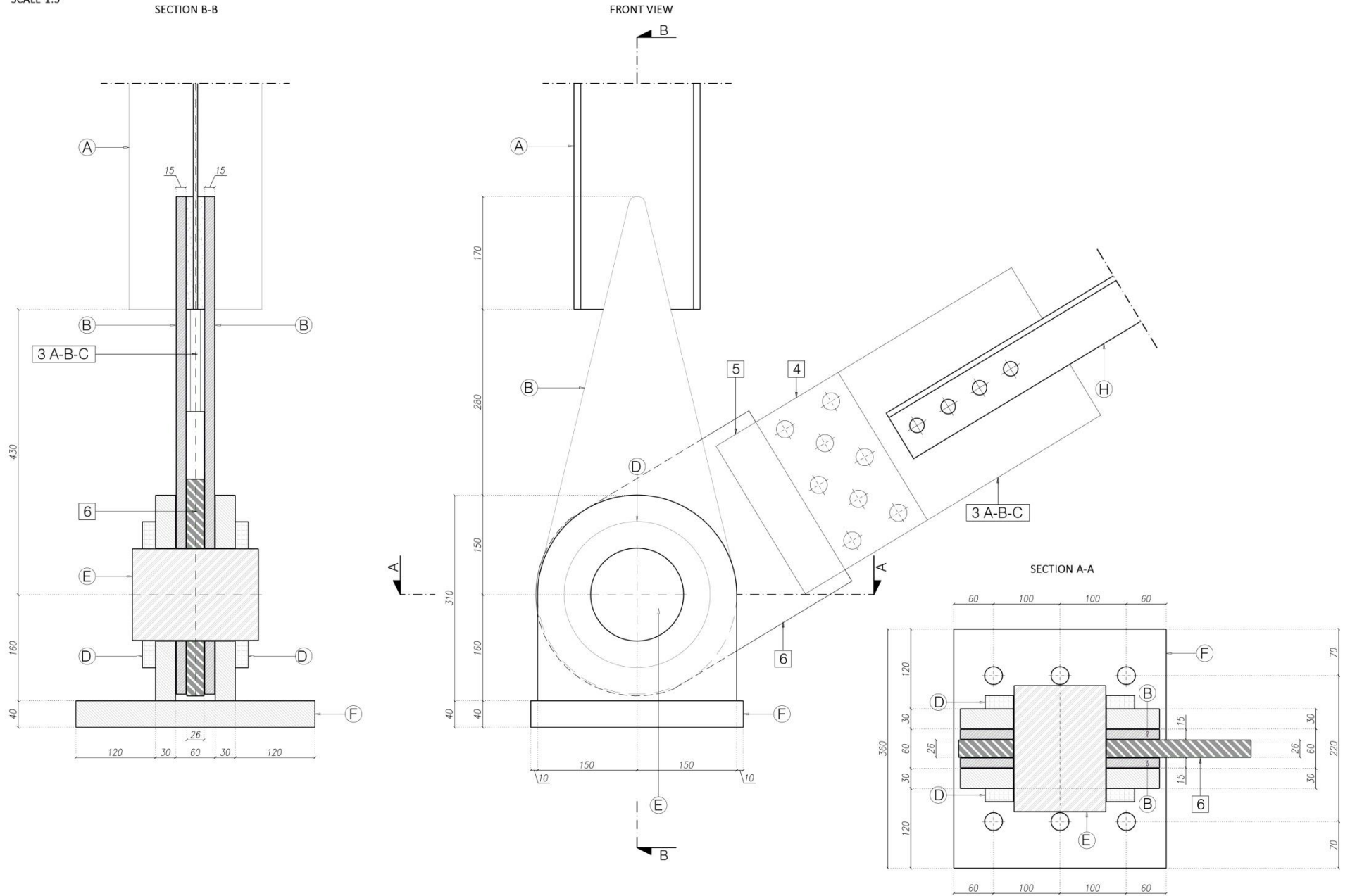


FRONT VIEW- BOLTS IDENTIFICATION
 SCALE 1:20

DET 1- RIGHT
SCALE 1:5



DET 1- LEFT
SCALE 1:5

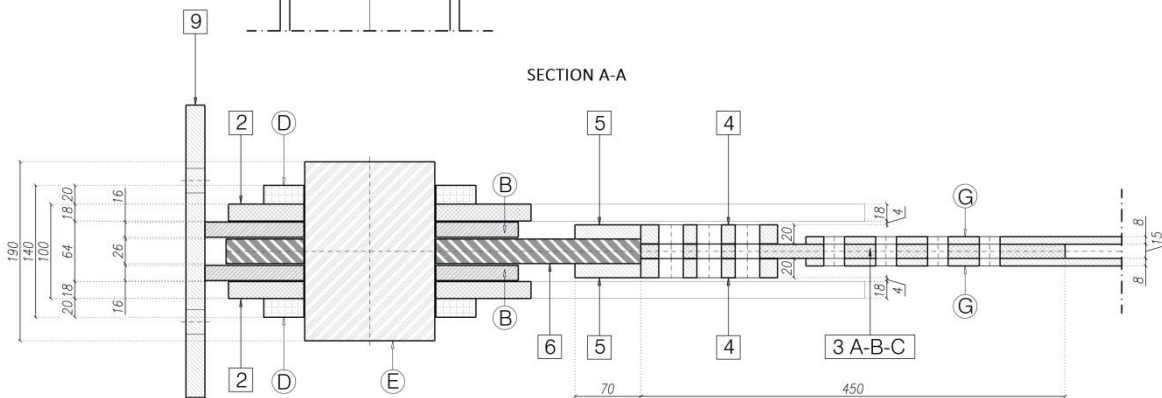
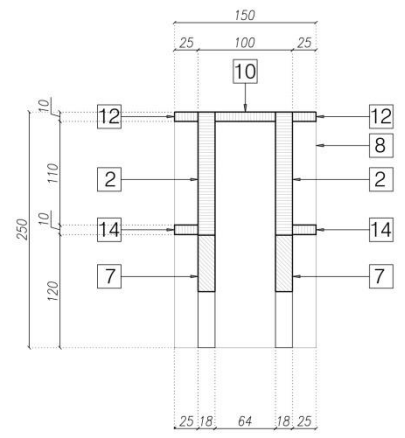
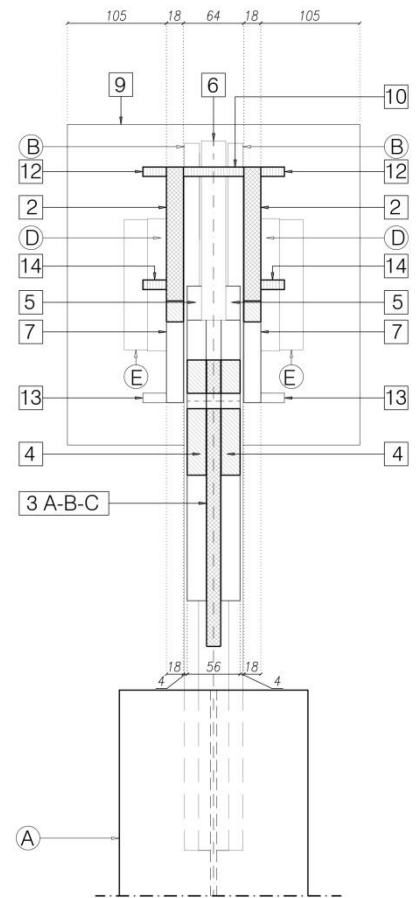
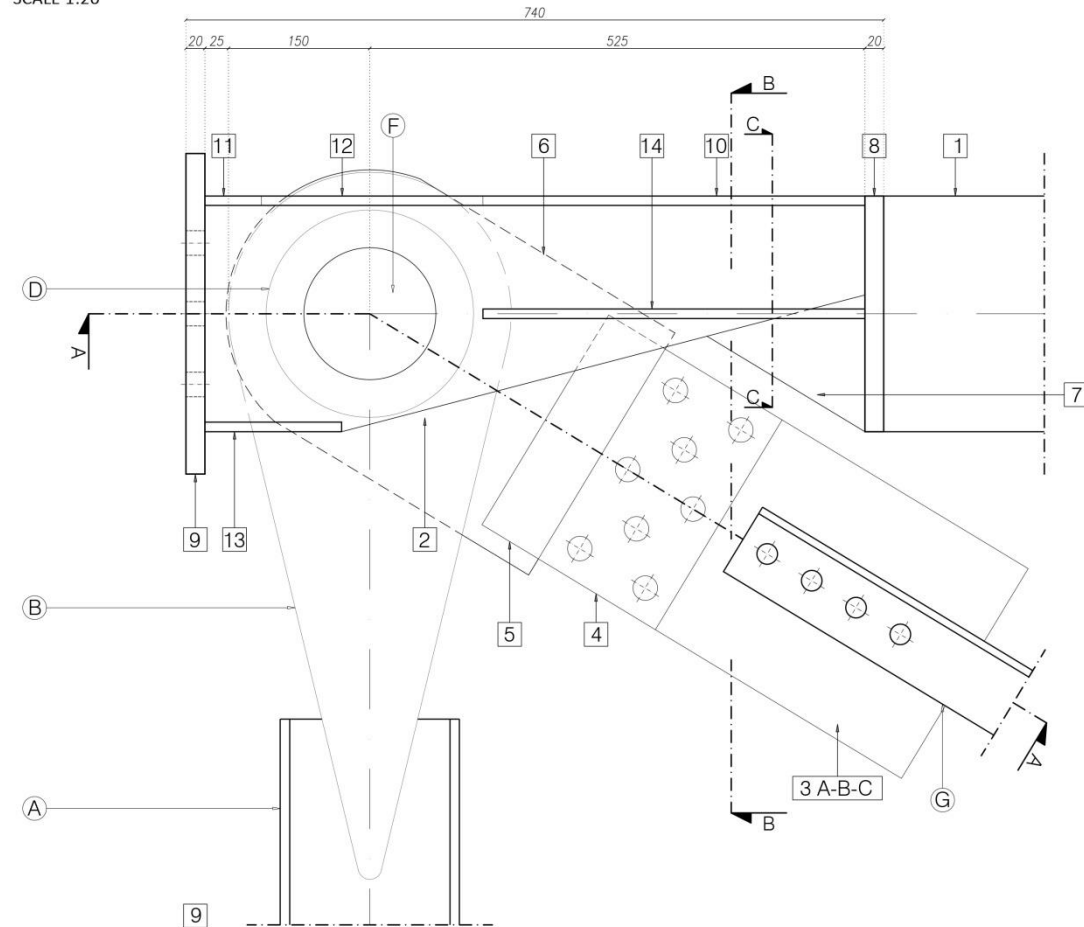


DET 2- LEFT
SCALE 1:20

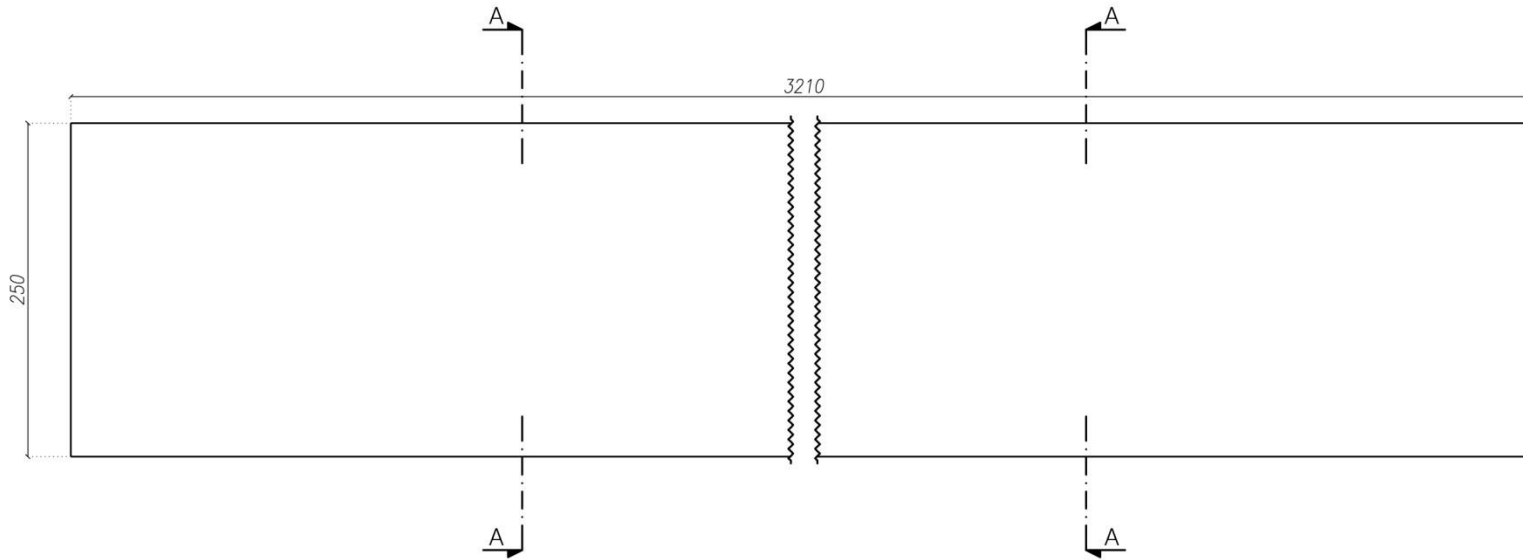
FRONT VIEW

SECTION B-B

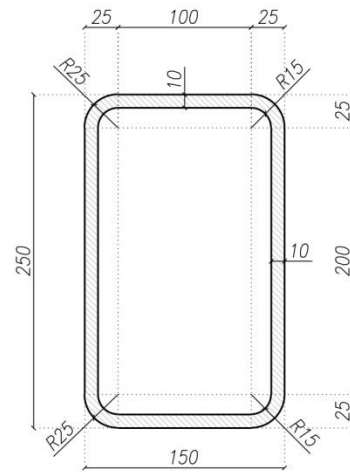
SECTION C-C



1 x HOLLOW PROFILE 150x250x8
HOT-ROLLED FORMED- LENGTH: 3210 mm
S355JR - 1:5

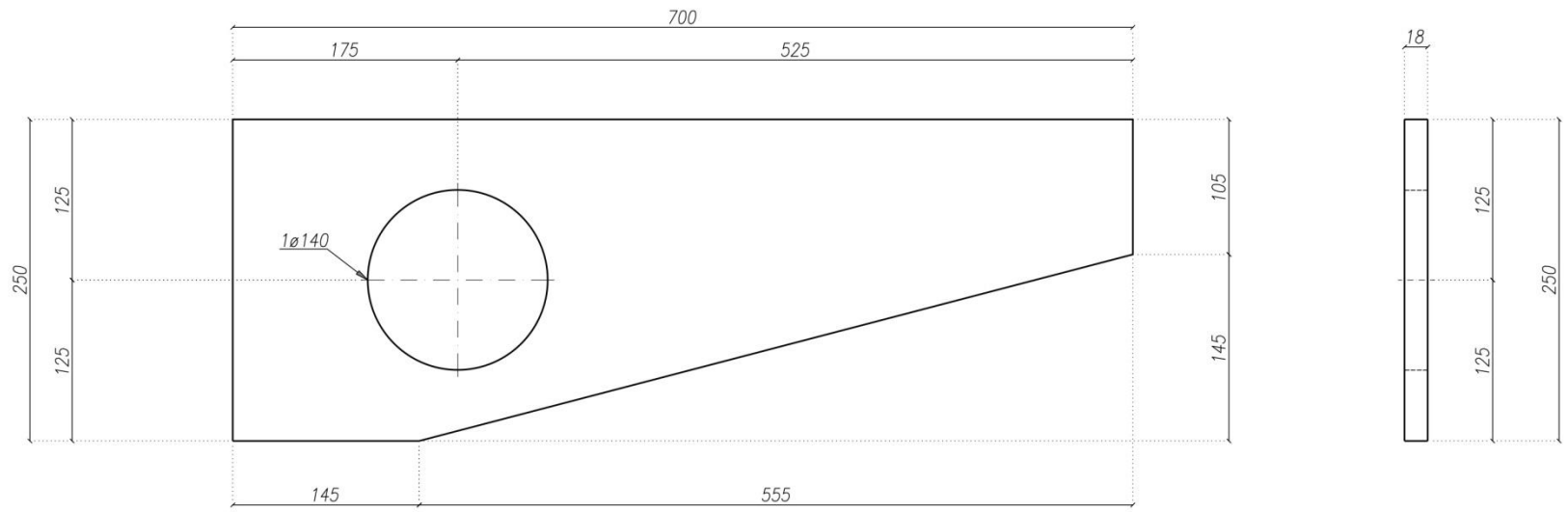


FRONT VIEW

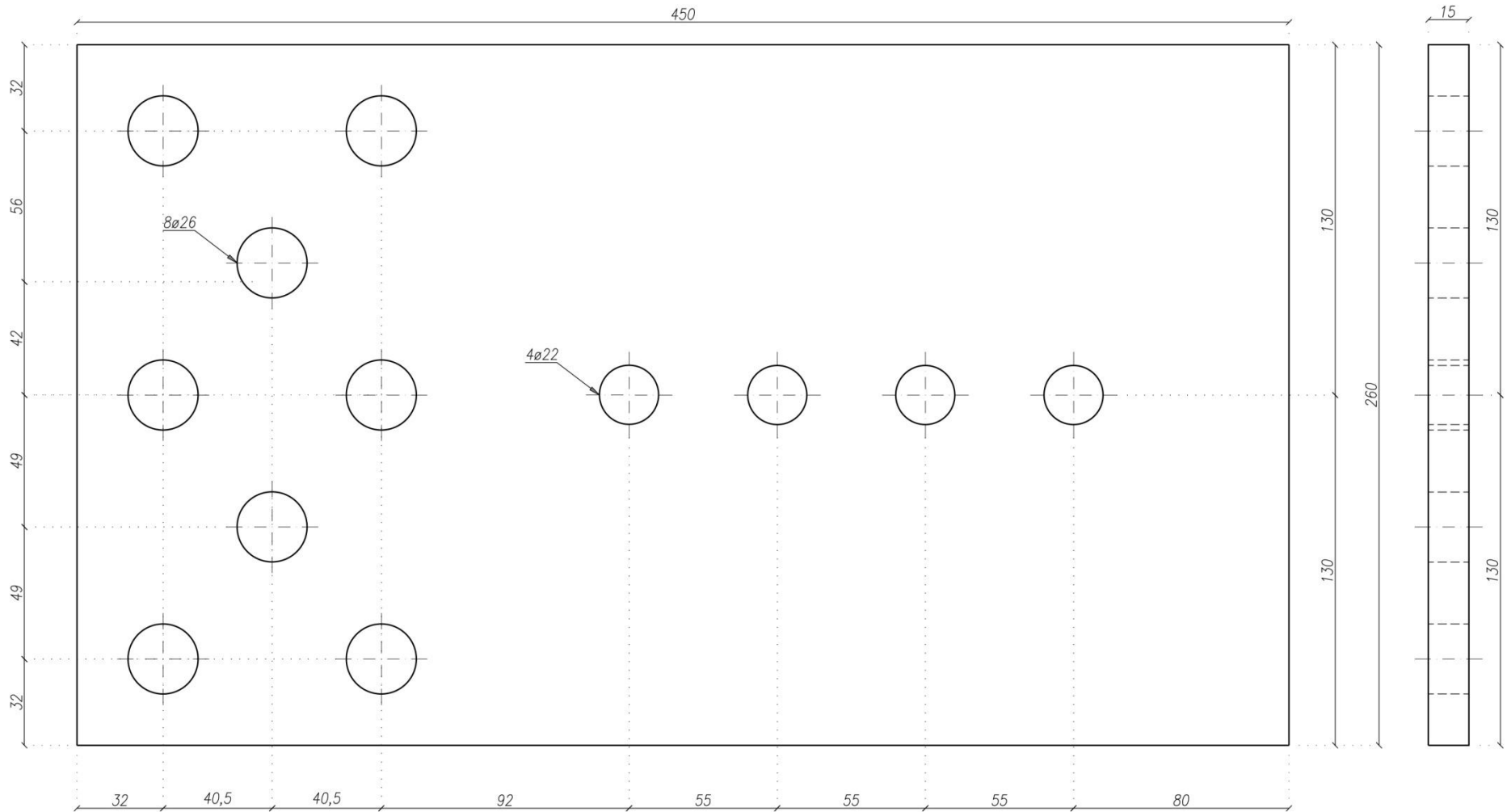


SECTION A-A

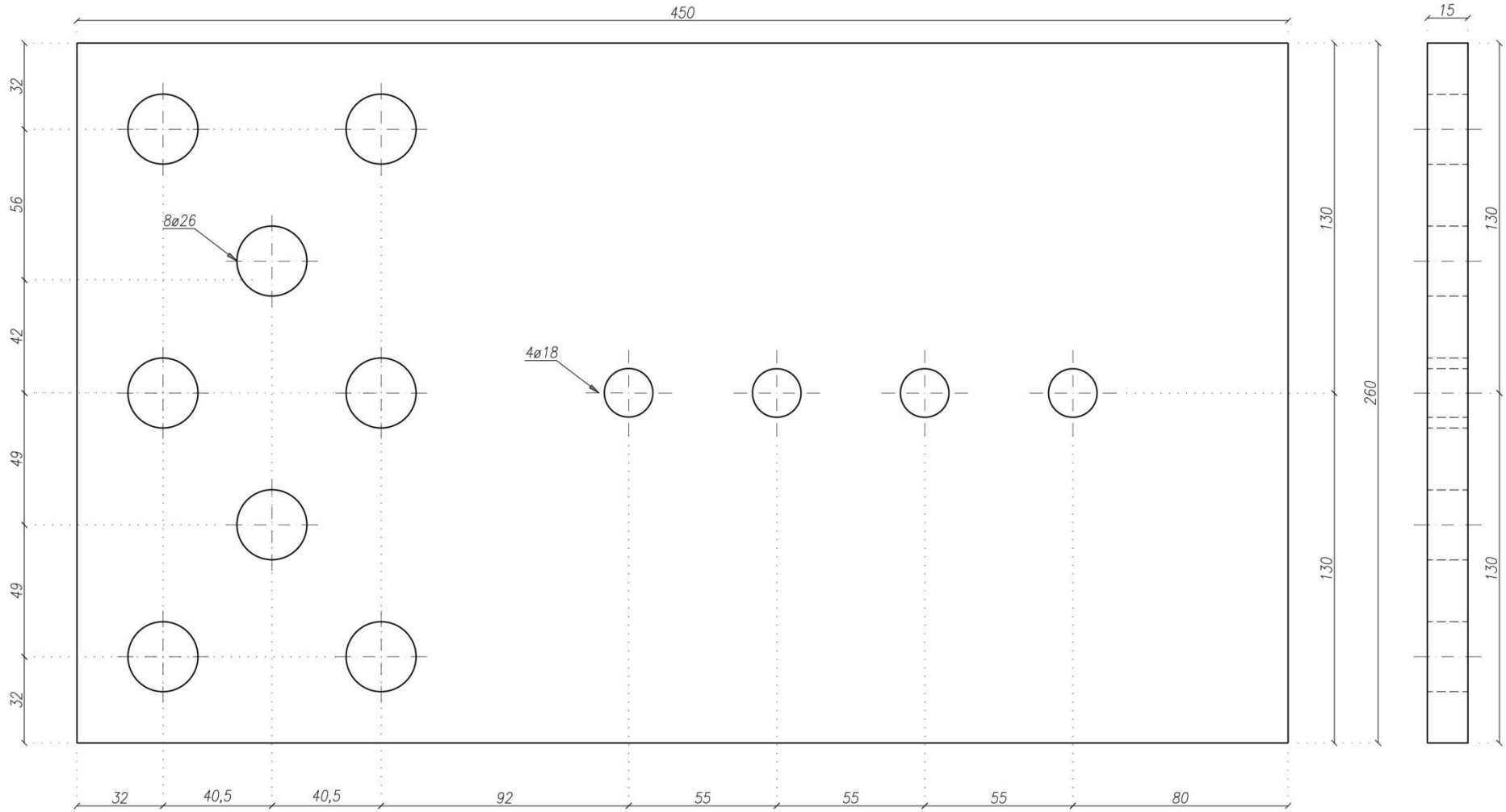
2 4x LAM 700x250x18
S355JR - 1:5



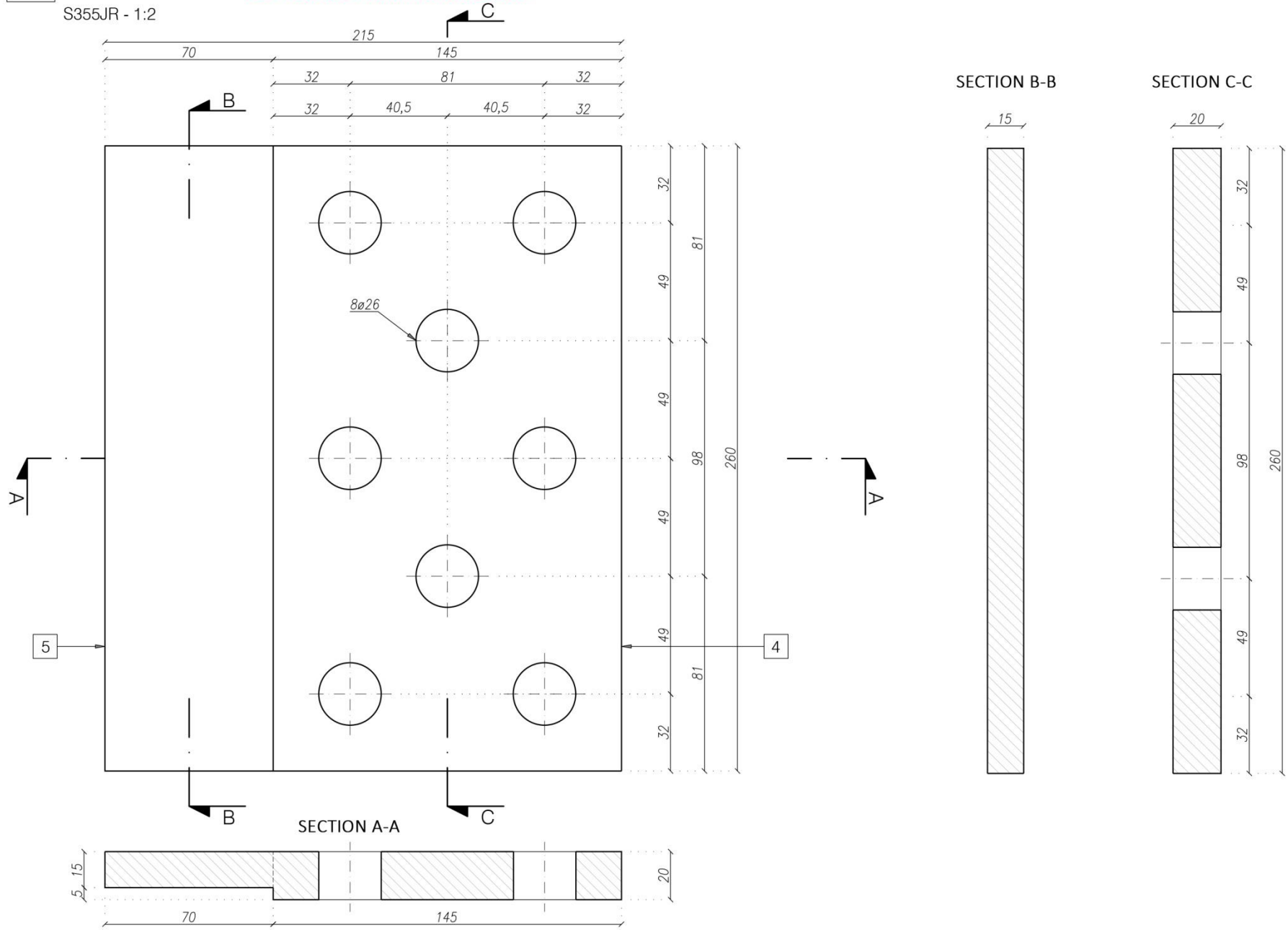
3 A B 24x LAM 450x260x15
S275JR - 1:2



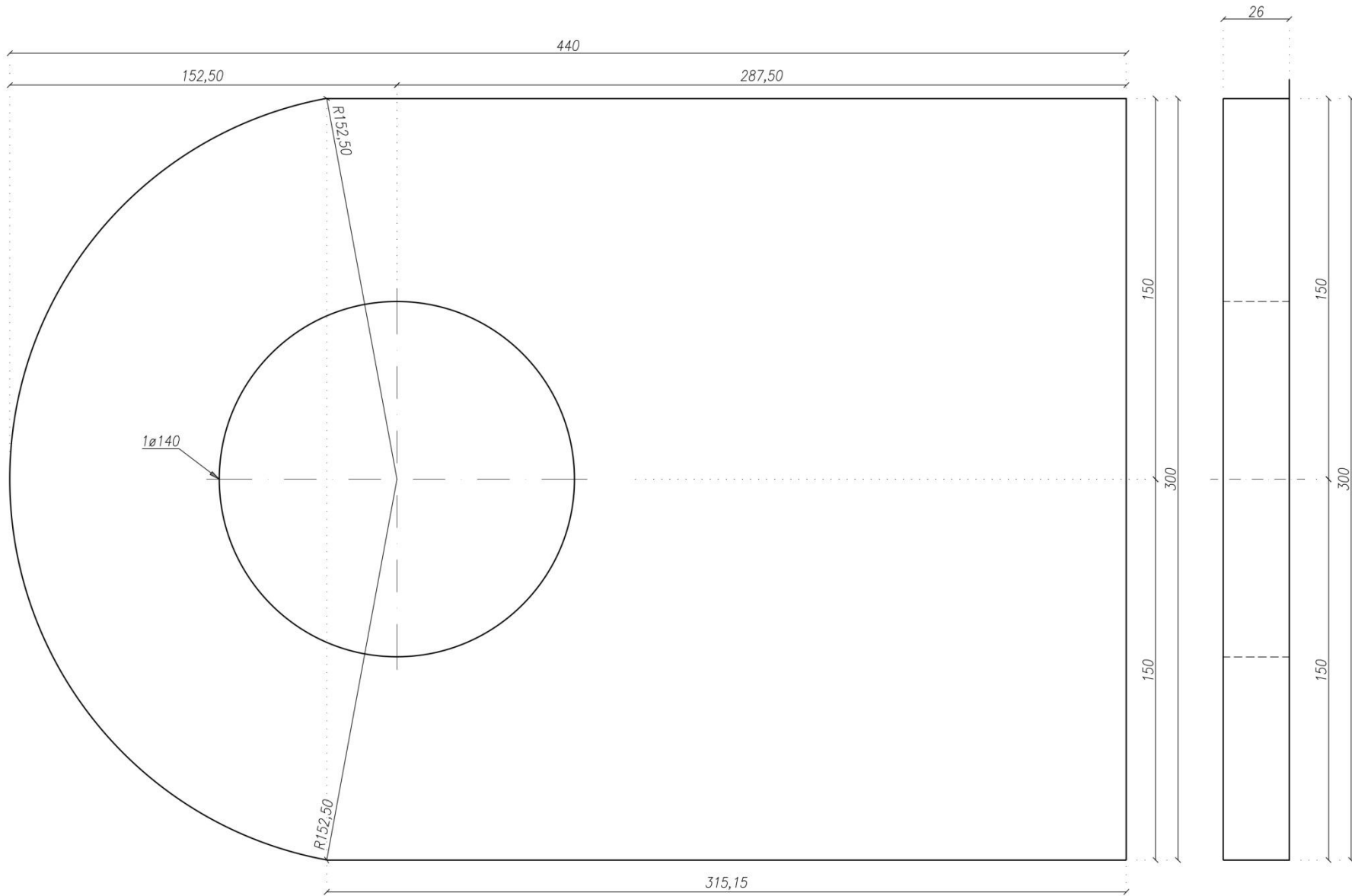
3 C 12x LAM 450x260x15
S275JR - 1:2



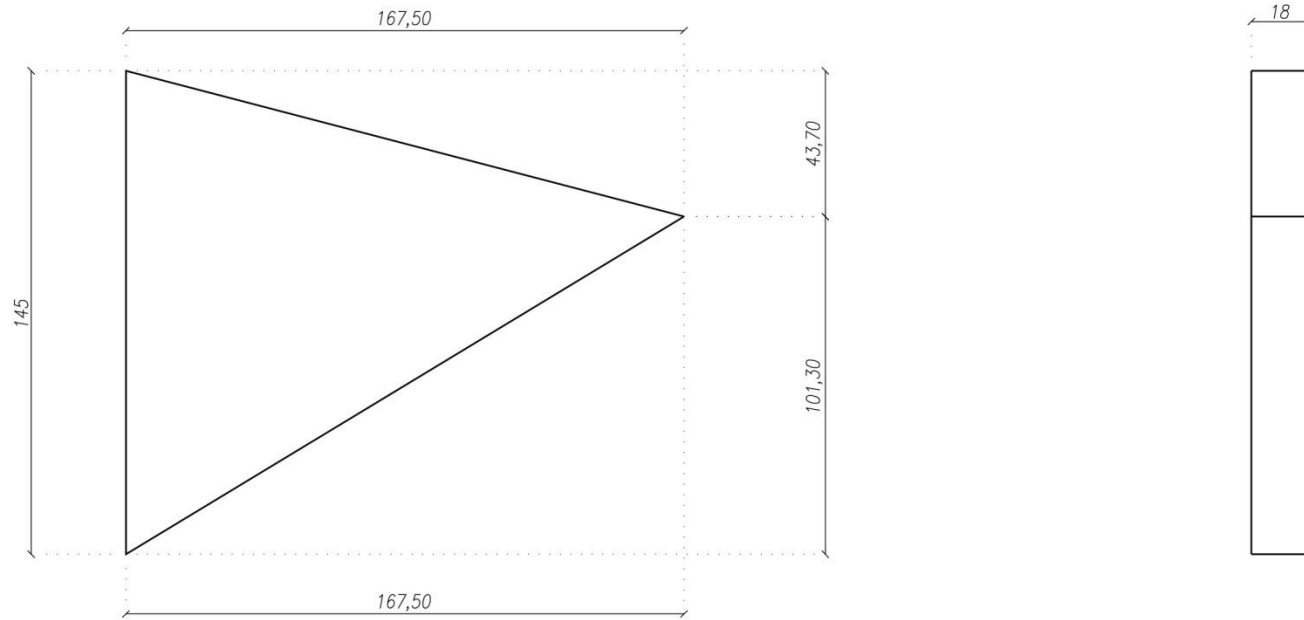
4+5 8x LAM 215x260x20/15 TO PRODUCE FROM A SINGLE PIECE
 S355JR - 1:2



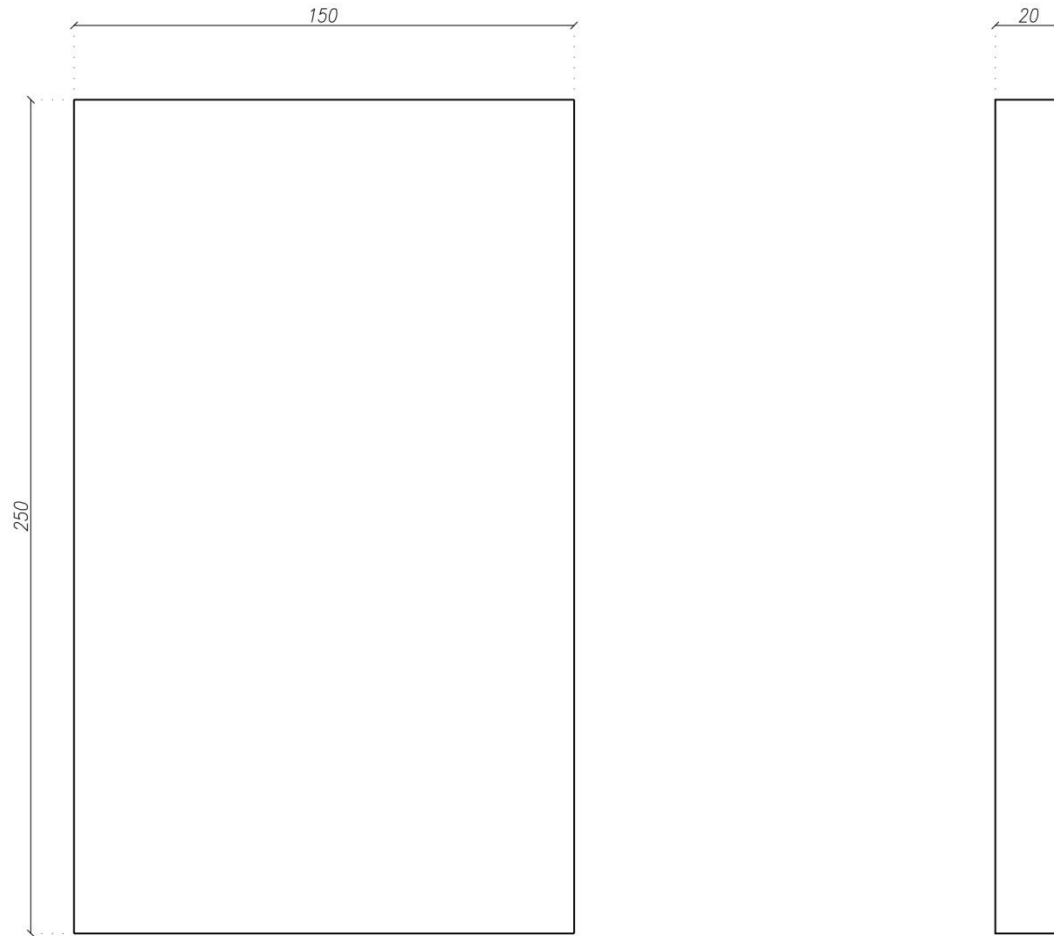
6 4x LAM 440x300x26
S355JR - 1:2



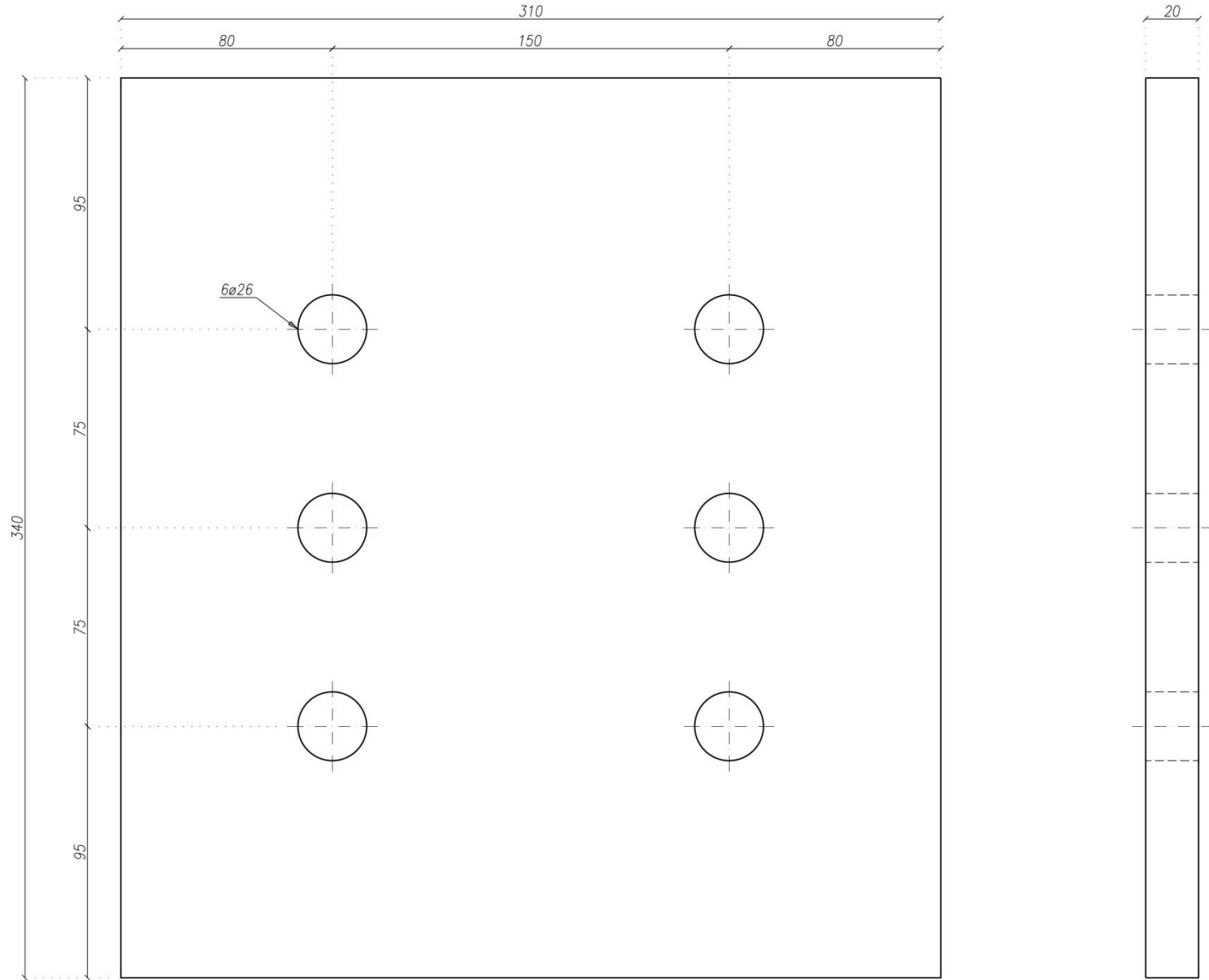
7 4x LAM 167.50x145x18
S355JR - 1:2



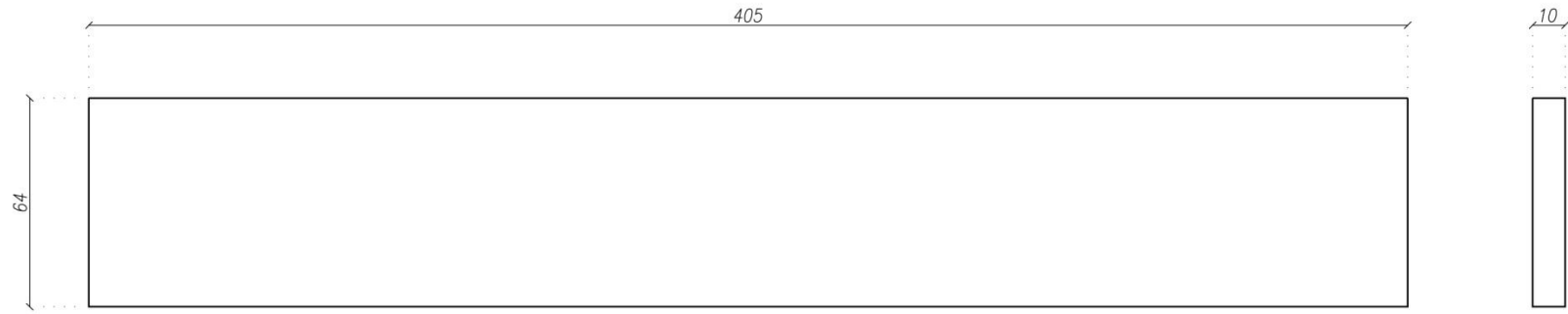
8 2x LAM 150x250x20
S355JR - 1:2



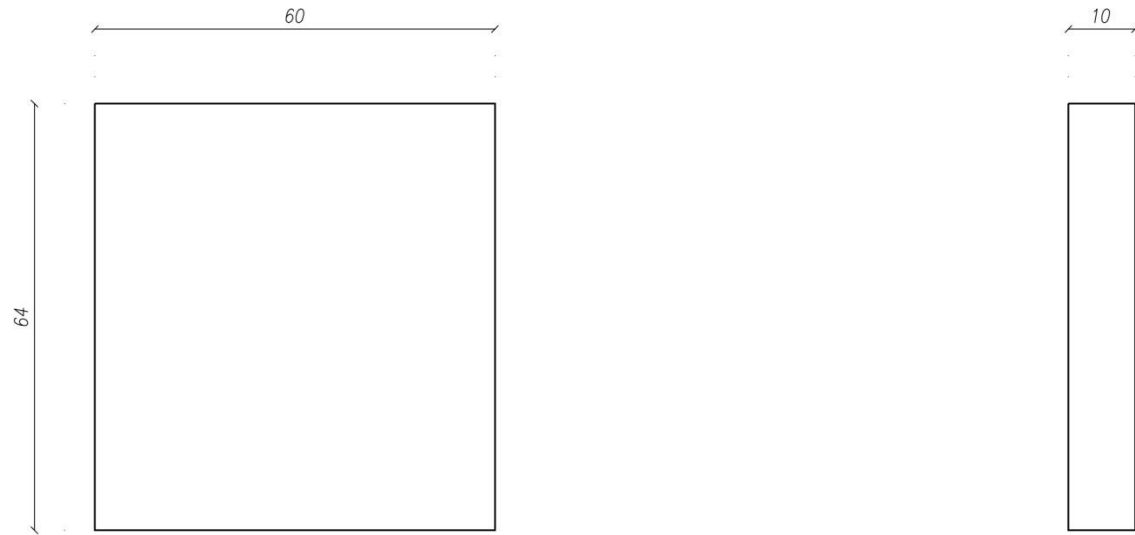
9 2x LAM 310x340x20
S355JR - 1:2



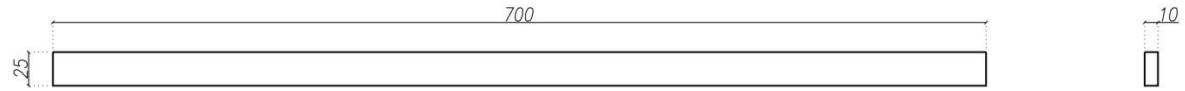
10 2x LAM 405x64x10
S355JR - 1:2



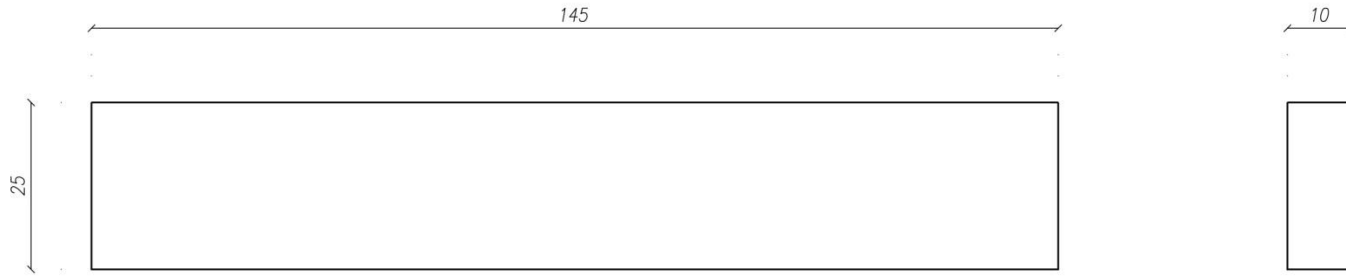
11 2x LAM 60x64x10
S355JR - 1:1



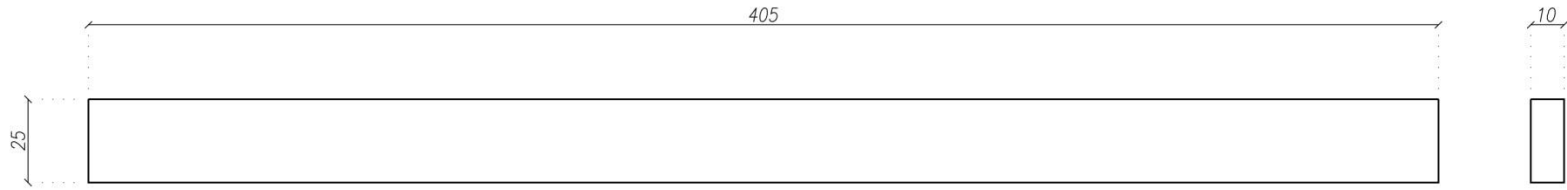
12 4x LAM 700x25x10
S355JR - 1:5



13 4x LAM 145x25x10
S355JR - 1:1

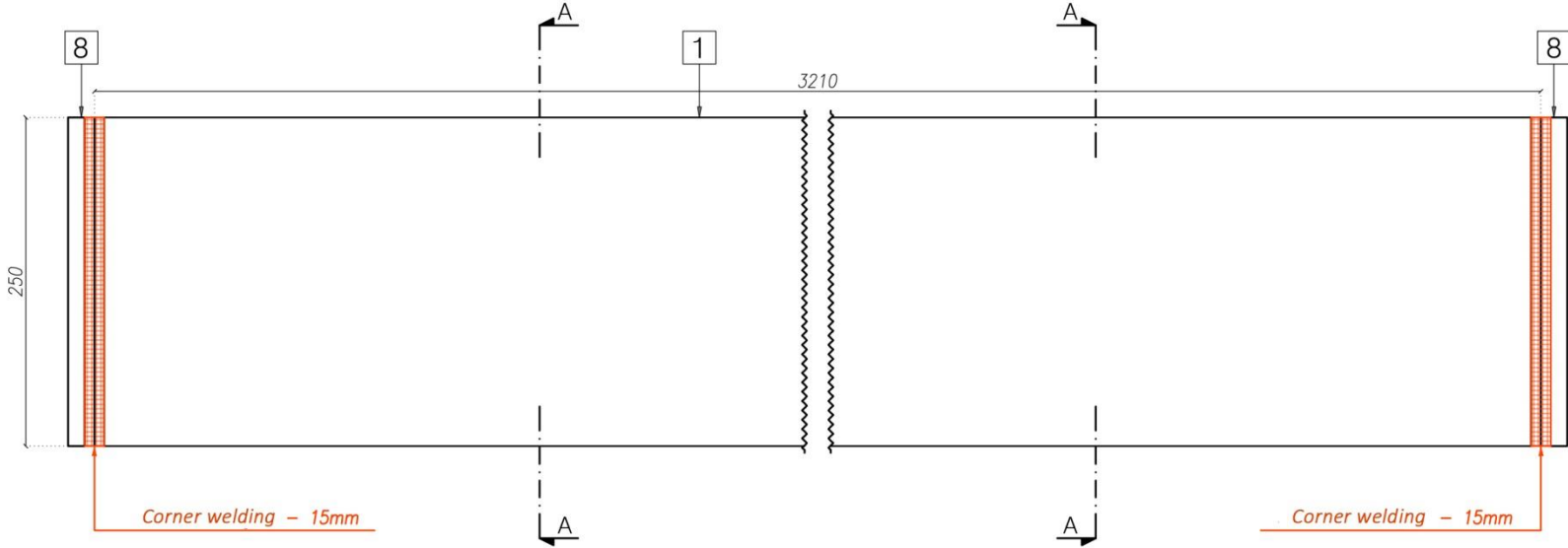


14 4x LAM 405x25x10
S355JR - 1:2

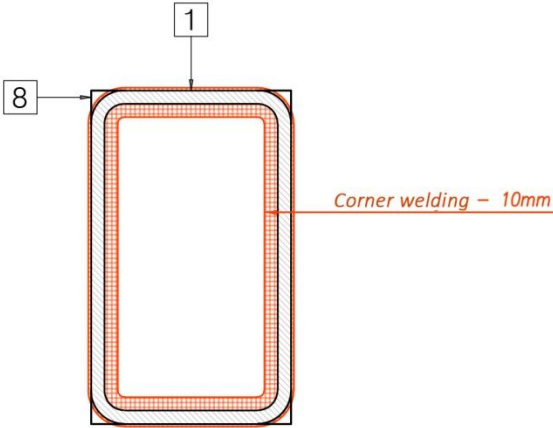


WELDING SCHEME - HOLLOW PROFILE

TO WELD 2x 8 ON ELEMENT 1

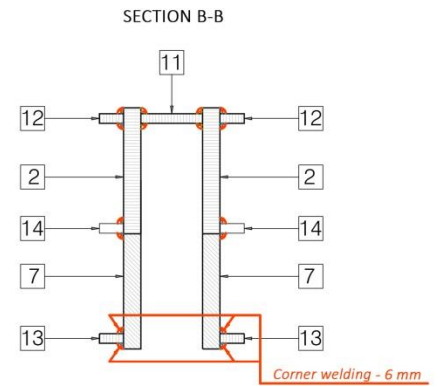
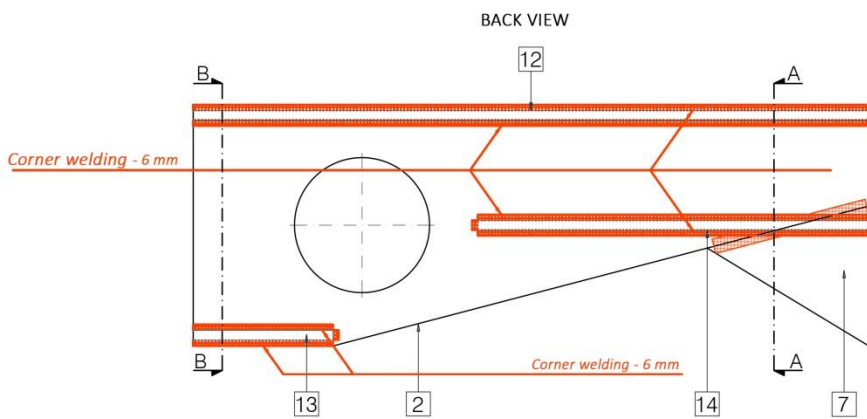
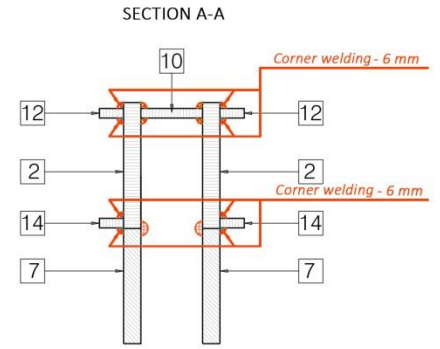
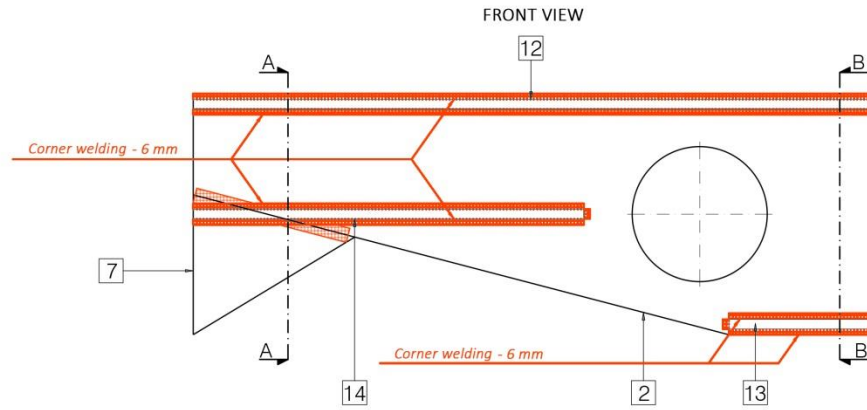


FRONT VIEW

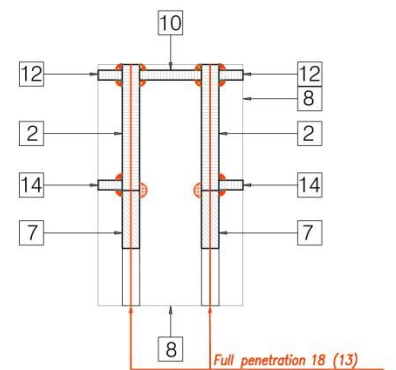
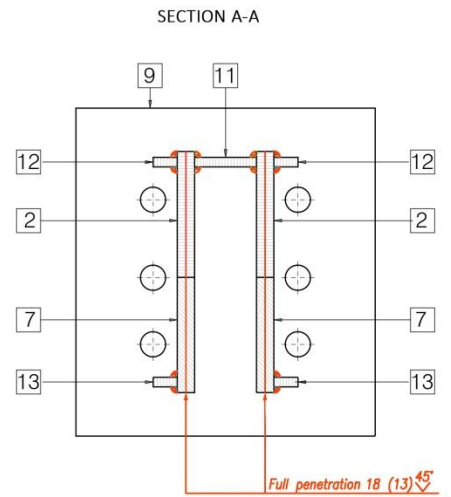
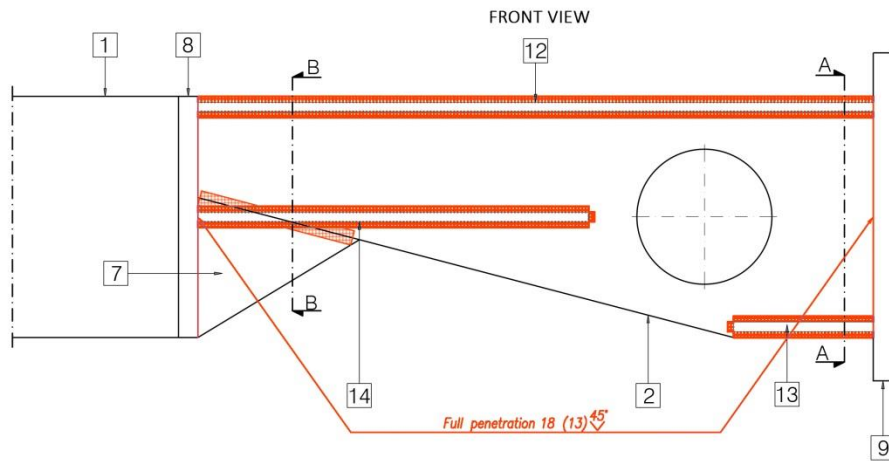


SECTION A-A

③ TO WELD 1x 12, 1x 13, 1x 14 ON ELEMENT 2+7 (REPEAT FOR OTHER ELEMENT 2+7)

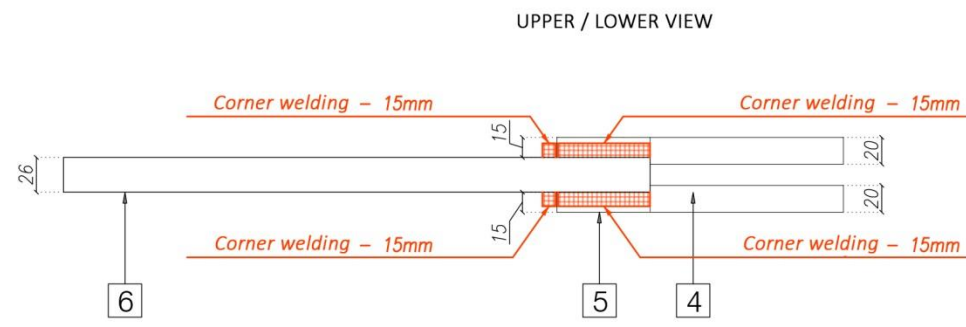
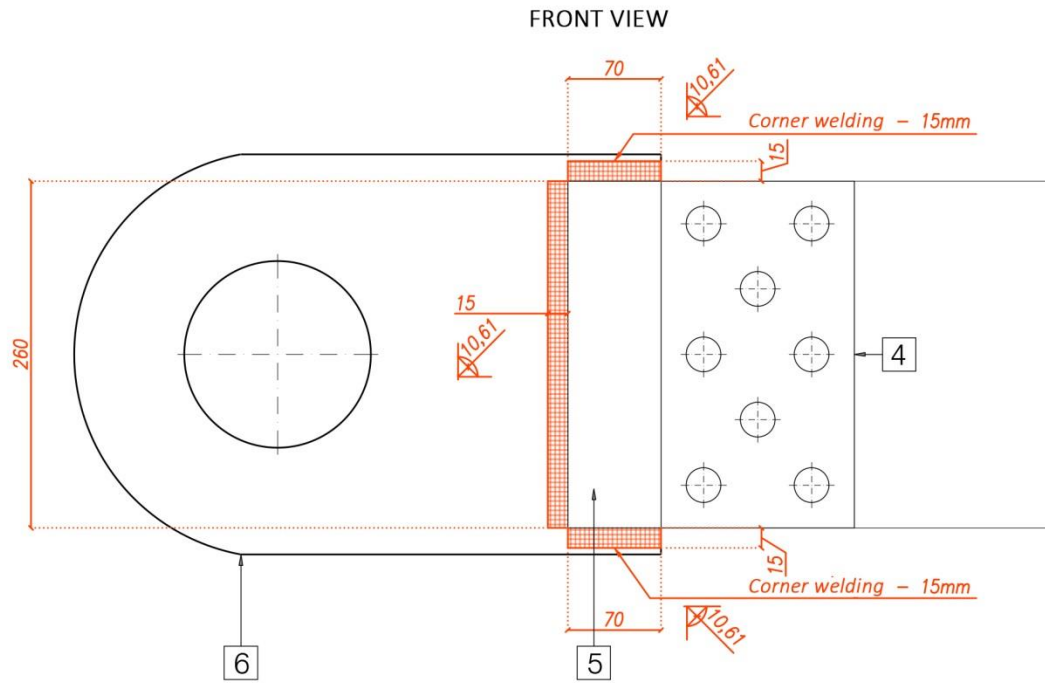


④ TO WELD 1x 9, 1x 1+2x8 ON ELEMENTS 2+7



WELDINGS SCHEME - BRACINGS PLATES

TO WELD 2x [4+5] ON ELEMENT [6] (TO REPEAT FOR EVERY ELEMENT 6)



APPENDIX C – BRACINGS BEARING CAPACITY

Bearing capacity brace-gusset plate connection

GEOMETRICAL CHARACTERISTICS OF BOLTED CONNECTION 70x7					
Parameter	L 60x60x8	L 70x70x7	L 80x80x8	Unit	Notes
d	16	20	20	mm	<i>bolts diameter</i>
d ₀	18	22	22	mm	<i>bolts holes diameter</i>
p ₁	55	55	55	mm	<i>bolts step</i>
e ₁	30	30	30	mm	<i>distance first bolt- profile edge, parallel to normal stress</i>
e ₂	25	30	40	mm	<i>distance first bolt- profile edge</i>
e	8	7	8	mm	<i>diagonal profile thickness</i>
t _{fazz.}	15	15	15	mm	<i>gusset thickness</i>
t _{min}	8	7	8	mm	<i>minimum thickness of connected elements</i>

DIMENSIONAL CHECK OF CONNECTION GEOMETRY 60X8 PROFILES				
$p_1 \geq 2.2 d_0$	55	\geq	39,60	verified
$p_1 \leq \min(14 t_{\min}, 200 \text{ mm})$	55	\leq	112,00	verified
$e_1 \geq 1.2 d_0$	30	\geq	21,60	verified
$e_1 \leq 40 \text{ mm} + 4 t_{\min}$	30	\leq	72,00	verified
$e_2 \geq 1.2 d_0$	25	\geq	21,60	verified
$e_2 \leq 40 \text{ mm} + 4 t_{\min}$	25	\leq	72,00	verified
TIGHTENING FORCE FOR EACH BOLT				
γ_{M7}	1		<i>safety coefficient</i>	
A_s	157	mm^2	<i>resistant area of bolt</i>	
f_{ub}	1000	N/mm^2	<i>bolt resistance</i>	
$F_{p,Cd}$	109,90	kN	<i>design pre-stress force</i>	
CONNECTION SLIP RESISTANCE (2 resistant sections per bolt)				
k_s	1		<i>normal clearance bolt-hole</i>	
μ	0,3		<i>frictional coefficient CLASS C</i>	
γ_{M3}	1,25		<i>safety coefficient</i>	
n	2		<i>resistant sections of bolt</i>	
n_b	4		<i>bolts number</i>	
$F_{s,Rd}$	52,752	kN	<i>design slip resistance of single bolt</i>	
$F_{s,Rd}$	211,008	kN	<i>connection slip resistance</i>	
DESIGN BEARING RESISTANCE OF THE UNION				
f_u	430	N/mm^2	<i>ultimate resistance gusset and profile</i>	
γ_{M2}	1,25		<i>safety coefficient</i>	
$\alpha_{b,bordo}$	0,56		<i>coefficients depending on bolts position (transfer load direction)</i>	
$\alpha_{b,interni}$	0,77			
k_1	2,19		<i>coefficients depending on bolts position (direction perpendicular to load transfer)</i>	
$F_{b,Rd,ext}$	53,55	kN	<i>bearing resistance of L-profile (edge bolt)</i>	
$F_{b,Rd,int}$	74,07	kN	<i>bearing resistance of L-profile (internal bolt)</i>	
$F_{b,Rd}$	551,51	kN	<i>connection bearing resistance of 2 L-profile coupled together</i>	
CONNECTION PROFILE RESISTANCE AT HOLE SECTION				
A_{L70x7}	903	mm^2	<i>gross-section area single profile</i>	
$A_{net,L70x7}$	758,5	mm^2	<i>net-section area at profile joint</i>	
$N_{u,Rd}$	234,83	kN	<i>design ultimate resistance of net-section</i>	
$F_{d,u,Rd}$	469,66	kN	<i>design resistance of connection profiles at hole section</i>	

DIMENSIONAL CHECK OF CONNECTION GEOMETRY 70X7 PROFILES				
$p_1 \geq 2.2 d_0$	55	\geq	48,40	verified
$p_1 \leq \min(14 t_{\min}; 200 \text{ mm})$	55	\leq	98,00	verified
$e_1 \geq 1.2 d_0$	30	\geq	26,40	verified
$e_1 \leq 40 \text{ mm} + 4 t_{\min}$	30	\leq	68,00	verified
$e_2 \geq 1.2 d_0$	30	\geq	26,40	verified
$e_2 \leq 40 \text{ mm} + 4 t_{\min}$	30	\leq	68,00	verified
TIGHTENING FORCE FOR EACH BOLT				
γ_{M7}	1		<i>safety coefficient</i>	
A_s	245	mm^2	<i>resistant area of bolt</i>	
f_{ub}	1000	N/mm^2	<i>bolt resistance</i>	
$F_{p,Cd}$	171,50	kN	<i>desing pre-stress force</i>	
CONNECTION SLIP RESISTANCE (2 resistant sections per bolt)				
k_s	1		<i>normal clearance bolt-hole</i>	
μ	0,3		<i>frictional coefficient CLASS C</i>	
γ_{M3}	1,25		<i>safety coefficient</i>	
n	2		<i>resistant sections of bolt</i>	
n_b	4		<i>bolts number</i>	
$F_{s,Rd}$	82,32	kN	<i>design slip resistance of single bolt</i>	
$F_{s,Rd}$	329,28	kN	<i>connection slip resistance</i>	
DESIGN BEARING RESISTANCE OF THE UNION				
f_u	430	N/mm^2	<i>ultimate resistance gusset and profile</i>	
γ_{M2}	1,25		<i>safety coefficient</i>	
$\alpha_{b,bordo}$	0,45		<i>coefficients depending on bolts position (transfer load direction)</i>	
$\alpha_{b,interni}$	0,58			
k_1	2,12		<i>coefficients depending on bolts position (direction perpendicular to load transfer)</i>	
$F_{b,Rd,ext}$	46,37	kN	<i>bearing resistance of L-profile (edge bolt)</i>	
$F_{b,Rd,int}$	59,51	kN	<i>bearing resistance of L-profile (internal bolt)</i>	
$F_{b,Rd}$	449,78	kN	<i>connection bearing resistance of 2 L-profile coupled together</i>	
CONNECTION PROFILE RESISTANCE AT HOLE SECTION				
A_{L70x7}	940	mm^2	<i>gross-section area single profile</i>	
$A_{net,L70x7}$	786	mm^2	<i>net-section area at profile joint</i>	
$N_{u,Rd}$	243,35	kN	<i>design ultimate resistance of net-section</i>	
$F_{d,u,Rd}$	486,69	kN	<i>design resistance of connection profiles at hole section</i>	

DIMENSIONAL CHECK OF CONNECTION GEOMETRY 80X8 PROFILES				
$p_1 \geq 2.2 d_0$	55	\geq	48,40	verified
$p_1 \leq \min(14 t_{\min}, 200 \text{ mm})$	55	\leq	112,00	verified
$e_1 \geq 1.2 d_0$	30	\geq	26,40	verified
$e_1 \leq 40 \text{ mm} + 4 t_{\min}$	30	\leq	72,00	verified
$e_2 \geq 1.2 d_0$	40	\geq	26,40	verified
$e_2 \leq 40 \text{ mm} + 4 t_{\min}$	40	\leq	72,00	verified
TIGHTENING FORCE FOR EACH BOLT				
γ_{M7}	1		<i>safety coefficient</i>	
A_s	245	mm^2	<i>resistant area of bolt</i>	
f_{ub}	1000	N/mm^2	<i>bolt resistance</i>	
$F_{p,Cd}$	171,50	kN	<i>desing pre-stress force</i>	
CONNECTION SLIP RESISTANCE (2 resistant sections per bolt)				
k_s	1		<i>normal clearance bolt-hole</i>	
μ	0,3		<i>frictional coefficient CLASS C</i>	
γ_{M3}	1,25		<i>safety coefficient</i>	
n	2		<i>resistant sections of bolt</i>	
n_b	4		<i>bolts number</i>	
$F_{s,Rd}$	82,32	kN	<i>design slip resistance of single bolt</i>	
$F_{s,Rd}$	329,28	kN	<i>connection slip resistance</i>	
DESIGN BEARING RESISTANCE OF THE UNION				
f_u	430	N/mm^2	<i>ultimate resistance gusset and profile</i>	
γ_{M2}	1,25		<i>safey coefficient</i>	
$\alpha_{b,bordo}$	0,45		<i>coefficients depending on bolts position (transfer load direction)</i>	
$\alpha_{b,interni}$	0,58			
k_1	2,50		<i>coefficients depending on bolts position (direction perpendicular to load transfer)</i>	
$F_{b,Rd,ext}$	62,55	kN	<i>bearing resistance of L-profile (edge bolt)</i>	
$F_{b,Rd,int}$	80,27	kN	<i>bearing resistance of L-profile (internal bolt)</i>	
$F_{b,Rd}$	606,69	kN	<i>connection bearing resistance of 2 L-profile coupled together</i>	
CONNECTION PROFILE RESISTANCE AT HOLE SECTION				
$A_{L70 \times 7}$	1225	mm^2	<i>gross-section area single profile</i>	
$A_{net,L70 \times 7}$	1049	mm^2	<i>net-section area at profile joint</i>	
$N_{u,Rd}$	324,77	kN	<i>design ultimate resistance of net-section</i>	
$F_{d,u,Rd}$	649,54	kN	<i>design resistance of connection profiles at hole section</i>	

Compression and tension brace resistance

Compression profile classification

COMPRESSION PROFILES CLASSIFICATION					
Parameter	L 60x60x8	L 70x70x7	L 80x80x8	Unit	Check
ϵ	0,92			-	
b	60	70	80	mm	
h	60	70	80	mm	
t	8	7	8	mm	
h/t	7,5	10	10	\leq	15 ϵ
$(b+h)/2t$	7,5	10	10	\leq	11,5 ϵ
PROFILES CLASS 3					

Tension diagonal strength

DIAGONALS TENSION RESISTANCE					
steel type	S275JR			Notes	Unit
profile type	L 60x60x8	L 70x70x7	L 80x80x8		
f_y	275	275	275	<i>steel yielding stress</i>	N/mm ²
f_u	430	430	430	<i>steel ultimate stress</i>	N/mm ²
E	210000	210000	210000	<i>steel Young modulus</i>	MPa
A_{L70x7}	902,5	940	1225	<i>gross-section area single profile</i>	mm ²
A_{2L70x7}	1805	1880	2450	<i>gross-section area coupled profiles</i>	mm ²
e	8	7	8	<i>profile thickness</i>	mm
d_0	18	22	22	<i>holes diameter</i>	mm
$A_{net,L70x7}$	758,5	786	1049	<i>single profile net-section area in correspondence of the bolt</i>	mm ²
$A_{net,L70x7}$	1517	1572	2098	<i>coupled profiles net-section area in correspondence of the bolt</i>	mm ²
p_1	55	55	55	<i>bolts step</i>	mm
β_3	0,50			<i>reduction coefficient that takes into account that connection affects only a flange of a profile</i>	-
γ_{M0}	1,00			<i>safety coefficient</i>	-
γ_{M2}	1,25				-
$N_{pl,Rd}$	496,38	517,00	673,75	<i>design plastic resistance of gross-section</i>	kN
$N_{u,Rd}$	260,92	270,38	360,856	<i>design ultimate resistance of gross-section</i>	kN

Buckling and strength of compression diagonal

1) RESISTANCE					
Parameter	L60x8	L70x7	L80x8	Unit	Notes
$N_{c,Rd}$	496,38	517,00	673,75	kN	<i>design compression resistance</i>
2) STABILITY					
L_{CON}	410			cm	<i>geometrical length of continuous diagonal (CON)</i>
L_{DIS}	195			cm	<i>geometrical length of discontinuous diagonal (DIS 1 and DIS 2)</i>
β	1			-	<i>effective length coefficient (pinned rod)</i>
2a) BOTH ACTIVE DIAGONALS					
A	1805	1880	2450	mm ²	<i>entire section area</i>
α	0,49			-	<i>imperfection coefficient (instability curve c)</i>
f_y	275			N/mm ²	<i>steel yielding stress</i>
γ_{M1}	1,05			-	<i>safety coefficient</i>
<u>respect to x-axis</u>					
J_x	58,40	84,60	144,4	cm ⁴	<i>moment of inertia with respect to x-axis</i>
$L_{0,x}$	205,00			cm	<i>free-length of inflexion in x-direction</i>
$N_{cr,x}$	288,02	417,24	712,16	kN	<i>bifurcation load in x-direction</i>
$\lambda_{rel,x}$	1,31	1,11	0,97	-	<i>relative slenderness</i>
ϕ_x	1,63	1,34	1,16	-	<i>χ-formula coefficient</i>
χ_x	0,38	0,48	0,56	-	<i>reduction coefficient for permanent instability mode</i>
$N_{b,Rd,x}$	188,81	235,01	356,74	kN	<i>bearing capacity</i>
<u>respect to y-axis</u>					
J_y	172,86	223,77	366,05	cm ⁴	<i>moment of inertia with respect to y-axis</i>
$L_{0,y}$	205			cm	<i>free-length of inflexion in y-direction</i>
$N_{cr,y}$	852,52	1103,60	1805,31	kN	<i>bifurcation load in y-direction</i>
$\lambda_{rel,y}$	0,76	0,68	0,10	-	<i>relative slenderness</i>
ϕ_y	0,93	0,85	0,79	-	<i>χ-formula coefficient</i>
χ_y	0,69	0,73	0,78	-	<i>reduction coefficient for permanent instability mode</i>
$N_{b,Rd,y}$	337,46	361,55	499,80	kN	<i>bearing capacity</i>

2b) ONLY TENSION DIAGONAL					
Parameter	L 60x8	L 70x7	L 80x8	Unit	Notes
A	1805	1880	2450	mm ²	gross-section area
α	0,490			-	imperfection coefficient (instability curve c)
f_y	275			N/mm ²	steel yielding stress
γ_{M1}	1,05			-	safety coefficient
respect to x-axis					
J_x	58,40	84,60	144,40	cm ⁴	moment of inertia with respect to x-axis
$L_{0,x}$	410,00			cm	free-length of inflexion in x-direction
$N_{cr,x}$	72,01	104,31	178,04	kN	bifurcation load in x-direction
λ_x	2,626	2,226	1,945	-	relative slenderness
ϕ_x	4,541	3,475	2,820	-	χ -formula coefficient
χ_x	0,121	0,163	0,206	-	reduction coefficient for permanent instability mode
$N_{b,Rd,x}$	57,33	80,16	132,00	kN	bearing capacity
respect to y-axis					
J_y	172,86	223,77	366,05	cm ⁴	moment of inertia with respect to y-axis
$L_{0,y}$	410,00			cm	free-length of inflexion in y-direction
$N_{cr,y}$	213,13	275,90	451,33	kN	bifurcation load in y-direction
λ_y	1,526	1,369	1,222	-	relative slenderness
ϕ_y	1,989	1,723	1,497	-	χ -formula coefficient
χ_y	0,306	0,361	0,423	-	reduction coefficient for permanent instability mode
$N_{b,Rd,y}$	144,76	177,74	271,74	kN	bearing capacity

Block tearing

BLOCK TEARING								
	2L70x7		2L60x8		2L80x8		Notes	Unit
	Standard s	Real	Standard s	Real	Standard s	Real		
A_{nt}	245	245	157	157	245	245	tension net-section area	mm ²
A_{nv}	413	413	265	265	413	413	shear net-section area	mm ²
f_y	275	491,00	275	349	275	346,67	steel yielding stress	N/mm ²
f_u	430	0,00	430	463,33	430	465	steel ultimate stress	N/mm ²
γ_{M2}	1,25	1	1,25	1	1,25	1	safety coefficient	-
γ_{M0}	1		1		1			-
$V_{eff,1,Rd}$	394,57	496,77	253,11	325,42	394,57	505,09	block tearing resistance for bolts group subjected to centroid load	kN
$V_{eff,2,Rd}$	352,43	438,13	226,10	289,05	352,43	448,12	block tearing resistance for bolts group subjected to non-centroid load	kN

APPENDICE D – DESIGN OF PINNED FRAME ELEMENTS

Hollow beam resistance and stability to compression according to EC3

GEOMETRICAL PROPERTIES OF THE SECTION				
<i>section type</i>	hot-rolled hollow profile			
<i>base</i>	b	150,00	mm	
<i>height</i>	h	250,00	mm	
<i>thickness</i>	t	10,00	mm	
<i>side B</i>	B	100,00	mm	
<i>side H</i>	H	200,00	mm	
<i>section area</i>	A	7255,00	mm ²	
<i>moment of inertia with respect to strong axis</i>	I_y	5823,17	cm ⁴	
<i>moment of inertia with respect to weak axis</i>	I_z	2633,56	cm ⁴	
<i>steel type</i>	S355JR			
<i>yielding stress</i>	f_y	355,00	N/mm ²	
<i>safety coefficient</i>	γ_{M0}	1,10		
<i>safety coefficient</i>	γ_{M1}	1,05		

1) CLASSIFICATION OF THE SECTION						
<i>limit slenderness coefficient</i>	ϵ	0,81	limit of slenderness class 1	limit of slenderness class 2	limit of slenderness class 3	
<i>slenderness side B</i>	L_B	10,00	26,85	30,92	34,17	<i>side B in class 1</i>
<i>slenderness side H</i>	L_h	20,00	26,85	30,92	34,17	<i>side H in class 1</i>
THE SECTION IS GLOBALLY IN CLASS 1						

2) CHECK RESISTANCE			
N_{ed} [kN]	\leq	$N_{c,Rd}$ [kN]	
700	\leq	2341,39	VERIFIED 3,34

STRONG AXIS						
<i>CRITICAL ELASTIC LOAD FOR FLEXURAL INSABILITY ALONG STRONG AXIS</i>						
<i>steel Young modulus</i>	E	210000	N/mm ²	N _{cr,y}	11426,46	kN
<i>beam length</i>	L _{0,y}	3250	mm			
<i>RELATIVE SLENDERNESS FOR STRONG AXIS</i>						
λ_y	0,47					
<i>REDUCTION COEFFICIENT EVALUATION</i>						
<i>parameter ϕ</i>	ϕ	0,64	χ_y	0,93		
<i>instability curve</i>	a					
<i>imperfection coefficient</i>	α	0,21				
WEAK AXIS						
<i>CRITICAL ELASTIC LOAD FOR FLEXURAL INSABILITY ALONG WEAK AXIS</i>						
<i>steel Young modulus</i>	E	210000	N/mm ²	N _{cr,z}	5167,68	kN
<i>beam length</i>	L _{0,z}	3250	mm			
<i>RELATIVE SLENDERNESS FOR WEAK AXIS</i>						
λ_z	0,71					
<i>REDUCTION COEFFICIENT EVALUATION</i>						
<i>parameter ϕ</i>	ϕ	0,80	χ_z	0,84		
<i>instability curve</i>	a					
<i>imperfection coefficient</i>	α	0,21				

<i>RESISTANCE TO BUCKLING</i>				
N _{b,Rd}	2072,49			kN
STABILITY CHECK				
N_{ed} [kN]	<=	N_{b,Rd} [kN]		
700	<=	2072,49	VERIFIED	2,96

Hollow beam resistance and stability to compression according to EC3

CHECK TO SHEAR OF BOLTED UNION ACCORDING TO 1993-1-8 : 2005			
<i>Category B: frictional connections resistant at service limit state, with high strength bolts prestressed with tightening torque evaluated according to UNII EN 1090-2 so to not develop slip at service limit state</i>			

DESIGN VALUES-INPUT			
<i>Design shear force at service limit state</i>	$F_{v,Ed,ser}$	600,00	kN
<i>Design shear force at ultimate limit state</i>	$F_{v,Ed}$	600,00	kN
<i>Safety partial coefficient for bolted connections</i>	γ_{Mb}	1,25	-
CONNECTION PLATES DATA-INPUT			
<i>Thickness of thinnest external connected element</i>	t	20,00	mm
<i>Steel type connected elements</i>	S355		
<i>Yielding stress</i>	f_y	355,00	N/mm ²
<i>Ultimate resistance</i>	f_u	510,00	N/mm ²
BOLTS DESIGN DATA			
<i>Nominal diameter of bolt</i>	d	22,00	mm
<i>Bolts class of resistance</i>	10,9	Prestressed	
<i>Bolt ultimate resistance</i>	f_{ub}	1000,00	N/mm ²
<i>Resistant area of thread portion</i>	A_s	303,00	mm ²
<i>Resistant area of unthread portion</i>	A	380,00	mm ²
<i>Bolts number</i>	n_b	10,00	
<i>Design shear force at service limit state on single bolt</i>	$F_{v,Ed,ser,b}$	60,00	kN
<i>Design shear force at ultimate limit state</i>	$F_{v,Ed,b}$	60,00	kN

1) PRESCRIPTIONS ABOUT BOLT-HOLE CLEARANCE			
<i>Hole type</i>	Standard circular holes		
<i>Clearance of bolt hole</i>	2,00	mm	
<i>Holes nominal diameter</i>	d_0	24,00	mm

2) DIMENSIONAL CHECK OF CONNECTION GEOMETRY			
Distance to the edge e_1	minimum[mm]	maximum* [mm]	adopted
Distance to the edge e_2	28,80	-	29,00
Distance L	28,80	-	29,00
Inter-axis p_1	52,80	200,00	53,00
Inter-axis p_2	57,60	200,00	58,00
<i>minimum plate base</i>	b [mm]	164,00	164,00
<i>minimum plate height</i>	h [mm]	232,00	232,00
3) CALCULATION OF TIGHTENING TORQUE FOR EACH BOLT			
<i>safety partial coefficient of the material</i>	γ_{M7}	1,00	-
pre-stress design force	$F_{p,Cd}$	212,10	kN
4) CALCULATION AND CHECK OF DESIGN RESISTANCE TO SLIP AT SLS			
<i>safety partial coefficient of the material</i>	$\gamma_{M3,ser}$	1,10	
<i>number of resistant sections for each bolt</i>	n	2	
<i>frictional coefficient</i>	μ	0,2	class D-untraited surfaces
<i>coefficient for hole type</i>	k_s	1	standard bolt-hole clearance
<i>tightening force or pre-load</i>	$F_{p,C}$	212,1	kN
design resistance to slip at SLS of a single bolt	$F_{S,Rd,ser}$	77,13	kN
design resistance to slip at ULS of a single bolt	$F_{d,S,Rd,ser}$	771,27	kN
5) CALCULATION AND CHECK OF DESIGN RESISTANCE TO SLIP AT ULS			
<i>safety partial coefficient of the material</i>	γ_{M3}	1,25	
<i>number of resistant sections for each bolt</i>	n	2	
<i>frictional coefficient</i>	μ	0,2	class D-untraited surfaces
<i>coefficient for hole type</i>	k_s	1	standard bolt-hole clearance
<i>tightening force or pre-load</i>	$F_{p,C}$	212,1	kN
design resistance to slip at SLS of a single bolt	$F_{S,Rd}$	67,87	kN
design resistance to slip at ULS of a single bolt	$F_{d,S,Rd}$	678,72	kN

6) CALCULATION AND CHECK OF TEARING RESISTANCE			
<i>safety partial coefficient of the material</i>	γ_{M2}	1,25	
edge bolts			
α_1	0,40	α_b	0,40
α_2	1,96		
α_3	1,00		
k_1	1,68	k_b	1,68
k_2	2,50		
Tearing resistance of edges bolts	$F_{b,Rd,est}$	121,72	kN
internal bolts			
α_1	0,49	α_b	0,49
α_2	1,96		
α_3	1,00		
k_1	1,68	k_b	1,68
k_2	2,50		
Tearing resistance of internal bolts	$F_{b,Rd,int}$	146,90	kN
7) CALCULATION AND CHECK OF PLATES ON HOLE SECTION			
<i>safety partial coefficient of the material</i>	γ_{M0}	1	
<i>safety partial coefficient of the material</i>	γ_{M2}	1,25	
<i>net-transversal area in correspondence of holes</i>	A_{net}	2720	mm ²
<i>trasversal gross-section area</i>	A	4640	mm ²
<i>ultimate design resistance of net section (single plate)</i>	$N_{u,Rd}$	998,784	kN
<i>plastic design resistance of net section (single plate)</i>	$N_{pl,Rd}$	1647,2	kN
<i>number of plates</i>	2		
ultimate design resistance (double plates)	$F_{d,u,Rd}$	1997,568	kN

Design slip resistance at SLS of a single bolt	$F_{S,Rd,ser}$	77,13	kN	>=	60,00	kN	<i>verified</i>	1,29
Design slip resistance at LS of a single bolt	$F_{d,S,Rd,ser}$	771,27	kN	>=	600,00	kN	<i>verified</i>	1,29

Design slip resistance at ULS of a single bolt	$F_{S,Rd}$	67,87	kN	>=	60,00	kN	<i>verified</i>	1,13
Design slip resistance at ULS of a single bolt	$F_{d,S,Rd}$	678,72	kN	>=	600,00	kN	<i>verified</i>	1,13
Tearing resistance of edges bolts	$F_{b,Rd,est}$	121,72	kN	>=	60,00	kN	<i>verified</i>	2,03
Tearing resistance of internal bolts	$F_{b,Rd,int}$	146,90	kN	>=	60,00	kN	<i>verified</i>	2,45
Ultimate design resistance (double plates)	$F_{d,u,Rd}$	1997,568	kN	>=	600,00	kN	<i>verified</i>	3,33

Weldings design and check

LATERAL WELDED SEAMS			
<i>welding stiffness</i>	t_{lat}	15,00	mm
<i>sezione di gola</i>	a_{lat}	10,61	mm
<i>seam length</i>	L_{lat}	70,00	mm
<i>number lateral seams</i>	n_{lat}	4,00	
<i>tension on critical section (sezione di gola) in direction parallel to seam axis</i>	τ_{par}	202,03	N/mm ²
<i>tension on critical section (sezione di gola) in direction perpendicular to seam axis</i>	τ_{per}	0,00	N/mm ²
<i>tension on critical section (sezione di gola) in direction perpendicular to seam axis</i>	σ_{per}	0,00	N/mm ²

LONGITUDINAL WELDED SEAMS			
<i>welding stiffness</i>	t_{lon}	15,00	mm
<i>sezione di gola</i>	a_{lon}	10,61	mm
<i>seam length</i>	L_{lon}	232,00	mm
<i>number lateral seams</i>	n_{lon}	2,00	
<i>tension on critical section (sezione di gola) in direction parallel to seam axis</i>	τ_{par}	0,00	N/mm ²
<i>tension on critical section (sezione di gola) in direction perpendicular to seam axis</i>	τ_{per}	86,21	N/mm ²
<i>tension on critical section (sezione di gola) in direction perpendicular to seam axis</i>	σ_{per}	86,21	N/mm ²

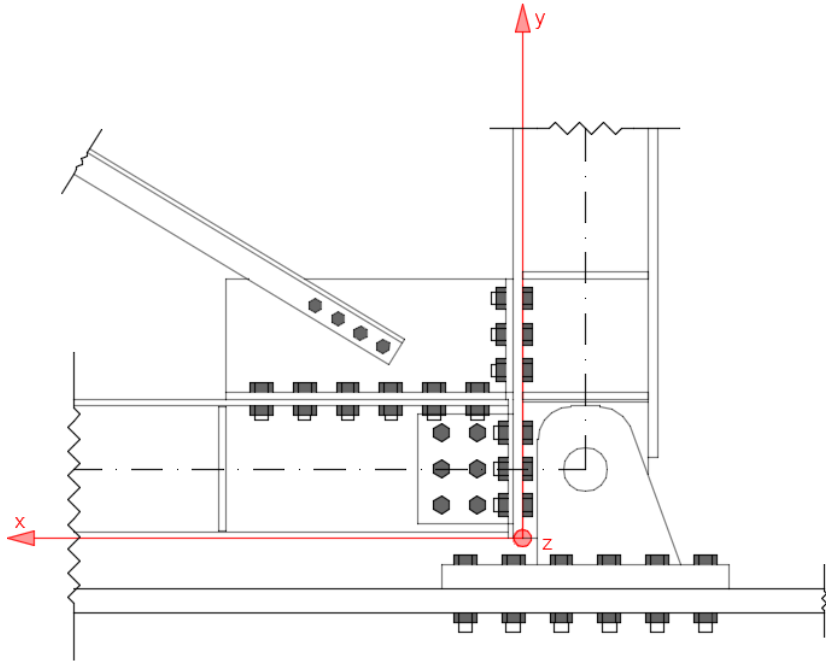
CHECK ACCORDING TO EC3 - DIRECTIONAL METHOD			
<i>nominal tension resistance of weakest element of the joint</i>	f_u	510	N/mm ²
<i>correlation coefficient (function of steel type)</i>	β_w	0,9	
<i>safety partial coefficient</i>	γ_{M2}	1,25	
LATERAL WELDED SEAMS			
σ_{Id}	<=	σ_{max}	
349,93		453,33	
LONGITUDINAL WELDED SEAMS			
σ_{Id}	<=	σ_{max}	
172,41		453,33	
σ_{per}	<=	σ_{max}	
86,21		367,20	

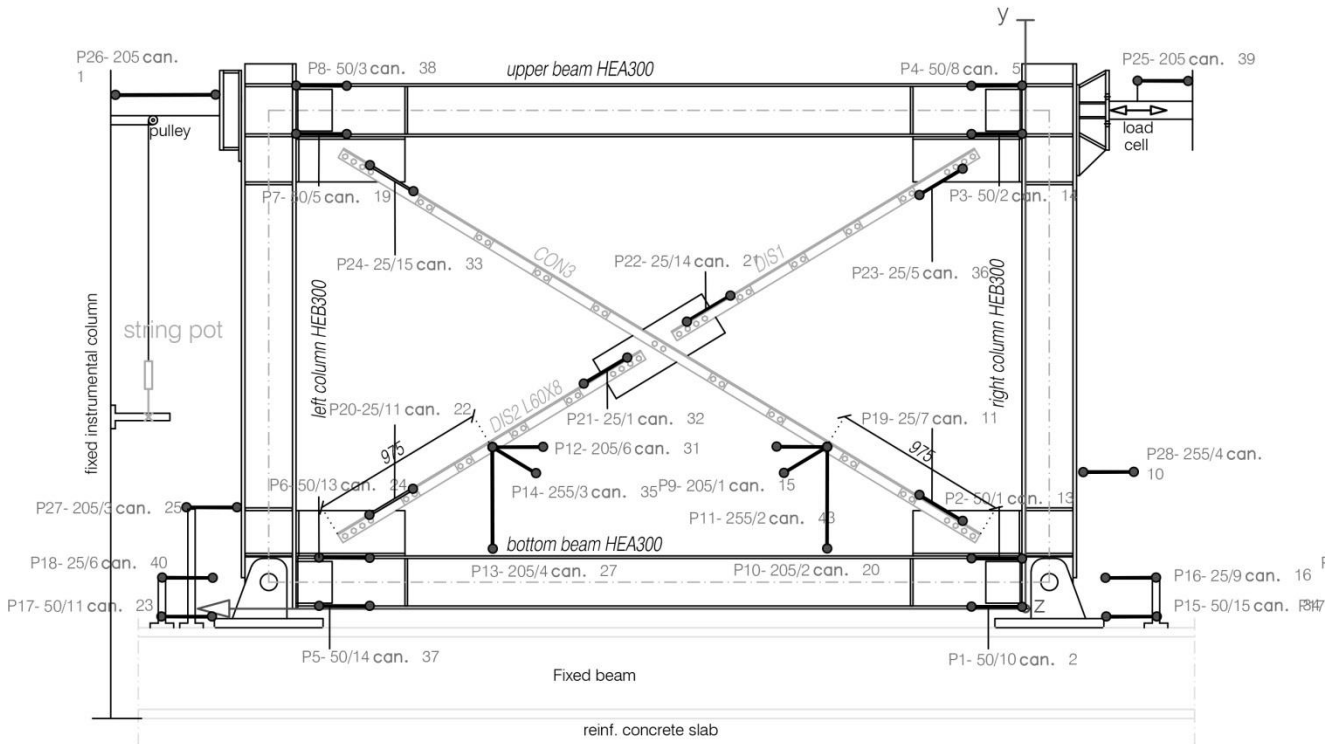
APPENDIX E – instrumentation layout

Potentiometers layouts

The following section presents for any test performed:

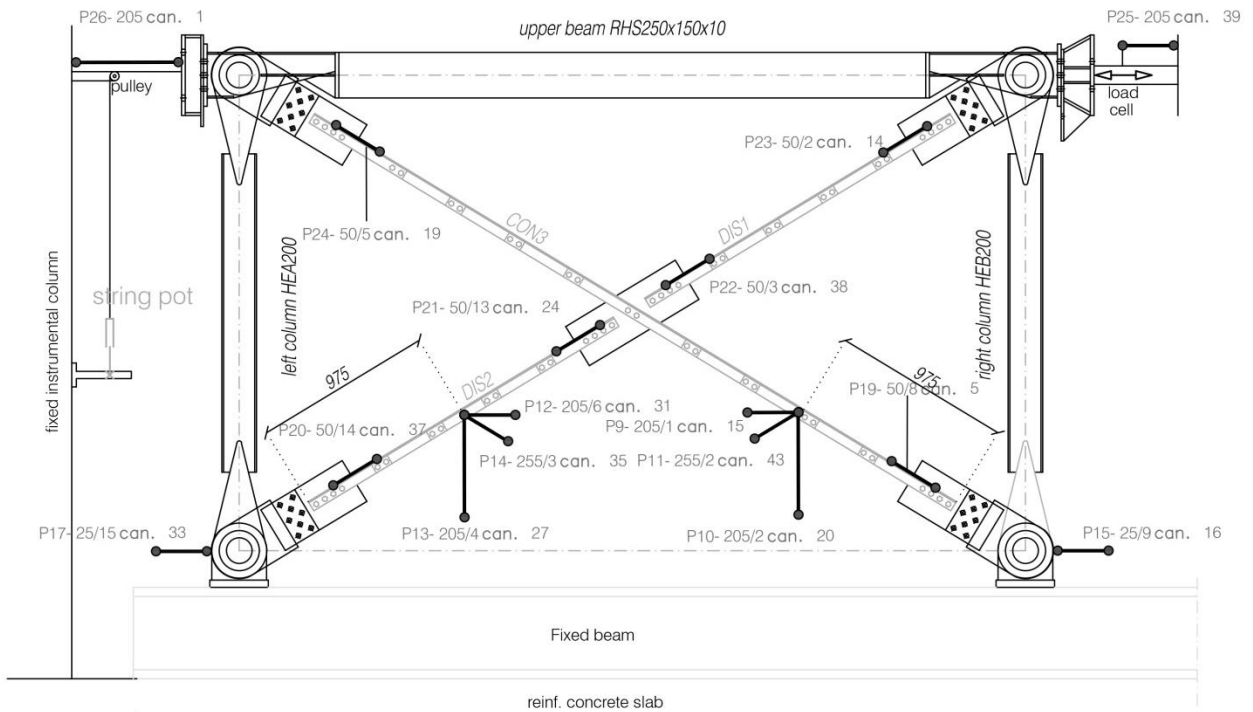
- potentiometers layout.





FRONT VIEW

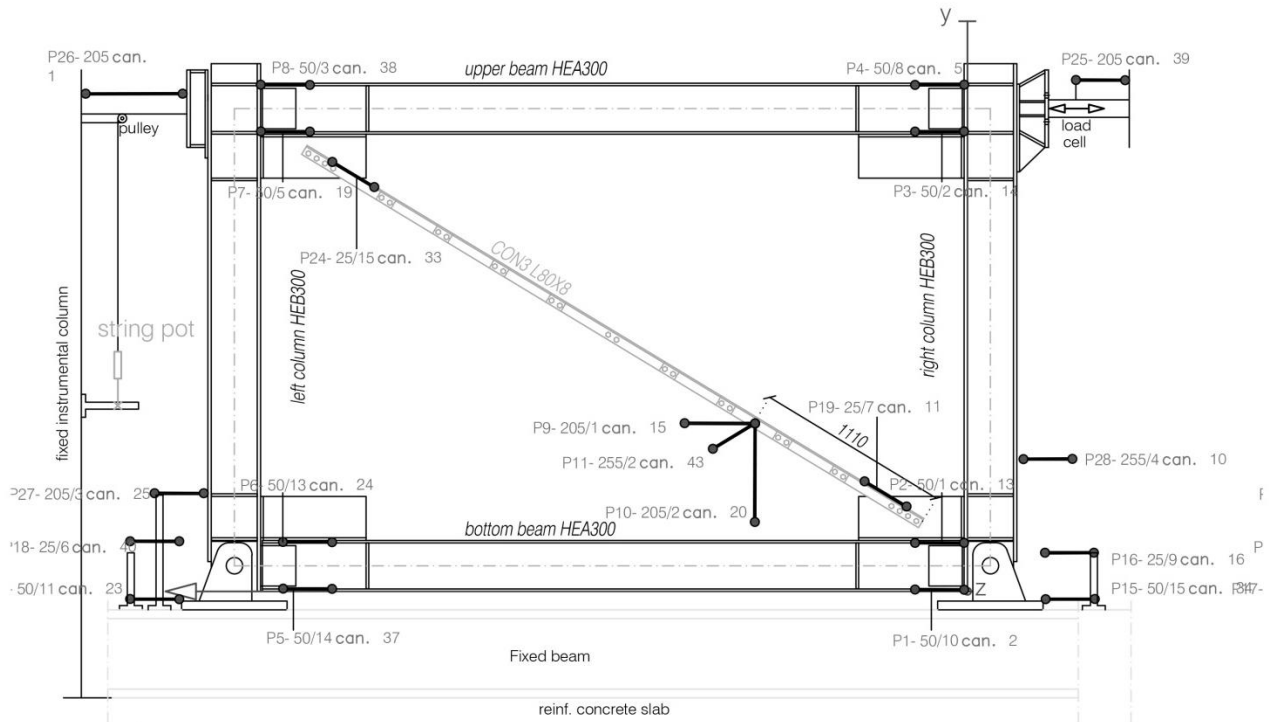
LEGEND:



FRONT VIEW

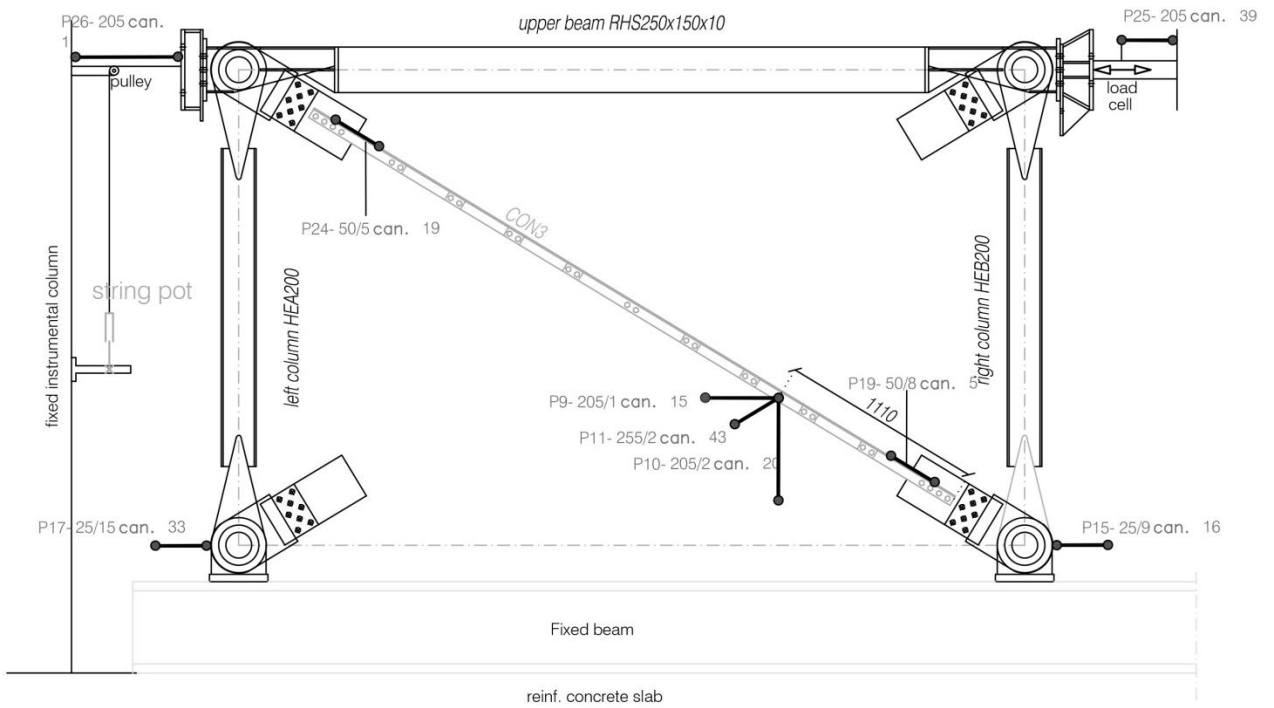
LEGEND:





FRONT VIEW

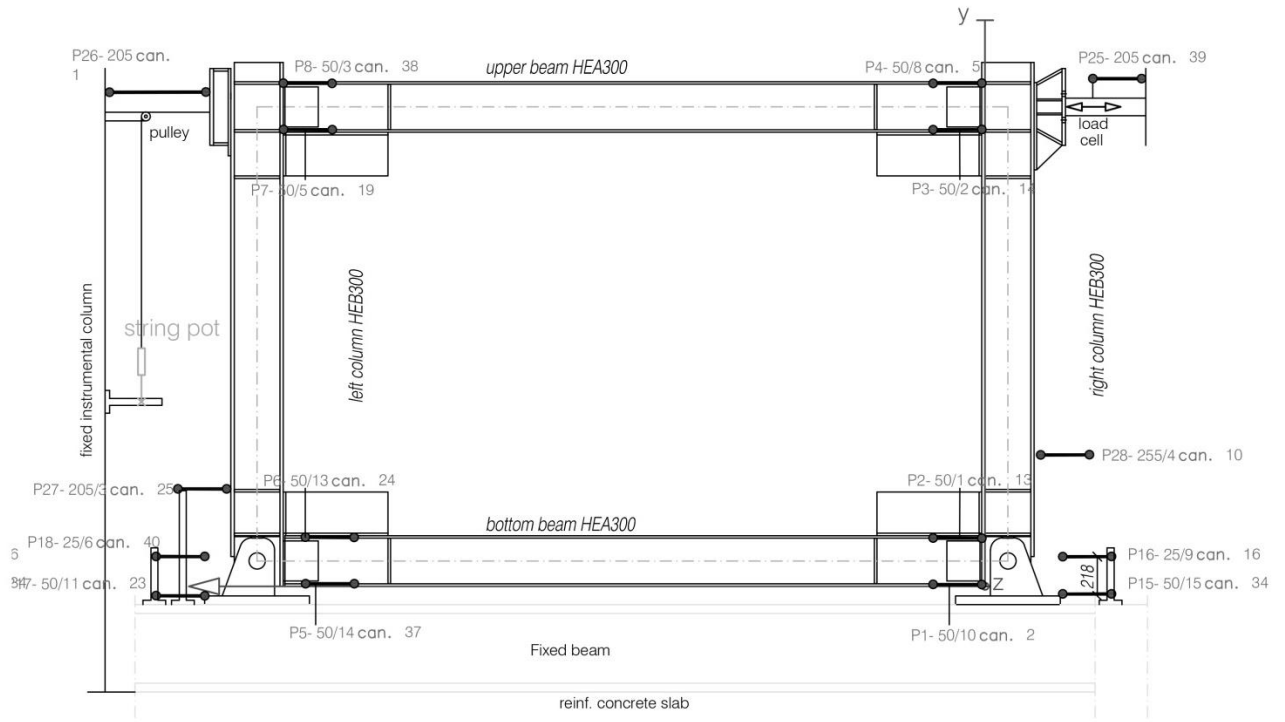
LEGEND:



FRONT VIEW

LEGEND:



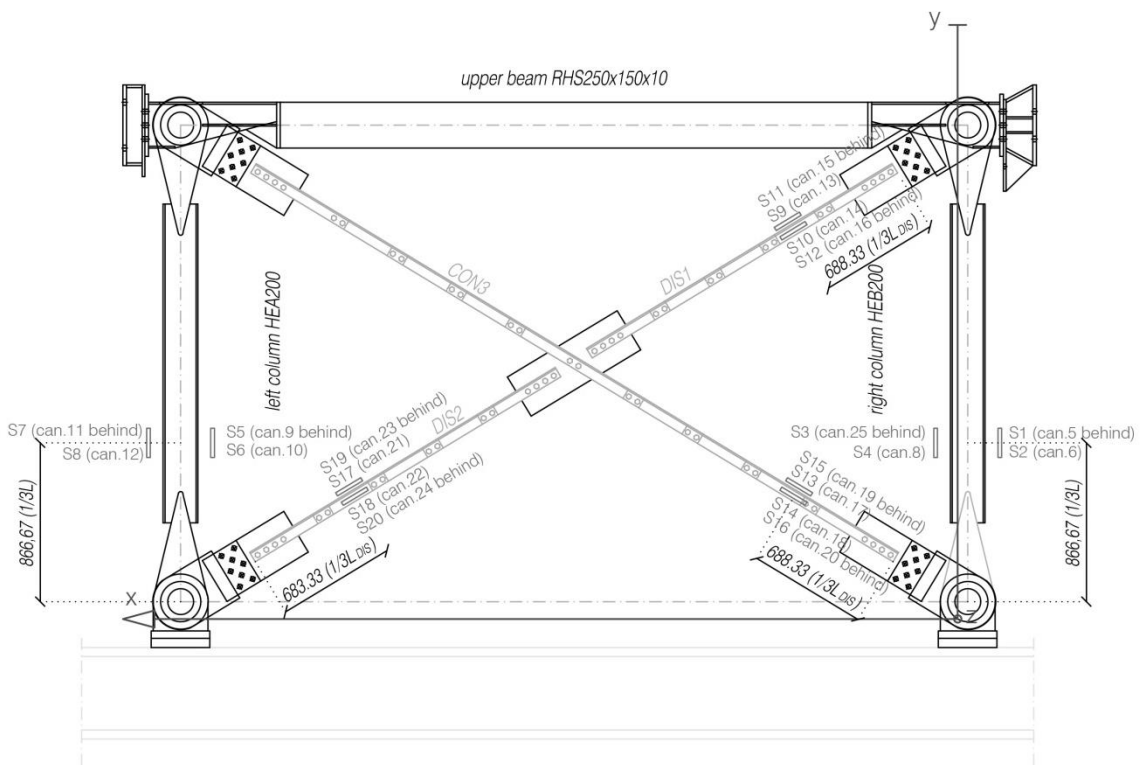
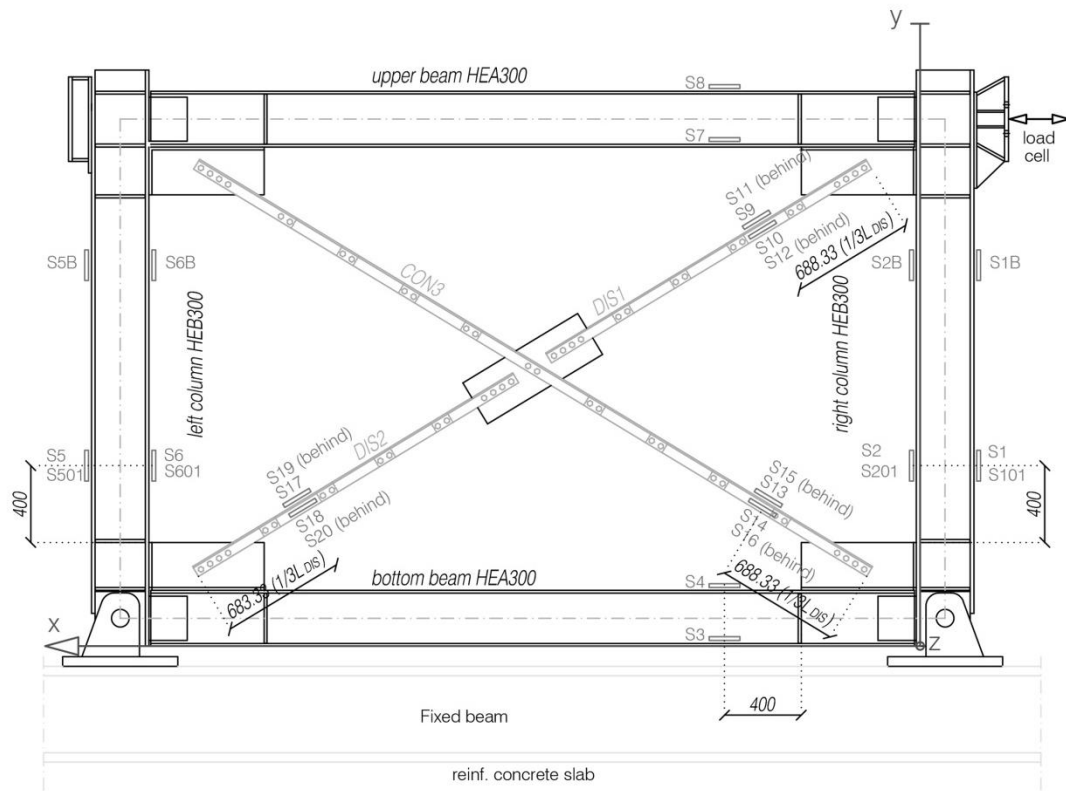


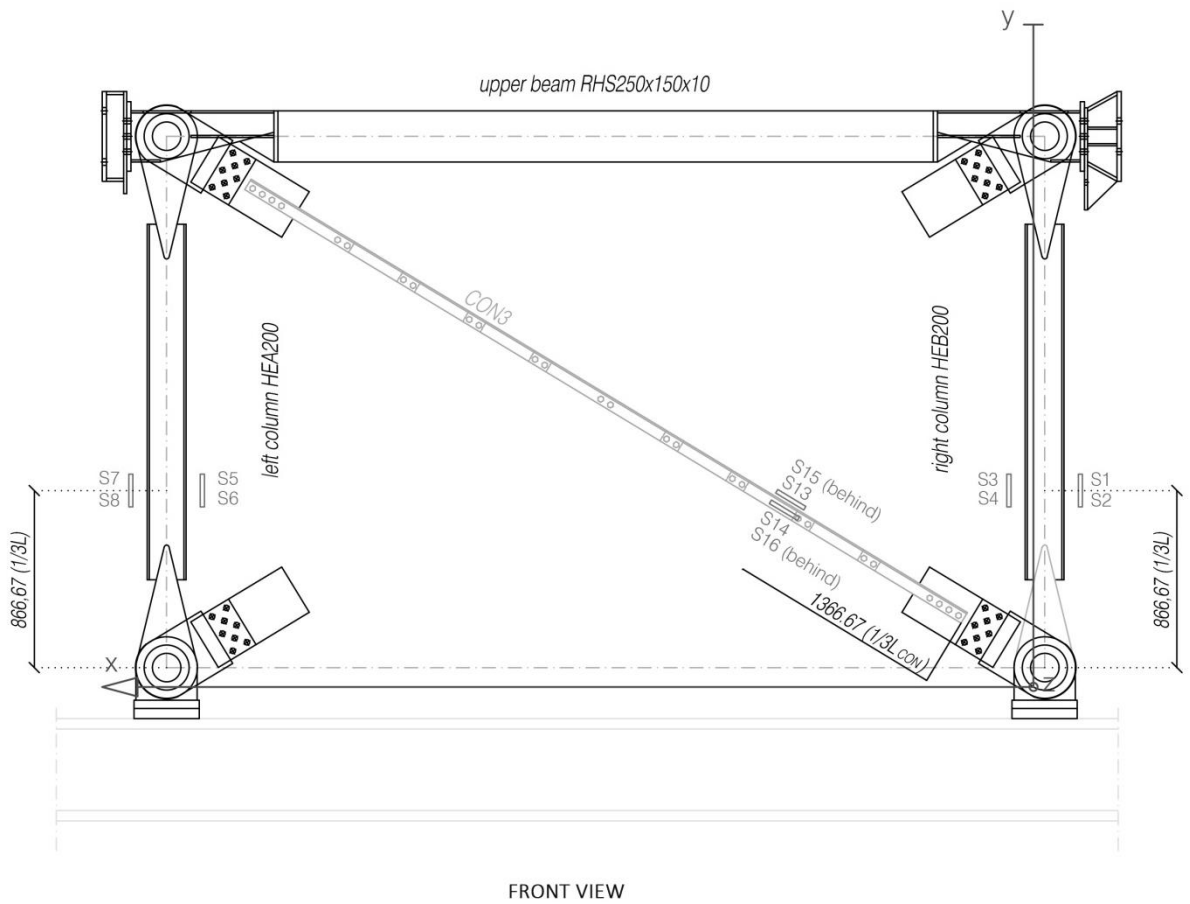
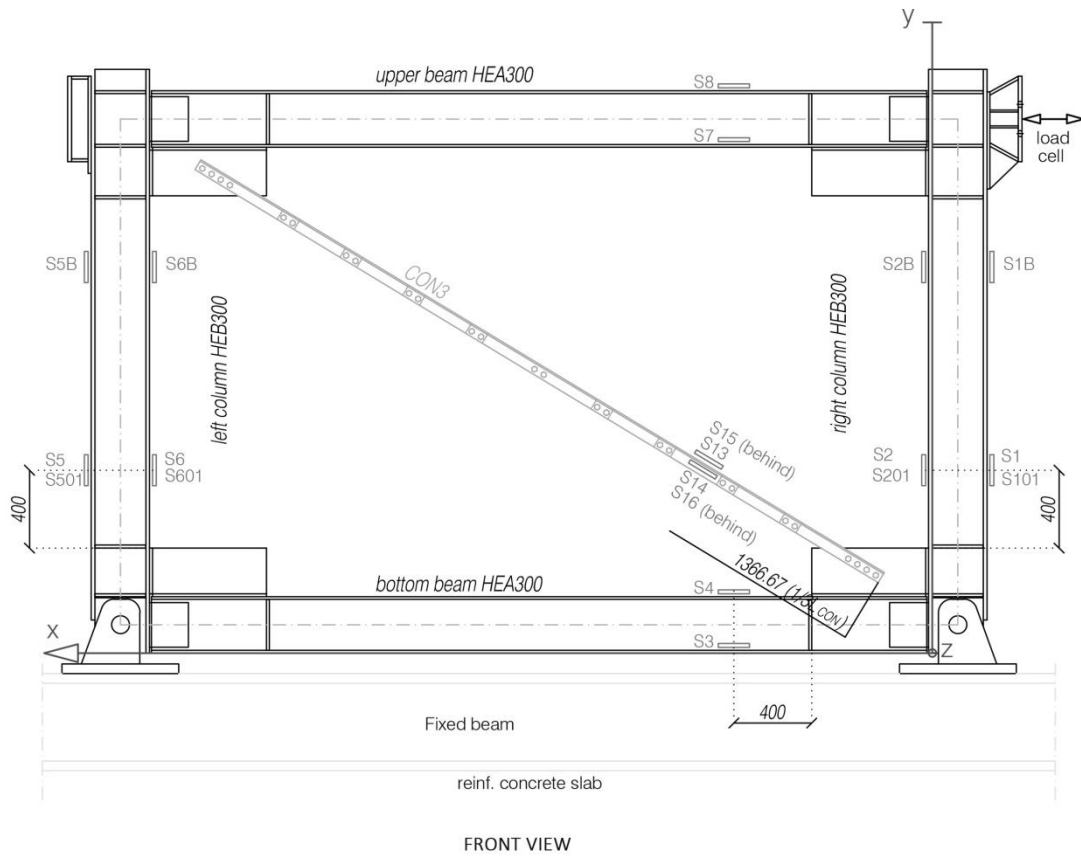
LEGEND:

FRONT VIEW



Strain gauges layouts





APPENDIX F – bolt slip

Graphs about measured displacements recorded by potentiometers at braces-gussets nodes, over time, quantify the relative displacements of main bolts connections nodes of the frame over time . They are reported below for each test performed. Additional notes will be reported for some tests.

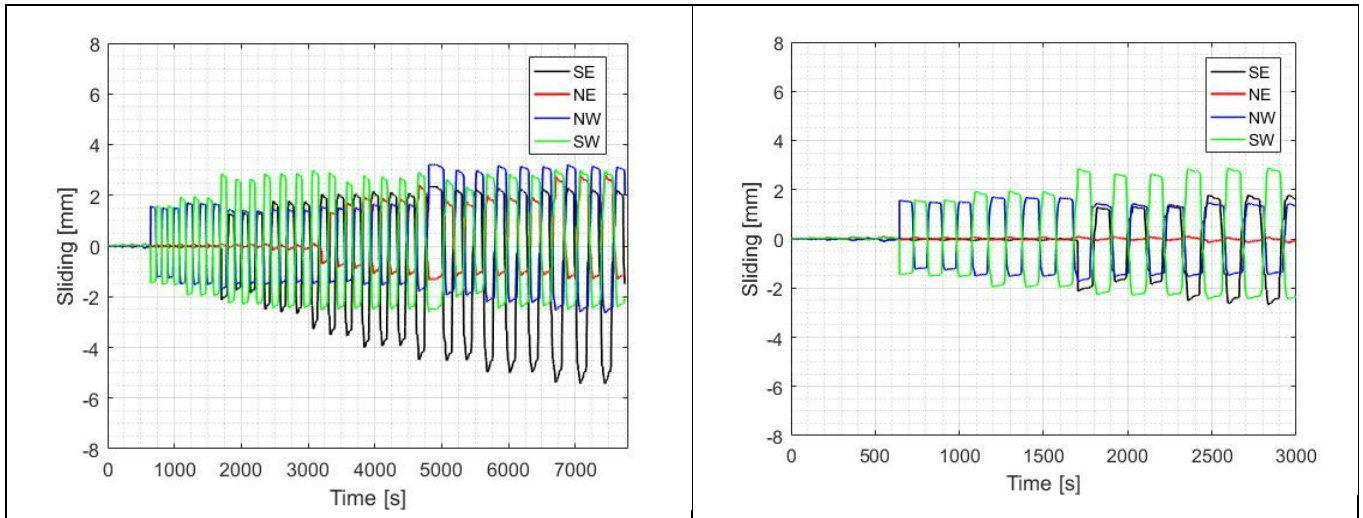


Figure 196. Test 1. Slip at bracing node.

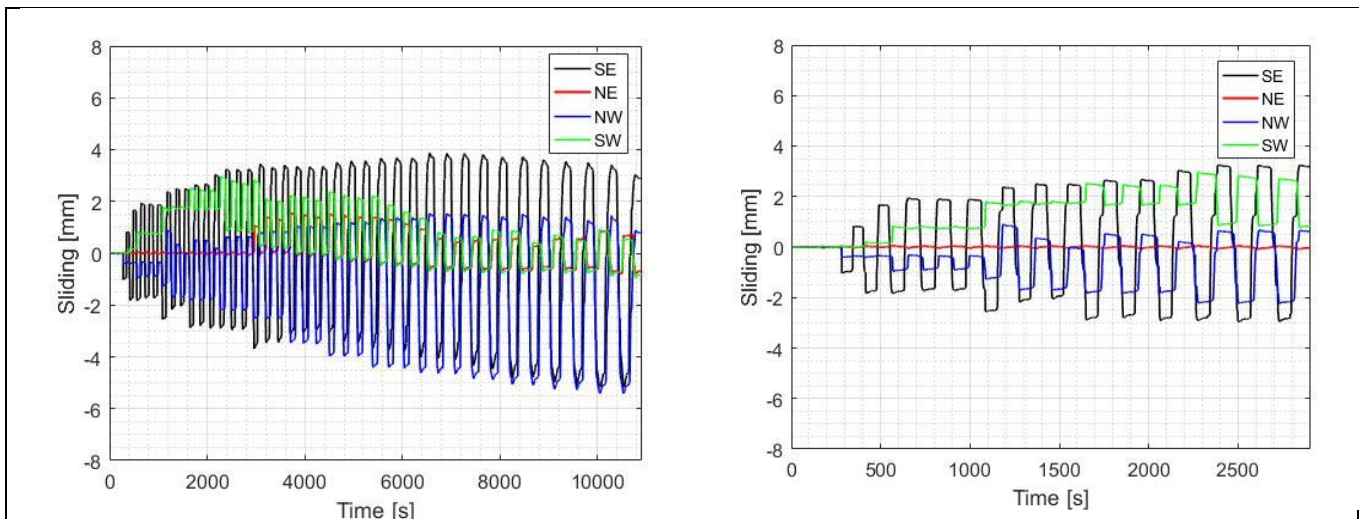


Figure 197. Test 2. Slip at bracing node.

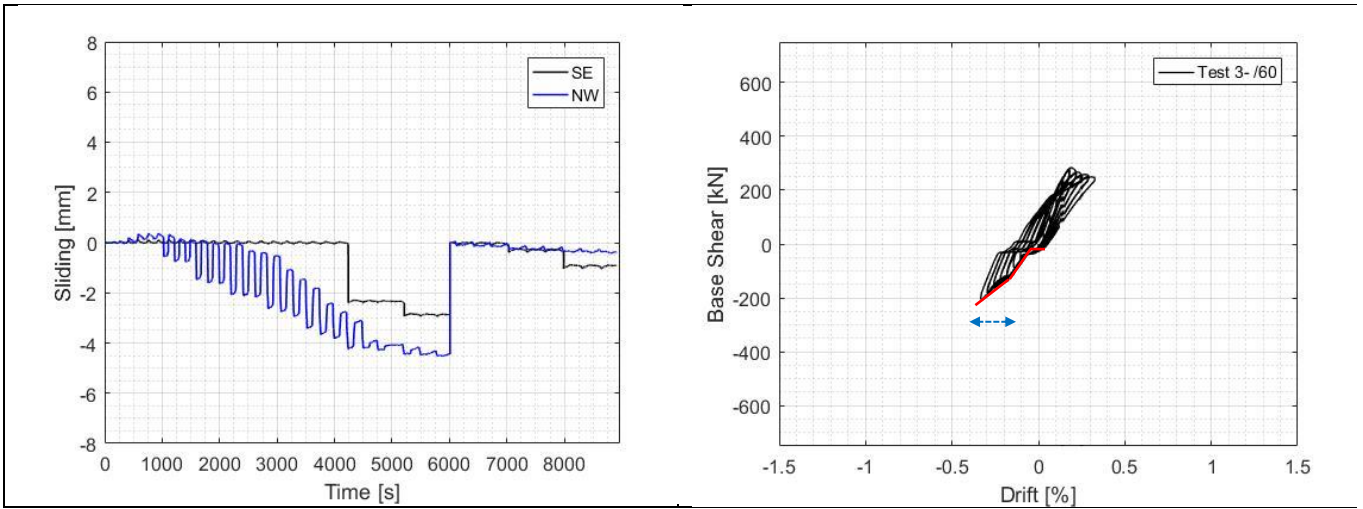


Figure 198. Test 3. Slip at bracings node.

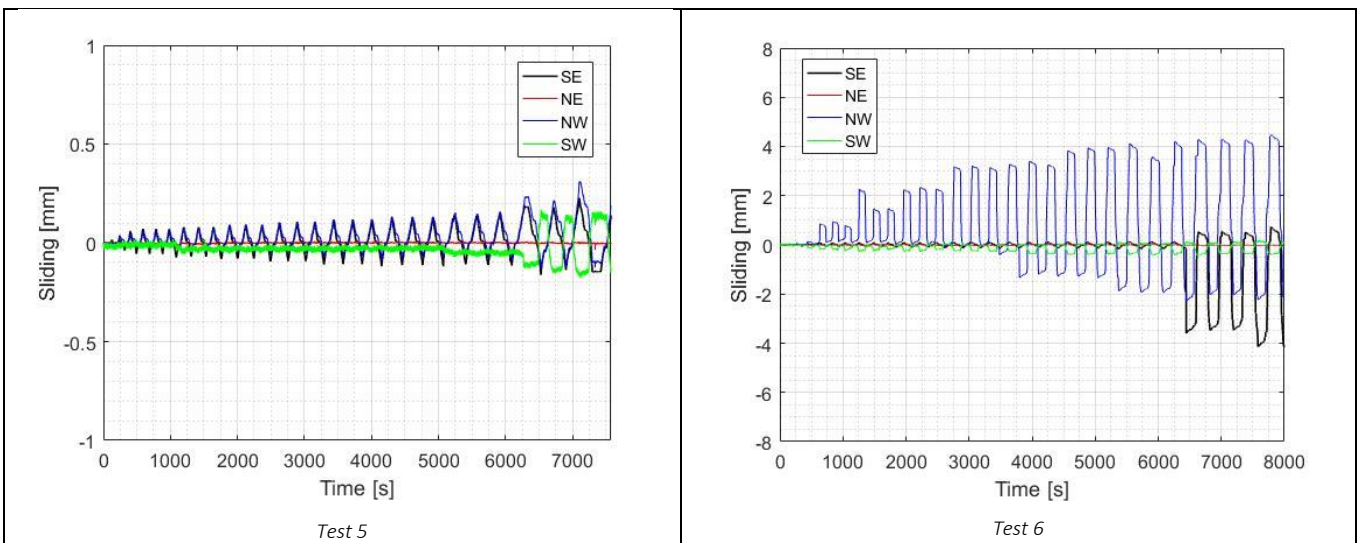


Figure 199. Slip at bracings node.

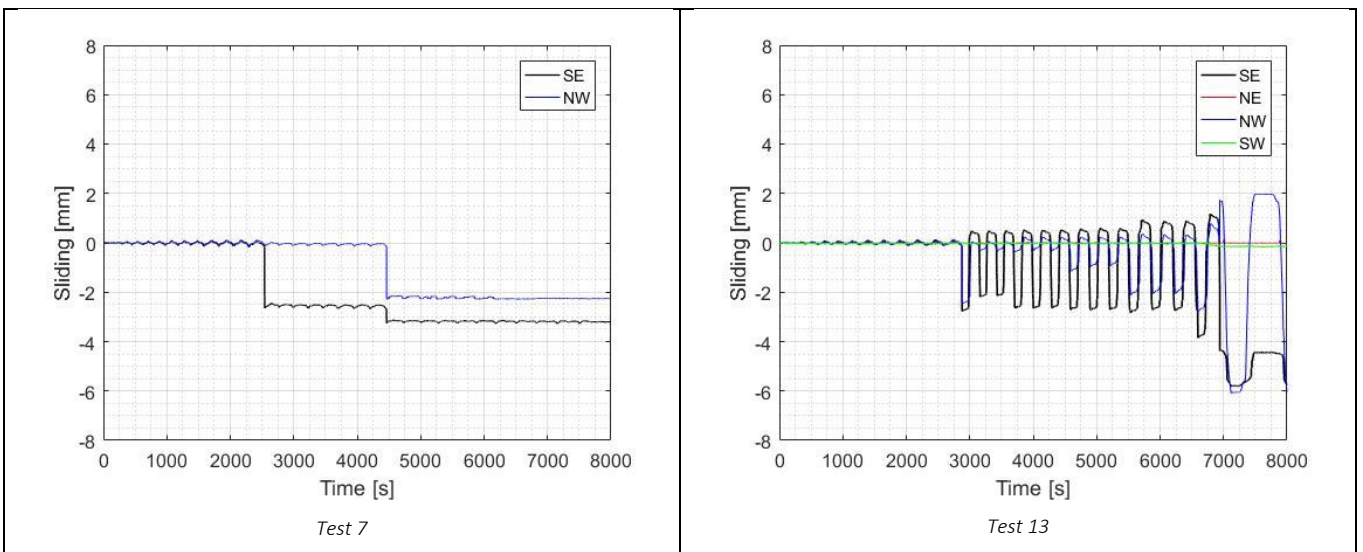


Figure 200. Slip at bracings node.

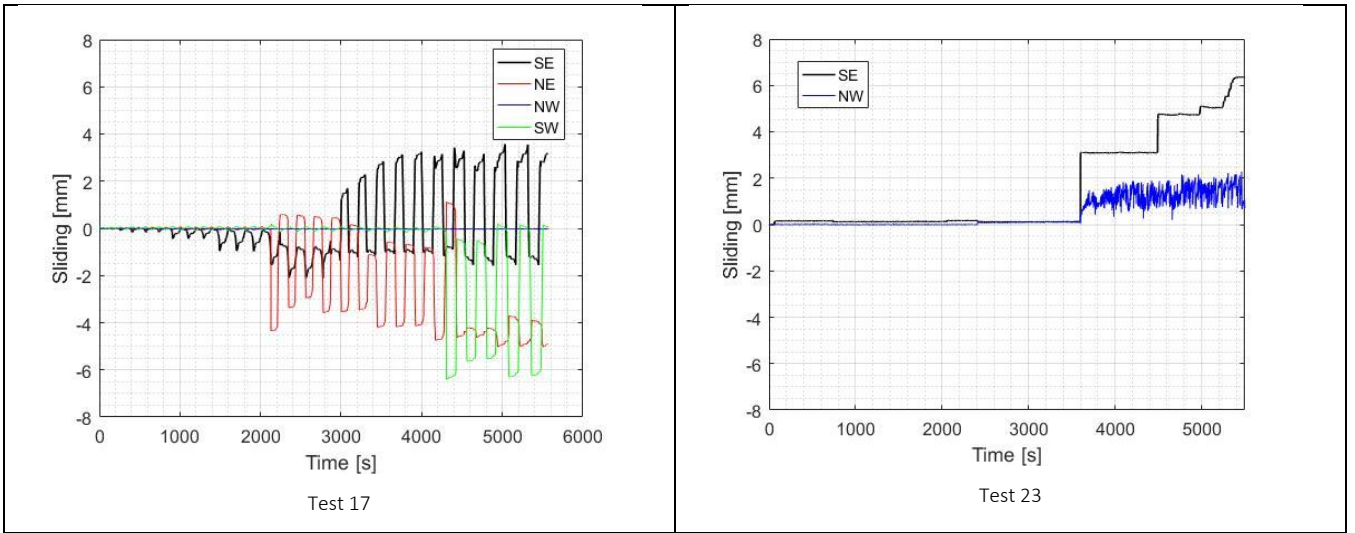


Figure 201. Slip at bracings node.

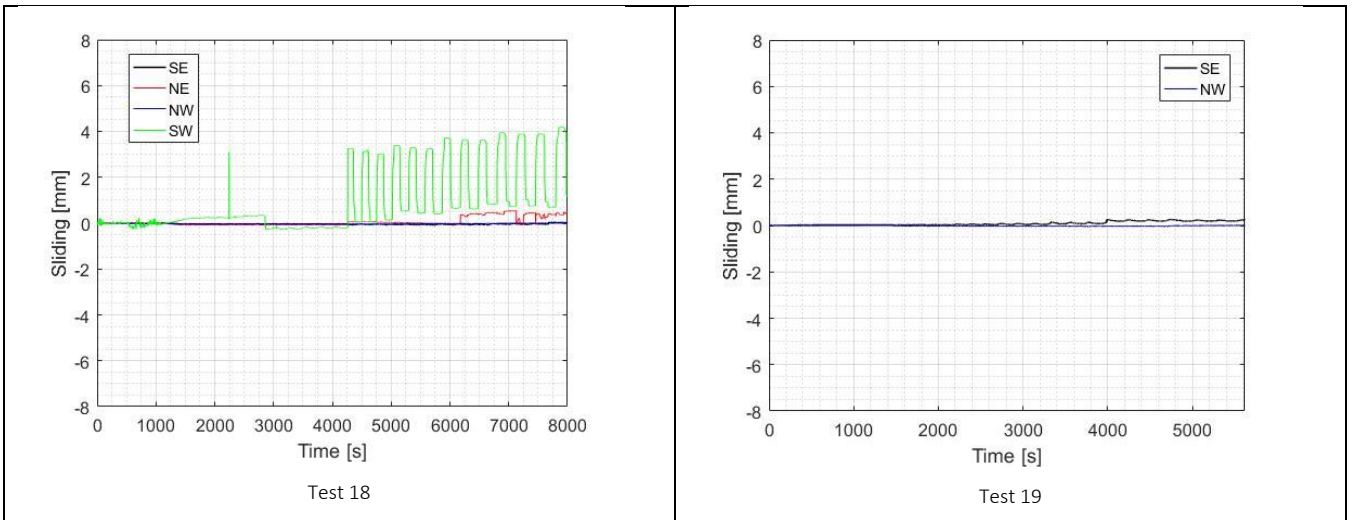


Figure 202. Slip at bracings node.

References

- [1] D. Mitchell and P. Paultre, **“Ductility and overstrength in seismic design of reinforced concrete structures”**, Canadian journal of civil Engineering”, Vol. 21, N°6, 1994.
- [2] A.S. Elnashai and A.M. Mwafy, **“Overstrength and force reduction factors of multistory reinforced concrete buildings.The structural design of tall buildings”**, 11(5).329-351, 2002.
- [3] M.A. Rahgozar and J.L.Humar, **“Accounting for overstrength in seismic design of steel structures”**, Canadian Journal of Civil Engineering”, pp.115, 1998.
- [4] Mazzolani F.M., Landolfo R., Della Corte G., Faggiano B.: **“Edifici con struttura in acciaio in zona sismica”**, IUSS Press, 2006.
- [2] Dall’Asta A., Landolfo R., Salvatore W.: **“Edifici industriali in acciaio ad uso industriale”**. Dario Flaccovio Editore, Palermo, 2009.
- [3] Tremblay R.: **“Inelastic seismic response of steel bracing members”**. Journal of Constructional Steel Research, Vol.58, pp 665-701, Elsevier Science, 2002.
- [4] Bruneau M., Uang C.M., Whittaker A.: **“Ductile Design of steel structures”**. McGraw-Hill, 1998.
- [5] Wakabayashi M., Nakamura T., Yoshida N.: **“Experimental studies on the elasticplastic behavior of braced frames under repeated horizontal loading”**. Bulletin, Disaster Prevention Research Institute, vol. 27 no. 251, pagine 121-154, 1977.
- [6] Popov E.P., Black G.: **“Steel Struts Under Severe Cyclic Loadings”**. Journal of the Structural Division, vol.107, 1981
- [7] Ballio G., Castiglioni C.A., Perotti F.: **“Numerical models for simulating the cyclic behavior and the seismic response of steel structures”**. Ninth world conference on earthquake Engineering, Tokyo - Kyoto, Japan (Vol.IV), 1988.
- [8] Ballio G., and Perotti, F.: **“Cyclic Behavior of Axially Loaded Members: Numerical Simulation and Experimental Verification”**. Journal of Constructional Steel Research 7, pagine 3-41, 1985.
- [9] Metelli G., Bregoli G., Marchina E.: **“Studio numerico e sperimentale del comportamento isteretico di controventi concentrici”**. Atti XV Convegno ANIDIS - L’Ingegneria Sismica in Italia, Padova 30 Giugno - 4 Luglio 2013. Padova University Press.
- [10] Bernuzzi C.: **“Progetto e verifica delle strutture in acciaio secondo le Norme Tecniche per le costruzioni e l’Eurocodice 3 (UNI EN 1993)”**. Hoepli, 2013.
- [11] Barberio G. **“Fondamenti di costruzioni in acciaio”**. Grafill, 2015.
- [12] Images from www.ecs.umass.edu
- [13] Gélinas A.: **“Étude expérimentale du comportement sismique des assemblages utilisés dans les contreventements en x en acier”**. École Polytechnique de Montréal, 2013.
- [14] ECCS-CECM-EKS **“Recommended Testing Procedure for Assessing the Behaviour of Structural Steel Elements under Cyclic Loads”**, Technical Working Group 1.3: Seismic Design, n.45, 1986.
- [15] Eurocode 3, Design of Steel Structure, 2003.
- [16] Eurocode 8, Design of structures for earthquake resistance, 2003.

- [17] UNI EN ISO 6892:2009 Materiali metallici – Prova di trazione – Parte 1: Metodo di prova a temperature ambiente.
- [18] R-UNI EN 10002-1:2004 Materiali metallici – Prova di trazione – Parte 1: Metodo di prova a temperature ambiente.
- [19] UNI EN 14399-5:2015 High-strength structural bolting assemblies for preloading – Part 4: System HV – Hexagon bolt and nut assemblies.
- [20] UNI 5397:1978 Prodotti finiti di acciaio laminati a caldo. Travi HE ad ali larghe parallele. Dimensioni e tolleranze.
- [21] UNI EN 10056-1:2000 Angolari ad ali uguali e disuguali di acciaio per impieghi strutturali. Dimensioni.

Acknowledgements

I wish to thank all that people who has not ceased to support me from the first to last day of this whole college career. Nevertheless the same university Politecnico of Milan that taught me so much for work as in life.

First and foremost, I'd like to special thanks to my family, that has always been close to me any times a bit 'darker of this experience with a lot of patience. In addition to the economic effort that has allowed me to reach this goal. Especially to my little sister, younger but yet stronger than me, that somehow gave me the maximum support with her kindness and smiles.

A big thank you goes to my thesis supervisors, Prof. Eng. Carlo Castiglioni and Eng. Alper Kanyilmaz, for their continued support during the process of preparation and performance of the tests and during the writing of the thesis. They gave me the freedom to select thesis topic which was unique to my abilities, and provided me with wise guidance whenever I needed it.

I have also to gratefully acknowledge my girlfriend Ilaria for her support. She has been besides me with extreme patience.

Then, a big hug goes to all Fossombrone's friends with which I grew up. The university has given me so much, but in return has taken potential moments that no one can bring back.

Thanks also to my colleague Alberto with whom I shared the preparation and the work during the first experimental evidence. A fair thanks to the staff of the Laboratory Testing and Materials in the Department of Structural Engineering of Politecnico di Milano, in particular Marco, Tonino and always available during the instrumentation and experimental testing.

Thank you, finally, but not like last, the fellow students, with whom I shared moments of real agony, sleepless nights and inhuman rhythms. The tenacity and the wish to accomplish its own objectives have allowed every day to give us strength to continue without any stop.